Tampere University

MARSEL GARIFULLIN

Component Method for High Strength Steel Rectangular Hollow Section T Joints

Tampere University Dissertations 45

Tampere University Dissertations 45

MARSEL GARIFULLIN

Component Method for High Strength Steel Rectangular Hollow Section T Joints

ACADEMIC DISSERTATION
To be presented, with the permission of
the Faculty Council of the Faculty of Built Environment
of Tampere University,
for public discussion in the auditorium RG202
of the Rakennustalo Building, Korkeakoulunkatu 5, Tampere,
on 26 April 2019, at 12 o'clock.

ACADEMIC DISSERTATION
Tampere University, Faculty of Built Environment
Finland

Responsible supervisor and Custos	Assistant Prof. Kristo Mela Tampere University Finland	
Supervisors	Prof. Markku Heinisuo Tampere University Finland	Associate Prof. Sami Pajunen Tampere University Finland
Pre-examiners	Prof.ir. Bert Snijder Eindhoven University of Technology The Netherlands	Prof. Jean-Pierre Jaspart Liège University Belgium
Opponents	Prof. Markus Knobloch Ruhr University Bochum Germany	Prof.ir. Bert Snijder Eindhoven University of Technology The Netherlands

The originality of this thesis has been checked using the Turnitin OriginalityCheck service.

Cover design: Roihu Inc.

ISBN 978-952-03-1042-4 (print)
ISBN 978-952-03-1043-1 (pdf)
ISSN 2489-9860 (print)
ISSN 2490-0028 (pdf)
http://urn.fi/URN:ISBN:978-952-03-1043-1

PunaMusta Oy – Yliopistopaino
Tampere 2019

Preface

This thesis represents the results of my work conducted at the Research Center of Metal Structures at Tampere University of Technology from 2015 to 2019. Although any doctoral thesis represents an individual author's work, this research became possible largely thanks to the fruitful cooperation of many brilliant contributors.

I started my doctoral studies in 2014 in the field of thin-walled cold-formed steel structures in Peter the Great St.Petersburg Polytechnic University, Russia. The key moment on my doctoral path occurred in December 2014, when I met Professor Markku Heinisuo and Senior Research Fellow Kristo Mela from Tampere University of Technology. They proposed me a challenging cooperation in tubular joints, which I accepted. On this stage, I am very thankful to my first supervisor, Professor Nikolai Vatin, who laid the corner stone in the cooperation between our universities and encouraged me to participate in this interesting collaboration.

As I started working on tubular joints, this research engaged me so actively that it became the topic my doctoral thesis. In 2015, a scholarship from the Ministry of Education and Science of the Russian Federation allowed me to move to Finland and start my doctoral studies in Tampere University of Technology. I am grateful for the painstaking guidance of my supervisor, Professor Markku Heinisuo, whose brilliant mind always inspired me throughout my doctoral studies. I am very thankful to my second supervisor, Kristo Mela, for his significant help in publishing papers and solving many organizational issues. I also appreciate the invaluable criticism and advice of Adjunct Professor Sami Pajunen and Professor Mikko Malaska.

In October 2017, I was awarded a grant for conducting a research on welding residual stresses in cooperation with Brandenburg University of Technology, Germany. I would like to thank Professor Hartmut Pasternak and researcher Benjamin Launert for their kind hospitality and KAUTE foundation for funding my two-month visit to Germany. The scientific cooperation with the German colleagues strengthened the relationship between our universities and brought fruitful results, which I included later into this doctoral thesis.

I also appreciate the help of Jarmo Havula, the Director of Research Unit at Häme University of Applied Sciences, who enriched my research with valuable experimental results. Many thanks to student Maria Bronzova, whose endless optimism and enthusiasm helped me to operate numerous Abaqus calculations. I must also mention my colleagues, Teemu Tiainen, Jolanta Bączkiewicz and Timo Jokinen, who created a wonderful atmosphere in our room.

My deepest bow is reserved to my parents, Gulnara and Rinat. Living in Finland, it was very important for me to remember that there is a house where I can always return and people who always love me, support me and wait for me, regardless of my success. At the end, this thesis

would have never been finished without the endless patience and care of my lovely Zemfira, who supported me during all my doctoral studies and believed in me, even when I did not believe in myself.

Tampere 04.02.2019

Marsel Garifullin

Abstract

Tubular joints cover a large range of applications, including bridges, lattice masts, frames and trusses, combining nice appearance and excellent structural properties. Currently, Eurocode and other standards provide engineers with clear and simple design rules for the design of tubular joints. However, the recent invention of new types of connections and high strength steels encourages researchers to develop new, more unified design rules to obtain all benefits of tubular structures in the construction industry.

One of the most reliable solutions for the design of tubular joints can be provided by the component method, which recently has been proposed as a unified approach for the design of most types of connections. The method has been extended for tubular joints in the comprehensive research conducted by CIDECT. Although the CIDECT recommendations present a consistent design approach for the resistance of joints, there are still many issues that remain unsolved.

Following the CIDECT studies conducted recently on this topic, this thesis specifies the component method for rectangular hollow section (RHS) T joints under arbitrary loading, including biaxial bending and axial loading. Employing simple mechanical models and extensive numerical analyses, the thesis develops theoretical solutions for the initial stiffness of RHS T joints under in-plane bending and axial loading. To incorporate the effect of chord axial stresses, the thesis proposes chord stress functions for the initial axial and rotational stiffness of joints. Moreover, the research investigates the most challenging issues of high strength steels in RHS T joints, including significant reduction factors for resistance and the extremely large throat thicknesses of full-strength fillet welds. In addition, the thesis discovers the improving effect of fillet welds on the structural properties of tubular joints. Attention is also paid to the influence of initial imperfections, such as geometrical imperfections and welding residual stresses. Finally, the thesis constructs a surrogate model for the initial rotational stiffness of RHS Y joints, demonstrating its effectiveness for solving engineering tasks with no analytical solution.

The results of the research can help to make a step forward in developing a sustainable and consistent approach for the design of tubular joints, including their resistance, initial stiffness and ductility.

Keywords: tubular joint; rectangular hollow section; resistance; initial stiffness; component method; initial imperfections; residual stresses; high strength steel.

Contents

List of Figures

List of Tables

List of Abbreviations

CIDECT	Comitè International pour le Dèveloppement et l'Etude de la Construction Tubulaire (International Committee for the Development and Study of Tubular Structures)
RHS	Rectangular Hollow Section
SHS	Square Hollow Section
CHS	Circular Hollow Section
HSS	High Strength Steel
HAZ	Heat Affected Zone
FE	Finite Element

List of Symbols

Geometry

A_0	chord cross-sectional area
a_w	fillet weld throat thickness
$a_{w,fs}$	full-strength fillet weld throat thickness
b_0	chord width
b_1	brace width
b_{eq}	equivalent brace width
h_0	chord height
h_1	brace height
L_0	chord length
t_0	chord wall thickness
t_1	brace wall thickness
$W_{el,0}$	chord elastic section modulus
z_{ip}	in-plane lever arm
z_{op}	out-of-plane lever arm
β	brace-to-chord width ratio, b_1 / b_0
γ	chord width-to-thickness ratio, $\gamma = b_0 / 2t_0$, usually considered as $2\gamma = b_0 / t_0$
η	brace height-to-chord width ratio, h_1 / b_0
φ	angle between chord axis and brace axis (Y joints)

Component method

b_{eff}	effective width (axial load)
$C_{j,ini,N}$	initial axial stiffness
k_i	stiffness of component i, $i = a, \ldots, e$
$k_{sn,ip}$	chord stress function for initial in-plane rotational stiffness
$k_{sn,op}$	chord stress function for initial out-of-plane rotational stiffness
$k_{sn,N}$	chord stress function for initial axial stiffness
l_{eff}	effective length (axial load)
$l_{eff,cf}$	effective width (in-plane bending moment)
$M_{ip,Ed}$	design in-plane bending moment
$M_{ip,Rd}$	design in-plane bending resistance
$M_{op,Ed}$	design out-of-plane bending moment
$M_{op,Rd}$	design out-of-plane bending resistance
N_{Ed}	design axial load
N_{Rd}	design axial resistance
$S_{j,ini,ip}$	initial in-plane rotational stiffness
$S_{j,ini,op}$	initial out-of-plane rotational stiffness

Steel properties

E	Young's (elastic) modulus
f_{u0}	chord steel ultimate tensile stress
f_{u1}	brace steel ultimate tensile stress
f_y	yield stress
f_{y0}	chord steel yield stress
f_{y1}	brace steel yield stress
ν	Poisson's ratio

Structural behavior

$C_{j,h}$	axial hardening stiffness
k_n	chord stress function for resistance
M_0	chord compensating moment
M_{ip}	in-plane bending moment
$M_{ip,1,Rd}$	design in-plane moment resistance according to EN 1993-1-8:2005
M_{max}	maximum moment load the joint can resist
M_{op}	out-of-plane bending moment
M_{pl}	plastic moment resistance
$M_{pl,exp}$	experimental plastic resistance
M_{ult}	ultimate moment resistance
$M_{w,Rd}$	weld design resistance
N	axial force
$N_{1\%b0}$	axial load corresponding to $0.01b_0$ displacement of the chord
$N_{3\%b0}$	axial load corresponding to $0.03b_0$ displacement of the chord
N_{max}	maximum axial load the joint can resist
N_{pl}	plastic axial resistance
N_{ult}	ultimate axial resistance
n	relative axial stress in chord
$S_{j,h}$	in-plane hardening stiffness
δ_{max}	displacement corresponding to N_{max}
σ_0	axial stress in chord
$\varphi_{3\%b0}$	rotation corresponding to $0.03b_0$ displacement of the chord
φ_{max}	rotation corresponding to M_{max}

Other symbols

k_{fw}	fillet welds correlation coefficient
k_{HSS}	high strength steel reduction factor
R^2	coefficient of determination
β_w	fillet welds strength factor
γ_{M0}	partial safety factor for the resistance of members and cross-sections
γ_{M2}	partial safety factor for the resistance of welds
γ_{M5}	partial safety factor for the resistance of hollow section joints
ε_0	allowable amplitude of initial geometrical imperfections

List of Original Publications

This thesis is based on the following original publications in peer-review scientific journals and conferences, which are references in the text as Articles I-VIII.

I. Garifullin, M., Pajunen, S., Mela, K. & Heinisuo, M., 2018. 3D component method for welded tubular T joints. In A. Heidarpour & X.-L. Zhao, eds. *Tubular Structures XVI: Proceedings of the 16th International Symposium for Tubular Structures (ISTS 2017, 4-6 December 2017, Melbourne, Australia)*. London: Taylor & Francis Group, pp. 165-173.

II. Garifullin, M., Pajunen, S., Mela, K., Heinisuo, M. & Havula, J., 2017. Initial in-plane rotational stiffness of welded RHS T joints with axial force in main member. *Journal of Constructional Steel Research*, 139, pp. 353-362.

III. Havula, J., Garifullin, M., Heinisuo, M., Mela, K. & Pajunen, S., 2018. Moment-rotation behavior of welded tubular high strength steel T joint. *Engineering Structures*, 172, pp. 523-537.

IV. Garifullin, M., Launert, B., Heinisuo, M., Pasternak, H., Mela, K. & Pajunen, S., 2018. Effect of welding residual stresses on local behavior of rectangular hollow section joints. Part 1 – Development of numerical model. *Bauingenieur*, 93(April), pp. 152-159.

V. Garifullin, M., Launert, B., Heinisuo, M., Pasternak, H., Mela, K. & Pajunen, S., 2018. Effect of welding residual stresses on local behavior of rectangular hollow section joints. Part 2 – Parametric studies. *Bauingenieur*, 93(May), pp. 207-213.

VI. Garifullin, M., Bronzova, M., Heinisuo, M., Mela, K. & Pajunen, S., 2018. Cold-formed RHS T joints with initial geometrical imperfections. *Magazine of Civil Engineering*, 4(80), pp. 81-90.

VII. Heinisuo, M., Garifullin, M., Jokinen, T., Tiainen, T. & Mela, K., 2016. Surrogate modeling for rotational stiffness of welded tubular Y-joints. In C. J. Carter & J. F. Hajjar, eds. *Connections in Steel Structures VIII*. Chicago, Illinois: American Institute of Steel Construction, pp. 285–294.

VIII. Garifullin, M., Bronzova, M., Pajunen, S., Mela, K., Heinisuo, M., 2019. Initial axial stiffness of welded RHS T joints. *Journal of Constructional Steel Research*, 153, pp. 459-472.

Author's contribution

I. The author conducted the research and wrote the manuscript as the corresponding author. The co-authors commented on the manuscript.

II. The author conducted the research and wrote the manuscript as the corresponding author. The co-authors commented on the manuscript.

III. The author developed the numerical model in close cooperation with Benjamin Launert. The author wrote the manuscript as the corresponding author. The co-authors commented on the manuscript.

IV. The author conducted the research and wrote the manuscript as the corresponding author. The co-authors commented on the manuscript.

V. The research program was prepared by the author. The finite element simulations were conducted by Maria Bronzova. The author wrote the manuscript as the corresponding author. The co-authors commented on the manuscript.

VI. The author conducted the finite element analyses and constructed the surrogate model. The effect of fillet weld was investigated in cooperation with Timo Jokinen. The author wrote the manuscript as the corresponding author. The co-authors commented on the manuscript.

VII. The experimental part was conducted by Jarmo Havula. The theoretical analyses were conducted by the author in cooperation with Jarmo Havula and Markku Heinisuo. The coauthors provided the text passages of their own expertise and commented on the manuscript. The author served as the corresponding author of the manuscript.

VIII. Initial axial stiffness was investigated by the author. The chord stress function was developed by the author in close cooperation with Maria Bronzova. The author wrote the manuscript as the corresponding author. The co-authors commented on the manuscript.

1 Introduction

All science is either physics or stamp collecting.

ERNEST RUTHERFORD

1.1 Background for the design of RHS T joints

1.1.1 Traditional approach

Rectangular hollow sections combine excellent structural properties, simple possibilities for connection and attracting appearance. Due to these advantages, they are widely used in a large range of applications, including bridges, lattice masts, trusses and buildings with large openings. The simplest RHS joint configuration, a T joint, is shown in FIGURE 1.

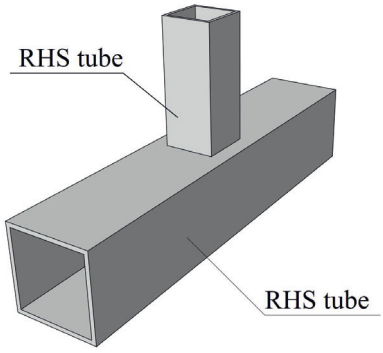

FIGURE 1. RHS T joint.

The first empirical equations for the resistance of RHS joints were proposed in 1970s by Eastwood & Wood (1971) and Davie & Giddings (1971). The equations were further developed in (Brockenbrough 1972; Korol et al. 1977; Kanatani et al. 1981). A comprehensive research on tubular joints was conducted by Wardenier (1982), who proposed the design approach based on the classical yield line theory of Johansen (1962). Currently, Wardenier's equations are employed in the failure mode approach realized in many design standards,

such as EN 1993-1-8:2005 (CEN 2005b), ISO 14346:2013 (IIW 2013) and CIDECT Design Guide No.3 (Packer et al. 2009).

The equations of Wardenier served as the basis for further investigations on RHS joints. Szlendak (1991) and Packer (1993) considered the design of RHS connections under in-plane bending moment. Yu (1997) conducted a comprehensive research for multiplanar RHS T and X joints. Lu et al. (1994) proposed the so-called $3\%b_0$ deformation limit to determine the resistance of joints with no peak loads in their load-deformation curves, limiting the deformations of joints in some specific cases. Later Zhao (2000) extended this limit to find the resistance of RHS joints with other failure modes.

However, the recent invention of new types of connections, e.g. bird-beak joints (Christitsas et al. 2007) or hybrid-column joints (Sadeghi et al. 2017), have shown that the current failure mode approach has a limited validity range and cannot serve as a universal design method for all RHS joints. In addition, the traditional approach does not allow to calculate the initial stiffness of joints. These problems can be solved by the component method.

1.1.2 Component method

The component method was originally proposed by Zoetemeijer (1974) for bolted beam-to-column connections and developed by Tschemmernegg et al. (1987). Later it was extended to column bases by Wald (1995) and Jaspart & Vandegans (1998). Grotmann & Sedlacek (1998) applied the component method to calculate the initial rotational stiffness of RHS T joints. In addition, the component method was also extended to steel joints subjected to fire (Leston-Jones 1997; Simões da Silva et al. 2001; Taib & Burgess 2011; Block et al. 2007), impact loading (Ribeiro et al. 2015; D'Antimo et al. 2018) and blast loading (Fang et al. 2013; Stoddart et al. 2013; Yim & Krauthammer 2012). For composite structures, it was used in (Haremza et al. 2016; Pitrakkos & Tizani 2015; Kozlowski 2016; Hoang et al. 2015; Demonceau & Jaspart 2004; Bučmys et al. 2018). The component method for joints under arbitrary loading was developed by Da Silva (2008). For bolted end-plate connections the method was used by Girão Coelho & Bijlaard (2007), Heinisuo et al. (2012) and Thai & Uy (2016). Perttola (2017) proposed a rakes-based component method for end-plate joints under arbitrary loading. Currently, the component method is implemented to EN 1993-1-8:2005 for joints connecting H or I sections.

For hollow section joints, the method was first proposed by Weynand & Jaspart (2001). The main concepts of the component method for RHS joints have been developed in the CIDECT projects 5BP (Jaspart et al. 2005) and 16F (Weynand et al. 2015). These documents develop a component model for tubular joints, identify potential components and provide equations for their resistance and stiffness. The documents are supported by detailed examples and guidelines. Although the authors present clear design rules for resistance, the equations for initial stiffness are not so straightforward and remain questionable.

1.1.3 Initial stiffness

The current design rules for tubular joints, such as EN 1993-1-8:2005 (CEN 2005b) and CIDECT Design Guide No. 3 (Packer et al. 2009), are based on the failure mode approach and allow calculating their design resistance, providing however no information for initial stiffness. At the same time, it has been shown that significant cost savings can be achieved by considering the initial rotational stiffness of semi-rigid joints, both in sway frames (Simões 1996; Grierson & Xu 1993) and in non-sway frames (Bzdawka 2012). In addition, many researchers (Boel 2010; Snijder et al. 2011; Haakana 2014) demonstrated that initial rotational stiffness plays the key role in the buckling of tubular truss members. In addition, axial stiffness plays a very important role in the design of shallow Vierendeel girders (Korol et al. 1977).

Many publications on tubular joints investigate the behavior of tubular joints under in-plane bending moment (Tabuchi et al. 1984; Szlendak 1991; Packer 1993; Yu 1997) and axial loading (Feng & Young 2008; Feng & Young 2010; Pandey & Young 2018; Zhao & Hancock 1991; Nizer et al. 2016; Becque & Wilkinson 2017; Davies & Crockett 1996). However, very few of them investigate initial stiffness. Mäkeläinen et al. (1988) presented a theoretical approach for the initial stiffness of CHS T joints. An extensive parametric study of axially loaded joints was conducted in (de Matos et al. 2015a), but no theoretical equation was proposed for their initial stiffness. Some equations for initial rotational stiffness of CHS joints were presented in (Wardenier 1982) and validated in (Boel 2010).

A considerable step forward in this issue was made by the invention of the component method, which allowed to compute the stiffness of the joint, decomposing it into simple components. Grotmann & Sedlacek (1998) presented the theoretical approach based on the component method for the rotational stiffness of RHS T joints. As a unified approach for all tubular joints, the component method was proposed in (Weynand & Jaspart 2001). The axial stiffness of a RHS-to-IPE web was presented in (Silva et al. 2003) and accepted later by CIDECT as the stiffness of the component “chord face in bending”. An alternative equation for the stiffness of this component was developed in (Málaga-Chuquitaype & Elghazouli 2010). The stiffness of the component “chord side walls in compression” was investigated in the doctoral thesis of Jaspart (1991) and later by López-Colina et al. (2011). An outstanding research on the component method in relation to RHS joints was conducted in the CIDECT reports 5BP (Jaspart et al. 2005) and 16F (Weynand et al. 2015). Although the documents developed a detailed design procedure for resistance, the initial stiffness of tubular joints is covered insufficiently. In addition, in contrast to resistance, the design rules for initial stiffness were validated with the very limited amount of experimental data and many uncertainties remain regarding their applicability and limitations.

As a rule, in addition to the brace loading, tubular joints are also loaded by an axial force and a bending moment in the chord. Such loading produces additional axial stresses in the chord, considerably affecting the structural behavior of joints. Originally this phenomenon was investigated by Wardenier (1982), who proposed a so-called chord stress function to consider the influence of axial stresses on the resistance of tubular joints. Later considerable research has been conducted on this issue and new chord stress functions were proposed in (Wardenier et al. 2007b) for RHS K gap joints and in (Liu et al. 2004; Wardenier et al. 2007a) for RHS X and T joints. Some recent studies have been published for RHS joints in (Nizer et al. 2016) and CHS joints in (Lipp

& Ummenhofer 2015). Currently, the chord stress functions are available for the resistance of joints in many design standards (CEN 2005b; IIW 2013; Packer et al. 2009) and handbooks (Ongelin & Valkonen 2016). At the same time, no such function exists for the initial stiffness of joints, neither axial nor rotational. The influence of chord axial loading on the stiffness of RHS joints was investigated in (de Matos et al. 2010); however, no chord stress function was developed.

1.1.4 Issues of high strength steels

The developments in manufacturing processes and material technologies increased the strength of steels available in the building market (Raoul 2005). As the strength of connected members becomes greater, the resistance of joints also increases, reducing the material consumption, the amount of welding works and the CO_2 emissions. However, the current design rules for tubular joints have been mostly developed and validated for regular steels and very limited research has been conducted for high strength steels. Generally, regular steels include the steel grades with $f_y \leq 355$ MPa, although Eurocodes from 1993-1-1 to EN 1993-1-11 specify the design rules for the steel grades with $f_y \leq 460$ MPa, where f_y denotes the nominal yield stress of the steel. EN 1993-1-12:2007 (CEN 2007) defines high strength steel as 460 MPa $< f_y \leq 700$ MPa.

Currently, the design of HSS tubular joints is regulated by the same Eurocode that is used for the joints made of regular steels, i.e. EN 1993-1-8:2005 (CEN 2005b). However, it specifies the additional coefficients (reduction factors) that reduce the resistance of HSS joints. In particular, clause 7.1.1(4) of EN 1993-1-8:2005 specifies the factor 0.9 for the design resistances of tubular joints if a nominal yield strength of their members exceeds 355 MPa. In addition, clause 2.8 of EN 1993-1-12:2007 (CEN 2007) presents the reduction factor 0.8 for steel grades greater than S460 up to S700. Identical requirements can be found in CIDECT Design Guide No.3 (Packer et al. 2009). For some joints, these factors lead to very conservative design and do not allow to obtain all benefits from using high strength steels. To maximize the usage of high strength steels in the construction industry, the reduction factors must be further clarified and specified.

According to (Zhao et al. 2014) and CIDECT Design Guide No.3 (Packer et al. 2009), the need for the reduction can be explained by the relatively larger deformations that take place in joints with nominal yield strengths of approximately 450 to 460 MPa, when the plastification of the connecting RHS face occurs. According to (Jiao et al. 2015; Pirinen 2013), the reduction can be caused by the softening of HAZ. Javidan et al. (2016) have shown that welding stresses can reduce the tensile strength of HSS tubes by 8%. Dunđer et al. (2007) presented the $t_{8/5}$ cooling time-hardness relationship for the HAZ softening of S420 steel, proving the influence of weld-heat input on the behavior of HSS joints. Nevertheless, no reduction due to the softening of HAZ is included in EN 1993-1-8:2005 and EN 1993-1-12:2007. To avoid this omission, corresponding reduction factors have been added to some National Annexes, e.g. the Finnish one (Ministry of Environment, 2017), which reduces the yield strength of steel with the coefficients 1.0 for S500, 0.85 for S700 with a linear interpolation between them. However, these reduction factors do not apply to clause 2.8/7.1.1(4) of EN 1993-1-12:2007, meaning that the discussed reduction factors (0.8 and 0.9) have another nature.

A broad discussion on the relevance of the reduction coefficients is provided in (Feldmann et al. 2016). Based on 100 tests on axially loaded HSS RHS joints, the document justified smaller reduction: the factor 0.9 for S700 and no reduction for S500. Having analyzed 23 RHS X joints, Björk & Saastamoinen (2012) showed that there is no need in the reduction factor of 0.9 for joints made of S420 grade. In any case, this issue remains open and requires considerable experimental research.

Another problem of HSS joints is the high cost of welding. This issue becomes particularly important for full-strength fillet welds, which are characterized by very large sizes. According to EN 1993-1-8:2005 (CEN 2005b) and (Ongelin & Valkonen 2016), the throat thickness of full-strength fillet welds can be significant: $1.48t_1$ for S420, $1.61t_1$ for S500 and $1.65t_1$ mm for S700. Taking into account the high costs of welding, such large welds considerably raise the cost of the welding process in HSS joints. However, some investigations show that the throat thicknesses of full-strength welds can be considerably reduced. In particular, Feldmann et al. (2016) demonstrated that for axially loaded RHS T joints the thicknesses can be reduced to $1.0t_1$ for S500, $1.2t_1$ for S700 and $1.4t_1$ for S960. Björk & Saastamoinen (2012) showed that the throat thickness of $1.11t_1$ can be used instead of $1.48t_1$ for RHS X joints made of S420.

The described issues state that the applicability and competitiveness of HSS tubular joints is challenged by the reduction coefficients and the very strict requirements regarding the thickness of welds. These obstacles complicate the active implementation of high strength steels into the modern building market; therefore, additional studies have to be conducted to overcome the mentioned challenges.

1.1.5 Initial imperfections

Finite element modeling represents a very effective tool in the analysis of tubular joints. To provide most reliable results, numerical simulations are carried out in such a way as to most accurately repeat the real behavior of structures. The current rules for FE modeling (CEN 2006b) oblige scientists and engineers to construct their numerical models considering initial imperfections. However, not all joints are sensitive to initial imperfections. Often consideration of initial imperfections brings no reasonable improvements in the accuracy of results, but severely complicates numerical simulations. In such cases, the influence of imperfections can be effectively replaced by a simple theoretical equation or neglected entirely.

Tubular welded joints are generally influenced by three types of imperfections:

- initial geometrical imperfections,
- welding residual stresses,
- residual stresses that occur from the cold-forming process (only for cold-formed members).

The latter have been studied in (Dubina et al. 2012; Jiao & Zhao 2003; Feldmann et al. 2016) and demonstrated a negligibly small influence on the behavior of tubular members. However, very little research has been conducted for the first two.

Although welding enables fast and simple connection of sections, it represents a complex thermomechanical process, which requires very high temperatures. When a welded joint is cooled to room temperature, the occurring shrinkage of the material leads to huge residual stresses in the welded zone. These stresses should be thoroughly investigated to ensure that they have no negative effect on the structural properties of tubular joints.

Many papers experimentally evaluate residual stresses in simple welded connections. Chen et al. (2017) have shown that residual stresses can lead to the reduction of tensile strength for butt-welded plates by 10%. Some authors came to the conclusion that the reduction of tensile strength of HSS butt joints can reach 3-8% (Hochhauser et al. 2012), and even 15% (Khurshid et al. 2015). In other publications, welding stresses are investigated numerically. Currently there are various programs for FE modeling and simulation of welding processes, including Abaqus (Teng et al. 2001), SYSWELD (Bate et al. 2009), Simufact Welding (Islam et al. 2014), Virfac (Majumdar & D'Alvise 2014) and many others. Günther et al. (2012) numerically and experimentally investigated the ultimate load and the behavior of longitudinal fillet welds in lap joints. Detailed recommendations for the FE simulation of residual stresses in welds are provided in (Knoedel et al. 2017).

However, very few publications evaluate welding residual stresses in relation to hollow section joints. Brar & Singh (2014) have shown a possibility to increase the tensile strength of tubular X joints by 24% by changing welding input parameters and reducing residual stresses in HAZ. A sophisticated study of residual stresses in SHS T joints has been carried out by Moradi Eshkafti (2017). The author concludes that the load-bearing capacity of joints can differ by 10% depending on the welding sequence. At the same time, the direct comparison of structural properties considering and neglecting welding residual stresses has not been conducted.

Another type of imperfection that requires consideration is initial geometrical imperfections. These imperfections occur during the manufacturing process, transportation and the construction process itself. Usually, geometrical imperfections are modelled using the common approach described in Appendix C.5 of EN 1993-1-5:2006 (CEN 2006b). It represents the simulation of equivalent imperfections, when buckling modes are obtained from a linear buckling analysis and implemented to a model with perfect geometry. Although the resulting distribution of imperfections represents a rather simplified pattern, this approach is widely used for thin-walled structures (Schafer & Peköz 1998; Nazmeeva & Vatin 2016).

The required magnitudes of local imperfections for RHS tubes can be found in the design rules. In particular, Appendix C.5 of EN 1993-1-5:2006 specifies local imperfections equal to $b_0/200$ and $h_0/200$. The same amplitudes are used in many publications (Hoang et al. 2014; Pavlovčič et al. 2007). Another value can be found in EN 10219-2:2006 (CEN 2006a), which limits the concavity and convexity of cold-formed RHS tubes by 0.8% with a minimum of 0.5 mm. This corresponds to the values of $b_0/125$ and $h_0/125$. The same limit can be found in (Ongelin & Valkonen 2016). It has been shown experimentally that real imperfections generally do not exceed these amplitudes (Hayeck et al. 2017; Ellobody & Young 2005; Jiao & Zhao 2003). Therefore, the latter can be effectively used as the most conservative limitation for modeling geometrical imperfections in RHS members and their joints.

1.1.6 Surrogate modeling

Many tasks dealing with the optimization of tubular structures require effective methods to calculate the structural properties of tubular joints. More to the point, these methods should be sufficiently fast to make the optimization procedure meaningful. Generally, analytical solutions provide the best option, since they can be easily programmed in the optimization software. However, for some tasks analytical solutions do not exist or are extremely complicated, requiring other methods to be employed. The solution can be found in surrogate modeling.

A surrogate model, also known as metamodel, represents an approximation of the Input/Output function that is employed by the developed simulation model (Kleijnen 2009). Generally, surrogate models are fitted to the data produced by an experiment or a simulation model and replace computationally expensive analytical solutions. Surrogate modeling is actively used in many engineering fields, including aerospace (Queipo et al. 2005) and structural (Roux et al. 1998) applications. In civil engineering, surrogate models have been employed in the design of semi-rigid steel connections (Jadid & Fairbairn 1996; de Lima et al. 2005; Guzelbey et al. 2006; Stavroulakis et al. 1997). Díaz et al. (2012) demonstrated the effectiveness of surrogate models for the optimum design of steel frames with semi-rigid joints.

The optimization of tubular trusses often requires extensive calculations of the initial rotational stiffness of the joints comprising these trusses (Bel Hadj Ali et al. 2009). Although there is a simple theoretical solution for the initial rotational stiffness of T joints (Grotmann & Sedlacek 1998), no such solution exists for Y joints. The finite element method can be employed for this purpose; however, it requires considerable efforts to develop a FE model for each joint, calculate it and extract the required outcome. Obviously, this method cannot be directly used in the optimization tasks that require thousands evaluations to be calculated extremely quickly. For such tasks, metamodeling can serve as the only possible method.

1.1.7 Discussion

The conducted literature review has shown that the component method has been actively applied for a wide variety of connections. The method has proved itself for its simplicity, clarity and versatility. Considerable research has been conducted on the expansion of the method to welded tubular joints. Although a clear and reliable procedure has been developed for the design resistance of tubular joints, the major concern of the method relate to the calculation of initial stiffness. Additional studies are required to check the equations for the stiffness of the components. In case of unsatisfactory results, new equations should be developed and experimentally verified. Another concern of the method is the influence of chord axial stresses on the behavior of joints. Although a number of chord stress functions exist to incorporate this effect to the resistance of tubular joints, very few publications investigate this issue in relation to initial stiffness.

In addition, attention should be paid on other issues of tubular joints that are common for both the traditional approach and the developed component method. The first issue is the design of tubular joints made of high strength steels. The current design rules apply the same approach for the design of HSS joints but specify the

additional reduction factors for the yield strength of connected members. These factors considerably reduce the design resistance of joints, making questionable the implementation of stronger steels in the construction industry. At the same, some experimental investigations on this topic have shown that in many cases joints demonstrate sufficient load-bearing capacity without the reduction factors or, at least, with "less strict" ones. Definitely, these observations cannot be extended for the whole range of joints and loading cases, but they prove that this issue demands significant additional studies supported with extensive experimental results.

The second issue to be considered is the influence of initial imperfections, such as geometrical imperfections and welding residual stresses. The current rules ignore imperfections in the design of welded tubular joints. To ensure that such disregard does not lead to unsafe results, some investigations should be conducted in this field. Moreover, very little research has been conducted to the influence of welds on the behavior of joints.

Some attention should be also paid on the practical aspects of the design. To enable extensive optimization procedures for tubular structures, fast and reliable methods should be developed to facilitate the design of connections. One method that has proved its reliability in civil engineering is surrogate modeling. However, very few surrogate models have been developed for the design of tubular joints.

1.2 Scope and aims of the thesis

The aim of this study is to present a fully consistent approach for the design of RHS T joints, including their resistance and initial stiffness. For this purpose, the thesis employs the component method, which has already proved its efficiency for many types of connections and loading cases. The thesis goes in line with the research conducted recently in this field, i.e. CIDECT projects 5BP (Jaspart et al. 2005) and 16F (Weynand et al. 2015), which made the first step in the extension of the component method to tubular joints. The thesis identifies and solves the most challenging issues of the component method in relation to RHS T joints. The following research tasks are going to be addressed in this doctoral thesis:

1. Develop a component model for RHS T joints under arbitrary loading and validate it against experimental data (Article I).
2. Develop a theoretical approach for the initial stiffness of RHS T joints under in-plane bending and axial brace loading (Articles II and VIII).
3. Determine the relevance of the reduction factors for the resistance of HSS RHS T joints (Article III).
4. Determine the influence of initial imperfections, such as welding residual stresses and geometrical imperfections, on the structural behavior of RHS T joints (Articles IV, V and VI).
5. Determine the influence of fillet welds on the structural behavior of RHS T joints (Article VII).
6. Develop a surrogate model for the initial rotational stiffness of RHS joints (Article VII).

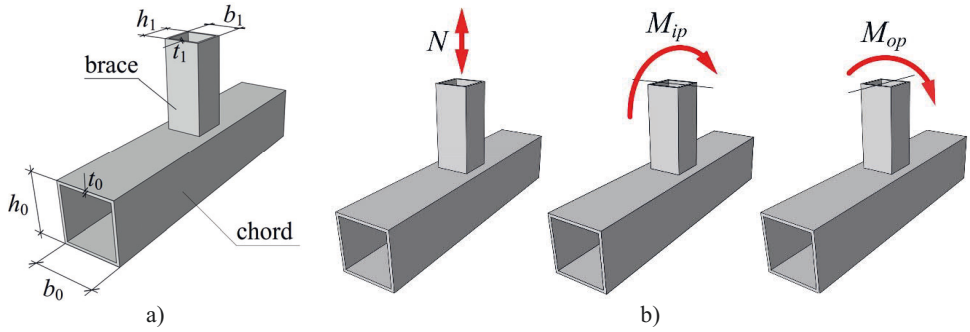

FIGURE 2. RHS T joint: a) notations; b) loading cases.

By these means, a unified validated and verified theory can be developed for the structural analysis of HSS RHS T joints, taking into account their resistance, stiffness and ductility in arbitrary loading cases, as well as the effects of residual stresses and initial imperfections. A T joint represents the simplest joint configuration, when a brace is welded to a chord at an angle of 90°, as shown in FIGURE 2a. The thesis considers only the joints that meet the requirements of EN 1993-1-8:2005 (CEN 2005b), implying the restrictions provided in TABLE 1. The joints are assumed to be comprised of cold-formed or hot-rolled sections, with the steel grades from S355 to S700. The joints are investigated under static arbitrary loading, which includes axial brace loading N, in-plane bending M_{ip} and out-of-plane bending M_{op}, as shown in FIGURE 2b.

TABLE 1. Eurocode limitations for RHS T joints.

Brace width	$0.25 \leq \beta \leq 1.0$
Section wall thickness	$10 \leq 2\gamma \leq 35$
Section aspect ratio	$0.5 \leq b_i/h_i \leq 2.0$, $i = 0; 1$
Cross-section class	1; 2

Some parts of the thesis consider other types of RHS joints, such as X and Y joints. An X joint represents a joint with two braces welded to a chord at an angle of 90°, as shown in FIGURE 3a. The study considers only X joints with equal braces, i.e. equal-brace X joints. A Y joint represents a joint with a brace welded to a chord at an arbitrary angle φ, as demonstrated.in FIGURE 3b. Generally, the angle φ is restricted to $30° \leq \varphi \leq 90°$, for the purposes of welding and symmetry. From that point of view, T joints can be considered as a particular case of Y joints with an angle of 90°.

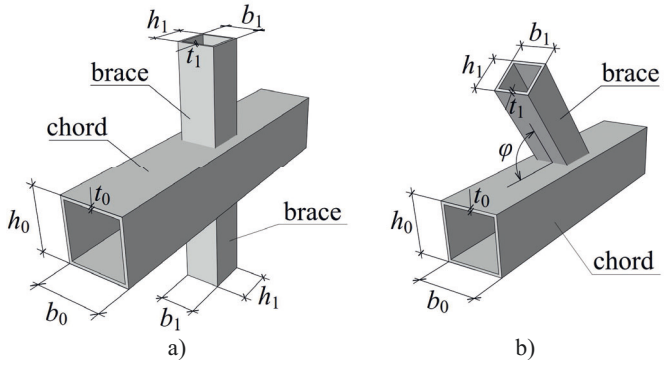

FIGURE 3. Other types of RHS joints: a) equal-brace X joint; b) Y joint.

2 Discussion

2.1 Component method for RHS T joints

This thesis investigates the structural behavior of RHS T joints employing the widely known component method. The basic concept of the component method represents the joint by means of basic elements (components) and calculates the behavior of the joint combining the resistances and stiffnesses of the introduced components. Due to its generic nature, the method can be applied to a wide variety of joints, including tubular joints. The method effectively correlates with the existing design methods, e.g., for tubular joints it employs the existing equations from the failure mode approach realized in the current Eurocode. One of the main advantages of the component method is the possibility to calculate the initial stiffness of joints, which is unavailable for tubular joints in the current Eurocode.

Article I applies the component method for RHS T joints considering three loading cases: axial loading, in-plane bending and out-of-plane bending. The paper is based on the CIDECT project 16F (Weynand et al. 2015), hereinafter in this section – CIDECT, which specified the method to tubular joints. This section shortly presents the main concept of the component method in relation to RHS T joints and discusses its main issues, which are solved in the further sections. The component method-based design rules for RHS T joints are collected in Section 2.10.

The component method models the joints by means of the combination of springs and gradually simplifies the model so that it can be effectively used in the design. In the first approximation, the component method assumes the load to be transferred from the brace to the chord through four loading zones located in the corners of the brace, as demonstrated in FIGURE 4a. This assumption can be justified by Wardenier (1982), who demonstrated a non-uniform distribution of elastic stresses along the cross-section of the brace, with considerable stress concentrations in its corners.

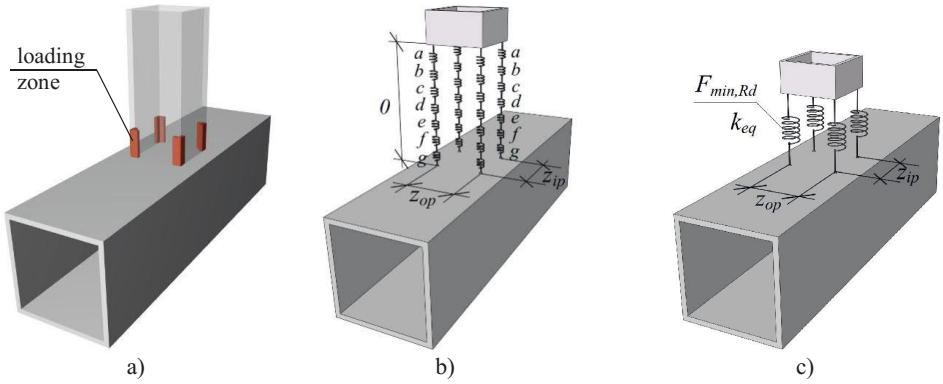

FIGURE 4. Local model for RHS T joint: a) loading zones, b) component model; c) simplified component model.

On the second step, every loading zone is replaced by a system of linear springs, as illustrated in FIGURE 4b. The springs correspond to the following components:

a) chord face in bending,
b) chord side walls in tension / compression,
c) chord side walls in shear,
d) chord face under punching shear,
e) brace flange / webs in tension / compression,
f) chord section in distortion,
g) welds.

The components from *a* to *f* were proposed by CIDECT. **Article I** proposes welds as a new independent component, based on the need to check weld resistance in case of undersized welds (welds smaller than full-strength welds). In addition, welds have been already proposed as a component in the previous CIDECT report (Jaspart et al. 2005) but have been excluded from the list of the components later. The distances between the springs along the face of the chord, i.e. lever arms, are calculated as

$$\begin{aligned} z_{ip} &= h_1 - t_1 \\ z_{op} &= b_1 - t_1 \end{aligned} \tag{1}$$

Each spring (component) has its own resistance $F_{i,Rd}$ and stiffness k_i, which are derived from mechanics. It should be noted that the resistance and stiffness of the components should differ for the three loading cases given above. For example, the component *a* has its individual resistances under axial loading, in-plane bending and out-of-plane bending denoted respectively as $F_{a,N,Rd}$, $F_{a,Mip,Rd}$ and $F_{a,Mop,Rd}$.

Further, the serially connected springs in every corner of the brace can be replaced by equivalent springs, which are characterized by equivalent resistance $F_{min,Rd}$ and stiffness k_{eq}. Such simplified model is shown in FIGURE 4c. The resistance of the equivalent springs is found as the minimum resistance among all the considered springs:

$$
\begin{aligned}
F_{N,\min,Rd} &= \min\left[F_{a,N,Rd},\ldots,F_{g,N,Rd}\right] \\
F_{Mip,\min,Rd} &= \min\left[F_{a,Mip,Rd},\ldots,F_{g,Mip,Rd}\right] \\
F_{Mop,\min,Rd} &= \min\left[F_{a,Mop,Rd},\ldots,F_{g,Mop,Rd}\right]
\end{aligned}
\tag{2}
$$

The stiffness of the equivalent springs can be calculated as the stiffness of serially connected springs:

$$
k_{eq,N} = \frac{1}{\sum_{i=a}^{i=g}\frac{1}{k_{i,N}}};\quad k_{eq,Mip} = \frac{1}{\sum_{i=a}^{i=g}\frac{1}{k_{i,Mip}}};\quad k_{eq,Mop} = \frac{1}{\sum_{i=a}^{i=g}\frac{1}{k_{i,Mop}}}
\tag{3}
$$

Very often, the resistance of some components under particular loading case can be very large in relation to the remaining components. In such cases, it is highly unlikely that these components can have the minimum resistance in Eq. (2), i.e. serve as a limiting component. To simplify the design, the list of the components can be shortened to include only "active" components, i.e. those that can be potentially considered as critical due to their relatively small resistance. Oppositely, "inactive" components are unlikely to be critical for the given loading type and do not have to be considered in Eq. (2). Similarly, some components may have extremely high stiffness in comparison to others, i.e. infinite stiffness; therefore, they do not considerably contribute to the stiffness of the equivalent strings. For this reason, they can be also considered as "inactive" and excluded from the further design. It should be noted that active and inactive components are different for resistance and stiffness. For example, the component *b* (chord side walls in compression / tension) is never critical (inactive) for joints with $\beta \leq 0.85$; however, it still contributes (active) to initial stiffness.

Finally, the RHS joint can be modelled by one linear and two rotational springs, which respectively represent its structural behavior under axial loading, in-plane bending and out-of-plane bending. In total, these springs form the local design model of the RHS T joint, which is illustrated in FIGURE 5. This local joint model can be used in the global frame analysis. The resistance and stiffness of these springs represent the resistance and initial stiffness of the joint under the considered loading types. They are computed by combining the corresponding values of the equivalent springs. In particular, the resistances are found as

$$
\begin{aligned}
N_{Rd} &= 4F_{N,\min,Rd} \\
M_{ip,Rd} &= 2F_{Mip,\min,Rd}\cdot z_{ip} \\
M_{op,Rd} &= 2F_{Mop,\min,Rd}\cdot z_{op}
\end{aligned}
\tag{4}
$$

The stiffnesses of the joint are calculated as

$$
\begin{aligned}
C_{j,ini,N} &= 4Ek_{eq,N} \\
S_{j,ini,ip} &= 2Eh_1^2 k_{eq,ip} \\
S_{j,ini,op} &= 2Eb_1^2 k_{eq,op}
\end{aligned}
\tag{5}
$$

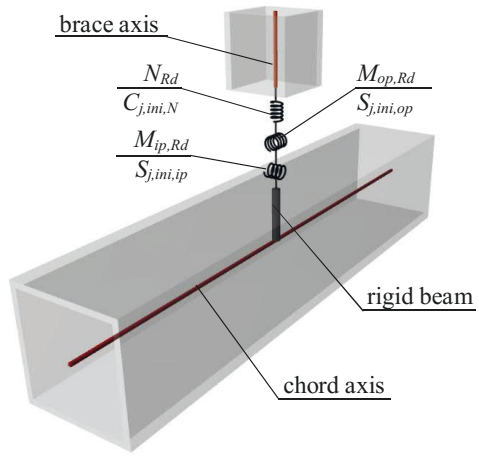

FIGURE 5. Local design model for RHS T joint.

This study assumes that the three loading cases do not interact and the behavior of the springs can be defined separately, as demonstrated in (Boel 2010; Haakana 2014). If the joint is subjected to combined bending and axial force, its resistance can be checked using the linear relationship, specified by Wardenier (1982) and EN 1993-1-8:2005 (CEN 2005b):

$$\frac{N_{Ed}}{N_{Rd}} + \frac{M_{ip,Ed}}{M_{ip,Rd}} + \frac{M_{op,Ed}}{M_{op,Rd}} \leq 1.0 \tag{6}$$

where indices *Ed* and *Rd* correspond to design internal force and design resistance, respectively.

Attention should be paid on the location of the local design model. For open section joints, considerable research on this issue has been conducted in (Sokol et al. 2002; Li et al. 1995; Wu & Chen 1990; Del Savio et al. 2009; da Silva et al. 2004; Bursi & Jaspart 1998), which can be also applied for tubular joints. At the moment, there is no agreement on the position of the local model in tubular joints. EN 1993-1-8:2005 (CEN 2005b) and some references (Rondal et al. 1992; Hornung & Saal 1998; Galambos 1998) position the model at the intersection of the midlines of the connected members. However, this thesis follows the conclusions of (Boel 2010; Snijder et al. 2011; Haakana 2014) and CIDECT, according to which the local model is located on the chord top face and connected with the axis of the chord by a rigid beam.

Another issue that requires attention is the influence of axial stresses in the chord on the structural behavior of tubular joints. For resistance, this effect is considered by the chord stress function presented in EN 1993-1-8:2005, which reduces the resistance of joints with compressive axial stresses. However, a similar effect is also observed for initial stiffness of joints, as can be seen in the following examples. The first evidence can be found in the tests of Zhao & Hancock (1991), who investigated the structural behavior of RHS T joints under a pure brace axial load and under its combination with chord bending. In particular, the behavior of a joint with $\beta = 1.0$ under these two loadings is presented in (Zhao & Hancock 1991, Figure 10a). The joint S1B1C12

is located on the rigid floor; therefore, it experiences no axial stresses in the chord, i.e. it is loaded by pure axial loading. Oppositely, the joint S3B1C12A2 is simply supported at the ends of the chord, which allowes bending of the chord resulted from the brace axial load. The bending of the chord creates axial stresses in the chord, as it is discussed in details in (Packer et al. 2017). The graph shows the local deformations of the joint, i.e. the deformation obtained from the chord bending are subtracted from the total deformation of the specimen. As can be seen, chord axial stresses considerably reduce the initial stiffness of the joint from the very beginning of the loading process. A similar phenomenon is observed also for a joint with $\beta = 0.50$, which is depicted in (Zhao & Hancock 1991, Figure 10b). Similarly, the joint S1B1C23 is located on a rigid floor (pure axial load), while the joints S3B1C23A0.5, S3B1C23A0.75 and S3B1C23A1.5 are simply supported with the spans of 0.5 m, 0.75 and 1.5 m, respectively. A particular reduction of initial stiffness is observed for the case S3B1C23A1.5, as it has the largest span.

Another example can be found in the tests of Nizer et al. (2016), where a simply supported RHS T joint is tested under a brace axial load in the combination with a varying chord axial load. The comparative experimental behavior of the joints is presented in (Nizer et al. 2016, Figure 5). The joints TN01N0 and TN02N0 are loaded with no axial force in the chord. In addition to a brace loading, the joints TN03N50+ and TN04N70+ are loaded with a tensile chord load leading to axial stresses accounting to 50% and 70% from the yield stress, respectively. Similarly, the joints TN05N70- and TN06N50- are loaded with corresponding compressive chord loads. As can be seen, chord axial stresses similarly affect the initial stiffness of the joint.

Another results can be found in (de Matos et al. 2015b), who conduct an extensive FE analysis of RHS T joints loaded by a brace axial load combined with a chord axial loading. According to the presented values of initial stiffness – see Table 6 in (de Matos et al. 2015b) – the stiffness of a joint with a compressed chord can reach only 64% from the stiffness of an identical joint with a chord in tension. Similar results are obtained by the FE analyses conducted for moment-loaded joints in **Article II**. As can be seen in Fig. 6, the initial stiffness of joints considerably differs for the joints with small β, even if $n \leq 1.0$ and no yielding appears in the chord.

The foresaid references clearly show that axial stresses in the chord considerably influence the initial stiffness of joints. It should be noted that this phenomenon is observed in the elastic stage of behavior, i.e. when no yielding is observed in the chord. Such effect can be taken into account by the introduction of a chord stress function, similar to the one that exists for resistance. Taking into account the chord stress functions, Eq. (5) should be modified as

$$\begin{aligned} C_{j,ini,N} &= 4Ek_{eq,N}k_{sn,N} \\ S_{j,ini,ip} &= 2Eh_1^2k_{eq,ip}k_{sn,ip} \\ S_{j,ini,op} &= 2Eb_1^2k_{eq,op}k_{sn,op} \end{aligned} \tag{7}$$

where $k_{sn,N}$, $k_{sn,ip}$ and $k_{sn,op}$ denote the chord stress functions under the corresponding loading type. As can be seen in Eq. (7), the chord stress functions are applied globally to the whole joint. However, this contradicts the general concept of the component method, which requires the functions to be applied to the individual components, as it is done for resistance. At the same time, the existing experimental results only allow to observe

the global influence on initial stiffness but do not allow to trace the components with which it is associated. In case of resistance, the influence of chord axial stresses can be associated with a certain component, since such component is easily determined from the list of all components as the one with the minimum resistance. However, the design of initial stiffness requires all components to contribute to the stiffness of the joint. And the contribution of these components cannot be easily defined. For example, if the component "chord face in bending" governs the behavior of a moment-loaded joint, then the observed chord stress function for resistance is directly connected with this component. However, in the design of its initial stiffness, all three components ("chord face in bending", "chord side walls in tension / compression" and "chord walls in shear") contribute to the stiffness of the joint. For this reason, the chord stress function for initial stiffness cannot be associated to a particular component, although it is clearly observed globally.

As can be seen in Fig. 6 of **Article II**, the influence of chord axial stresses on initial stiffness is particularly pronounced for small β and decreases for greater β. This allows to conclude that the major part of the chord stress function accounts for the component "chord face in bending", which governs the behavior of joints with small β. However, it is not possible to determine the exact "share" of this component. Based on these conclusions, the chord stress functions for initial stiffness are introduced only globally. To be in line with the component method, the functions can be specified in the further research.

The second part of **Article I** verifies the component method with EN 1993-1-8:2005 (CEN 2005b) and validates it with the experimental results available in the literature. The considered examples of the joints under three loading types allow to make the following conclusions:

1. To calculate the resistance of joints, the component method employs the inverted equations from the failure mode approach realized in EN 1993-1-8:2005. For this reason, the method provides exactly the same resistance as EN 1993-1-8:2005, however requires more computations.
2. Employing the Eurocode equations, the component method should follow its limitations in terms of steel properties. EN 1993-1-8:2005 and EN 1993-1-12:2007 specify the reduction factors 0.9 and 0.8 for the joints with a nominal yield strength higher than 355 N/mm^2. To be consistent with the current Eurocode, these reduction factors must be also considered in the design of resistance, as shown in the examples. A detailed discussion on the relevance of these factors is provided in Section 2.6.
3. The major concerns of the component method are related to the design of initial stiffness. The sufficiently accurate initial in-plane rotational stiffness was obtained only using the improved equation for the component *a*. The design of axial stiffness was found to overestimate the experimental stiffness of joints. Moreover, the strict validity requirements for the stiffness of the component *a* allow applying it only for the joints with very small braces. The design of out-of-plane rotational stiffness is not covered at all.

These issues are considered further in this thesis. The final design rules for RHS T joints based on the component method are provided in Section 2.10.

2.2 Resistance of hollow section joints

The behavior of tubular joints is best described by load-deformation curves. However, the direct analysis of these curves represents quite a difficult task; therefore, the behavior of joints is usually evaluated by their structural properties, such as initial stiffness and resistance, which are determined from these curves. Although initial stiffness can be easily extracted from a load-deformation curve, the determination of resistance often represents a challenging issue, which is still under discussion among the scientific community. Based on the existing publications, this section provides a short summary to determine the resistance of RHS T joints. The procedure is considered simultaneously for all the three loading cases analyzed in this thesis, i.e. axial loading, in-plane and out-of-plane bending moments, given the similarities between the load-deformation curves for these loading cases. Currently there are two options to determine the resistance of such joints.

The first method was developed for joints with a noticeable hardening phase and used later in many publications, e.g. (Packer et al. 1980), (Zhao & Hancock 1991) and (Grotmann & Sedlacek 1998). The load-deformation curve for such joints is depicted in FIGURE 6. In the beginning of the loading, the joint demonstrates elastic behavior. This phase is called elastic and characterized by initial stiffness $S_{j,ini}$ ($C_{j,ini}$). As the stresses reach the yield strength of steel, chord face bending starts to develop, followed by a noticeable decline in the slope. Due to a considerable membrane effect, the joint continues to resist the load, and the curve exhibits a clearly observed hardening phase, which is characterized by so-called hardening (membrane) stiffness $S_{j,h}$ ($C_{j,h}$). When the joint cannot resist any more load, it fails by cracking in HAZ, which corresponds to the maximum load M_{max} (N_{max}). Obviously, the maximum load corresponds to very large deformations φ_{max} (δ_{max}); therefore, it cannot be considered as the resistance of the joint. In this regard, the method determines the resistance of the joint as the intersection of two straight lines adjusted to initial and hardening stiffnesses. Such resistance is called plastic resistance M_{pl} (N_{pl}), or yield load. As can be seen, the method is applied mainly for the joints that have a noticeable hardening phase, i.e. governed by chord face failure. Therefore, it cannot be applicable if the hardening phase is negligible.

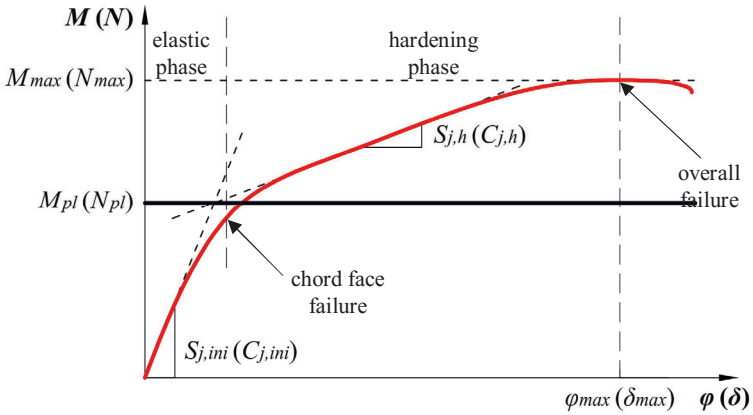

FIGURE 6. Plastic resistance of RHS T joint.

The second method was proposed by Zhao (2000), based on the deformation limit of Lu et al. (1994), which restricts the deformation of tubular joints to $0.03b_0$. The resistance is called ultimate resistance and it depends on the position of the maximum load in relation to the deformation limit. If the maximum load N_{max} corresponds to a deformation larger than $0.03b_0$, the resistance depends on the ratio of the load $N_{3\%b0}$ to the serviceability load $N_{1\%b0}$. If the ratio $N_{3\%b0} / N_{1\%b0}$ is less than 1.5, the ultimate resistance is determined as $N_{3\%b0}$, as shown in FIGURE 7a. If the ratio $N_{3\%b0}/ N_{1\%b0}$ exceeds 1.5, the ultimate resistance is taken as $1.5N_{1\%b0}$, as illustrated in FIGURE 7b. If the joint has a peak load N_{max} at a deformation smaller than $0.03b_0$, the peak load N_{max} is assumed to be the ultimate resistance of the joint, as shown in FIGURE 8. Analytically, this approach can be represented by Eq. (8).

$$N_{ult} = \begin{cases} N_{3\%b0}, & \delta_{max} > 0.03b_0 \bigcup N_{3\%b0} / N_{1\%b0} < 1.5 \\ 1.5N_{1\%b0}, & \delta_{max} > 0.03b_0 \bigcup N_{3\%b0} / N_{1\%b0} > 1.5 \\ N_{max}, & \delta_{max} < 0.03b_0 \end{cases} \tag{8}$$

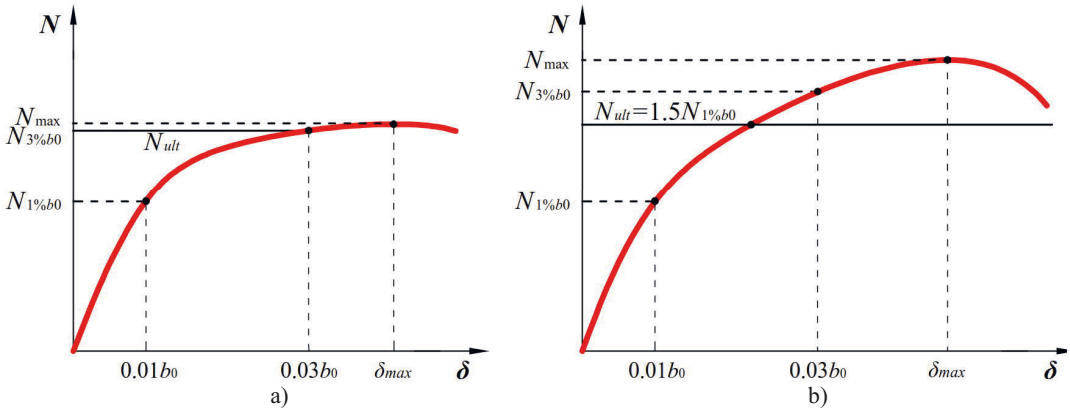

FIGURE 7. Ultimate resistance of RHS T joint, $\delta_{max} > 0.03b_0$: a) $N_{3\%b0} / N_{1\%b0} \leq 1.5$; b) $N_{3\%b0} / N_{1\%b0} > 1.5$.

Although this procedure was developed for axially loaded joints, it can be also extended to joints under in-plane and out-of-plane bending due to the similarities between the load-deformation curves for these loading cases. This method requires no curve-fitting procedure; therefore, it can be employed for any joint, regardless of its hardening phase.

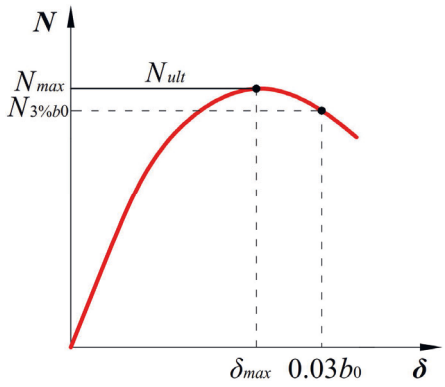

FIGURE 8. Ultimate resistance of RHS T joint, $\delta_{max} < 0.03b_0$.

Currently, the scientific community has no single opinion regarding the most suitable approach to determine the resistance of tubular joints. As plastic resistance obviously corresponds to the initiation of a yielding mechanism in the chord, it should correspond to the ultimate limit state. Oppositely, the second approach was developed based on the serviceability limit state, restricting the deformation of the joint to 3% of the chord. Since the thesis primarily investigates the ultimate limit state of tubular joints, it employs plastic resistance to calculate the strength of tubular joints. The comparison of the discussed two approaches in (Garifullin 2018) demonstrates that plastic resistance leads to 10-20% lower resistance than ultimate resistance. This allows to ensure that the application of plastic resistance does not result in unsafe results. If plastic resistance cannot be determined due to an inconsiderable hardening phase in a curve, the thesis employs the second approach.

2.3 FE model for RHS T joints

This thesis actively employs the FE analysis in the design of tubular joints. This section shortly describes the used FE model for RHS T joints under two loading cases, such as axial loading and in-plane bending moment. The model was constructed using the general-purpose FE software Abaqus/Standard (Abaqus 2012). To exclude a possible effect of the chord end conditions, the length of the chord was selected as $6b_0$ (van der Vegte & Makino 2010), while the brace length was chosen as $4b_1$. According to (van der Vegte et al. 2010), the model was constructed using quadratic solid finite elements with reduced integration (C3D20R), with two elements in the thickness direction. Material properties were modelled either using true stress-strain curves obtained from tensile coupon tests or employing one of the simplified models proposed in Appendix C.6 of EN 1993-1-5:2006 (CEN 2006b). FIGURE 9a depicts the FE model constructed following the provided recommendations.

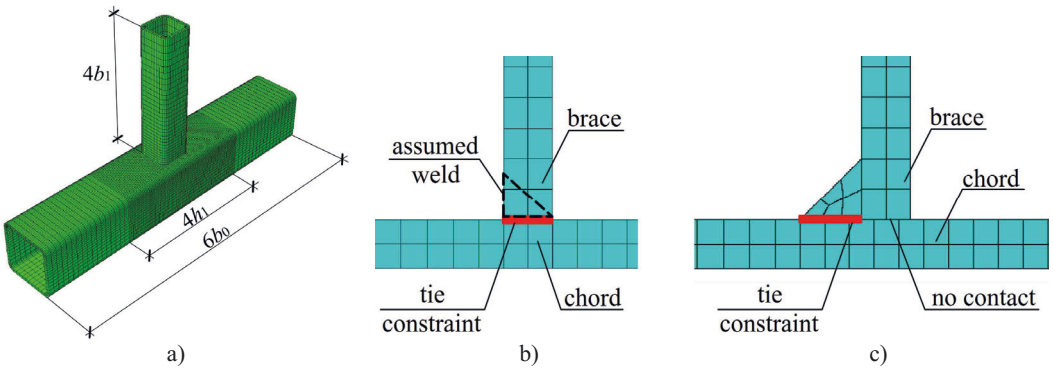

FIGURE 9. FE model: a) meshing; b) butt welds modeling; c) fillet welds modeling.

Particular attention was paid to the modelling of welds. Butt welds were modelled as the base material of the brace, as shown in FIGURE 9b. The contact between the connected members was modelled using the tie constraint, which ties two surfaces together such that there is no relative motion between them. This tool is used by many researchers (Heinisuo et al. 2014; AlHendi & Celikag 2015; Haakana 2014) and it allows to use independent meshes for the connected members without matching their nodes, thus considerably reducing the labor intensity of the modelling process. Fillet welds were modelled as a part of the brace, as shown in FIGURE 9c. The contact between the weld and the chord was modelled with the tie constraint; however, no interaction was introduced between the chord and the brace itself. Strictly speaking, the latter should be modelled with the contact interaction to avoid possible penetration of brace nodes into the chord resulting from compressive loads (Tuominen et al. 2018). However, it has been shown in **Article IV** that the penetration takes place only at very large deformations and does not influence the results in the practical range of interest. It should be noted that when the chord and the brace are of equal width ($\beta = 1.0$), fillet welds parallel to the chord axis cannot be performed and are replaced by partial/full penetration butt welds.

Loading was performed with a force-controlled nonlinear static analysis. The load was applied by a concentrated in-plane moment M or an axial force N to the reference point connected rigidly with the end of the brace. If the joint is simply supported on its ends, the axial force N in the brace causes in-plane bending of the chord, producing additional axial stresses on its faces. These stresses affect the structural behaviour of tubular joints, reducing their resistance (Packer et al. 2017). To consider the behaviour of joints under pure axial load, this effect should be eliminated by several possible approaches. The most reliable one employs a contact interaction with a "rigid floor" modelled with extremely stiff elements, as shown in FIGURE 10a. Although this method is the most accurate, it is computationally very demanding. The second approach introduces constraints against vertical displacements along the length of the chord, as shown in FIGURE 10b. This technique is rather simple but it allows no disconnection between the contacted surfaces during the loading process. For this reason, it slightly overestimates the stiffness of the model. The third method applies compensating moments $M_0 = 0.25N(L_0 - h_1)$ at the ends of the chord, resulting to zero bending moment in the area of connection (Packer et al. 2017), as shown in FIGURE 10c. In the thesis, this method was found to provide excessive

stiffness of joints compared to the first two. Based on the presented comparison, the thesis employed the second approach (FIGURE 10b), as the one that provides accurate results with relatively simple modeling.

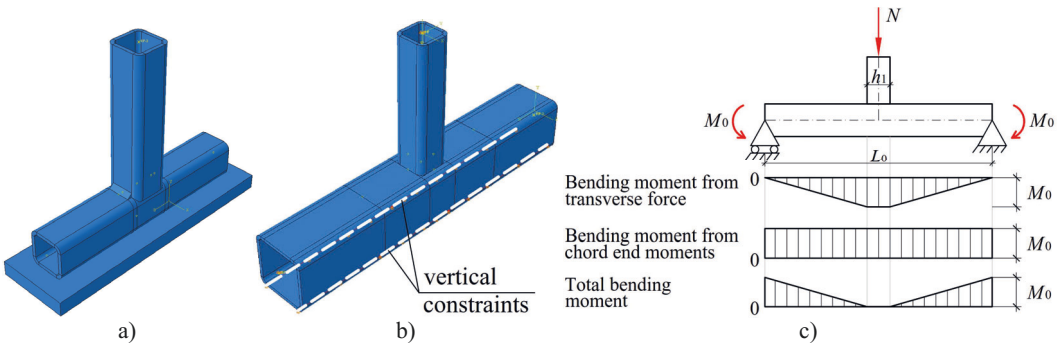

FIGURE 10. Possibilities to eliminate chord bending: a) contact interaction with "rigid floor"; b) vertical constraints; b) compensating moments.

To analyze the local behavior of the joint, its local deformations are extracted from the results of the FE analysis. For moment-loaded joints, this procedure is described in **Article III**, for other loading cases it is performed similarly. The constructed model was used as for the joints that are governed by chord face failure ($\beta \leq 0.85$), as well as for those that fail from chord side walls buckling ($\beta > 0.85$). The model was actively employed to develop the initial stiffness of joints with the corresponding chord stress functions (**Articles II** and **VIII**). Numerical simulations were also conducted for studying initial geometrical imperfections (**Article VI**) and the influence of fillet welds (**Article VII**). A similar model with some required adjustments was also used to investigate welding residual stresses (**Articles IV** and **V**). In addition, extensive FE analyses were used to calculate the responses of the sample points in the surrogate modeling (**Article VII**).

2.4 Initial in-plane rotational stiffness

Article II finds a theoretical solution for the initial rotational stiffness of tubular joints under in-plane bending. As a starting point, the paper evaluates the existing approach, which is based on the component method and presented by CIDECT (Weynand et al. 2015). According to the report, only three components contribute to the initial rotational stiffness of RHS T joints:

- Chord face in bending (component *a*),
- Chord side walls in compression (component *b*),
- Chord side walls in shear (component *c*).

The stiffness of the remaining components is assumed to be infinite and does not affect the stiffness of the joint. Therefore, the stiffness of the joint $S_{j,ini}$ can be presented as:

$$S_{j,ini} = \frac{Eh_1^2}{\frac{2}{k_a} + \frac{2}{k_b} + \frac{1}{k_c}} = Eh_1^2 \frac{k_a k_b k_c}{2k_b k_c + 2k_a k_c + k_a k_b} \tag{9}$$

where k_a, k_b and k_c denote the stiffnesses of the corresponding components. In Eq. (9), the components k_a and k_b are counted twice, since they are considered independently for the compressive and tensile parts of the joint. Generally, k_a limits the behavior of joints with $\beta \leq 0.85$, being considerably smaller than the stiffness of the remaining components:

$$k_a < 0.1k_b; \quad k_a < 0.1k_c; \tag{10}$$

This simplifies Eq. (9) to

$$S_{j,ini} = Eh_1^2 \frac{k_a k_b k_c}{2k_b k_c + 2k_a k_c + k_a k_b} \approx Eh_1^2 \frac{k_a k_b k_c}{2k_b k_c} = \frac{Eh_1^2}{2} k_a \tag{11}$$

As can be seen, the accuracy of Eq. (11) primarily depends on the accuracy of the component k_a. The stiffness of this component can be found in the CIDECT report (Weynand et al. 2015). However, this thesis employs an equation, which is proposed in the other CIDECT report (Grotmann & Sedlacek 1998):

$$k_a = \frac{8t_0^3 l_{eff,cf}}{(1-\beta)^3 b_0^3} \cdot \frac{1}{2 + \frac{6\beta}{1-\beta}} \tag{12}$$

where $l_{eff,cf}$ is the effective width determined as

$$l_{eff,cf} = t_1 + 2b_0\sqrt{1-\beta} \tag{13}$$

The validation against the experimental data have shown that the proposed theoretical approach significantly underestimates the initial stiffness of RHS T joints. For most of joints, the predicted stiffness accounted 30-45% from the experimental values. Given the leading contribution of the component *a* to the stiffness of the joint, a new equation has been proposed for its stiffness:

$$k_a = \frac{20t_0^3 l_{eff,cf}}{(1-\beta)^3 b_0^3} \cdot \frac{1}{2 + \frac{6\beta}{1-\beta}} \tag{14}$$

Eq. (14) was developed based on the direct fitting of the theoretical stiffness to the experimental values. For the investigated joints, Eq. (14) allowed to predict initial stiffness in the range from 0.64 to 0.94 from the experimental values. Still observed underestimation for some joints is connected with the influence of fillet welds, which considerably increase the experimental stiffness of joints but are not considered in the theoretical calculations.

The second part of the paper investigated the influence of chord axial stresses on the initial rotational stiffness of RHS T joints. For resistance, the influence of chord axial stresses is taken into account in EN 1993-1-8:2005 (CEN 2005b) by the chord stress function:

$$k_n = \begin{cases} 1.3 - \dfrac{0.4|n|}{\beta} \le 1.0, & n > 0 \\ 1.0, & n < 0 \end{cases} \tag{15}$$

where n is the relative normal stress:

$$n = \frac{\sigma_0}{f_{y0}} = \frac{N_0}{A_0 f_{y0}} + \frac{M_0}{W_{el0} f_{y0}} \tag{16}$$

where N_0 and M_0 are respectively axial force and bending moment applied in the chord, A_0 and W_{el0} are respectively the cross-sectional area and elastic section modulus of the chord.

However, no such function exists for initial stiffness. The paper numerically investigated the effect of axial stresses on the stiffness of RHS T joints. The FE analyses were conducted in two steps. On the first one, an axial force was applied to the chord to create axial stresses. On the second step, the joint was loaded by an in-plane bending moment using a single increment. The joints were analyzed on the whole range specified by EN 1993-1-8:2005: $0.25 \le \beta \le 1.0$, $10 \le 2\gamma \le 35$, considering a single steel grade S500. The results demonstrated that tensile axial stresses increase rotational stiffness of joints, while compressive stresses, oppositely, reduce it. The effect was found particularly pronounced for the joints with small β and high 2γ (+30% of stiffness for tension and -50% for compression). Some examples are demonstrated in FIGURE 11, where S/S_0 denotes stiffness in relation to the stiffness with no axial force in the chord. For joints with $\beta = 1.0$, the effect was found independent on 2γ.

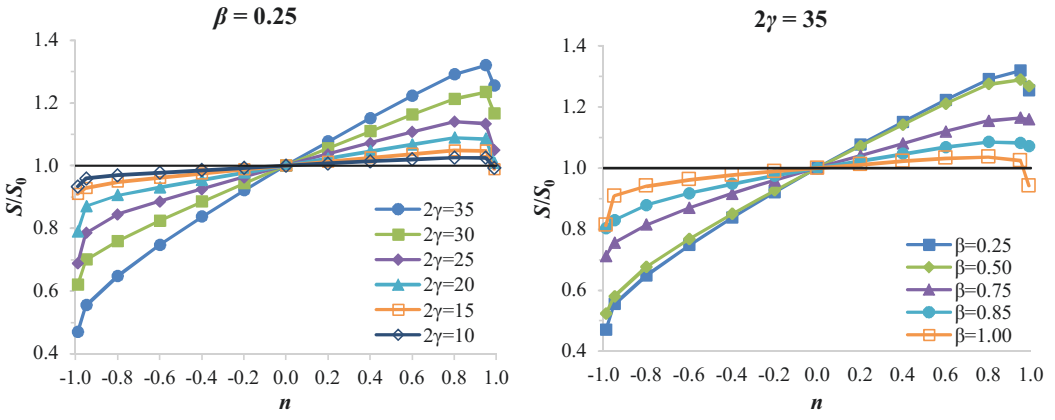

FIGURE 11. Influence of chord axial stresses on initial rotational stiffness of RHS T joints.

To take this influence into account, the paper developed a following chord stress function $k_{sn,ip}$:

For $0.25 \le \beta \le 0.85$:

$$k_{sn,ip} = \begin{cases} 1+0.001\left(1+1.7\beta-2.6\beta^2\right)n\gamma^2-2.7\left(|n|-0.8\right)^2, & -0.99 \le n < -0.8 \\ 1+0.001\left(1+1.7\beta-2.6\beta^2\right)n\gamma^2, & -0.8 < n < 0.8 \\ 1+0.001\left(1+1.7\beta-2.6\beta^2\right)n\gamma^2-3.1\left(n-0.8\right)^2, & 0.8 < n \le 0.99 \end{cases}$$

For $0.85 < \beta < 1.0$: (17)

$k_{sn,ip}$ is the linear interpolation between $\beta = 0.85$ and $\beta = 1.0$

For $\beta = 1.0$:

$$k_{sn,ip} = \begin{cases} 1+0.06n-3.5\left(|n|-0.8\right)^2, & -0.99 \le n < -0.8 \\ 1+0.06n, & -0.8 < n < 0.8 \\ 1+0.06n-2.8\left(n-0.8\right)^2, & 0.8 < n \le 0.99 \end{cases}$$

The function was validated against a series of independent FE analyses, considering the joints made of steel grades S355 and S700. The validation demonstrated that the influence of axial stresses depends on the steel grade, i.e. the changes of stiffness were more pronounced for S700 than for S355, as shown in FIGURE 12. Based on the numerical data for S500, the chord stress function provided the results intermediate between S355 and S700. However, the function demonstrated a satisfactory correlation with the numerical results and was found suitable for the design.

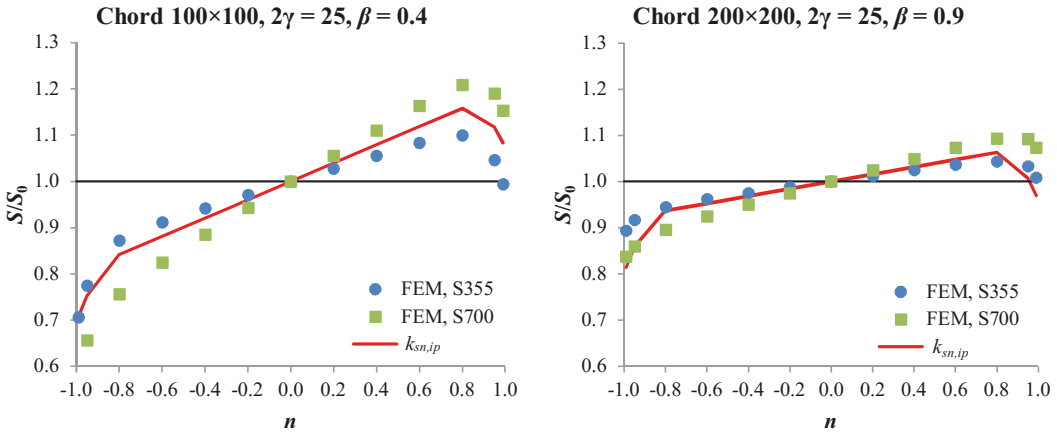

FIGURE 12. Validation of the proposed chord stress function.

2.5 Initial axial stiffness

Article VIII develops a theoretical solution for the initial axial stiffness of RHS T joints on the basis of the component method. As was determined in **Article I**, only two components contribute to the initial axial stiffness of RHS T joints:

- Chord face in bending (component *a*),
- Chord side walls in compression (component *b*).

The remaining components are not considered due to their relatively high stiffness. Based on that, the initial axial stiffness $C_{j,ini}$ of the RHS T joint with $\beta \leq 0.85$ can be expressed as

$$C_{j,ini} = \frac{E}{\frac{1}{k_a} + \frac{1}{k_b}} \tag{18}$$

where k_a and k_b denote the stiffnesses of the corresponding components. For joints with $\beta > 0.85$, the component *a* becomes irrelevant, and the axial stiffness of the joint can be simplified to

$$C_{j,ini} = Ek_b \tag{19}$$

The stiffnesses of the components *a* and *b* are proposed in the CIDECT report (Weynand et al. 2015). For the component *a*, CIDECT presents two options for its stiffness (see Section 1.1.3). As a starting point, the paper validated the existing approach against the experimental results available in the literature. Despite the similarities between the behavior of T and X joints, the latter demonstrated significantly greater initial stiffness and were excluded from the analysis. The validation allowed to make the following conclusions:

1. For the joints with $\beta \leq 0.85$, theoretical stiffness noticeably (2.0 times in average) overestimated experimental stiffness for T joints, if the stiffness of the component *a* was calculated using the first CIDECT option. Moreover, the vast majority of the considered joints violated the validity range of this equation. Only the joints with very small braces were found to meet the introduced limitations.
2. If stiffness was calculated using the second CIDECT option for the component *a*, then the results were considerably underestimated (0.08 from experimental). This equation was found inapplicable for tubular joints and was not considered further in the paper.
3. For the joints with $\beta > 0.85$, theoretical stiffness also (2.1 times) overestimated experimental stiffness for T joints. Since in this case the stiffness of the joint is represented by a single component *b*, Eq. (19), the equation for the stiffness of this component was found inaccurate.
4. The stiffness of the component *b* does not take into account the brace-to-chord width ratio β, meaning that the same equation is proposed for joints with both $\beta = 1.0$ and $\beta < 1.0$.

The observed unsatisfactory prediction of the stiffness by the theoretical approach demonstrated that none of the proposed equations for the stiffness of the components can be effectively used in the design of RHS T joints. Based on simple mechanical models, the paper developed the equations for the stiffness of the components *a* and *b*. The equations employed the concept of the effective length and width, which were determined based on the extensive numerical simulations. The following equation was proposed for the stiffness of the component *a*:

$$k_a = \frac{4 l_{eff} t_0^3}{\left(L - b_1\right)^3} \tag{20}$$

where $L = b_0 - 2t_0$; l_{eff} is the effective length determined as

$$l_{eff} = h_1\left(2 - \beta\right) + 1.25 b_0\left(1 - \beta\right) \tag{21}$$

The following equation was proposed for the stiffness of the component *b*:

$$k_b = \frac{2 b_{eff} t_0}{h_0 - t_0} \tag{22}$$

where b_{eff} is the effective width determined as

$$b_{eff} = 0.025\left(h_1\left(9\beta - 1\right) + \frac{2.4 b_0}{1.2 - \beta} \right) \tag{23}$$

The reliability of the proposed equations was validated against the same experimental data. The joints demonstrated sufficient agreement between theoretical and experimental stiffness, particularly when the influence of fillet welds was taken into account.

The second part of the paper investigated the effect of chord axial stresses on the axial stiffness of RHS T joints. The paper analyzed the joints on the whole range specified by EN 1993-1-8:2005 (CEN 2005b): $0.25 \le \beta \le 1.0$, $10 \le 2\gamma \le 35$, considering three steel grades S355, S500 and S700. Similar to initial rotational stiffness, tensile axial stresses increased the axial stiffness of joints, with the opposite influence for compressive stresses. The effect was found particularly pronounced for the joints with small β and high 2γ and high steel grades (+30% of stiffness for tension and -60% for compression). Some examples are demonstrated in FIGURE 13, where C/C_0 denotes stiffness in relation to the stiffness with no axial force in the chord. For the joints with $\beta = 1.0$, the effect did not depend on 2γ.

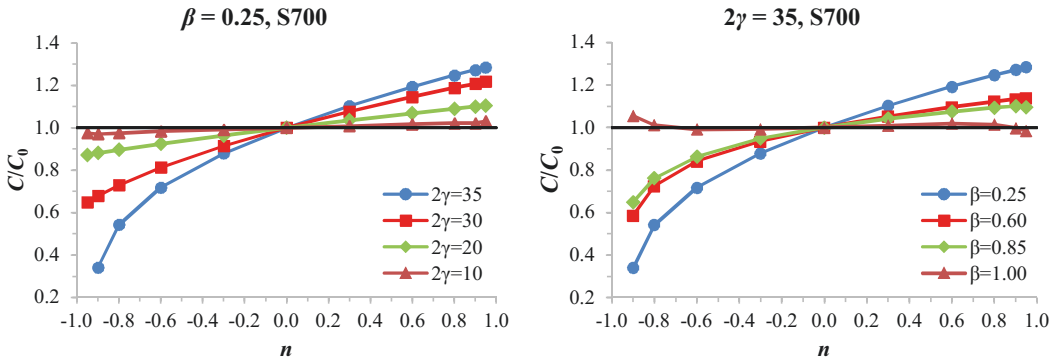

FIGURE 13. Influence of axial stresses on initial axial stiffness of RHS T joints.

To consider the influence of chord axial stresses in the design, the paper developed a corresponding chord stress function. In contrast to the function for initial rotational stiffness (Section 2.4), the developed chord stress function took into account the influence of the steel grade:

$$
\begin{aligned}
&\text{For } 355 \text{ MPa} \le f_{y0} \le 500 \text{ MPa}: \\
&k_{sn,N} = 1 + 10^{-5} f(\beta) f(\gamma) f\left(f_{y0}\right) n \\
&\text{For } 500 \text{ MPa} < f_{y0} < 700 \text{ MPa}: \\
&k_{sn,N} \text{ is the linear interpolation between S500 and S700} \\
&\text{For } f_{y0} = 700 \text{ MPa}: \\
&k_{sn,N} = 1 + 0.0008 f(\beta) f(\gamma)\left(n^3 - 1.25n^2 + 0.01 f\left(f_{y0}\right) n\right)
\end{aligned}
\tag{24}
$$

where

$$
\begin{aligned}
&f(\beta) = -2\beta^2 + 1.6\beta + 0.3 \\
&f(\gamma) = 1.3\gamma^2 - 38 \\
&f\left(f_{y0}\right) = 0.02 f_{y0}^{\,1.4}
\end{aligned}
\tag{25}
$$

Tthe validity of the proposed function was limited to the joints that meet the following requirements:

$$2\gamma \ge 12; \quad \beta \le 0.9; \quad 40\beta - 2\gamma \le 11 \tag{26}$$

Outside this domain, axial stresses demonstrated a very small influence on axial stiffness. In these cases, the introduction of the chord stress function had no practical reason, since the possible error of the function was comparable to the error obtained from its ignorance.

The validation of the proposed chord stress function was conducted with a series of independent FE results and employing the same FE model. The validation was considered for the joints with a different chord size

100×100 and steel grades S420 and S600. The function demonstrated good agreement with the numerical results, as can be seen in FIGURE 14.

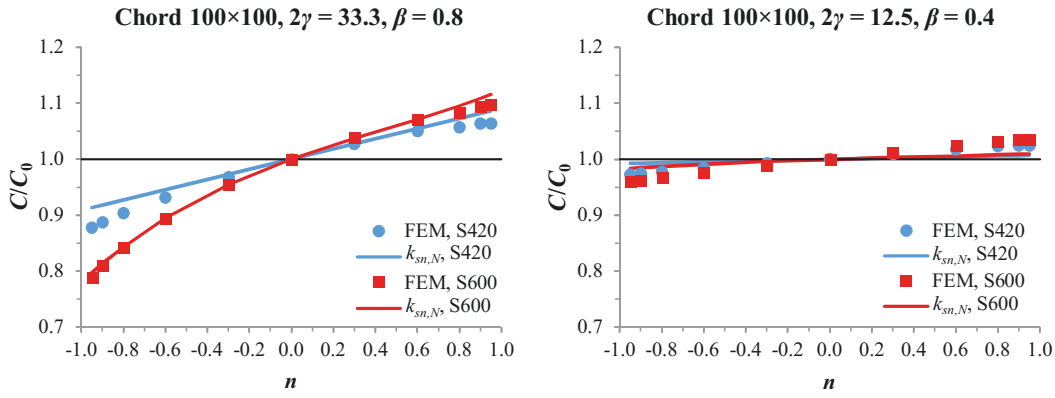

FIGURE 14. Validation of the proposed chord stress function.

2.6 Issues of high strength steels

As was mentioned before, the design of HSS tubular joints is complicated by the two following issues:

- very conservative reduction factors for resistance of joints
- very large throat thicknesses of full-strength fillet welds

The reduction factors k_{HSS} are determined according to EN 1993-1-8:2005 (CEN 2005b) and EN 1993-1-12:2007 (CEN 2007) in relation to the nominal steel grade of the chord:

$$k_{HSS} = \begin{cases} 0.9, & 355 \text{ MPa} < f_{y0} \leq 460 \text{ MPa} \\ 0.8, & 460 \text{ MPa} < f_{y0} \leq 700 \text{ MPa} \end{cases} \tag{27}$$

Both issues are discussed in **Article III**, which presents the experimental tests conducted in Häme University of Applied Sciences (HAMK). The tests included twenty HSS SHS T joints under in-plane bending. The paper considered joints with $\beta = 0.67$ and 0.80, three steel grades (S420, S500 and S700) and three types of welds (6 mm and 10 mm fillet welds and 1/2v butt welds). The details of the tested joints are presented in TABLE 2, where the naming of the test specimens is presented in the format [chord steel]_[brace steel]_[weld type]. Index *WiPF* denotes robot welding. All fillet welds were undersized (throat thickness was smaller than that of full-strength fillet welds), as shown by the relative weld size a_w / $a_{w,fs}$. The analyses were performed with measured section dimensions and the material properties obtained from tensile coupon tests.

TABLE 2. In-plane bending tests: tests matrix.

Joint	b_0 [mm]	h_0 [mm]	t_0 [mm]	Chord Steel	b_1 [mm]	h_1 [mm]	t_1 [mm]	β	Brace Steel	a_w [mm]	$a_w / a_{w,fs}$
S420_S420_a6	150	150	8	S420	100	100	8	0.67	S420	6	0.51
S500_S420_a6				S500	100	100	8	0.67	S420		0.51
S500_S500_a6				S500	100	100	8	0.67	S500		0.47
S700_S420_a6				S700	100	100	8	0.67	S420		0.51
S700_S500_a6				S700	100	100	8	0.67	S500		0.47
S700_S500_a6_WiPF				S700	100	100	8	0.67	S500		0.47
S700_S700_a6				S700	120	120	8	0.80	S700		0.45
S420_S420_a10	150	150	8	S420	100	100	8	0.67	S420	10	0.84
S500_S420_a10				S500	100	100	8	0.67	S420		0.84
S500_S500_a10				S500	100	100	8	0.67	S500		0.78
S700_S420_a10				S700	100	100	8	0.67	S420		0.84
S700_S500_a10				S700	100	100	8	0.67	S500		0.78
S700_S500_a10_WiPF				S700	100	100	8	0.67	S500		0.78
S700_S700_a10				S700	120	120	8	0.80	S700		0.76
S420_S420_1/2v	150	150	8	S420	100	100	8	0.67	S420	butt	-
S500_S420_1/2v				S500	100	100	8	0.67	S420		
S500_S500_1/2v				S500	100	100	8	0.67	S500		
S700_S420_1/2v				S700	100	100	8	0.67	S420		
S700_S500_1/2v				S700	100	100	8	0.67	S500		
S700_S700_1/2v				S700	120	120	8	0.80	S700		

All twenty tests were performed until the overall failure of the specimens. All joints demonstrated clearly seen plastification of the chord face (chord face failure), which is typical for joints $\beta \leq 0.85$. At the same time, the joints experienced considerable post-yielding behavior (hardening phase) due to strain hardening and the membrane effect. Finally, all joints failed from cracking in HAZ (punching shear failure). The example of the deformation pattern for joint S420_S420_a6 is presented in FIGURE 15a. The plastic resistance of the joints $M_{pl,exp}$ was determined as the intersection of the tangent lines corresponding to initial and hardening stiffness, as shown in FIGURE 15b. Experimental resistance was compared to the current theoretical solution presented in EN 1993-1-8:2005 (CEN 2005b) as:

$$M_{ip,1,Rd} = f_{y0} t_0^2 h_1 \left(\frac{1}{2\eta} + \frac{2}{\sqrt{1-\beta}} + \frac{\eta}{1-\beta} \right) \tag{28}$$

To determine the necessity for HSS reduction coefficients, the resistance of joints was normalized in respect to steel grade and geometry. FIGURE 16 presents non-dimensional moment resistance $M_{pl,exp}/(f_{y0} \cdot t_0^2 \cdot h_1)$ in relation to β, where the joints are grouped by the weld size. The detailed comparison between the theoretical and experimental results is provided in TABLE 3. As can be seen, all joints with 10 mm fillet welds ($a_w/a_{w,fs} = 0.76 \ldots 0.84$) demonstrate safe results: experimental resistance clearly exceeds the theoretical prediction with sufficient safety margins. Even without the reduction, theoretical resistance is rather conservative. Obviously, no reduction of resistance is required for these joints.

a)

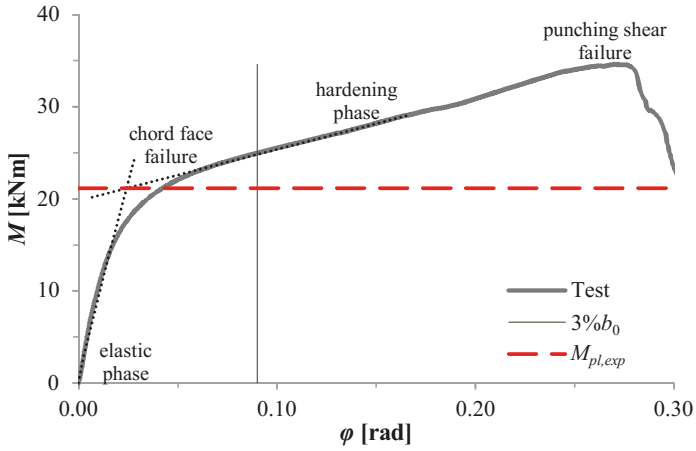

b)

FIGURE 15. Joint S420_S420_a6: a) chord face failure; b) definition of resistance.

The joints with 6 mm fillet welds ($a_w/a_{w,fs}$ = 0.45…0.51) depend on the case: the theoretical results are very close to the experimental values with extremely small safety margins. Moreover, the ratio $M_{ip,1,Rd}$ / $M_{pl,exp}$ exceeds 1.0 in two cases, S700_S420_a6 and S700_S500_a6 (both have the chord made of S700). This means that reduction is needed only for the joints with the chord made of grade S700, or the grades above S500, more generally. However, k_{HSS} = 0.9 was found to be sufficient, instead of the original value of 0.8. No reduction is required for the joints made of grade S500 and below. Regarding the butt-welded joints, none of them show safe results, with the ratio $M_{ip,1,Rd}$ / $M_{pl,exp}$ exceeding 1.0 in all cases. With the reduction factors, all joints show safe performance. Therefore, the reduction factors are required for butt-welded joints in all cases.

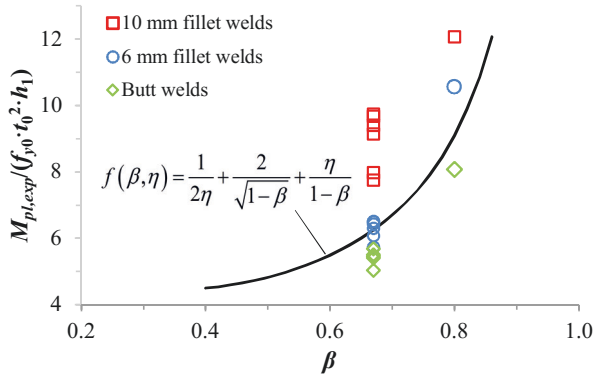

FIGURE 16. Comparison of normalized experimental resistance with EN solution.

TABLE 3. Comparison of experimental and theoretical resistance.

Joint	β	a_w / $a_{w,fs}$	$M_{ip,1,Rd}$ [kNm]	k_{HSS}	$M_{pl,exp}$ [kNm]	$M_{ip,1,Rd}$ / $M_{pl,exp}$	k_{HSS}*$M_{ip,1,Rd}$ / $M_{pl,exp}$
S420_S420_a6	0.66	0.51	20.0	0.9	21.2	0.95	0.85
S500_S420_a6	0.67	0.51	24.1	0.8	24.3	0.99	0.79
S500_S500_a6	0.67	0.47	24.1	0.8	25.0	0.96	0.77
S700_S420_a6	0.67	0.51	30.1	0.8	27.7	1.09	0.87
S700_S500_a6	0.67	0.47	30.1	0.8	29.4	1.02	0.82
S700_S500_a6_WiPF	0.67	0.47	30.1	0.8	31.2	0.96	0.77
S700_S700_a6	0.80	0.45	52.6	0.8	61.2	0.86	0.69
Average						**0.98**	**0.79**
S420_S420_a10	0.67	0.84	20.1	0.9	31.6	0.64	0.57
S500_S420_a10	0.67	0.84	24.1	0.8	35.1	0.69	0.55
S500_S500_a10	0.67	0.78	24.1	0.8	37.2	0.65	0.52
S700_S420_a10	0.67	0.84	29.9	0.8	38.5	0.78	0.62
S700_S500_a10	0.67	0.78	30.1	0.8	45.5	0.66	0.53
S700_S500_a10_WiPF	0.67	0.78	30.0	0.8	37.6	0.80	0.64
S700_S700_a10	0.80	0.76	53.1	0.8	70.1	0.76	0.61
Average						**0.71**	**0.58**
S420_S420_1/2v	0.67	-	20.2	0.9	18.5	1.09	0.98
S500_S420_1/2v	0.67	-	24.2	0.8	21.1	1.15	0.92
S500_S500_1/2v	0.67	-	24.2	0.8	21.0	1.15	0.92
S700_S420_1/2v	0.67	-	30.0	0.8	24.2	1.24	0.99
S700_S500_1/2v	0.67	-	30.4	0.8	26.4	1.15	0.92
S700_S700_1/2v	0.81	-	54.6	0.8	46.8	1.17	0.93
Average						**1.16**	**0.94**

The observed results are in good correlation with other publications on this issue. In particular, Feldmann et al. (2016) proposed the following reduction factors for axially loaded RHS T joints: 1.0 for S500, 0.9 for S700 and 0.8 for S960. Björk & Saastamoinen (2012) demonstrated that axially loaded RHS X joints made of S420 grade provide sufficient resistance without the reduction factor of 0.9. TABLE 4 presents the summary of the recommended reduction factors based on this paper and other publications for the four steel grades commonly used in the construction industry. It should be noted that Article II employed plastic resistance to determine the experimental strength of the joints. At the same time, Section 2.2 shows that plastic resistance leads to 10-20% smaller resistance than ultimate resistance based on the 3%b_0 deformation limit. This allows to conclude that if the latter was used to determine the resistance of the joints, the theoretical calculation would have been even more conservative, leading to more beneficial (greater) reduction factors.

TABLE 4. Proposed reduction factors.

	Eurocode	Proposal, butt welds	Proposal, fillet welds	Feldmann et al. (2016)	Björk & Saastamoinen (2012)
Loading case	all	in-plane bending	in-plane bending	axial	axial
S420	0.9	0.9	1.0	no data	1.0
S500	0.8	0.8	1.0	1.0	no data
S700	0.8	0.8	0.9	0.9	no data
S960	no data	no data	no data	0.8	no data

The observed difference between the experimental resistances of the joints with various types of welds can be explained by the considerable improving effect of fillet welds. Fillet welds enlarge the cross-section of the

brace at the connection area, effectively increasing β and resulting to greater resistance. For this reason, the lowest experimental resistance is observed for the butt-welded joints, while the greatest one corresponds to the joints with 10 mm fillet welds. A detailed comparison of the experimental resistances of these joints is provided in Section 2.8.1. At the same time, the Eurocode solution does not take into account the beneficial influence of fillet welds, providing the same equation regardless the type and the size of welds. This means that the conclusions on the reduction factors are considerably influenced by the effect of fillet welds. If the effect was taken into account, as it is proposed in Section 2.8 by using an enlarged β, this could have led to higher theoretical resistance of the joints, as shown in FIGURE 17. Therefore, this could have led to smaller safety margins between the experimental and theoretical resistances or even unsafe results, requiring greater reduction and less favorable (smaller) HSS reduction factors. Until the beneficial influence of fillet welds is incorporated into the standards, the reduction factors proposed in the thesis can be recommended for the design of RHS T joints. If the influence of fillet welds is included into the standards, the HSS reduction factors have to be redefined to avoid possible unsafe results.

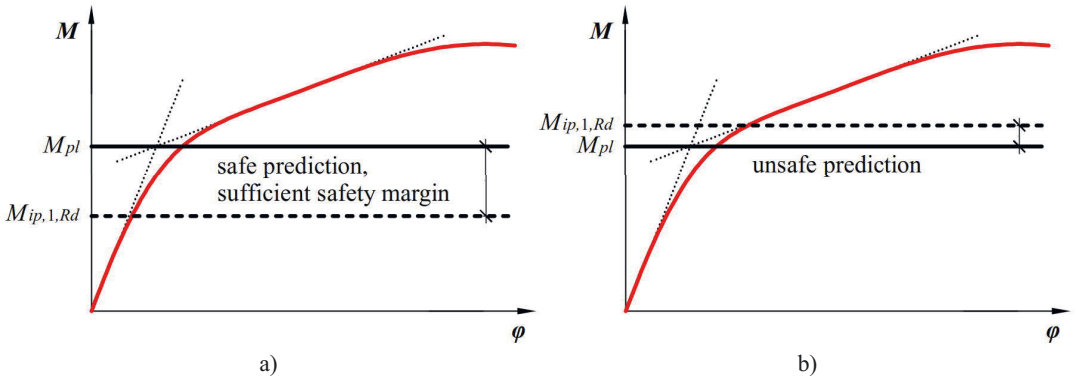

FIGURE 17. Behavior of RHS T joint: a) influence of fillet welds is ignored, no reduction is needed; b) influence of fillet welds is considered, greater theoretical resistance, reduction is needed.

Article III also considered the ductility of the joints, evaluating their ability to provide sufficient rotation capacity. The rotation capacity of the joint was determined as the rotation φ_{max} corresponding to the maximum resistance of the joint and was compared to the $3\%b_0$ deformation limit $\varphi_{3\%b0}$ of Lu et al. (1994). The results showed that all joints demonstrated sufficient rotation capacity, with the $\varphi_{3\%b0} / \varphi_{max}$ ratio in the range of 0.33…0.61 for the joints with $\beta = 0.67$ and 0.68…0.88 for the joints with $\beta = 0.80$. This finding has shown the reliability of joints with welds smaller than full-strength fillet welds.

In addition, **Article III** proposed the design procedure for the resistance of welds. The equations are based on the Directional method provided in EN 1993-1-8:2005 (CEN 2005b) and are developed separately for fillet and butt welds. The comparison of weld resistance $M_{w,Rd}$ with the maximum resistance M_{max} of the joints (the maximum load the joint can resist) demonstrates that the proposed equation for fillet welds is safe but rather conservative, as shown in FIGURE 18a. The resistance of butt welds was found to be unsafe, clearly exceeding

maximum resistance for all the considered joints, as depicted in FIGURE 18b. This indicates that the developed equations can be limited only for the joints with fillet welds, requiring additional studies for butt-welded joints.

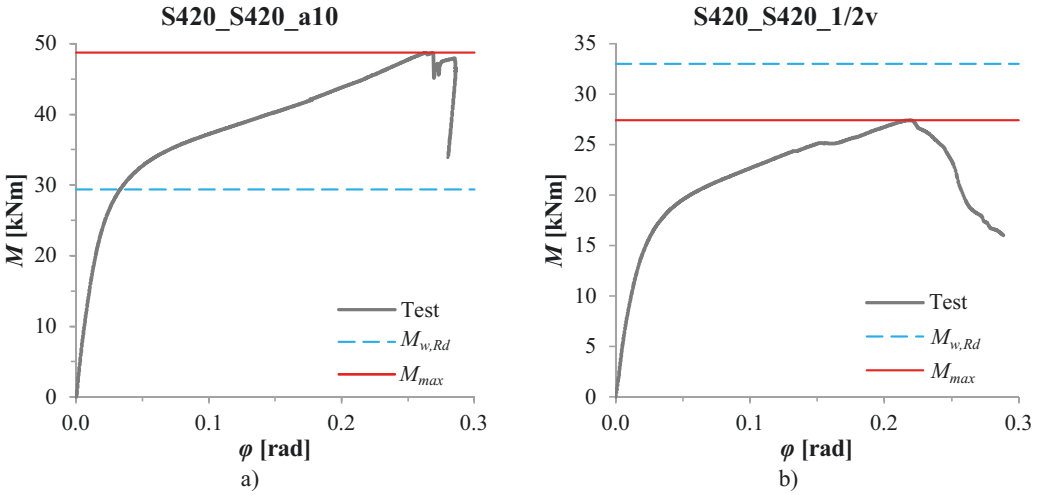

FIGURE 18. Resistance of welds: a) joint with fillet welds; b) joint with butt welds.

It should be noted that the results obtained in **Article III** are based on the joints with $\beta < 0.85$, $2\gamma = 18$ and subjected to in-plane bending. The need for a reduction factor may also depend on the failure mode: ductile, e.g. chord face in bending, or brittle, e.g. punching shear or weld failure. More research is required to develop more generalized conclusions, considering joints with various geometry, steel grades and loading cases, including axial loading and out-of-plane bending.

In addition to the 0.8 and 0.9 reduction factors addressed in the thesis, the last discussions in CEN SC3/TC250 WG8 have recently led to the introduction of an extra coefficient of 0.8 for the steel yield stress for some failure modes. By the time of the thesis, this proposal was not available; therefore, this coefficient was not considered.

2.7 Influence of initial imperfections

This section investigates the influence of initial imperfections on the structural behavior of RHS T joints. In particular, this thesis analyzes initial geometrical imperfections and welding residual stresses.

2.7.1 Initial geometrical imperfections

The effect of initial geometrical imperfection has been investigated in **Article VI** by means of the FE analysis. Since the deformation of the joint is governed by the deformation of the chord (chord face bending and chord side walls buckling), the paper considered only the local imperfections of the chord. The analyses measured

the resistance and initial stiffness of joints under two loading cases: in-plane bending and axial brace loading. Imperfections were modelled using the traditional approach for thin-walled sections, when buckling modes are scaled in accordance with allowable fabrication tolerances and applied to the perfect model. The buckling modes were obtained from the linear buckling analysis and were applied in the most unfavorable ways, so that the obtained imperfect geometry replicated the deformed shape of the joint under a corresponding loading as closely as possible. The allowable amplitude of imperfections was determined according to EN 10219-2:2006 (CEN 2006a), which limits the concavity and convexity of cold-formed RHS tubes by $\varepsilon_0 = 0.8\%$. Both perfect and imperfect joints were then loaded by a nonlinear static analysis.

The first part of the article investigated different buckling modes and their applicability to simulate initial imperfections. For axial loading, the most conservative results were obtained when imperfections were simulated by the mode that repeated as close as possible the deformation pattern under the compressive axial force. This pattern represented the convexity of the chord side walls in the area of the connection, as illustrated in FIGURE 19a. The corresponding buckling mode is shown in FIGURE 19b. The consideration of other buckling modes and their possible combinations brought no reasonable changes in the results and was found unnecessary. For moment loading, all the obtained buckling modes demonstrated the maximum deformations in the brace; therefore, none of them was found suitable for the simulation of imperfections located in the chord. For this reason, initial imperfections for moment-loaded joints were modelled using the buckling modes obtained from axial loading.

The second part of the paper conducted several parametric studies, evaluating the influence of initial imperfections by comparing joints with perfect and imperfect geometry. Geometrical imperfections demonstrated a small negative effect on the structural behavior of joints, both those governed by chord face failure ($\beta \leq 0.85$), and those governed by chord side walls failure ($\beta > 0.85$). The effect was more pronounced for the joints with comparatively thin walls but was found independent on the steel grade and brace-to-chord width ratio β. The maximum observed reduction of resistance accounted 3% and 5% for in-plane bending and axial loading, respectively. Initial stiffness decreased correspondingly by 4% and 7%. These findings allow to conclude that geometrical imperfections do not seriously affect the structural behavior of RHS T joints in the range specified in the current design rules. For this reason, this type of imperfections can be safely ignored in the design.

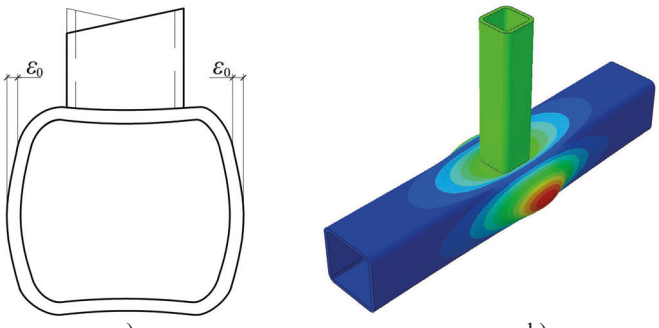

FIGURE 19. a) Deformation pattern under axial loading; b) corresponding buckling mode.

2.7.2 Welding residual stresses

The influence of welding residual stresses has been numerically investigated in **Articles IV** and **V**. **Article IV** develops and validates the FE model for a RHS T joint, simulating fillet welds in Abaqus Welding Interface, which represents an Abaqus plugin for the simulation of welding processes. To allow modeling of the welding process with significant thermal and stress gradients, the FE model from the previous numerical analyses (Section 2.3) required considerable adjustments. The new model had a noticeably finer mesh, particularly in welds and in the connection area. The conducted mesh convergence study recommended the optimal mesh size equal to the minimum between $t_0/3$ and $a_w/3$. The number of elements in the thickness direction was also increased from two to three. To meet the requirements of Abaqus Welding Interface, the model was created as a single part with corresponding partitioning, instead of using a tie constraint to connect the chord and the brace. For the correct interpretation of the connection by means of fillet welds, a small gap was introduced between the brace and the chord. To reduce calculation time, significantly increased due to better FE discretization, quadratic finite elements were replaced by linear finite elements (C3D8). In addition, the model required the accurate introduction of the thermal steel properties, including heat capacity, thermal conductivity and thermal expansion. All these properties, including mechanical ones, were introduced as temperature-dependent. Attention was paid particularly on the calibration of the weld heat input, i.e. the welding speed and the corresponding target torch heat-up temperature. The validation with the existing experimental results has shown that the developed model properly captures the local behavior of joints and can be effectively used for further studies.

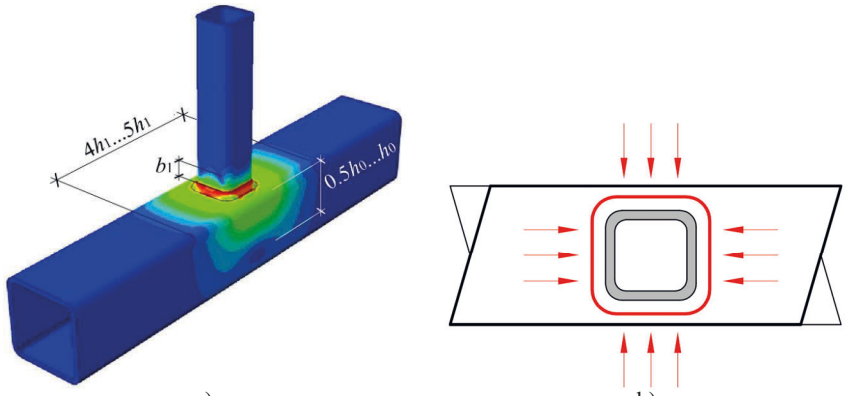

FIGURE 20. a) Distribution of welding residual stresses; b) idealized welding sequence.

The companion paper, **Article V**, determines the influence of welding residual stresses on the structural behavior of RHS T joints, employing the model developed in **Article IV**. The model with obtained welding residual stresses was considered under in-plane bending and axial loading, conducting nonlinear static analyses in Abaqus/Standard. Firstly, the paper analyzed the welding sequences that are mostly often employed for RHS T joints. The results have showed that the considered welding sequences resulted to the same distribution of welding residual stresses in the joint, illustrated in FIGURE 20a. The maximum welding stresses occur in the weld, spreading to the surface of the chord and the brace. In addition, all considered sequences led to the same

structural behavior of joints, with equal resistance and initial stiffnesses under in-plane bending and axial loading. To reduce computational efforts in the analyses, the paper proposed an idealized welding sequence, when the whole weld is performed simultaneously at the same time, as shown in FIGURE 20b. This sequence allowed to reduce calculation time more than four times in comparison to the other considered sequences.

The conducted parametric studies demonstrated a positive effect of residual stresses on the resistance of the joints. The maximum observed improvement accounted for 19% for moment resistance and 17% for axial resistance. The behaviour of a joint with varying wall thickness, with and without welding stresses is illustrated in FIGURE 21, where index *w* corresponds to joints with welding stresses. In case of in-plane bending, the improving effect was more pronounced for higher steel grades, smaller chord wall thickness and smaller welds. For axial loading, the effect was found to increase only for smaller chord wall thickness. At the same time, residual stresses reduced initial rotational and axial stiffness by 5-14%. No changes were observed for maximum resistance and deformation capacity.

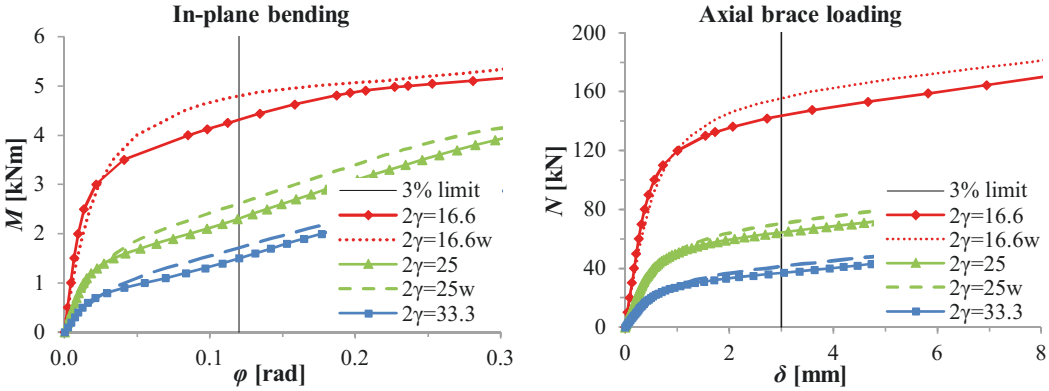

FIGURE 21. Influence of welding stresses (chord 100×100 mm, brace 50×50 mm, S355).

The nature of the observed phenomenon is not fully clear. The conducted comparative analysis has demonstrated that the positive effect is not caused by welding-induced deformations but primarily connected with welding residual stresses. The same values of maximum resistance (the maximum load the joint can resist) for the joints with and without residual stresses show that residual stresses do not increase the load-bearing capacity of joints but postpone the initiation of yielding in the area of the connection. This allows joints to resist an additional load in the elastic phase of the loading process. In reality, welding residual stresses are always present in tubular joints and obviously cannot be avoided. The obtained results demonstrate the difference between the two approaches for the FE simulation of the behaviour of tubular joints: one considering welding residual stresses and one neglecting them. The disregard of welding stresses underestimates the resistance of joints, providing thus an additional safety margin. At the same time, the observed underestimation is not so large to be considered as conservative. Given the considerable computational efforts required for the simulation of welding stresses, they can be safely ignored in the design of tubular joints.

It should be noted that **Articles IV** and **V** considered only fillet-welded joints with $\beta \leq 0.85$, i.e. governed by chord face bending. The conclusions regarding the influence of welding residual stresses can be different for butt-welded joints, as well as for joints with other governing failure modes. Additional research is also required for the joints under out-of-plane bending. The observed results can be validated experimentally by comparing welded joints with the joints that received a stress-relief heat treatment before the loading. This will allow to directly compare the behaviour of tubular joints with and without welding residual stresses.

2.8 Influence of fillet welds

Currently, most RHS joints are welded using two weld types: butt welds and fillet welds. A joint with idealized full-penetration butt welds is presented in FIGURE 22a. Butt welds are comparatively compact and therefore can be considered as the continuation of the brace. From that point of view, it can be assumed that butt welds do not increase the cross-section of the brace and do not influence the structural behaviour of RHS joints.

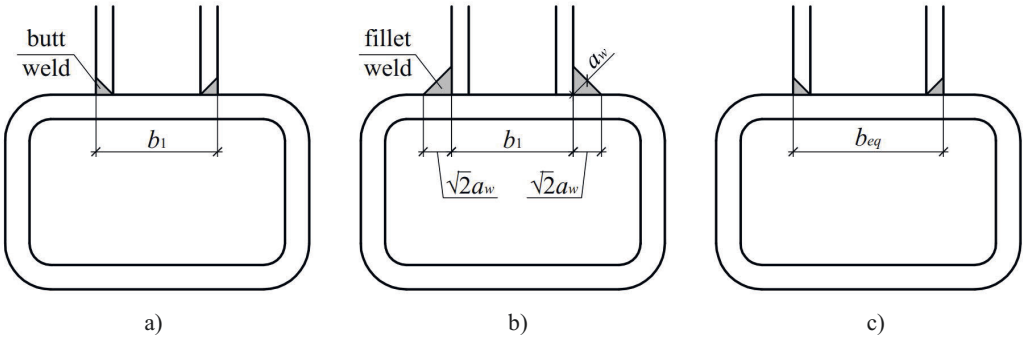

FIGURE 22. Idealization of welds: a) butt welds; b) fillet welds; c) equivalent joint with butt welds.

In contrast, fillet welds enlarge the cross-section of the brace in the area of connection, increasing simultaneously its brace-to-chord width ratio β, as can be seen in FIGURE 22b. The increased β leads to higher resistance and stiffness in comparison to the joint with the same geometry and butt welds. Such improvement of structural properties can be particularly noticeable for joints with full-strength fillet welds, which have very large throat thickness. The equation for calculating the throat thickness of full-strength fillet welds can be found in (Ongelin & Valkonen 2016):

$$a_w \geq 2 \cdot \frac{\beta_w}{\sqrt{2}} \cdot \frac{\gamma_{M2}}{\gamma_{M0}} \cdot \frac{f_y}{f_u} \cdot t_1 \tag{29}$$

where β_w is the strength factor. It should be noted that yield strength f_y and ultimate tensile strength f_u are considered in relation to the brace material. TABLE 5 provides the throat thicknesses of full-strength fillet welds calculated in accordance with Eq. (29) for the steels that are commonly used in construction. As can be seen, full-strength fillet welds have very large throat thicknesses, particularly for high strength steels. Such

welds can increase the cross-section of the brace so severely that neglecting them can lead to the very conservative design of resistance and stiffness. These statements are supported by the following examples.

TABLE 5. Throat thicknesses of full-strength fillet welds.

Brace material	S355	S460	S500	S550	S700
a_w	$1.20t_1$	$1.53t_1$	$1.60t_1$	$1.62t_1$	$1.64t_1$

2.8.1 HAMK tests

The first example considers the results of the HAMK tests discussed earlier in Section 2.6. As can be found in TABLE 3, the ratio $M_{ip,1,Rd}$ / $M_{pl,exp}$ (theoretical resistance in relation to experimental resistance) accounts for 1.16, 0.98 and 0.71 for the joints with butt welds, the joints with 6 mm fillet welds and the joints with 10 mm fillet welds, respectively. This means that the joints with 10 mm fillet welds have in average 1.16 / 0.71 = 1.63 times higher experimental resistance than the joints with butt welds. The similar trend is observed also for initial rotational stiffness: it is increased by 63% for the 10 mm fillet-welded joints in comparison to the joints with butt welds. It should be noted that in the tests, the largest fillet welds accounted 0.85 from full-strength fillet welds. If the latter were used instead, the results could have been even more conservative. The significant effect of fillet welds can be clearly demonstrated in FIGURE 23, which directly compares the behaviour of the joints with matching geometry and steel grades but varying welds. The joints are named in the way [chord steel grade]_[brace steel grade], while a10, a6 and 1/2v denote 10 mm fillet welds, 6 mm fillet welds and butt welds, respectively.

2.8.2 Numerical simulations

The second example represents a short numerical study conducted in **Article VII**. A comparative FE analysis was performed on SHS Y joints with butt and full-strength fillet welds, measuring their initial in-plane rotational stiffness. The results are presented in FIGURE 24, which plots the ratio S_{fillet} / S_{butt} (initial stiffness of fillet-welded joint in relation to butt-welded joint) for steel grades S355 and S700. The joints are named in the manner [“C”b_0×t_0]-[“B”b_1×t_1]-[φ] and are arranged in the ascending order of β. As can be seen, fillet welds significantly increase the initial stiffness of the joints. The influence is particularly strong for the joints with high β, reaching more than 2.0 times for S355 and more than 3.0 times for S700. Obviously, if the improving effect of fillet welds is disregarded, it may lead to very the conservative design of tubular joints.

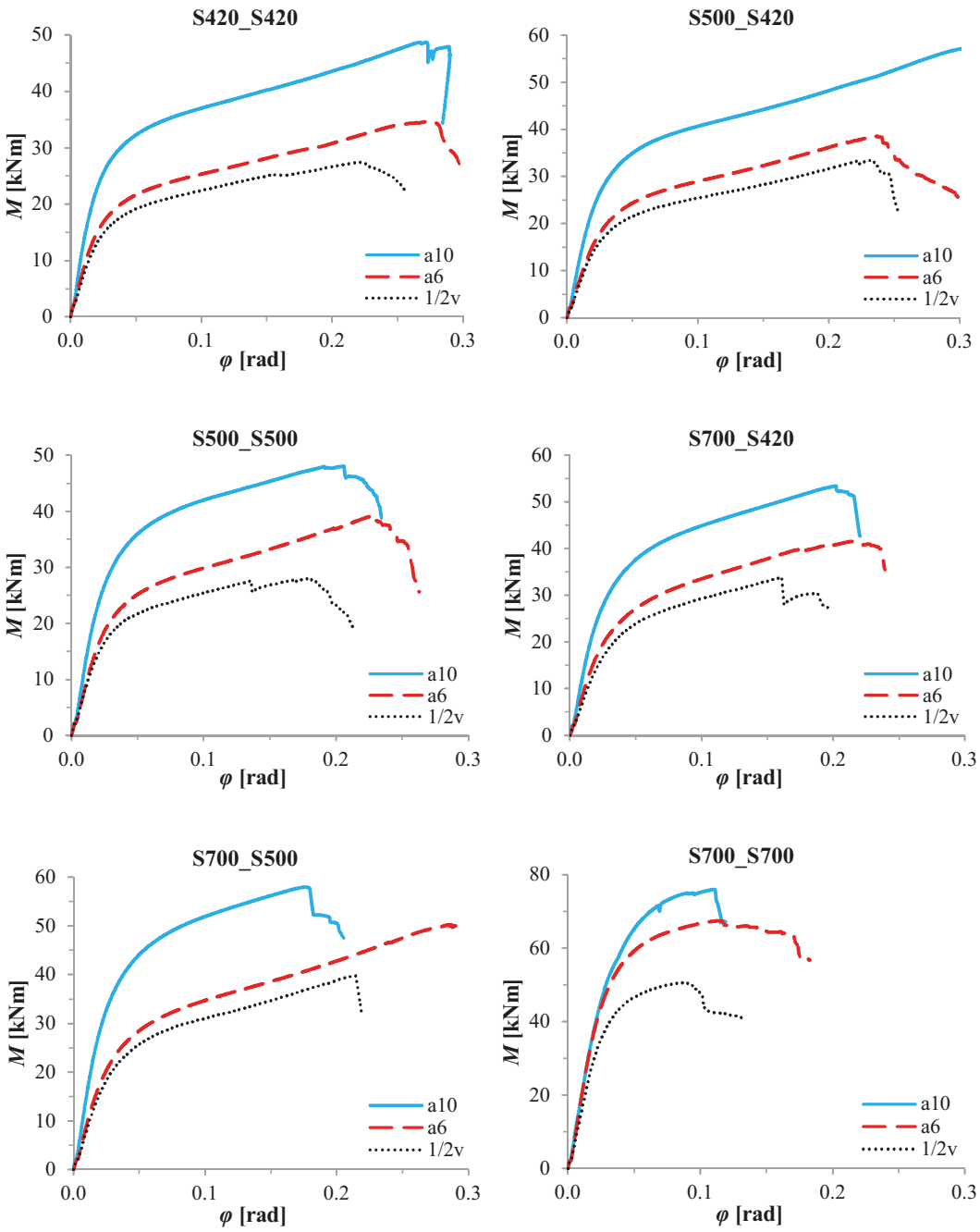

FIGURE 23. Structural behaviour of joints with varying weld types.

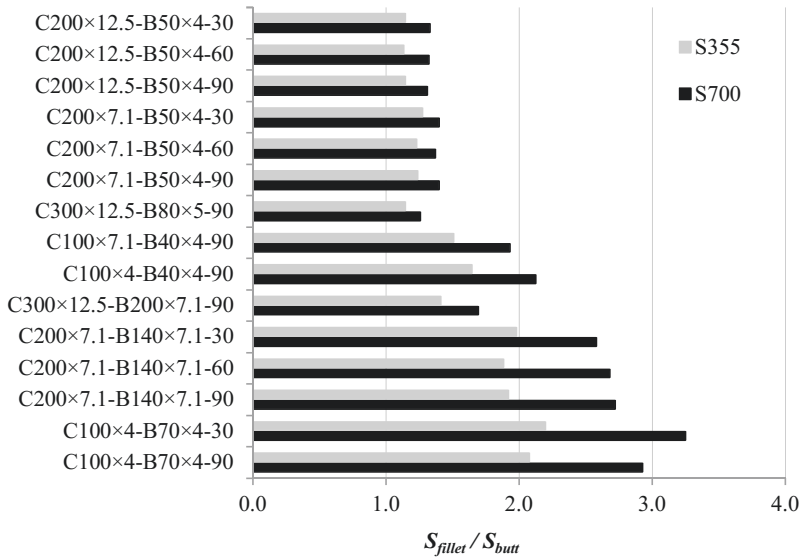

FIGURE 24. Comparison of initial stiffness of Y joints with butt welds and full-strength fillet welds.

In addition, **Article VII** attempted to take into account the effect of fillet welds on the initial stiffness of RHS Y joints. It was assumed that a joint with fillet welds can be considered as a butt-welded joint with the equivalent width $b_{eq} > b_1$ so that both joints have the same stiffness (FIGURE 22c). According to FIGURE 22b, the equivalent width b_{eq} was limited by the following boundaries:

$$b_1 < b_{eq} < b_1 + 2\sqrt{2}a_w \tag{30}$$

Therefore, an exact equation for b_{eq} was searched in the following way:

$$b_{eq} = b_1 + 2\sqrt{2}a_w \cdot k_{fw} \tag{31}$$

where k_{fw} is a correlation coefficient. In the paper, it was determined by FE analyses through several steps. On the first step, the stiffness of a joint with fillet welds was obtained from the analysis. On the second step, a butt-welded joint with the equivalent width b_{eq} was found such that its stiffness fitted that of the given fillet-welded joint. The equivalent width b_{eq} was first determined randomly and then refined through several iterations. Finally, when b_{eq} was known, the correlation coefficient k_{fw} was calculated according to Eq. (31). For all the joints, the correlation coefficient k_{fw} was found in the range 0.42…0.79. Based on that, a following simplified rule was proposed for k_{fw}:

$$k_{fw} = \begin{cases} 0.6, & \text{S355} \\ 0.7, & \text{S700} \\ \text{linear interpolation between} \end{cases} \tag{32}$$

Introducing Eq. (32) to Eq. (31), the equation for b_{eq} can be presented as

$$b_{eq} = \begin{cases} b_1 + 1.7a_w, & \text{S355} \\ b_1 + 2.0a_w, & \text{S700} \\ \text{linear interpolation between} \end{cases} \tag{33}$$

TABLE 6. Influence of fillet welds: validation of the proposed equation.

Joint	b_1 [mm]	β	k_{fw}	b_{eq} [mm]	β_{eq}	$S_{j,ini}$ [kNm/rad]				
						no welds	with welds	test	no welds / test	with welds / test
S420_S420_a6	100.3	0.66	0.62	110.8	0.73	804	1010	1115	0.72	0.91
S500_S420_a6	100.2	0.67	0.62	110.7	0.74	892	1131	1083	0.82	1.04
S500_S500_a6	100.7	0.67	0.64	111.6	0.74	890	1140	995	0.89	1.15
S700_S420_a6	101.0	0.67	0.62	111.5	0.74	862	1092	1082	0.80	1.01
S700_S500_a6	100.5	0.67	0.64	111.4	0.74	859	1097	1108	0.78	0.99
S700_S500_a6_WiPF	100.6	0.67	0.64	111.5	0.74	859	1097	1282	0.67	0.86
S700_S700_a6	120.6	0.80	0.70	132.5	0.88	1982	2865	1990	1.00	1.44
Average									**0.81**	**1.06**
S420_S420_a10	100.9	0.67	0.62	118.4	0.78	814	1235	1692	0.48	0.73
S500_S420_a10	100.8	0.67	0.62	118.3	0.79	894	1370	1701	0.53	0.81
S500_S500_a10	100.5	0.67	0.64	118.7	0.79	895	1397	1452	0.62	0.96
S700_S420_a10	100.8	0.67	0.62	118.3	0.78	847	1287	1521	0.56	0.85
S700_S500_a10	100.6	0.67	0.64	118.8	0.79	856	1325	1705	0.50	0.78
S700_S500_a10_WiPF	100.6	0.67	0.64	118.7	0.79	852	1316	1455	0.59	0.90
S700_S700_a10	120.6	0.80	0.70	140.4	0.93	2009	3593	2268	0.89	1.58
Average									**0.59**	**0.94**
S420_S420_1/2v	100.3	0.67	-	100.3	0.67	828	828	893	0.93	0.93
S500_S420_1/2v	100.8	0.67	-	100.8	0.67	896	896	977	0.92	0.92
S500_S500_1/2v	100.6	0.67	-	100.6	0.67	897	897	1003	0.89	0.89
S700_S420_1/2v	100.9	0.67	-	100.9	0.67	854	854	971	0.88	0.88
S700_S500_1/2v	100.2	0.67	-	100.2	0.67	873	873	961	0.91	0.91
S700_S700_1/2v	121.5	0.81	-	121.5	0.81	2084	2084	1990	1.05	1.05
Average									**0.93**	**0.93**

This thesis validates the proposed equation against the results of the HAMK tests, discussed earlier in Section 2.8.1. The theoretical stiffness of the joints is calculated using the approach developed in **Article II** (Section 2.3), which also provides the experimental values of stiffness. The results of the validation are collected in TABLE 6, where "no welds", "with welds" and "test" respectively denote theoretical stiffness ignoring the influence of welds, theoretical stiffness including it and experimental stiffness. As can be seen, the consideration of welds allows to obtain significantly more accurate prediction of stiffness. It should be noted that the stiffness is noticeably overestimated for the cases with the nominal $\beta = 0.80$. Such error can be caused by the greater influence of β on the stiffness of joints when β approaches 0.85. In addition, Eq. (33) correlates with the solution of de Matos et al. (2015), who proposed a similar equation for axially loaded T joints:

$$b_{eq} = b_1 + 1.6a_w \tag{34}$$

The developed approach can be recommended as a rule of thumb to consider the improving effect of fillet welds on the rotational stiffness of RHS Y joints, including T joints. At the same time, an additional research is required to extend it to other loading cases as well as develop a similar equation for resistance.

It should be noted that the beneficial effect of fillet welds significantly influences the conclusions on HSS reduction factors (see Section 2.6): using an increased β can require the introduction of less favorable (smaller) HSS reduction factors. If the influence of fillet welds is included into the standards, the HSS reduction factors have to be carefully redefined to avoid unsafe results.

2.9 Surrogate model for initial stiffness of RHS Y joints

Sometimes the optimization of tubular structures requires their structural properties to be calculated extremely fast. In the absence of an analytical solution, surrogate modeling can serve as a reliable solution for such tasks. **Article VII** developed a surrogate model for the initial rotational stiffness of SHS Y joints. The study considered only butt-welded Y joints that followed the requirements of EN 1993-1-8:2005 (CEN 2005b) and were made of the cold-formed tubes from the catalogue of the steel manufacturer SSAB (Ongelin & Valkonen 2016).

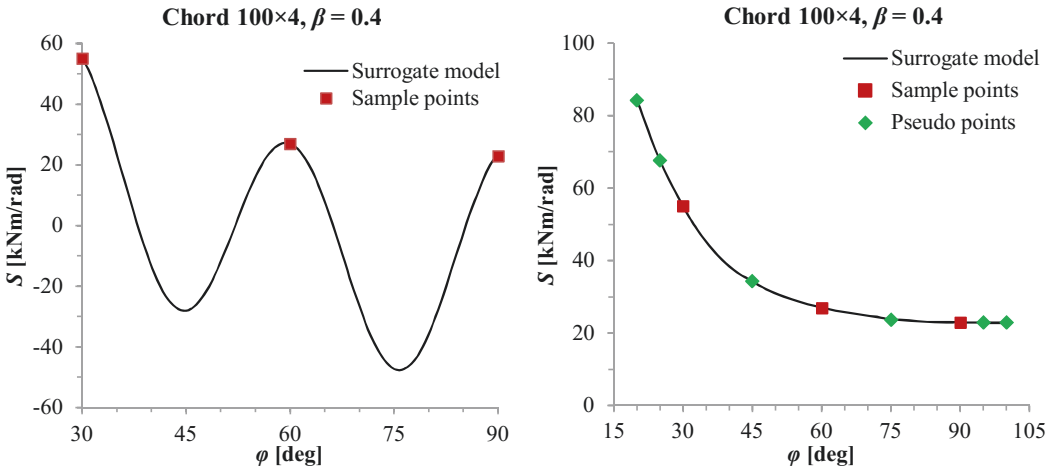

FIGURE 25. Behavior of the surrogate model: a) no pseudo points; b) with pseudo points.

The surrogate modeling employed the ooDACE toolbox for Matlab (Couckuyt et al. 2014), which was developed for the construction of metamodels by the Kriging method. The model was considered as a function of four independent variables: b_0, t_0, β and φ (FIGURE 3b). The sampling was conducted in such a way as to evenly cover the practical scope of interest and meet the requirements of the design rules. The outcome of the sample points (initial stiffness) was calculated numerically, employing the FE model developed in Section 2.3. The first attempts were unsuccessful and led to negative stiffness for some joints, as shown in FIGURE 25a,

where S denotes initial stiffness. The problem was solved by the implementation of the so-called "pseudo" points, which stabilized the behavior of the model by introducing additional boundary conditions, as demonstrated in FIGURE 25b. The pseudo points were calculated manually in MS Excel, extrapolating and interpolating the values of the sample points by polynomial regressions. This technique allowed to significantly increase the amount of the sample points without computationally demanding FE analyses. The behavior of the model in relation to some variables is provided in FIGURE 26.

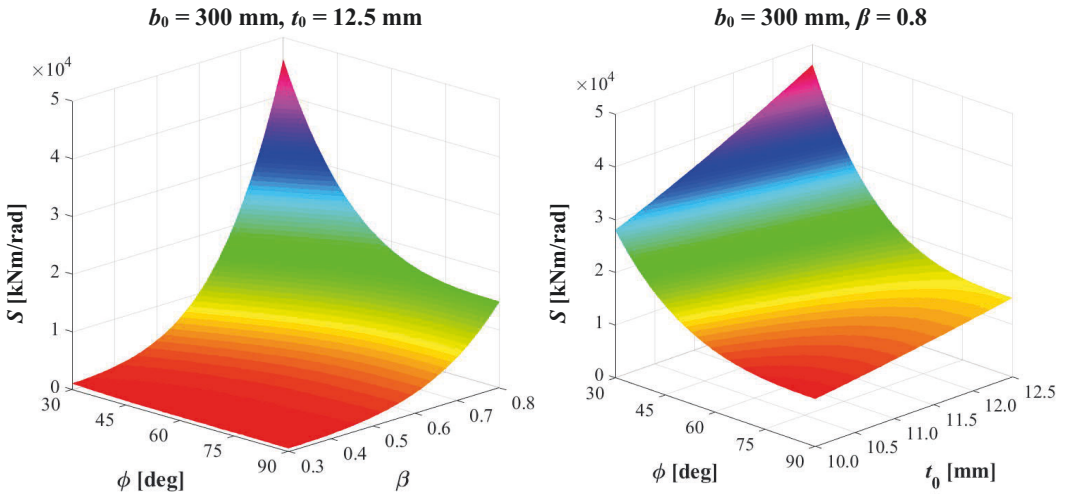

FIGURE 26. Behavior of the surrogate model in relation to the pairs of variables.

The developed model was tested using a set of independent validation points, which were calculated similarly to sample points. The validation demonstrated a good correlation with the numerical results, with $R^2 = 0.99$, average error of 4% and the maximum error of 16%. In addition, this thesis validates the model against the experimental data, which are provided in **Article II**. TABLE 7 summarizes the results of the validation, which includes the HAMK tests (Havula et al. 2018), the tests of TH Karlsruhe (Mang & Bucak 1982), the tests of the Kobe University (Kanatani et al. 1981) and the University of Thrace tests (Christitsas et al. 2007). In the table, S_{sm} and S_{exp} respectively denote initial stiffness determined by the surrogate model and experimentally. For the HAMK tests, the stiffness of the joints is computed taking into account the improving influence of fillet welds (Section 2.8); for the remaining tests, this influence is ignored since the joints violate the validity range of the proposed equation by steel properties. The accuracy of the model was evaluated by the coefficient of determination R^2. According to (Díaz et al. 2012), a metamodel can be considered as accurate if $R^2 \geq 0.85$.

TABLE 7. Validation of surrogate model.

Tests	Joint	b_0 [mm]	t_0 [mm]	β	φ [deg]	S_{sm} [kNm/rad]	S_{exp} [kNm/rad]	S_{sm} / S_{exp}	R^2
HAMK	S420_S420_a6	151.7	7.98	0.73	90	1693	1115	1.52	0.89
	S500_S420_a6	149.6	7.97	0.74	90	1844	1083	1.70	
	S500_S500_a6	149.9	7.97	0.74	90	1806	995	1.81	
	S700_S420_a6	150.7	7.91	0.74	90	1806	1082	1.67	
	S700_S500_a6	150.6	7.91	0.74	90	1779	1108	1.61	
	S700_S500_a6_WiPF	150.8	7.91	0.74	90	1781	1282	1.39	
	S700_S700_a6	150.8	7.91	0.88	90	4022	1990	2.02	
	S420_S420_a10	151.4	7.98	0.78	90	2442	1692	1.44	
	S500_S420_a10	149.7	7.97	0.79	90	2608	1701	1.53	
	S500_S500_a10	149.5	7.97	0.79	90	2634	1452	1.81	
	S700_S420_a10	151.2	7.91	0.78	90	2450	1521	1.61	
	S700_S500_a10	150.9	7.91	0.79	90	2573	1705	1.51	
	S700_S500_a10_WiPF	151.2	7.91	0.79	90	2623	1455	1.80	
	S700_S700_a10	150.5	7.91	0.93	90	4687	2268	2.07	
	S420_S420_1/2v	150.6	7.98	0.67	90	1067	893	1.20	
	S500_S420_1/2v	149.7	7.97	0.67	90	1039	977	1.06	
	S500_S500_1/2v	149.6	7.97	0.67	90	1034	1003	1.03	
	S700_S420_1/2v	150.7	7.91	0.67	90	1012	971	1.04	
	S700_S500_1/2v	150.5	7.91	0.67	90	1059	961	1.10	
	S700_S700_1/2v	150.1	7.91	0.81	90	2992	1990	1.50	
	Average							1.52	
TH Karlsruhe & Kobe University	M44	160	4	0.63	90	249	130	1.91	0.96
	M45	160	5	0.63	90	301	260	1.16	
	S12	200	9	0.75	90	3528	2000	1.76	
	S23	250	6	0.70	90	903	875	1.03	
	Average							1.47	
University of Thrace	80c150t5	150	5	0.53	90	121	135	0.89	0.94
	80c150t6	150	6	0.53	90	181	208	0.87	
	80c150t8	150	8	0.53	90	359	407	0.88	
	100c150t5	150	5	0.67	90	273	301	0.91	
	100c150t6	150	6	0.67	90	448	494	0.91	
	100c150t8	150	8	0.67	90	1125	712	1.58	
	120c150t5	150	5	0.80	90	853	741	1.15	
	120c150t6	150	6	0.80	90	1361	1366	1.00	
	120c150t8	150	8	0.80	90	2825	1927	1.47	
	Average							1.07	

As can be seen from the table, R^2 exceeds 0.85 for all the tests, meaning that the model correlates with the experimental results. However, a considerable deviation of stiffness is observed for some points, which is connected with the insufficient amount of the sample points. Increasing the amount of the sample points could have reduced the observed errors. The second reason that affects the accuracy of the results is the deviation of Young's modulus: the model employs the theoretical value of E = 210 GPa, while in the tests the values are generally lower (in the range of 190-200 GPa).

The constructed model has showed its efficiency to solve engineering tasks, for which no theoretical solution can be found. It should be noted that the model is based on the Kriging method; therefore, it behaves accurately only for the joints inside the domain of the sample points. However, outside the domain, the accuracy of results

is not guaranteed. Generally, as a surrogate model might have a considerable amount of variables, the validity range of the model should be carefully defined. Although the variation of the individual parameters can be easily determined, this can be not so straightforward when the variables are considered in combinations with each other.

2.10 Design rules for RHS T joints

This part summarizes the design rules for the resistance and initial stiffness of RHS T joints under axial loading, in-plane bending moment and out-of-plane bending moment. The rules follow the component method and contain the equations from the CIDECT report 16F (Weynand et al. 2015), hereinafter – CIDECT, as well as the equations developed in this thesis.

2.10.1 Resistance

The active components for resistance are selected in accordance with TABLE 8, where an alphanumerical code corresponds to the component in TABLE 9. The symbol "–" corresponds to an inactive component. Attention should be paid to the following issues:

1. The chord stress function for the component *b* (chord side walls in tension / compression), $k_{N,chord,b}$, is provided in CIDECT, but is not presented in EN 1993-1-8:2005 (CEN 2005b). Probably, it was included in CIDECT since it appears in the ongoing version of Eurocode. However, new Eurocode specifies it only for the case of axial loading with no extension to moment loading.
2. CIDECT provides no resistance for the component *f* (chord section in distortion), assuming that the distortion of the chord has to be prevented in the design. However, EN 1993-1-8:2005 provides a corresponding equation for this component, which has been also included in TABLE 9.
3. The equation for the component *e* (brace flange / webs in tension / compression) in the case of in-plane bending is taken from CIDECT. The same equation can be found in the new version of Eurocode. However, current EN 1993-1-8:2005 provides a slightly different equation:

$$F_{e,ip,Rd} = \frac{W_{pl,1} - \left(1 - b_{eff} / b_1\right) b_1 t_1 h_1}{2 t_1 \left(h_1 - t_1\right)} \tag{35}$$

4. The resistances of the component *g* (welds) are developed in Section 2.6.

TABLE 8. Active components for resistance.

Compo-nent	Axial force			In-plane moment		Out-of-plane moment	
	$\beta \le 0.85$	$0.85 < \beta \le (1–1/\gamma)$	$\beta > (1–1/\gamma)$	$\beta \le 0.85$	$0.85 < \beta \le 1.0$	$\beta \le 0.85$	$0.85 < \beta \le 1.0$
a	a-1	–	–	a-2	–	a-3	–
b	–	b-1	b-1	–	b-2	–	b-3
c	–	–	–	–	–	–	–
d	–	d-1	–	–	–	–	–
e	–	e-1	e-1	–	e-2	–	e-3
f	–	–	–	–	–	–	f-1
g	g-1	g-1	g-1	g-2	g-2	g-3	g-3

TABLE 9. Resistances of components.

<table>
<tr><td rowspan="2">a</td><td colspan="3">$F_{a,Rd} = 0.25 f_{y0} \cdot t_0^2 \cdot \left(0.5\overline{l}_{eff,1,a} + \overline{l}_{eff,2,a}\right) \cdot k_{N,chord,a} / \gamma_{M5}$</td></tr>
<tr><td>$\overline{l}_{eff,1,a}$</td><td>$\overline{l}_{eff,2,a}$</td><td>$k_{N,chord,a}$</td></tr>
<tr><td>a-1</td><td>$\dfrac{4\eta}{1-\beta}$</td><td>$\dfrac{4}{\sqrt{1-\beta}}$</td><td rowspan="3">$k_{N,chord,a} = \begin{cases} 1.3 - 0.4n/\beta, & n > 0 \\ 1.0, & n \le 0 \end{cases}$</td></tr>
<tr><td>a-2</td><td>$\dfrac{h_1}{h_1 - t_1}\left(\dfrac{4\eta}{1-\beta} + \dfrac{2}{\eta} + \dfrac{8t_1}{h_1\sqrt{1-\beta}}\right)$</td><td>$\dfrac{4}{\sqrt{1-\beta}}$</td></tr>
<tr><td>a-3</td><td>$\dfrac{2h_1(1+\beta)}{(b_1 - t_1)(1-\beta)}$</td><td>$\dfrac{2b_1}{b_1 - t_1}\sqrt{\dfrac{2(1+\beta)}{\beta(1-\beta)}}$</td></tr>
<tr><td rowspan="2">b</td><td colspan="3">$F_{b,Rd} = b_{eff,b} \cdot k_{N,chord,b} \cdot \chi \cdot f_{y0} \cdot t_0 / \gamma_{M5}$</td></tr>
<tr><td>$b_{eff,b}$</td><td>χ</td><td>$k_{N,chord,b}$</td></tr>
<tr><td>b-1</td><td>For $\beta = 1.0$:
$0.5(h_1 + 5t_0)$ [1)]</td><td>$\chi = \begin{cases} 1.0, & \text{tension} \\ f(\bar{\lambda}), & \text{compression} \end{cases}$ [2)]</td><td rowspan="3">$k_{N,chord,b} = \begin{cases} 1.3 - 0.4n/\beta, & n > 0 \\ 1.0, & n \le 0 \end{cases}$</td></tr>
<tr><td>b-2</td><td>$\dfrac{(h_1 + 5t_0)^2}{4(h_1 - t_1)}$</td><td>1.0</td></tr>
<tr><td>b-3</td><td>$\dfrac{(b_0 - t_0)(h_1 + 5t_0)}{2(b_1 - t_1)}$</td><td>1.0</td></tr>
<tr><td rowspan="2">d</td><td colspan="3">$F_{d,Rd} = b_{eff,d} \cdot f_{y0} \cdot t_0 / \sqrt{3} / \gamma_{M5}$</td></tr>
<tr><td>$b_{eff,d}$</td><td>$b_{e,p}$</td><td></td></tr>
<tr><td>d-1</td><td>$0.5(h_1 + b_{e,p})$</td><td>$10 t_0 \beta \le b_1$</td><td></td></tr>
<tr><td rowspan="2">e</td><td colspan="3">$F_{e,Rd} = b_{eff,e} \cdot f_{y1} \cdot t_1 / \gamma_{M5}$</td></tr>
<tr><td>$b_{eff,e}$</td><td>b_{eff}</td><td></td></tr>
<tr><td>e-1</td><td>$0.5(h_1 - 2t_1 + b_{eff})$</td><td rowspan="2">$10 t_0 \beta \cdot \dfrac{f_{y0} t_0}{f_{y1} t_1} \le b_1$</td><td></td></tr>
<tr><td>e-2</td><td>$\dfrac{W_{pl,1} - (1 - b_{eff}/b_1) b_1 t_1 (h_1 - t_1)}{2 t_1 (h_1 - t_1)}$</td><td></td></tr>
</table>

e-3	$\dfrac{W_{pl,1}-0.5\left(1-b_{eff}/b_1\right)^2 b_1^2 t_1}{2t_1\left(b_1-t_1\right)}$		
f	$F_{f,Rd}=b_{eff,f}\cdot f_{y0}\cdot t_0/\gamma_{M5}$		
	$b_{eff,f}$		
f-1	$\dfrac{h_1 t_0+\sqrt{b_0 h_0 t_0\left(b_0+h_0\right)}}{b_1-t_1}$		
g	$F_{g,Rd}=\dfrac{A_{eff}\,f_u}{2\sqrt{2}\beta_w\gamma_{M2}}$ [3)]		
	A_{eff}	f_u	β_w
g-1	$a_w\left(b_1+h_1\right)$	$\min\left\{f_{u0};\,f_{u1}\right\}$	$\beta_w=\begin{cases}0.80, & \text{S235}\\ 0.85, & \text{S275}\\ 0.90, & \text{S235}\\ 1.00, & \text{S420, S460}\end{cases}$
g-2	$a_w b_1$		
g-3	$a_w h_1$		

[1)] For $0.85 \le \beta \le 1.0$ linear interpolation between the component a at $\beta = 0.85$ and the component b at $\beta = 1.0$.

[2)] χ is the reduction factor for flexural buckling obtained from EN 1993-1-1 (CEN 2005a) using the relevant buckling curve and a normalized slenderness $\bar{\lambda}$ determined from:

$$\bar{\lambda}=3.46\frac{h_0/t_0-2}{\pi\sqrt{E/f_{y0}}} \tag{36}$$

[3)] Only fillet welds with a throat thickness of a_w.

Limiting resistances are determined among the active ones as

$$\begin{aligned}F_{N,\min,Rd}&=\min_{i=a}^{i=g}F_{i,N,Rd}\\ F_{ip,\min,Rd}&=\min_{i=a}^{i=g}F_{i,ip,Rd}\\ F_{op,\min,Rd}&=\min_{i=a}^{i=g}F_{i,op,Rd}\end{aligned} \tag{37}$$

Finally, the resistances of the joint are computed using the following equations:

$$\begin{aligned}N_{Rd}&=4F_{N,\min,Rd}\\ M_{ip,Rd}&=2F_{ip,\min,Rd}\cdot\left(h_1-t_1\right)\\ M_{op,Rd}&=2F_{op,\min,Rd}\cdot\left(b_1-t_1\right)\end{aligned} \tag{38}$$

For steel grades with a nominal yield strength greater than 355 MPa, the resistances should be multiplied by the HSS reduction factors, which are collected in TABLE 10 for the three loading cases and four steel grades. For intermediate grades, the factor can be computed by a linear interpolation.

TABLE 10. HSS reduction factors.

	Axial loading	In-plane bending		Out-of-plane bending
		butt welds	fillet welds	
S420	1.0	0.9	1.0	no data
S500	1.0	0.8	1.0	no data
S700	0.9	0.8	0.9	no data
S960	0.8	no data	no data	no data

2.10.2 Initial stiffness

The active components for initial stiffness are selected in accordance with TABLE 11, where an alphanumerical code corresponds to the component in 0. The symbol "∞" corresponds to an inactive component (a component with "infinite" stiffness).

TABLE 11. Active components for initial stiffness.

Component	Axial force		In-plane moment		Out-of-plane moment	
	$\beta \le 0.85$	$0.85 < \beta \le 1.0$	$\beta \le 0.85$	$0.85 < \beta \le 1.0$	$\beta \le 0.85$	$0.85 < \beta \le 1.0$
a	a-1	∞	a-2	∞	a-3	∞
b	b-1	b-1	b-2	b-2	b-3	b-3
c	∞	∞	c-1	c-1	∞	∞
d	∞	∞	∞	∞	∞	∞
e	∞	∞	∞	∞	∞	∞
f	∞	∞	∞	∞	f-1	f-1
g	∞	∞	∞	∞	∞	∞

It should be noted that the equations for the stiffness of the components were simplified to be presented in the shortest and most convenient form, e.g. the stiffness of the component *a* for in-plane bending was simplified as follows:

$$k_{a,ip} = \frac{20 t_0^3 l_{eff}}{(1-\beta)^3 b_0^3} \cdot \frac{1}{2+\frac{6\beta}{1-\beta}} = \frac{20 t_0^3 l_{eff}}{(1-\beta)^3 b_0^3} \cdot \frac{1-\beta}{2+4\beta} = \frac{20 t_0^3 l_{eff}}{(1-\beta)^2 b_0^3 (2+4\beta)} \tag{39}$$

In addition, **Articles II** and **VIII**, which respectively considered initial in-plane and axial stiffness, employed the different definition of components than is used in the original concept of the component method (**Article I**). To avoid a possible confusion and go in line with the originally denoted components, the stiffness equations were modified in the corresponding way. For example, the component *a* (chord face in bending) in case of axial stiffness was developed for the whole section of the brace, which corresponds to four strings working simultaneously:

TABLE 12. Stiffnesses of components.

a	k_a	l_{eff}	
a-1	$\frac{l_{eff}t_0^3}{\left(b_0-2t_0-b_1\right)^3}$	$h_1\left(2-\beta\right)+1.25b_0\left(1-\beta\right)$	
a-2	$\frac{10t_0^3 l_{eff}}{\left(1-\beta\right)^2 b_0^3\left(2+4\beta\right)}$	$t_1+2b_0\sqrt{1-\beta}$	
a-3	not solved		
b	k_b	b_{eff}	$l_{eff,cw}$
b-1	$\frac{0.5b_{eff}t_0}{h_0-t_0}$	$0.025\left(h_1\left(9\beta-1\right)+\frac{2.4b_0}{1.2-\beta}\right)$	
b-2	$\frac{b_{eff}t_0}{h_0-3t_0}$	$1.4l_{eff,cw}+t_1$	$\max\begin{cases}\sqrt{0.5t_0b_0}\le 2.5t_0\\ 0.5b_0\sqrt{1-\beta}\le 0.5h_0\end{cases}$
b-3	not solved		
c	k_c		
c-1	$\frac{0.38t_0\left(h_0-t_0\right)}{h_1}$		
f	k_f		
f-1	not solved		

$$k_{a,N}=\frac{4l_{eff}t_0^3}{\left(b_0-2t_0-b_1\right)^3} \tag{40}$$

To apply it for a single string located in the corner of the brace, the stiffness was divided by 4:

$$k_{a,N}=\frac{l_{eff}t_0^3}{\left(b_0-2t_0-b_1\right)^3} \tag{41}$$

Similarly, the component *a* in case of in-plane bending, Eq. (39), was developed for the compressed flange of the brace, which corresponds to two strings. To apply it for a single string located in the corner of the brace, the stiffness was divided by 2:

$$k_{a,ip}=\frac{10t_0^3 l_{eff}}{\left(1-\beta\right)^2 b_0^3\left(2+4\beta\right)} \tag{42}$$

Equivalent stiffnesses can be calculated as

$$k_{eq,N}=\frac{1}{\sum_{i=a}^{i=g}\frac{1}{k_{i,N}}};\quad k_{eq,ip}=\frac{1}{\sum_{i=a}^{i=g}\frac{1}{k_{i,ip}}};\quad k_{eq,op}=\frac{1}{\sum_{i=a}^{i=g}\frac{1}{k_{i,op}}} \tag{43}$$

The inactive components (the components with infinite stiffness) do not have to be included in Eq. (43). The components *a* and *b* in case of in-plane bending ($k_{a,ip}$ and $k_{b,ip}$) must be included in Eq. (43) separately for a compressive and a tensile parts.

Finally, the initial stiffnesses of the joint are computed using the following equations:

$$\begin{aligned} C_{j,ini,N} &= 4Ek_{eq,N}k_{sn,N} \\ S_{j,ini,ip} &= 2Eh_1^2 k_{eq,ip}k_{sn,ip} \\ S_{j,ini,op} &= 2Eb_1^2 k_{eq,op}k_{sn,op} \end{aligned} \tag{44}$$

Unless actual Young's modulus is not known, the value of E = 210 GPa is recommended in Eq. (44).

The chord stress function for initial axial stiffness:

$$\begin{aligned} k_{sn,N} &= \begin{cases} 1+10^{-5}\cdot f(\beta)f(\gamma)f\left(f_{y0}\right)n; & 355\ \text{MPa} \le f_{y0} \le 500\ \text{MPa} \\ \text{linear interpolation between S500 and S700}; & 500\ \text{MPa} < f_{y0} < 700\ \text{MPa} \\ 1+0.0008\cdot f(\beta)f(\gamma)\left(n^3-1.25n^2+1.92n\right); & f_{y0} = 700\ \text{MPa} \end{cases} \\ &-0.95 \le n \le 0.95 \end{aligned} \tag{45}$$

where

$$\begin{aligned} f(\beta) &= -2\beta^2 + 1.6\beta + 0.3 \\ f(\gamma) &= 1.3\gamma^2 - 38 \\ f\left(f_{y0}\right) &= 0.02 f_{y0}^{\ 1.4} \end{aligned} \tag{46}$$

The chord stress function for initial in-plane rotational stiffness:

$$\begin{aligned} &\text{For } 0.25 \le \beta \le 0.85: \\ &k_{sn,ip} = \begin{cases} 1+0.001\gamma^2\left(1+1.7\beta-2.6\beta^2\right)\cdot n - 2.7\left(|n|-0.8\right)^2, & -0.99 \le n < -0.8 \\ 1+0.001\gamma^2\left(1+1.7\beta-2.6\beta^2\right)\cdot n, & -0.8 < n < 0.8 \\ 1+0.001\gamma^2\left(1+1.7\beta-2.6\beta^2\right)\cdot n - 3.1\left(n-0.8\right)^2, & 0.8 < n \le 0.99 \end{cases} \\ &\text{For } 0.85 < \beta < 1.0: \\ &k_{sn,ip} \text{ is the linear interpolation between } \beta = 0.85 \text{ and } \beta = 1.0 \\ &\text{For } \beta = 1.0: \\ &k_{sn,ip} = \begin{cases} 1+0.06n - 3.5\left(|n|-0.8\right)^2, & -0.99 \le n < -0.8 \\ 1+0.06n, & -0.8 < n < 0.8 \\ 1+0.06n - 2.8\left(n-0.8\right)^2, & 0.8 < n \le 0.99 \end{cases} \end{aligned} \tag{47}$$

No chord stress function has been developed for initial out-of-plane rotational stiffness.

3 Conclusions

3.1 The outcome of the research

The main objective of this thesis was to make a step forward in the application of the component method to the design of tubular joints. Following the existing research conducted by CIDECT, the study tried to solve the most challenging issues of the component method in relation to RHS T joints under three loading cases, namely axial loading, in-plane bending and out-of-plane bending. The verification of the component method with EN 1993-1-8:2005 demonstrated that the method employs the inverted Eurocode equations and therefore provides the same resistance of joints. However, the main concerns of the method relate to the design of initial stiffness.

To employ extensive numerical studies in the analyses, the thesis developed a FE model for RHS T joints. The model was constructed with two quadratic solid finite elements in the thickness direction. Some recommendations are proposed in regards to the required length of the members and the possibilities for the modeling of butt and fillet welds. In addition, the thesis presented three methods to investigate pure axial loading of the joint, preventing the in-plane bending of the chord. The FE model was employed further in the thesis to develop the design equations for the initial stiffness of joints, investigate the influence of initial imperfections and fillet welds, as well as the surrogate modeling.

The main attention of the thesis was paid to the initial stiffness of RHS T joints. The validation with the experimental results showed that the theoretical solution provided by CIDECT considerably underestimates the in-plane rotational stiffness of joints. A more accurate equation was proposed for the component “chord face in bending”. The equation demonstrated good correlation with the experimental data. In terms of initial axial stiffness, the CIDECT report showed consid-

erable overestimation of the experimental values. New equations were developed for the components “chord face in bending” and “chord side walls in compression”. In addition, the thesis numerically investigated the influence of chord axial stresses on the initial rotational and axial stiffness of RHS T joints. The compressive stresses were found to reduce considerably the stiffness of joints, with the opposite trend for tensile stresses. The influence was found particularly strong for the joints with small braces ($\beta = 0.25$) and wall thickness ($2\gamma = 35$). To consider this effect in the design, the thesis developed and verified corresponding chord stress functions.

Another part of the thesis investigated the beneficial effect of fillet welds on the structural behavior of tubular joints. The FE analyses of RHS Y joints demonstrated that the joints with full-strength fillet welds had considerably higher initial stiffness than the identical joints with butt welds. The influence was particularly strong for the joints with high β, reaching more than 2.0 times for S355 and more than 3.0 times for S700. The observed phenomenon was also supported by a series of experimental results on RHS T joints, which demonstrated the difference of 60% between the resistance and stiffness of the joints with large fillet welds and the butt-welded joints. The current building standards do not take this effect into account, providing the same resistance regardless the type and the size of welds. To avoid conservative results, the thesis proposed a simple equation to consider the influence of fillet welds on the initial in-plane stiffness of RHS Y joints. Although the equation is based on a limited number of joints, additional studies can be conducted to develop a more general solution, incorporating resistance and other loading cases.

Attention was also paid to the issue of the reduction factors for HSS tubular joints. A study analyzed the experimental results of HSS RHS T joints under in-plane bending with varying geometry, steel grades and three types of welds. The comparison between the experimental results and the existing Eurocode equation for moment resistance demonstrated the need for the reduction factors only for butt-welded joints. The joints with large fillet welds showed sufficiently safe resistance without any reduction. Applying the factors for these joints would have led to excessively conservative results. The necessity of the reduction for the joints with small fillet welds depended on the steel grade: the factors were needed only for the joints with steel grades above S500. In all cases, the required reduction coefficients were greater than those specified by Eurocode, leading to smaller reduction of resistance. The thesis proposes certain values of the reduction coefficients (factors) for moment-loaded joints, depending on the steel properties and the relative throat thickness of the weld. The proposed coefficients well correlate with the observations of other researchers for axially loaded RHS joints. It should be noted that the recommended values of the reduction factors do not consider the substantial beneficial influence of fillet welds. If this effect is accepted in the standards, the recommended values of the HSS reduction factors have to be further specified.

The same experimental data was used to evaluate the ductility of HSS RHS joints. The results showed that all considered joints demonstrated sufficient rotation capacity, clearly exceeding the

specified 3%b_0 deformation limit for tubular joints. This finding allows to conclude that RHS T joints can be safely designed with undersized welds (welds smaller than full-strength fillet welds), provided that the resistance of welds is checked. This finding is supported for axially loaded joints by the recent European research (Feldmann et al. 2016).

In addition, the thesis considered the influence of initial imperfections on the behavior of RHS T joints, such as welding residual stresses and initial geometric imperfections. Welding residual stresses were investigated numerically, with the simulation of the welding process and the subsequent static loading of the joint under in-plane bending moment and axial loading. The results showed that the welding sequence did not influence the structural behavior of the analyzed joints; therefore, the idealized simplified sequence was proposed to reduce computational efforts. In the considered range of joints, welding residual stresses were found to increase the resistance of joints. The conducted parametric studies demonstrated that the improving effect was particularly pronounced for the joints with small wall thickness (large 2γ ratio), reaching 19% for in-plane bending and 17% for axial loading. The observed influence on initial stiffness was insignificant. The obtained results allow to conclude that welding residual stresses can be safely ignored in the theoretical and numerical design of RHS T joints, with no unbeneficial consequences.

The influence of initial geometrical imperfections was investigated numerically, considering RHS T joints under in-plane bending and axial loading. The analyses employed the common approach for the modeling of geometrical imperfections on thin-walled structures, applying scaled buckling modes to the joint with perfect geometry. The buckling modes were scaled according to the allowable tolerances specified in Eurocode. In case of axial loading, the most conservative results were observed when imperfections were modelled by the buckling mode that repeats the deformation pattern under the corresponding loading. In case of in-plane bending moment, none of the buckling modes was found suitable for modeling imperfections; therefore, they were simulated using the modes from axial loading. The conducted parametric studies demonstrated the reducing effect of imperfections on the resistances and initial stiffness of the tested joints, both those governed by chord face failure ($\beta \leq 0.85$), and those governed by chord side walls failure ($\beta > 0.85$). However, the effect was inconsiderable, reaching 5% for resistance and 7% for initial stiffness. In practice, such small reductions do not have to be considered in the design.

Finally, the thesis developed a surrogate model for initial rotational stiffness of RHS Y joints. The model was constructed employing the Kriging method and using the sample points calculated numerically. The model considered the joints in the whole range of the practical interest, following the limitations of Eurocode. The model allowed to receive an immediate and relatively accurate outcome without considerable computational efforts. Such a method demonstrated that surrogate modeling can represent a very effective tool for the engineering tasks with extensive computations and for which no analytical solution exists.

3.2 The need for further research

3.2.1 Initial stiffness of joints

It should be noted that to derive the stiffness equations, the thesis employs the "effective length" concept, which is associated to the formation of a yield mechanism. In reality, the effective length to be considered in the elastic range is not the same as the one used in the design of resistance. To overcome this obstacle for the components of open section joints, the relation has been derived between the "elastic effective length" and the "plastic effective length". Based on that, Eurocode presents stiffness equations that artificially depend on the "plastic effective lengths", while in reality they are based on elastic effective length values. A similar concept can be also utilized in future works for tubular joints to develop stiffness coefficients that are in line with the existing design of resistance.

3.2.2 Out-of-plane bending

Although the structural behavior of tubular joints under axial loading and in-plane bending has been investigated in this thesis and many other publications, there is still a lack of research on RHS T joints under out-of-plane bending. Some additional research can be conducted to check the reliability of the Eurocode equation for chord distortion. In addition, considerable research is required to investigate initial stiffness under this type of loading.

A series of tests on HSS RHS T joints under out-of-plane bending is planned to be conducted in the nearest future. The experimental program includes the joints with varying geometry (β, 2γ), steel grades (S420, S500, S700) and weld types (fillet welds with different throat thickness). The geometry of the joints is selected so that the joints are going to fail from chord face bending, chord side walls buckling and the combination of the two. The aims of the tests include:

- to check the existing component method rules for the resistance of joints
- to determine the relevance of the reduction factors for HSS joints
- to evaluate the influence of fillet welds on the structural behavior of joints
- to develop and validate equations for initial out-of-plane rotational stiffness with corresponding chord stress functions

3.2.3 Beneficial influence of fillet welds

The experimental research and the extensive numerical simulations conducted in this thesis demonstrated a considerable improving effect of fillet welds on the structural behavior of RHS joints. The current design guides for tubular joints do not consider this influence, providing the same theoretical equation regardless the type of welds. However, this thesis demonstrated that a

RHS T joint might have 60% higher resistance and stiffness if large fillet welds are used instead of butt welds. In addition, some Y joints with full-strength fillet welds showed 3 times higher initial rotational stiffness than the butt-welded joints with matching geometry. Such underestimation of structural behavior may lead to the situation that the whole potential of high strength steels is not realized in the construction industry, making the application of high strength steels not as beneficial as it can be.

This thesis proposed an equation to take into account the size of fillet welds in the design of initial rotational stiffness of SHS Y joints. Additional numerical studies supported by experimental tests are required to develop a similar rule of thumb for resistance, considering RHS joints in the whole scope of applications specified by the design rules. However, the beneficial effect of fillet welds on the resistance of tubular joints can noticeably affect the HSS reduction factors. If the former is accepted in the standards, the HSS reduction factors have to be correspondingly adjusted to avoid unsafe results due to the simultaneous consideration of these two issues.

3.2.4 Issues of high strength steels

The thesis shows that the existing design rules cannot be applied for HSS joints without corresponding adjustments by the reduction factors. At the same time, the conducted research demonstrates that no single conclusion can be made in relation to the relevance of these factors. In this research, the reduction factors were investigated for SHS T joints with chord face failure as a governing failure mode, a single 2γ ratio and under in-plane bending. Additional experimental studies are required to extend the presented conclusions to joints with other failure modes and loading cases, considering the geometry on the whole scope specified by the design standards.

3.2.5 Practical aspects in the design of tubular joints

This thesis pays particular attention to the design of initial stiffness of RHS joints, since it has been shown to be the main parameter that affects the buckling of members in tubular trusses. In particular, previous studies have shown that in a tubular truss, the consideration of initial stiffness can reduce the effective lengths of compressed diagonals or posts. However, the actual practical benefits resulted from this assumption are not yet clear. In the future, this issue can be further investigated by conducting a design of a tubular truss, taking into account the initial stiffness of joints. The design should also incorporate the issues addressed in this thesis, i.e. the chord stress functions for initial stiffness and the beneficial influence of fillet welds. A similar design can be also conducted for welded portal frames, which are widely utilized in industry. Such frames usually operate under heavy loads with considerable chord stress functions in joints.

References

Abaqus, 2012. *Abaqus 6.12. Getting Started with Abaqus: Interactive Edition*, Dassault Systèmes, 695 p.

AlHendi, H. & Celikag, M., 2015. Behavior of reverse-channel and double-reverse-channel connections to tubular columns with HSS. *Journal of Constructional Steel Research*, 112, pp. 271–281.

Bate, S.K., Charles, R. & Warren, A., 2009. Finite element analysis of a single bead-on-plate specimen using SYSWELD. *International Journal of Pressure Vessels and Piping*, 86(1), pp. 73–78.

Becque, J. & Wilkinson, T., 2017. The capacity of grade C450 cold-formed rectangular hollow section T and X connections: An experimental investigation. *Journal of Constructional Steel Research*, 133, pp. 345–359.

Bel Hadj Ali, N., Sellami, M., Cutting-Decelle, A.-F. & Mangin, J.-C., 2009. Multi-stage production cost optimization of semi-rigid steel frames using genetic algorithms. *Engineering Structures*, 31(11), pp. 2766–2778.

Björk, T. & Saastamoinen, H., 2012. Capacity of CFRHS X-joints made of double-grade S420 steel. In L. Gardner, ed. *Tubular Structures XIV - Proceedings of the 14th International Symposium on Tubular Structures, ISTS 2012, London, United Kingdom, 12-14 September 2012*. London: Taylor & Francis Group, pp. 167–176.

Block, F.M., Burgess, I.W., Davison, J.B. & Plank, R.J., 2007. The development of a component-based connection element for endplate connections in fire. *Fire Safety Journal*, 42(6–7), pp. 498–506.

Boel, H., 2010. *Buckling length factors of hollow section members in lattice girders*, Master Thesis. Eindhoven: Eindhoven University of Technology.

Brar, G.S. & Singh, C.S., 2014. FEA of residual stress in cruciform welded joint of hollow sectional tubes. *Journal of Constructional Steel Research*, 102, pp. 44–58.

Brockenbrough, R.L., 1972. Strength of square-tube connections under combined loads. *Journal of the Structural Division*, 98(12), pp. 2753–2768.

Bučmys, Ž., Daniūnas, A., Jaspart, J.-P. & Demonceau, J.F., 2018. A component method for cold-formed steel beam-to-column bolted gusset plate joints. *Thin-Walled Structures*, 123(October 2016), pp. 520–527.

Bursi, O.S. & Jaspart, J.-P., 1998. Basic issues in the finite element simulation of extended end plate connections. *Computers & Structures*, 69(3), pp. 361–382.

Bzdawka, K., 2012. *Optimization of office building frame with semi-rigid joints in normal and fire conditions*, Doctor of Science thesis. Tampere: Tampere University of Technology, Publication 1038.

CEN, 2006a. *Cold formed welded structural hollow sections of non-alloy and fine grain steels. Part 2: Tolerances, dimensions and sectional properties (EN 10219-2:2006)*, Brussels.

CEN, 2005a. *Eurocode 3: Design of steel structures – Part 1-1: General rules and rules for buildings (EN 1993-1-1:2005)*, Brussels.

CEN, 2005b. *Eurocode 3: Design of steel structures – Part 1-8: Design of joints (EN 1993-1-8:2005)*, Brussels.

CEN, 2007. *Eurocode 3 – Design of steel structures – Part 1-12: Additional rules for the extension of EN 1993 up to steel grades S 700 (EN 1993-1-12: 2007)*, Brussels.

CEN, 2006b. *Eurocode 3 – Design of steel structures – Part 1-5: Plated structural elements (EN 1993-1-5:2006)*, Brussels.

Chen, C., Zhao, M.-S., Fung, T.-C., Chiew, S.P. & Lee, C.-K., 2017. Influence of welding on mechanical properties of high strength steel butt joints. In *The 8th European Conference on Steel and Composite Structures (Eurosteel 2017). Copenhagen, Denmark, 13–15 September 2017*.

Christitsas, A.D., Pachoumis, D.T., Kalfas, C.N. & Galoussis, E.G., 2007. FEM analysis of conventional and square bird-beak SHS joint subject to in-plane bending moment — experimental study. *Journal of Constructional Steel Research*, 63(10), pp. 1361–1372.

Couckuyt, I., Dhaene, T. & Demeester, P., 2014. ooDACE Toolbox: a flexible object-oriented Kriging implementation. *Journal of Machine Learning Research*, 15, pp. 3183–3186.

D'Antimo, M., Latour, M., Rizzano, G., Demonceau, J.F. & Jaspart, J.-P., 2018. Preliminary study on beam-to-column joints under impact loading. *The Open Construction and Building Technology Journal*, 12(Suppl-1, M5), pp. 112–123.

Davie, J. & Giddings, T.W., 1971. Research into the strength of welded lattice girder joints in structural hollow sections. *CIDECT report 5EC/71/7/E*.

Davies, G. & Crockett, P., 1996. The strength of welded T-DT joints in rectangular and circular hollow section under variable axial loads. *Journal of Constructional Steel Research*, 37(1), pp. 1–31.

Demonceau, J.F. & Jaspart, J.-P., 2004. Experimental and analytical investigations on single-sided composite joint configurations. In J. C. Walraven, J. Blaauwendraad, T. Scarpas, & H. H. Snijder, eds. *Proceedings of the 5th International PhD Symposium in Civil Engineering*. Delft, the Netherlands: Balkema, pp. 341–349.

Díaz, C., Victoria, M., Querin, O.M. & Martí, P., 2012. Optimum design of semi-rigid connections using metamodels. *Journal of Constructional Steel Research*, 78, pp. 97–106.

Dubina, D., Ungureanu, V. & Landolfo, R., 2012. *Design of Cold-formed Steel Structures: Eurocode 3: Design of Steel Structures, Part 1-3: Design of Cold-formed Steel Structures*, ECCS.

Dunđer, M., Samardžić, I. & Klarić, Š., 2007. Influence of cooling time Δt8/5 on welded joint

properties of the thermal cycle simulated TStE 420 specimens. *Technical Gazette*, 14(1–2), pp. 47–57.

Eastwood, W. & Wood, A.A., 1971. The static strength of welded joints in structural hollow sections. *Constructional Steelwork*, 01, pp. 6–20.

Ellobody, E. & Young, B., 2005. Structural performance of cold-formed high strength stainless steel columns. *Journal of Constructional Steel Research*, 61(12), pp. 1631–1649.

Fang, C., Izzuddin, B.A., Elghazouli, A.Y. & Nethercot, D.A., 2013. Modeling of semi-rigid beam-to-column steel joints under extreme loading. *Frontiers of Structural and Civil Engineering*, 7(3), pp. 245–263.

Feldmann, M., Schillo, N., Schaffrath, S., Virdi, K., Björk, T., Tuominen, N., Veljkovic, M., Pavlovic, M., Manoleas, P., Heinisuo, M., Mela, K., Ongelin, P., Valkonen, I., Minkkinen, J., Erkkilä, J., Pétursson, E., Clarin, M., Seyr, A., Horváth, L., Kövesdi, B., Turán, P. & Somodi, B., 2016. *Rules on high strength steel*, Luxembourg: Publications Office of the European Union.

Feng, R. & Young, B., 2008. Experimental investigation of cold-formed stainless steel tubular T-joints. *Thin-Walled Structures*, 46(10), pp. 1129–1142.

Feng, R. & Young, B., 2010. Tests and behaviour of cold-formed stainless steel tubular X-joints. *Thin-Walled Structures*, 48(12), pp. 921–934.

Galambos, T. V, 1998. *Guide to stability design criteria for metal structures* 5th ed., John Wiley & Sons.

Garifullin, M., 2018. Experimental moment resistance of rectangular hollow section T joints A. Borodinecs, V. Sergeev, & N. Vatin, eds. *MATEC Web of Conferences*, 245(08003).

Girão Coelho, A.M. & Bijlaard, F.S.K., 2007. Experimental behaviour of high strength steel end-plate connections. *Journal of Constructional Steel Research*, 63(9), pp. 1228–1240.

Grierson, D.E. & Xu, L., 1993. Design optimization of steel frameworks accounting for semi-rigid connections. In G. I. N. Rozvany, ed. *Optimization of Large Structural Systems, Volume II*. Dordrecht: Kluwer Academic Publisher, pp. 873–881.

Grotmann, D. & Sedlacek, G., 1998. *Rotational stiffness of welded RHS beam-to-column joints. Cidect 5BB-8/98*, Aachen: RWTH-Aachen.

Günther, H.-P., Hildebrand, J., Rasche, C., Versch, C., Wudtke, I., Kuhlmann, U., Vormwald, M. & Werner, F., 2012. Welded connections of high-strength steels for the building industry. *Welding in the World*, 56(5–6), pp. 86–106.

Guzelbey, I.H., Cevik, A. & Gögüş, M.T., 2006. Prediction of rotation capacity of wide flange beams using neural networks. *Journal of Constructional Steel Research*, 62(10), pp. 950–961.

Haakana, Ä., 2014. *In-plane buckling and semi-rigid joints of tubular high strength steel trusses*, Master of Science Thesis. Tampere: Tampere University of Technology.

Haremza, C., Santiago, A., Demonceau, J.F., Jaspart, J.-P. & Da Silva, L.S., 2016. Composite joints under M-N at elevated temperatures. *Journal of Constructional Steel Research*, 124, pp. 173–186.

Havula, J., Garifullin, M., Heinisuo, M., Mela, K. & Pajunen, S., 2018. Moment-rotation behavior of welded tubular high strength steel T joint. *Engineering Structures*, 172, pp. 523–537.

Hayeck, M., Nseir, J., Saloumi, E. & Boissonnade, N., 2017. Experimental characterization of steel tubular beam-columns resistance by means of the Overall Interaction Concept. *Thin-Walled Structures*, In press.

Heinisuo, M., Perttola, H. & Ronni, H., 2014. A step towards the 3D component method for modelling beam-to-column joints. *Steel Construction*, 7(1), pp. 8–13.

Heinisuo, M., Ronni, H., Perttola, H., Aalto, A. & Tiainen, T., 2012. End and base plate joints with corner bolts for rectangular tubular member. *Journal of Constructional Steel Research*, 75, pp. 85–92.

Hoang, V.L., Demonceau, J.F. & Jaspart, J.-P., 2014. Resistance of through-plate component in beam-to-column joints with circular hollow columns. *Journal of Constructional Steel Research*, 92, pp. 79–89.

Hoang, V.L., Jaspart, J.-P. & Demonceau, J.F., 2015. Extended end-plate to concrete-filled rectangular column joint using long bolts. *Journal of Constructional Steel Research*, 113, pp. 156–168.

Hochhauser, F., Ernst, W., Rauch, R., Valiant, R. & Enziger, N., 2012. Influence of the soft zone on the strength of welded modern HSLA steels. *Welding in the World*, 56(5–6), pp. 77–85.

Hornung, U. & Saal, H., 1998. A method for calculating the out-of-plane buckling length of diagonals of truss girders with hollow sections and K-joints. *Journal of Constructional Steel Research*, 46(1–3), p. 489.

IIW, 2013. *ISO 14346:2013. Static design procedure for welded hollow-section joints — Recommendations*, International Institute of Welding.

Islam, M., Buijk, A., Rais-Rohani, M. & Motoyama, K., 2014. Simulation-based numerical optimization of arc welding process for reduced distortion in welded structures. *Finite Elements in Analysis and Design*, 84, pp. 54–64.

Jadid, M.N. & Fairbairn, D.R., 1996. Neural-network applications in predicting moment-curvature parameters from experimental data. *Engineering Applications of Artificial Intelligence*, 9(3), pp. 309–319.

Jaspart, J.-P., 1991. *Etude de la semi-rigidité des noeuds pouter-colonne et son influence sur la résistance et la stabilité des ossatures en acier*, Doctor of Science thesis. University of Liège (in French).

Jaspart, J.-P., Pietrapertosa, C., Weynand, K., Busse, E. & Klinkhammer, R., 2005. *Development of a full consistent design approach for bolted and welded joints in building frames and trusses between steel members made of hollow and / or open sections – Application of the*

component method. Volume 1 – Practical guidelines, CIDECT Report: 5BP-4/05.

Jaspart, J.-P. & Vandegans, D., 1998. Application of the component method to column bases. *Journal of Constructional Steel Research*, 48(2–3), pp. 89–106.

Javidan, F., Heidarpour, A., Zhao, X.-L., Hutchinson, C.R. & Minkkinen, J., 2016. Effect of weld on the mechanical properties of high strength and ultra-high strength steel tubes in fabricated hybrid sections. *Engineering Structures*, 118, pp. 16–27.

Jiao, H. & Zhao, X.-L., 2003. Imperfection, residual stress and yield slenderness limit of very high strength (VHS) circular steel tubes. *Journal of Constructional Steel Research*, 59(2), pp. 233–249.

Jiao, H., Zhao, X.-L. & Lau, A., 2015. Hardness and compressive capacity of longitudinally welded very high strength steel tubes. *Journal of Constructional Steel Research*, 114, pp. 405–416.

Johansen, K.W., 1962. *Yield line theory*, London: Cement and Concrete Association.

Kanatani, H., Fujiwara, K., Tabuchi, M. & Kamba, T., 1981. *Bending tests on T-joints of RHS chord and RHS or H-shape branch*, CIDECT Programme 5AF.

Khurshid, M., Barsoum, Z. & Barsoum, I., 2015. Load carrying capacities of butt welded joints in high strength steels. *Journal of Engineering Materials and Technology*, 137(4), p. 41003.

Kleijnen, J.P.C., 2009. Kriging metamodeling in simulation: A review. *European Journal of Operational Research*, 192(3), pp. 707–716.

Knoedel, P., Gkatzogiannis, S. & Ummenhofer, T., 2017. Practical aspects of welding residual stress simulation. *Journal of Constructional Steel Research*, 132, pp. 83–96.

Korol, R.M., El-Zanaty, M. & Brady, F.J., 1977. Unequal width connections of square hollow sections in Vierendeel trusses. *Canadian Journal of Civil Engineering*, 4(2), pp. 190–201.

Kozlowski, A., 2016. Component method model for predicting the moment resistance, stiffness and rotation capacity of minor axis composite seat and web site plate joints. *Steel and Composite Structures*, 20(3), pp. 469–486.

Leston-Jones, L., 1997. *The influence of semi-rigid connections on the performance of steel framed structures in fire*, PhD Thesis. University of Sheffield.

Li, T.Q., Choo, B.S. & Nethercot, D.A., 1995. Connection element method for the analysis of semi-rigid frames. *Journal of Constructional Steel Research*, 32(2), pp. 143–171.

de Lima, L.R.O., Vellasco, P.C.G. da S., de Andrade, S.A.L., da Silva, J.G.S. & Vellasco, M.M.B.R., 2005. Neural networks assessment of beam-to-column joints. *Journal of the Brazilian Society of Mechanical Sciences and Engineering*, 27(3), pp. 314–324.

Lipp, A. & Ummenhofer, T., 2015. Influence of tensile chord stresses on the strength of CHS X-joints – Experimental and numerical investigations. In E. de M. Batista, P. Vellasco, & L. R. O. de Lima, eds. *Tubular Structures XV: Proceedings of the 15th International*

Symposium on Tubular Structures, Rio de Janeiro, Brazil, 27-29 May 2015. London: Taylor & Francis Group, pp. 379–386.

Liu, D.K., Wardenier, J. & van der Vegte, G.J., 2004. New chord stress functions for rectangular hollow section joints. In *The Fourteenth International Offshore and Polar Engineering Conference*. International Society of Offshore and Polar Engineers, pp. 178–185.

López-Colina, C., Serrano-López, M.A., Gayarre, F.L. & Del Coz-Díaz, J.J., 2011. Stiffness of the component 'lateral faces of RHS' at high temperature. *Journal of Constructional Steel Research*, 67(12), pp. 1835–1842.

Lu, L.H., de Winkel, G.D., Yu, Y. & Wardenier, J., 1994. Deformation limit for the ultimate strength of hollow section joints. In P. Grundy, A. Holgate, & B. Wong, eds. *Tubular Structures VI, 6th International Symposium on Tubular Structures, Melbourne, Australia*. Rotterdam: Balkema, pp. 341–347.

Majumdar, A. & D'Alvise, L., 2014. Application of welding simulation method to simulate additive manufacturing. In *Proceedings of the International Symposium on Visualization in Joining&Welding Science through Advanced Measurements and Simulation (Visual-JW2014)*. pp. 105–106.

Mäkeläinen, P., Puthli, R. & Bijlaard, F., 1988. Strength, stiffness and nonlinear behaviour of simple tubular joints. *IABSE congress report*, 13, pp. 635–640.

Málaga-Chuquitaype, C. & Elghazouli, A.Y., 2010. Component-based mechanical models for blind-bolted angle connections. *Engineering Structures*, 32(10), pp. 3048–3067.

Mang, F. & Bucak, Ö., 1982. *Hohlprofilkonstruktionen. Stahlbauhandbuch*, Köln: Stahlbau-Verlag-GmbH.

de Matos, R.M.M.P., Costa-Neves, L.F. & de Lima, L.R.O., 2010. Influence of chord axial load on the stiffness and resistance of welded T joints of shs members. In E. D. M. Batista, P. C. G. S. Vellasco, & L. R. O. de Lima, eds. *SDSS'Rio 2010 International Colloquium on Stability and Ductility of Steel Structures*. Rio de Janeiro: Federal University of Rio de Janeiro, pp. 247–254.

de Matos, R.M.M.P., Costa-Neves, L.F., Lima, L.R.O. de, Vellasco, P.C.G.S. & da Silva, J.G.S., 2015a. Resistance and elastic stiffness of RHS "T" joints: part I – axial brace loading. *Latin American Journal of Solids and Structures*, 12(11), pp. 2159–2179.

de Matos, R.M.M.P., Costa-Neves, L.F., Lima, L.R.O. de, Vellasco, P.C.G.S. & da Silva, J.G.S., 2015b. Resistance and elastic stiffness of RHS "T" joints: part II – combined axial brace and chord loading. *Latin American Journal of Solids and Structures*, 12(11), pp. 2180–2207.

Ministry of Environment, 2017. *Finnish National Annex to standard SFS-EN 1993-1-12 Part 1-12: Extension of EN 1993 up to steel grades S700*.

Moradi Eshkafti, M., 2017. *Influence of various welding sequence schemes on the load bearing capacity of square hollow section T-joint*, PhD thesis. Cottbus: Brandenburg University of Technology.

Nazmeeva, T. V & Vatin, N.I., 2016. Numerical investigations of notched C-profile compressed members with initial imperfections. *Magazine of Civil Engineering*, 62(2), pp. 92–101.

Nizer, A., de Lima, L.R.O., Vellasco, P.C.G. da S., Andrade, S.A.L. de, Goulart, E. da S., Silva, A.T. da & Costa-Neves, L.F., 2016. Experimental and numerical assessment of RHS T-joints subjected to brace and chord axial forces. *Steel Construction*, 9(4), pp. 315–322.

Ongelin, P. & Valkonen, I., 2016. *SSAB Domex Tube. Structural hollow sections. EN 1993 – Handbook 2016*, SSAB Europe Oy.

Packer, J., Puthli, R., van der Vegte, G.J. & Wardenier, J., 2017. Discussion on the paper "Experimental and numerical assessment of RHS T-joints subjected to brace and chord axial forces", by Nizer et al., Steel Construction 9 (2016), No. 4, pages 315–322. *Steel Construction*, 10(1), pp. 89–90.

Packer, J.A., 1993. Moment connections between rectangular hollow sections. *Journal of Constructional Steel Research*, 25(1–2), pp. 63–81.

Packer, J.A., Davies, G. & Coutie, M.G., 1980. Yield strength of gapped joints in rectangular hollow section trusses. *Proceedings of the Institution of Civil Engineers*, 69(4), pp. 995–1013.

Packer, J.A., Wardenier, J., Zhao, X.-L., van der Vegte, G.J. & Kurobane, Y., 2009. *Design guide for rectangular hollow section (RHS) joints under predominantly static loading. CIDECT Design Guide No. 3.* 2nd ed., LSS Verlag.

Pandey, M. & Young, B., 2018. High strength steel tubular X-joints — an experimental insight under axial compression. In A. Heidarpour & X.-L. Zhao, eds. *Tubular Structures XVI: Proceedings of the 16th International Symposium for Tubular Structures (ISTS 2017, 4-6 December 2017, Melbourne, Australia)*. London: Taylor & Francis Group, pp. 223–230.

Pavlovčič, L., Detzel, A., Kuhlmann, U. & Beg, D., 2007. Shear resistance of longitudinally stiffened panels—Part 1: Tests and numerical analysis of imperfections. *Journal of Constructional Steel Research*, 63, pp. 337–350.

Perttola, H., 2017. *3D Component Method Based on the Rakes*, Doctor of Science thesis. Tampere: Tampere University of Technology, Publication 1517.

Pirinen, M., 2013. *The effects of welding heat input on the usability of high strength steels in welded structures*, Doctor of Science thesis. Lappeenranta: Lappeenranta University of Technology.

Pitrakkos, T. & Tizani, W., 2015. A component method model for blind-bolts with headed anchors in tension. *Steel and Composite Structures*, 18(5), pp. 1305–1330.

Queipo, N. V, Haftka, R.T., Shyy, W., Goel, T., Vaidyanathan, R. & Kevin Tucker, P., 2005. Surrogate-based analysis and optimization. *Progress in Aerospace Sciences*, 41, pp. 1–28.

Raoul, J., 2005. *Use and application of high-performance steels for steel structures*, Zürich, Switzerland: IABSE-AIPC-IVBH.

Ribeiro, J., Santiago, A., Rigueiro, C. & da Silva, L.S., 2015. Analytical model for the response of T-stub joint component under impact loading. *Journal of Constructional Steel Research*, 106, pp. 23–34.

Rondal, J., Würker, K.-G., Dutta, D., Wardenier, J. & Yeomans, N., 1992. *Structural stability of hollow sections*, Köln: Verlag TÜV Rheinland GmbH.

Roux, W.J., Stander, N. & Haftka, R.T., 1998. Response surface approximations for structural optimization. *International Journal for Numerical Methods in Engineering*, 42(3), pp. 517–534.

Sadeghi, S.N., Heidarpour, A., Zhao, X.-L. & Al-Mahaidi, R., 2017. An innovative I-beam to hybrid fabricated column connection: Experimental investigation. *Engineering Structures*, 148, pp. 907–923.

Del Savio, A.A., Nethercot, D.A., Vellasco, P.C.G.S., Andrade, S.A.L. & Martha, L.F., 2009. Generalised component-based model for beam-to-column connections including axial versus moment interaction. *Journal of Constructional Steel Research*, 65(8–9), pp. 1876–1895.

Schafer, B.W. & Peköz, T., 1998. Computational modeling of cold-formed steel: characterizing geometric imperfections and residual stresses. *Journal of Constructional Steel Research*, 47, pp. 193–210.

Silva, L.A.P., Neves, L.F.N. & Gomes, F.C.T., 2003. Rotational stiffness of rectangular hollow sections composite joints. *Journal of Structural Engineering*, 129(4), pp. 487–494.

da Silva, L.S., 2008. Towards a consistent design approach for steel joints under generalized loading. *Journal of Constructional Steel Research*, 64(9), pp. 1059–1075.

da Silva, L.S., de Lima, L.R.O., Vellasco, P.C.G. da S. & de Andrade, S.A.L., 2004. Behaviour of flush end-plate beam-to-column joints under bending and axial force. *Steel and Composite Structures*, 4(2), pp. 77–94.

Simões da Silva, L., Santiago, A. & Vila Real, P., 2001. A component model for the behaviour of steel joints at elevated temperatures. *Journal of Constructional Steel Research*, 57(11), pp. 1169–1195.

Simões, L.M.C., 1996. Optimization of frames with semi-rigid connections. *Computers & Structures*, 60(4), pp. 531–539.

Snijder, H.H., Boel, H.D., Hoenderkamp, J.C.D. & Spoorenberg, R.C., 2011. Buckling length factors for welded lattice girders with hollow section braces and chords. In L. Dunai, M. Iványi, K. Jármai, N. Kovács, & L. G. Vigh, eds. *Proceedings of the 6th European Conference on Steel and Composite Structures (Eurosteel 2011), 31 August - 2 September 2011, Budapest, Hungary*. Brussels: ECCS, pp. 1881–1886.

Sokol, Z., Wald, F., Delabre, V., Muzeau, J.-P. & Švarc, M., 2002. Design of end plate joints subject to moment and normal force. In A. Lamas & L. S. da Silva, eds. *Third European conference on steel structures — Eurosteel 2002*. Coimbra: Cmm Press, pp. 1219–1228.

Stavroulakis, G.E., Avdelas, A. V, Abdalla, K.M. & Panagiotopoulos, P.D., 1997. A neural network approach to the modelling, calculation and identification of semi-rigid connections in steel structures. *Journal of Constructional Steel Research*, 44(1–2), pp. 91–105.

Stoddart, E.P., Byfield, M.P., Davison, J.B. & Tyas, A., 2013. Strain rate dependent component based connection modelling for use in non-linear dynamic progressive collapse analysis. *Engineering Structures*, 55, pp. 35–43.

Szlendak, J., 1991. Beam-column welded RHS connections. *Thin-Walled Structures*, 12(1), pp. 63–80.

Tabuchi, M., Kanatani, H. & Kamba, T., 1984. *The local strength of welded RHS T joints subjected to bending moment. CIDECT report 5AF-84/5E*, Boston, Massachusetts: International Institute of Welding.

Taib, M. & Burgess, I., 2011. A component-based model for fin-plate connections in fire. *Journal of Structural Fire Engineering*, 4(2), pp. 113–122.

Teng, T., Fung, C.-P., Chang, P.-H. & Yang, W.-C., 2001. Analysis of residual stresses and distortions in T-joint fillet welds. *International Journal of Pressure Vessels and Piping*, 78(8), pp. 523–538.

Thai, H.T. & Uy, B., 2016. Rotational stiffness and moment resistance of bolted endplate joints with hollow or CFST columns. *Journal of Constructional Steel Research*, 126, pp. 139–152.

Tschemmernegg, F., Tautschnig, A., Klein, H., Braun, C. & Humer, C., 1987. Zur Nachgiebigkeit von Rahmenknoten – Teil 1. *Stahlbau*, 56(10), p. 299–306 (in German).

Tuominen, N., Björk, T. & Ahola, A., 2018. Effect of bending moment on capacity of fillet weld. In A. Heidarpour & X.-L. Zhao, eds. *Tubular Structures XVI: Proceedings of the 16th International Symposium for Tubular Structures (ISTS 2017, 4-6 December 2017, Melbourne, Australia)*. London: Taylor & Francis Group, pp. 675–683.

van der Vegte, G.J. & Makino, Y., 2010. Further research on chord length and boundary conditions of CHS T- and X-joints. *Advanced Steel Construction*, 6(3), pp. 879–890.

van der Vegte, G.J., Wardenier, J. & Puthli, R.S., 2010. FE analysis for welded hollow-section joints and bolted joints. *Proceedings of the Institution of Civil Engineers — Structures and Buildings*, 163(SB6), pp. 427–437.

Wald, F., 1995. *Column bases*, Prague: CTU Prague.

Wardenier, J., 1982. *Hollow section joints*, Delft: Delft University Press.

Wardenier, J., van der Vegte, G.J. & Liu, D.K., 2007a. Chord stress function for rectangular hollow section X and T joints. In *Proceedings of the Seventeenth International Offshore and Polar Engineering Conference*. International Society of Offshore and Polar Engineers, pp. 3363–3370.

Wardenier, J., van der Vegte, G.J. & Liu, D.K., 2007b. Chord stress functions for K gap joints of rectangular hollow sections. *International Journal of Offshore and Polar Engineering*, 17(3),

pp. 225–232.

Weynand, K. & Jaspart, J.-P., 2001. Extension of the component method to joints in tubular construction. In R. S. Puthli & S. Herion, eds. *Tubular Structures IX: Proceedings of the Ninth International Symposium and Euroconference, Dusseldorf, Germany, 3-5 April 2001*. Rotterdam: Balkema, pp. 517–524.

Weynand, K., Jaspart, J.-P., Demonceau, J.F. & Zhang, L., 2015. *Component method for tubular joints*, CIDECT Report 16F – 3/15.

Wu, F.-H. & Chen, W.-F., 1990. A design model for semi-rigid connections. *Engineering Structures*, 12(2), pp. 88–97.

Yim, H.C. & Krauthammer, T., 2012. Mechanical properties of single-plate shear connections under monotonic, cyclic, and blast loads. *Engineering Structures*, 37, pp. 24–35.

Yu, Y., 1997. *The static strength of uniplanar and multiplanar connections in rectangular hollow sections*, PhD thesis. Delft: Delft University of Technology.

Zhao, X.-L., 2000. Deformation limit and ultimate strength of welded T-joints in cold-formed RHS sections. *Journal of Constructional Steel Research*, 53(2), pp. 149–165.

Zhao, X.-L. & Hancock, G.J., 1991. T-Joints in Rectangular Hollow Sections Subject to Combined Actions. *Journal of Structural Engineering*, 117(8), pp. 2258–2277.

Zhao, X.-L., Heidarpour, A. & Gardner, L., 2014. Recent developments in high-strength and stainless steel tubular members and connections. *Steel Construction*, 7(2), pp. 65–72.

Zoetemeijer, P., 1974. Design method for the tension side of statically loaded, bolted beam-to-column connections. *Heron*, 20(1), pp. 1–59.

Appendix

Appendix A1. Moment-rotation curves, HAMK tests.

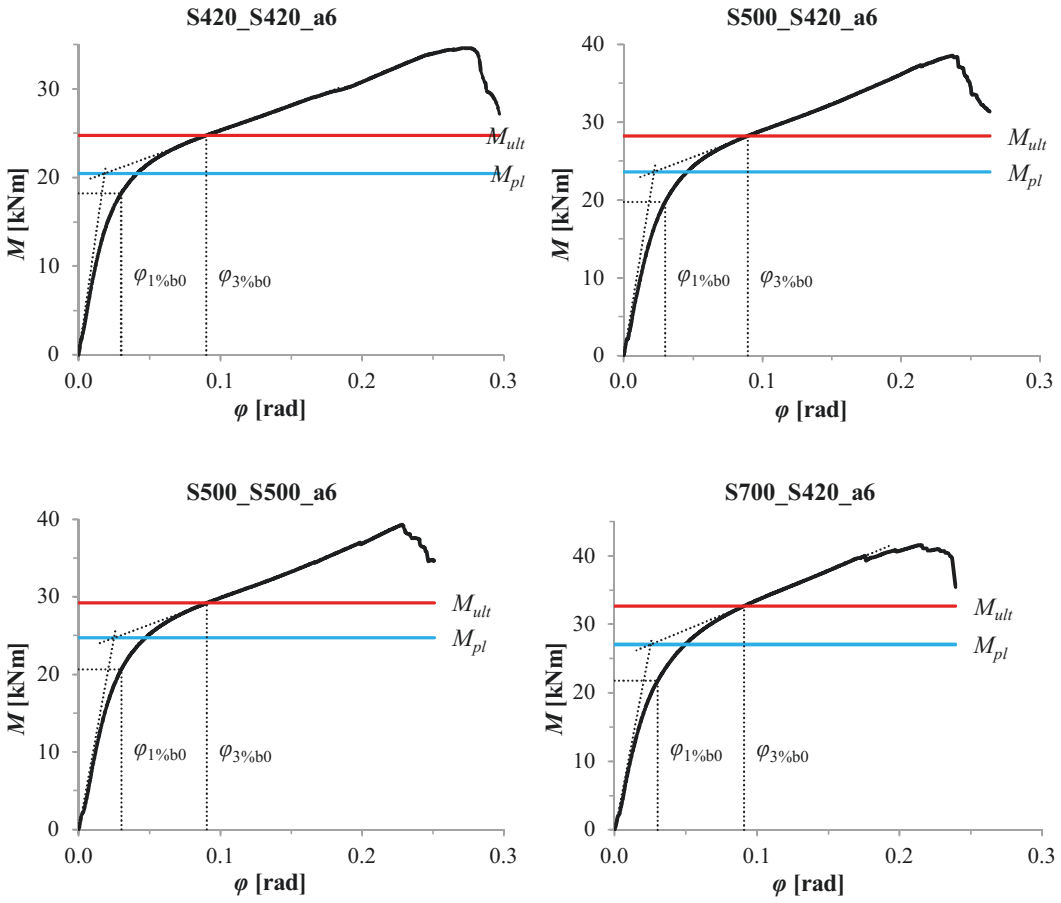

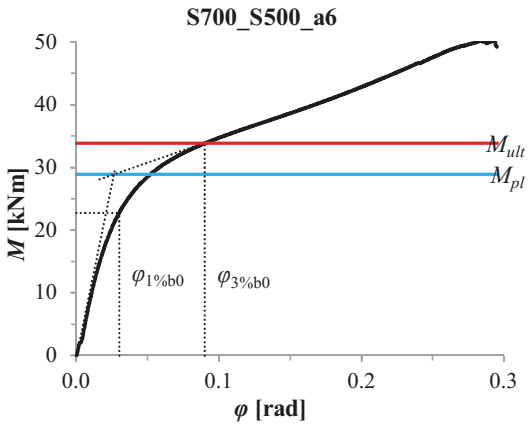
S700_S500_a6
M [kNm]
φ [rad]
M_ult
M_pl
φ1%b0
φ3%b0

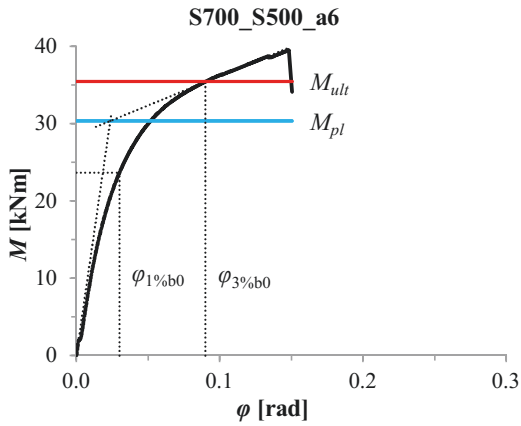
S700_S500_a6
M [kNm]
φ [rad]
M_ult
M_pl
φ1%b0
φ3%b0

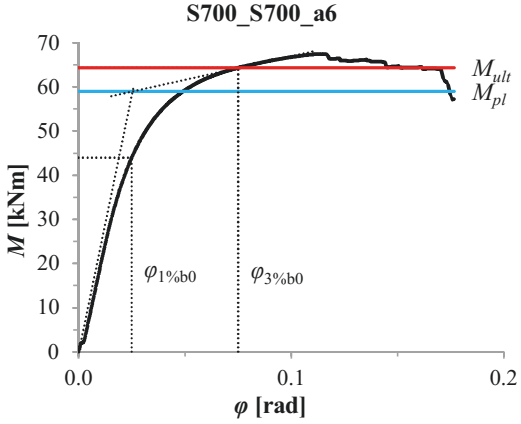
S700_S700_a6
M [kNm]
φ [rad]
M_ult
M_pl
φ1%b0
φ3%b0

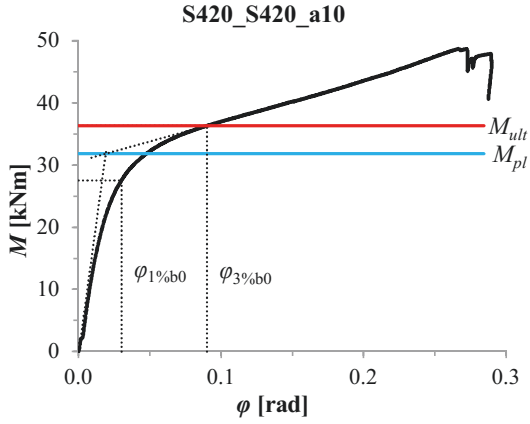
S420_S420_a10
M [kNm]
φ [rad]
M_ult
M_pl
φ1%b0
φ3%b0

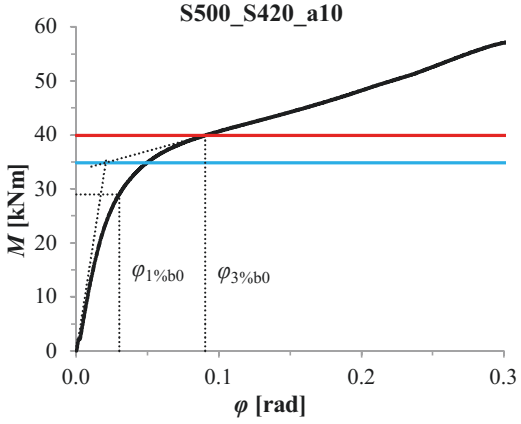
S500_S420_a10
M [kNm]
φ [rad]
φ1%b0
φ3%b0

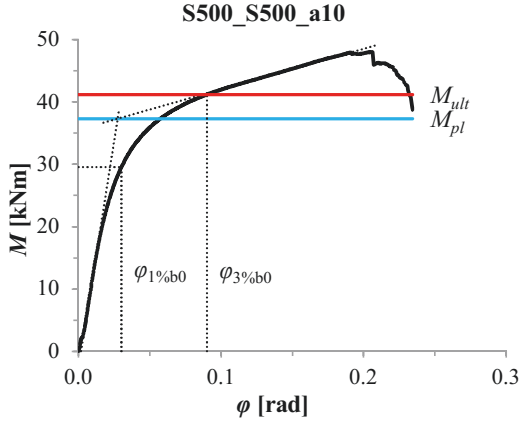
S500_S500_a10
M [kNm]
φ [rad]
M_ult
M_pl
φ1%b0
φ3%b0

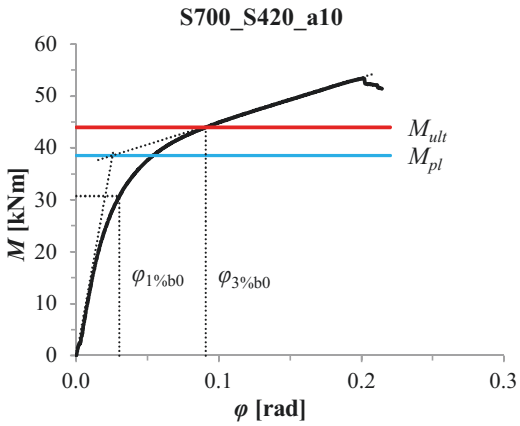
S700_S420_a10
M [kNm]
φ [rad]
M_ult
M_pl
φ1%b0
φ3%b0

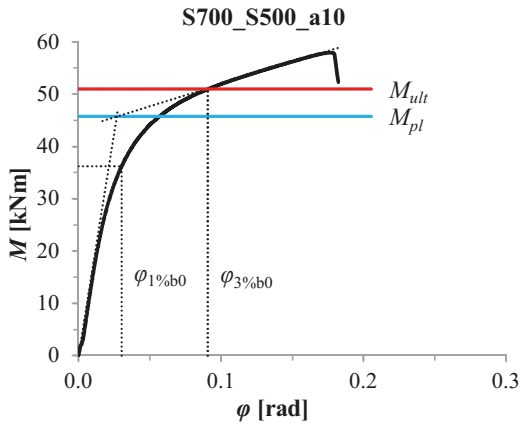
S700_S500_a10
M [kNm]
φ [rad]
M_ult
M_pl
φ1%b0
φ3%b0

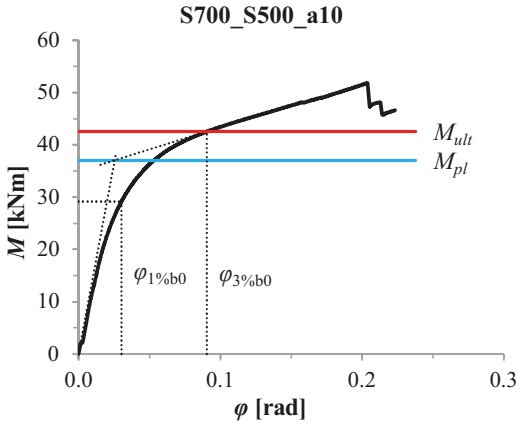
S700_S500_a10
M [kNm]
φ [rad]
M_ult
M_pl
φ1%b0
φ3%b0

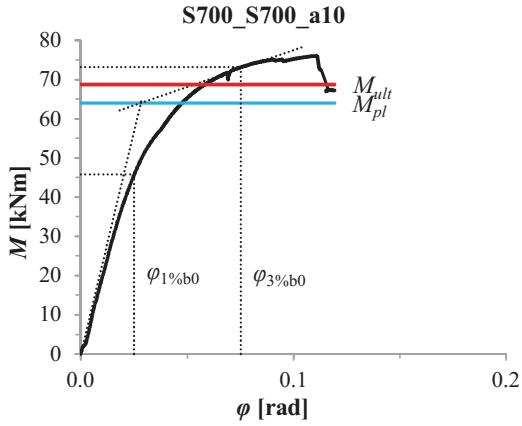
S700_S700_a10
M [kNm]
φ [rad]
M_ult
M_pl
φ1%b0
φ3%b0

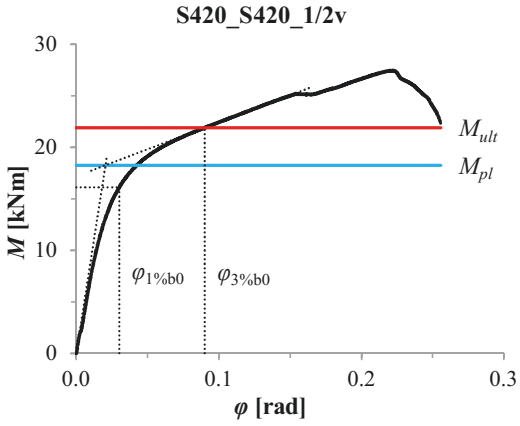
S420_S420_1/2v
M [kNm]
φ [rad]
M_ult
M_pl
φ1%b0
φ3%b0

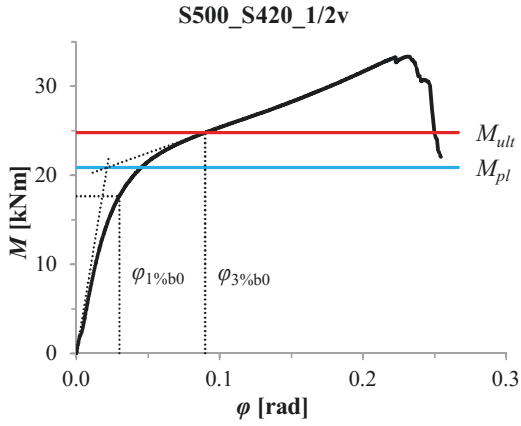
S500_S420_1/2v
M [kNm]
φ [rad]
M_ult
M_pl
φ1%b0
φ3%b0

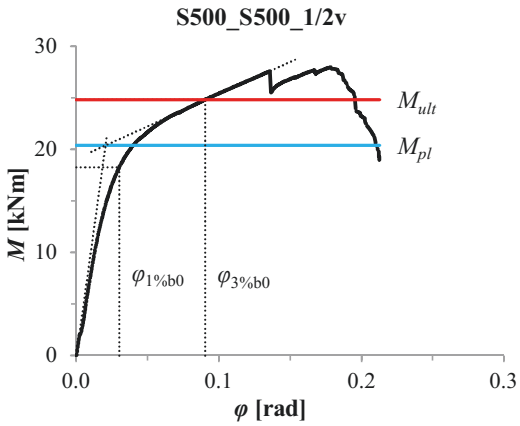
S500_S500_1/2v
M [kNm]
φ [rad]
M_ult
M_pl
φ1%b0
φ3%b0
0
10
20
30
0.0
0.1
0.2
0.3

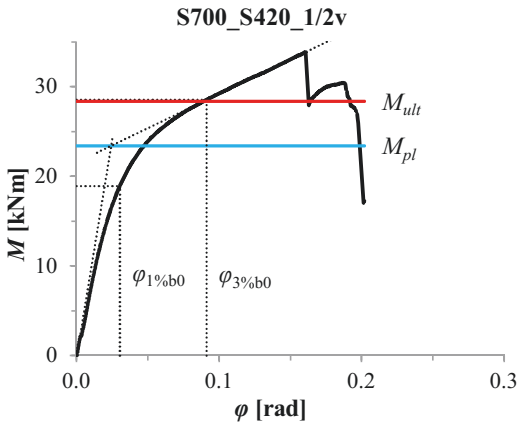
S700_S420_1/2v
M [kNm]
φ [rad]
M_ult
M_pl
φ1%b0
φ3%b0
0
10
20
30
0.0
0.1
0.2
0.3

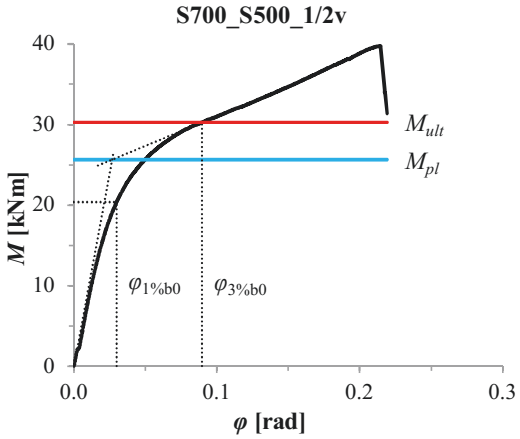
S700_S500_1/2v
M [kNm]
φ [rad]
M_ult
M_pl
φ1%b0
φ3%b0
0
10
20
30
40
0.0
0.1
0.2
0.3

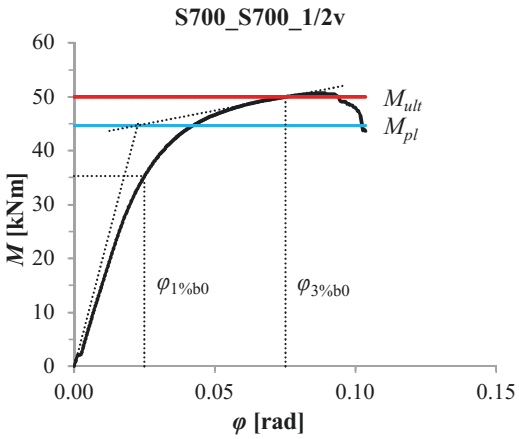
S700_S700_1/2v
M [kNm]
φ [rad]
M_ult
M_pl
φ1%b0
φ3%b0
0
10
20
30
40
50
60
0.00
0.05
0.10
0.15

ORIGINAL PAPERS

I

3D COMPONENT METHOD FOR WELDED TUBULAR T JOINTS

by

Garifullin M., Pajunen S., Mela K. & Heinisuo M., 2018

Tubular Structures XVI: Proceedings of the 16th International Symposium for Tubular Structures (ISTS 2017, 4-6 December 2017, Melbourne, Australia), pp. 165-173

II

INITIAL IN-PLANE ROTATIONAL STIFFNESS OF WELDED RHS T JOINTS WITH AXIAL FORCE IN MAIN MEMBER

by

Garifullin M., Pajunen S., Mela K., Heinisuo M. & Havula J., 2017

Journal of Constructional Steel Research vol. 139, 353-362

Journal of Constructional Steel Research 139 (2017) 353–362

Contents lists available at ScienceDirect

Journal of Constructional Steel Research

Initial in-plane rotational stiffness of welded RHS T joints with axial force in main member

Marsel Garifullin [a,b,*], Sami Pajunen [b], Kristo Mela [b], Markku Heinisuo [b], Jarmo Havula [c]

[a] Peter the Great St. Petersburg Polytechnic University, Saint Petersburg, Russia
[b] Tampere University of Technology, Tampere, Finland
[c] HAMK University of Applied Sciences, Hämeenlinna, Finland

ARTICLE INFO

Article history:
Received 6 June 2017
Received in revised form 25 September 2017
Accepted 30 September 2017
Available online xxxx

Keywords:
Welded tubular T joint
In-plane moment load
Chord stress function
Rotational stiffness

ABSTRACT

In the frame analysis, the local analysis model of the joint must follow the behavior of the joint. When completing the elastic global analysis, the initial rotational stiffness of the joints should be known to obtain the reliable moment distribution between the members of the frame. This paper evaluates the existing calculation approach for the initial rotational stiffness of welded rectangular hollow section T joints. Validation with the experiments shows that the current calculation approach significantly underestimates their initial rotational stiffness. Based on the existing experimental data, the paper proposes the improvement for determining the initial stiffness. The second part of the article investigates the effect of the axial force in the main member on the initial rotational stiffness of the joint. The conducted numerical study on square hollow section T joints shows that the reduction of their initial stiffness can reach 50%, when the main member experiences the normal stresses close to yielding. Using the curve fitting approach, the paper proposes and validates a corresponding chord stress function, similar to the existing ones for the moment resistance.

1. Introduction

Feasibility study dealing with safety of the structure starts from the global analysis of the structure. In the frame analysis, which is conducted using beam elements, the local analysis model of the joint must follow the behavior of the joint. In this regard, the stiffness, in this case the initial rotational stiffness, becomes the important quantity of joints. It has been shown that significant cost savings can be achieved by considering the initial rotational stiffness of semi-rigid joints, both in sway frames [1,2] and in non-sway frames [3]. Moreover, the rotational stiffness has a significant effect on the buckling behavior of members [4–6].

Comprehensive research on tubular joints loaded by in-plane bending moments was conducted by Wardenier [7], who proposed the design resistance equations, which are currently presented in many design standards, such as EN 1993-1-8:2005 [8] and ISO 14346:2013 [9]. After that, extensive studies have been undertaken dealing with the strength of hollow section joints. Tabuchi et al. [10] presented experimental results for in-plane moment loaded rectangular hollow section (RHS) T joints and examined their local failures. Szlendak [11] and Packer [12] developed design procedures for RHS connections under the moment loading. Intensive research for uniplanar and multiplanar RHS joints was conducted by Yu [13]. The deformation limit of RHS joints was investigated by Lu [14] and Zhao [15].

In the joint, normal stresses may occur at the surface of the main member, where the connected member is located. Generally, the effect of these stresses is measured using the so-called chord stress functions, which are available for the resistances of joints in many design standards [8,9] and handbooks [16]. The design equation for the chord stress function was originally presented in [7] for the resistance of hollow section joints. Later considerable research has been conducted worldwide dealing, however, only with the resistance of joints. The results for RHS K gap joints are provided in [17] and for RHS X and T joints in [18,19]. Recent studies have been published for RHS joints in [20] and circular hollow section (CHS) joints in [21].

At the same time, considerably less research has considered the rotational stiffness of tubular joints. Korol & Mirza [22] described several methods to determine the behavior of joints, including the post-elastic phase. Mäkeläinen et al. [23] presented the rotational stiffness of circular hollow sections (CHS) T joints, based on the semi-analytical models. The component method, the origin of which can be tracked back to [24], enables calculating the stiffness of the joint, decomposing it to the basic components. Calculation methods for the rotational stiffness of RHS T joints are presented in [25,26]. Both based on the component method, they employ different mechanical models and equations to determine the stiffnesses of the components. However, in contrast to the resistance, the initial stiffness design rules were validated with the very

* Corresponding author at: Tampere University of Technology, Tampere, Finland.
E-mail address: marsel.garifullin@tut.fi (M. Garifullin).

https://doi.org/10.1016/j.jcsr.2017.09.033
0143-974X/

limited amount of experimental data. Moreover, none of the presented publications considers the effect of the axial forces in the main member on the stiffnesses of the joint.

The focus of the present study is on the local initial rotational stiffness of welded RHS T joints loaded by the in-plane bending moment. The T joint is a joint where a RHS member is connected in an angle of 90° to another RHS member, called the main member. The connected member can be a brace of a truss or a beam of a frame, whereas the main member usually represents a chord of a truss or a column. Fig. 1a shows a RHS T joint loaded with the in-plane moment M acting on the connected member and with the axial force N acting on the main member. The main properties of such joint are its brace-to-chord width ratio β and chord width-to-thickness ratio γ:

$$\beta = \frac{b_1}{b_0}; \quad \gamma = \frac{b_0}{2t_0} \tag{1}$$

As can be seen in Fig. 1a, shear forces and bending moments occur in the main member to compensate the moment M. Considering the chord stress function in the joint, it is essential to construct the test specimen and its mechanical model so that the stresses on the surface on the main member correspond with the actual stresses [13,27]. In Fig. 1a, the mechanical model assumes the axial stresses in the joint to be anti-symmetric with respect to the mid-line of the joint, when the axial force in the main member is zero. At the symmetric axis, the axial stresses are zero, and this is considered as the case without axial stresses in the main member.

The first section of this paper provides the theoretical background for the initial rotational stiffness of joints [25] and proposes the improved stiffness equation for one of the components. Section 2 validates the proposed improvements with the experimental data. Section 3 studies the effect of the axial force in the main member on the initial rotational stiffness and proposes the corresponding chord stress function, using the curve-fitting approach.

1.1. Theoretical background for the design of initial rotational stiffness

1.1.1. Local analysis model

The different beam element local analysis models for welded tubular joints have been evaluated in [4,5]. This paper employs the best variation of [4], which is composed of the elastic and rigid beams, as presented in Fig. 1b, where S_j denotes the in-plane rotational stiffness of the joint. It should be noted, that the rotation of the joint and, consequently, its rotational stiffness, are defined at the point where the member is connected to the surface of the main member, not at the intersection point of the connected and main member midlines, as is defined in [8]. The motivation for such assumption is provided in [28,29]. This assumption is also used in [26], where it is shown that the local analysis model is located at the top flange of the main member. The properties of the beam elements should follow those they represent, *i.e.*, the connected and main members.

1.1.2. Initial rotational stiffness

The initial rotational stiffness is determined using the component method, which is currently employed by [8] for the joints connecting H and I sections. It was also applied for RHS joints in [25]. According to [8], the initial rotational stiffness of the joint, $S_{j,ini}$, is calculated as

$$S_{j,ini} = \frac{Ez^2}{\sum_i \frac{1}{k_i}} \tag{2}$$

where E is the Young's modulus; $z = h_1$ is the lever arm; k_i is the stiffness coefficient for basic joint component i. Based on [25], the following stiffness coefficients k_i should be considered when calculating the initial stiffness of the welded RHS T joint:

- k_{cf} is the coefficient for the deformation of the main member surface, where the connected member is welded;
- k_{cw} is the coefficient for compression and tension deformation of the main member webs;
- k_{sh} is the coefficient for the shear deformation of the main member webs, denoted as k_i in [25].

Other coefficients, which relate to the weld deformations and the axial deformations of the brace, are not considered for RHS joints. Normally, the coefficient k_{cf} is the smallest, which means that the deformation of the main member face is the most essential when defining the rotational stiffness of the joint, particularly for the joints with small β.

1.1.2.1. Coefficient k_{cf}. Following Eq. (2.5.19) in [25], the coefficient k_{cf} is calculated as

$$k_{cf} = \frac{8t_0^3 l_{eff,cf}}{(1-\beta)^3 b_0^3} \cdot \frac{1}{2 + \frac{6\beta}{1-\beta}} \tag{3}$$

Table 2.5.1 in [25] presents two options for calculating the effective width $l_{eff,cf}$:

$$l_{eff,cf} = t_1 + 2 \cdot b_0 \sqrt{1-\beta} \tag{4}$$

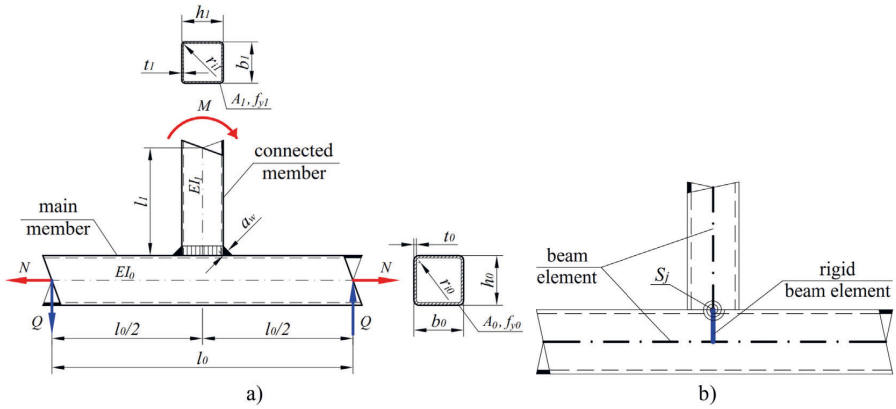

Fig. 1. a) RHS T joint; b) its local design model.

$$l_{eff,cf} = \frac{h_1}{2} + b_0 \cdot \sqrt{1-\beta} \tag{5}$$

Based on the classical yield line theory of Johansen [30], it can be seen that Eq. (4) represents the length of the total yield line pattern for the chord loaded with a perpendicular load in the flange of the brace. Eq. (5) represents the extension of Eq. (4) to the case where the chord is loaded with a half of the brace. In this paper, the effective width $l_{eff,cf}$ is determined using Eq. (4). The local design model of the joint consists of the compressive and tensile parts, which are assumed to behave similarly [25]. Therefore, the coefficient k_{cf} can be used also for the tensile part of the model and thus is counted twice in Eq. (2).

Validation with the experimental data has shown that Eq. (3) significantly underestimates the stiffness of the component, leading thus to very conservative results of the overall initial rotational stiffness. To avoid this, a more accurate solution is proposed in Eq. (6). The justification for that is presented in Section 2.

$$k_{cf} = \frac{20 t_0^3 l_{eff,cf}}{(1-\beta)^3 b_0^3} \cdot \frac{1}{2 + \frac{6\beta}{1-\beta}} \tag{6}$$

1.1.2.2. Coefficient k_{cw}. Following clause 2.6.2 of [25], the coefficient k_{cw} is defined as

$$k_{cw} = \frac{2 \cdot t_0 \cdot b_{eff,cw,el}}{h_0 - 3t_0} \tag{7}$$

where

$$b_{eff,cw,el} = 2 \cdot 0.7 \cdot l_{eff,cw} + t_1 \tag{8}$$

$$l_{eff,cw} = \max \begin{cases} t_0 \cdot \sqrt{\frac{b_0}{2 \cdot t_0}} \le 2.5 \cdot t_0 \\ \frac{b_0}{2} \cdot \sqrt{1-\beta} \le \frac{h_0}{2} \end{cases} \tag{9}$$

The first part of Eq. (9) limits the spread of the yield to $2.5t_0$ at both sides of the flange of the brace, while the origin of the second part comes from the yield condition. Similarly to k_{cf}, the coefficient k_{cw} is the same in tension and compression and is taken into account twice in Eq. (2).

1.1.2.3. Coefficient k_{sh}. According to clause 6.11 of [8], the shear coefficient k_{sh} is determined as

$$k_{sh} = 0.38 \cdot \frac{A_{VC}}{rz} \tag{10}$$

where $r \approx 1$ is the transformation parameter (Table 5.4, [8]), z is the lever arm and, following Eq. (2.7.8) in [25], the shear area is:

$$A_{VC} = 2t_0(h_0 - t_0) \tag{11}$$

The coefficient k_{sh} is taken into account only once in Eq. (2).

1.1.3. Initial rotational stiffness

Taking into account all the above, the initial rotational stiffness is calculated as

$$S_{j,ini} = \frac{Ez^2}{\frac{2}{k_{cf}} + \frac{2}{k_{cw}} + \frac{1}{k_{sh}}} \tag{12}$$

2. Validation of the initial rotational stiffness for RHS T joints

This section validates the calculation approach for the initial rotational stiffness with the experimental tests available in the literature. The steel grades of the members are provided in the following way: steel grade of the main member/steel grade of the connected member. The theoretical initial rotational stiffness $S_{j,ini}$ is compared to the experimental value $S_{j,ini,exp}$. For the theoretical values, the coefficient k_{cf} is calculated using both Eq. (3), presented in [25], and the proposed Eq. (6). The $S_{j,ini}/S_{j,ini,exp}$ ratio is provided in the following way: the absolute value, the average value and the (standard deviation).

2.1. HAMK tests

Consider first the tests of [31], which represent twenty experiments of HSS square hollow section T joints with varying section dimensions, steel grades, weld sizes and welding types (Table 1). Although only the nominal values of member sizes are provided, the theoretical initial stiffness is calculated using their measured values. It can be seen that the original approach, Eq. (3), considerably underestimates the initial rotational stiffness of the joints. On the contrary, Eq. (6) provides more accurate prediction, particularly for the butt-welded joints. However, for the joints with fillet welds, the results are still underestimated.

2.2. Tests of TH Karlsruhe and Kobe University

The next validation (Table 2) is conducted using the results of the TH Karlsruhe [32] and the Kobe University [33]. The initial rotational stiffnesses are extracted from the moment-rotation curves (Figs. 2 and 3), provided in [25]. As in the case with HAMK tests, the calculation is much more accurate, if Eq. (6) is used instead of Eq. (3).

2.3. University of Thrace tests

This validation is conducted using the tests of Christitsas et al. [34], who present the experimental stiffness of the square hollow section X joints subject to in-plane bending moment (Table 3). The results are in line with the previous observations: Eq. (6) yields more accurate prediction of the initial rotational stiffness.

2.4. Discussion concerning initial stiffness

As can be seen from the validation results, Eq. (3), originally proposed in [25], provides very conservative results: the $S_{j,ini}/S_{j,ini,exp}$ ratio is 0.29…0.45 for HAMK tests, 0.35 for the tests of TH Karlsruhe and the Kobe University and 0.41 for the University of Thrace tests. Oppositely, Eq. (6) provides considerably more accurate values, with the $S_{j,ini}/S_{j,ini,exp}$ ratio close to one.

Comparing the results of HAMK tests, it can be noted that the joints with fillet welds have significantly higher initial stiffness than those with butt welds, in average 13% higher for the 6 mm weld joints and 36% higher for the 10 mm weld joints. This allows making a conclusion that fillet welds significantly affect the initial rotational stiffness of joints. This corresponds well with the results of [35], who proposed a simple rule to calculate the initial rotational stiffness of Y joints using the equivalent brace width:

$$b_{1,eq} = b_1 + 2\sqrt{2} a_w k_{fw} \tag{13}$$

where a_w is the fillet weld size, k_{fw} is a correlation coefficient, determined as 0.6 for S355 and 0.7 for S700. Overall, Eq. (13) leads to the additional width of $(0.6…0.7) \cdot \sqrt{2} a_w$ at both sides of the connected member, which is very close to the proposal $0.8 \cdot \sqrt{2} a_w$ for open cross-sections in Fig. 6.8 of [8].

Table 1
HAMK tests.

Case	Main member	Connected member	Steel grade	a_w [mm]	β	$S_{j,ini}$ [kNm/rad]		$S_{j,ini,exp}$ [kNm/rad]	$S_{j,ini}/S_{j,ini,exp}$			
						Eq. (3)	Eq. (6)		Eq. (3)		Eq. (6)	
1111	150 × 150 × 8	100 × 100 × 8	S420/S420	6	0.66	401	913	1115	0.36	0.39 (0.06)	0.82	0.87 (0.10)
2111	150 × 150 × 8	100 × 100 × 8	S500/S420	6	0.67	422	956	1083	0.39		0.88	
2211	150 × 150 × 8	100 × 100 × 8	S500/S500	6	0.67	421	954	995	0.42		0.96	
3111	150 × 150 × 8	100 × 100 × 8	S700/S420	6	0.67	405	919	1082	0.37		0.85	
3211	150 × 150 × 8	100 × 100 × 8	S700/S500	6	0.67	403	916	1108	0.36		0.83	
3214	150 × 150 × 8	100 × 100 × 8	S700/S500	6	0.67	403	916	1282	0.31		0.71	
3311	150 × 150 × 8	120 × 120 × 8	S700/S700	6	0.80	1030	2113	1990	0.52		1.06	
1121	150 × 150 × 8	100 × 100 × 8	S420/S420	10	0.67	407	924	1692	0.24	0.29 (0.07)	0.55	0.64 (0.13)
2121	150 × 150 × 8	100 × 100 × 8	S500/S420	10	0.67	423	958	1701	0.25		0.56	
2221	150 × 150 × 8	100 × 100 × 8	S500/S500	10	0.67	424	959	1452	0.29		0.66	
3121	150 × 150 × 8	100 × 100 × 8	S700/S420	10	0.67	397	903	1521	0.26		0.59	
3221	150 × 150 × 8	100 × 100 × 8	S700/S500	10	0.67	401	913	1705	0.24		0.54	
3224	150 × 150 × 8	100 × 100 × 8	S700/S500	10	0.67	399	908	1455	0.27		0.62	
3321	150 × 150 × 8	120 × 120 × 8	S700/S700	10	0.80	1048	2141	2268	0.46		0.94	
1131	150 × 150 × 8	100 × 100 × 8	S420/S420	Butt	0.67	414	940	893	0.46	0.45 (0.05)	1.05	1.00 (0.06)
2131	150 × 150 × 8	100 × 100 × 8	S500/S420	Butt	0.67	424	960	977	0.43		0.98	
2231	150 × 150 × 8	100 × 100 × 8	S500/S500	Butt	0.67	425	961	1003	0.42		0.96	
3131	150 × 150 × 8	100 × 100 × 8	S700/S420	Butt	0.67	401	911	971	0.41		0.94	
3231	150 × 150 × 8	100 × 100 × 8	S700/S500	Butt	0.67	409	930	961	0.43		0.97	
3331	150 × 150 × 8	120 × 120 × 8	S700/S700	Butt	0.81	1100	2222	1990	0.55		1.12	

Table 2
Tests of TH Karlsruhe and Kobe University.

Case	Main member	Connected member	Steel grade	a_w [mm]	β	$S_{j,ini}$ [kNm/rad]		$S_{j,ini,exp}$ [kNm/rad]	$S_{j,ini}/S_{j,ini,exp}$			
						Eq. (3)	Eq. (6)		Eq. (3)		Eq. (6)	
M44	160 × 160 × 4	100 × 100 × 3	S235/S235	3	0.63	41	100	130	0.31	0.35 (0.10)	0.77	0.82 (0.20)
M45	160 × 160 × 5	100 × 100 × 3	S235/S235	3	0.63	79	191	260	0.30		0.73	
S12	200 × 200 × 9	150 × 150 × 6	S235/S235	6	0.75	1043	2325	2000	0.52		1.16	
S23	250 × 250 × 6	175 × 175 × 6	S235/S235	6	0.70	226	550	875	0.26		0.63	

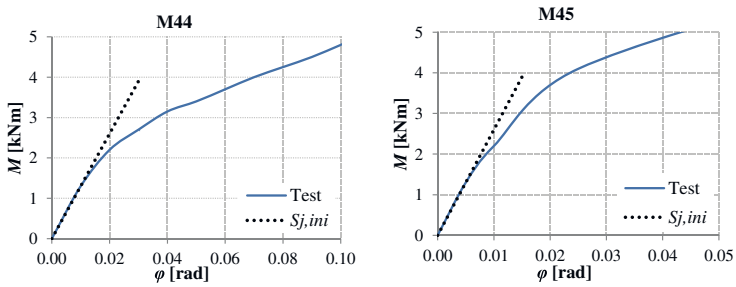

Fig. 2. Initial rotational stiffness extracted from the tests of the TH Karlsruhe, [25], Annex B.3.

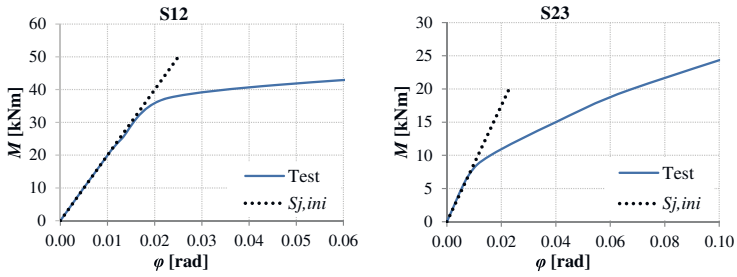

Fig. 3. Initial rotational stiffness extracted from the tests of the Kobe University, [25], Annex B.4.

Table 3
University of Thrace tests.

Case	Main member	Connected member	Steel grade	a_w [mm]	β	$S_{j,ini}$ [kNm/rad]		$S_{j,ini,exp}$ [kNm/rad]	$S_{j,ini}/S_{j,ini,exp}$			
						Eq. (3)	Eq. (6)		Eq. (3)		Eq. (6)	
80c150t5	150 × 150 × 5	80 × 80 × 5	S235/S235	6	0.53	46	111	135	0.34	0.41 (0.08)	0.82	0.94 (0.17)
80c150t6	150 × 150 × 6	80 × 80 × 5	S235/S235	6	0.53	78	189	208	0.38		0.91	
80c150t8	150 × 150 × 8	80 × 80 × 5	S235/S235	6	0.53	183	430	407	0.45		1.06	
100c150t5	150 × 150 × 5	100 × 100 × 5	S235/S235	6	0.67	104	249	301	0.34		0.83	
100c150t6	150 × 150 × 6	100 × 100 × 5	S235/S235	6	0.67	177	417	494	0.36		0.84	
100c150t8	150 × 150 × 8	100 × 100 × 5	S235/S235	6	0.67	408	924	712	0.57		1.30	
120c150t5	150 × 150 × 5	120 × 120 × 5	S235/S235	6	0.80	279	634	741	0.38		0.86	
120c150t6	150 × 150 × 6	120 × 120 × 5	S235/S235	6	0.80	469	1028	1366	0.34		0.75	
120c150t8	150 × 150 × 8	120 × 120 × 5	S235/S235	6	0.80	1041	2119	1927	0.54		1.10	

Table 4
FEM parameters.

Main member	$300\times300\times t_0$						
	t_0 [mm]	8.5	10	12	15	20	30
	2γ	35	30	25	20	15	10
Connected member	$b_1\times b_1\times t_1$						
	b_1 [mm]	75	150	225	255	300	
	β	0.25	0.50	0.75	0.85	1.00	
Steel grade	S500 (both for main and connected members)						
n	−0.99, −0.95, −0.80, −0.60, −0.40, −0.20, 0, 0.20, 0.40, 0.60, 0.80, 0.95, 0.99						

3. Chord stress function for initial rotational stiffness

The axial forces acting in the main member are known to reduce the resistance of the joint [7]. This reduction is defined by chord stress functions, the simplest of which, Eq. (14), is presented in Eurocode [8]. The extensive research on the chord stress functions for RHS joints is also provided in [18,19].

$$k_n = \begin{cases} 1.3 - \dfrac{0.4|n|}{\beta} \le 1.0, & n>0 \\ 1.0, & n<0 \end{cases} \tag{14}$$

where n is the ratio of the normal stress in the main member to its yield strength:

$$n = \frac{\sigma_0}{f_{y0}} = \frac{N_0}{A_0 f_{y0}} + \frac{M_0}{W_{el0} f_{y0}} = \frac{N_0}{A_0 f_{y0}} \tag{15}$$

where A_0 is the cross-sectional area of the main member and N_0 is the axial load in the main member. In Eurocode [8], negative n means

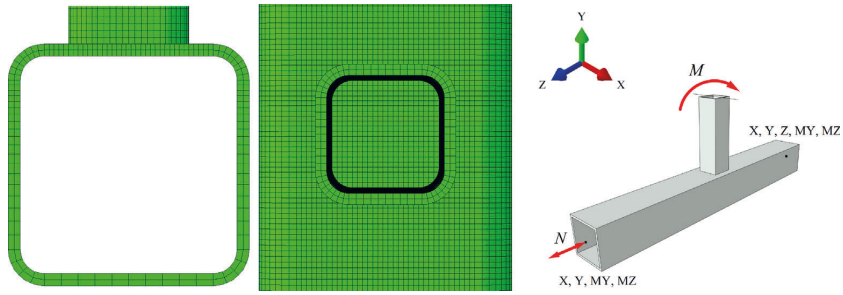

Fig. 4. a) Meshing; b) boundary conditions.

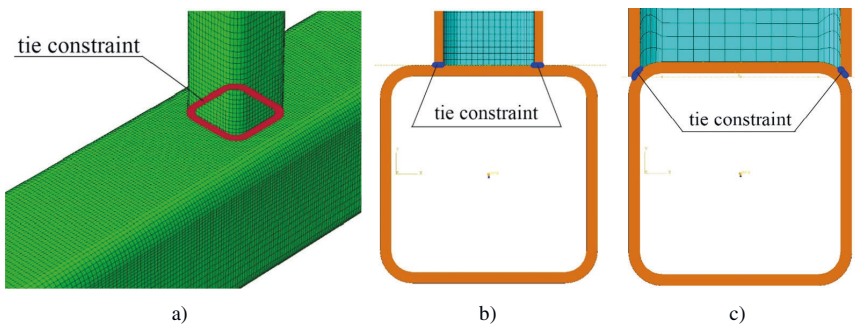

Fig. 5. a) Tie constraint; b) FE model for $\beta = 0.50$; c) FE model for $\beta = 1.0$.

tension in the main member, while the positive one indicates compression. However, many publications [18,19,21] employ the inverse order for n, which is also used in this paper.

As has been proposed in [36], such phenomenon can be observed not only for resistance of joints, but also for their initial stiffness. Although in predominantly statically loaded trusses there is no need to take into account joint stiffnesses for the load distribution if the critical parts have sufficient rotation capacity, in frame structures stiffnesses of joints have to be considered in the global analysis. From that point of view, such an effect can lead to the noticeable redistribution of forces in the members of frames, making the results of the analysis unreliable. This fact justifies the necessity to develop the chord stress function for the initial stiffness of joints. For that reason, Eq. (2) should be modified in the following way:

$$S_{j.ini} = \frac{k_{sn.ip} E z^2}{\sum_i \frac{1}{k_i}} \tag{16}$$

where $k_{sn,ip}$ is the chord stress function for the initial rotational stiffness.

This section evaluates the effect of the axial force in the main member on the initial in-plane rotational stiffness of hollow section T joints. On the first step, the FEM analysis is conducted to investigate the effect of the chord stress on the initial stiffness. The obtained results are then approximated using the linear and polynomial regressions, proposing the final chord stress function.

3.1. FEM

The numerical analyses were performed with the FE package ABAQUS/Standard [37]. The described FE model was verified and validated against experimental results in [38]. The scope of the study was restricted to square hollow sections, since RHS joints would have required considering the additional variable b_0/h_0, thus leading to the significant increase of the sample points. The FEM analyses were conducted for a single main member size 300 × 300. Following the requirements of the [8], the main member wall thickness t_0 varied from 8.5 mm ($2\gamma = 35$) to 30 mm ($2\gamma = 10$), whereas the connected member width changed from 75 mm ($\beta = 0.25$) to 300 mm ($\beta = 1.00$), as shown in Table 4. The wall thickness t_1 of the connected member was chosen so that it did not exceed the thickness of the main member t_0. According to [39], all the sections were modelled with round corners, meaning cold-formed sections. To exclude the possible effects of the main member end conditions, its length was selected as $10b_0$, as recommended in [40], while the connected member length was chosen as $4b_1$, following [13]. The relative stress in the main member, n, was determined using Eq. (15). The analyses were conducted for a single steel grade S500, both for main and connected members, as

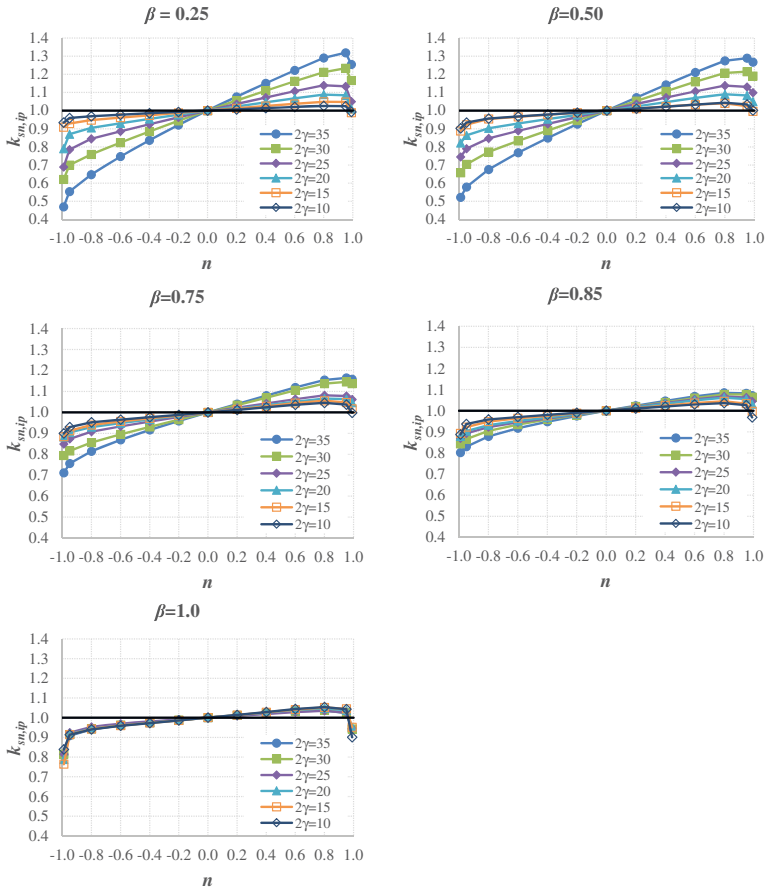

Fig. 6. Chord stress function depending on γ. The function weakens with the decrease of γ. For $\beta = 1.0$, the difference is negligibly little.

the average steel grade in the range of ones considered in this paper (S355…S700).

The sections were modelled using 20-noded solid quadratic finite elements with reduced integration (C3D20R in Abaqus), with two elements in thickness direction (Fig. 4a). Since the deformation of the main member top face represents the dominating failure mode, its mesh was refined closer to the connected face (Fig. 4a). Fig. 4b illustrates the boundary conditions of the FE model. The T joints were modelled with butt welds, meaning no welds, using the tie constraint of Abaqus (Fig. 5a), which ties two separate surfaces together so that there is no relative motion between [37]. This approach allows using individual meshes for the main and connected members without matching their nodes (Fig. 5b) and is employed by many researchers [41,42]. The joints with $\beta = 1.0$ were modelled with end preparations of the connected member (Fig. 5c).

The analyses were conducted in two steps: after the axial load was applied to the main member on the first step, the end of the connected member was loaded with the concentrated in-plane moment M_{ip} using only one increment, corresponding approximately to 0.1 rad and meaning no yielding at the joint area. All calculations employed the same ideal plastic material model for S500 steel, with $E = 210$ GPa and $\nu = 0.3$. The outcome of the FEM was the overall rotation in the end of the connected member φ_{FEM}. To obtain the rotation φ_j corresponding to the in-plane rotational stiffness $S_{j,ini}$, φ_{FEM} was reduced by the rotation of the brace φ_{br} and the rotation of the chord φ_{ch}:

$$\varphi_j = \varphi_{FEM} - \varphi_{br} - \varphi_{ch} \tag{17}$$

The rotation of the brace was found as

$$\varphi_{br} = \frac{M_{ip} l_1}{EI_{1,ip}} \tag{18}$$

where l_1 and $I_{1,ip}$ are the length and the in-plane moment of inertia of the brace, respectively.

The rotation of the chord was determined as

$$\varphi_{ch} = \frac{M_{ip} l_0}{12EI_{0,ip}} \tag{19}$$

where l_0 and $I_{0,ip}$ are the length and the in-plane moment of inertia of the chord, respectively.

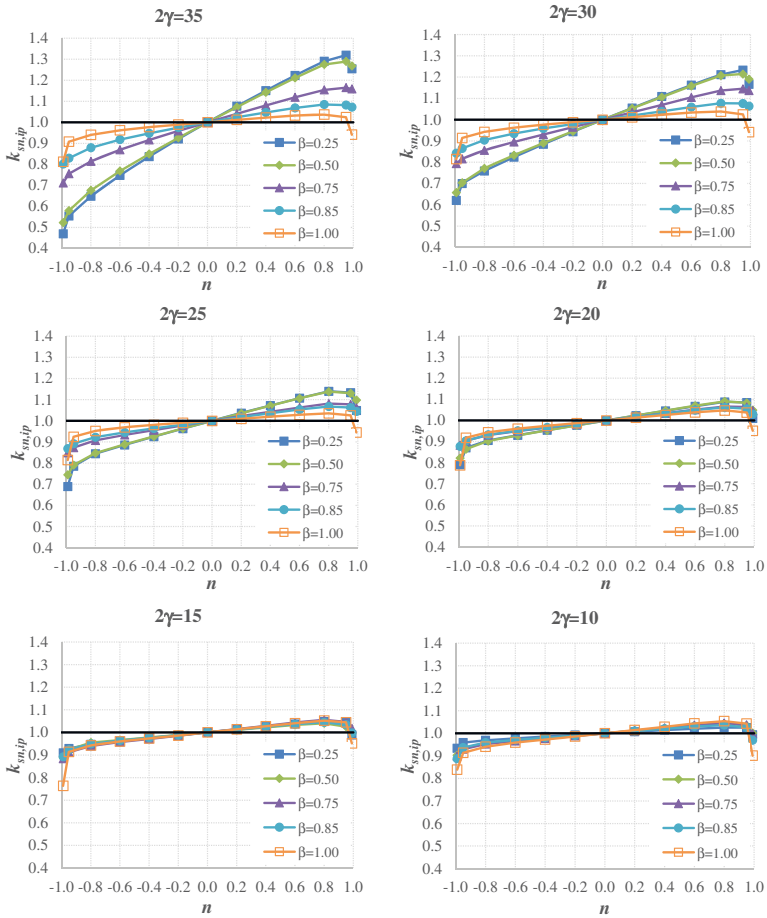

Fig. 7. Chord stress function depending on β. The function weakens with the increase of β. For small γ ($2\gamma = 15$ and $2\gamma = 10$), the difference is negligibly little.

Table 5
Approximation based on the existing chord stress functions for the moment resistance.

Case	Equation	A	B	C	R^2	Δ_{av} [%]	Δ_{max} [%]
1	$k_{sn,ip}=\begin{cases}1.3-\frac{0.4\lvert n\rvert}{\beta}\le 1.0, & n<0\\ 1.0, & n>0\end{cases}$	–	–	–	0.34	12.7	160.5
2	$k_{sn,ip}=1+A\frac{n}{\beta+B}, \quad -0.99\le n\le 0.99$	0.419	0.917	–	0.63	10	37.1
3	$k_{sn,ip}=\begin{cases}(1-\lvert n\rvert)^{0.6-0.5\beta}, & n<0\\ (1-\lvert n\rvert)^{0.1}, & n>0\end{cases}$	–	–	–	0.32	20.9	88.0
4	$k_{sn,ip}=(1+n)^{A+B\beta}$	−0.148	0.031	–	0.25	13.6	93.2
5	$k_{sn,ip}=(1-n^2)^{0.8-0.8\beta+0.01\gamma}$	–	–	–	0.04	26.0	96.0
6	$k_{sn,ip}=(1-n^2)^{A+B\beta+C\gamma}$	0.018	−0.035	0.004	0.05	7.8	55.7

Finally, the initial rotational stiffness was be presented as

$$S_{j,ini}=\frac{M_{ip}}{\varphi_j} \tag{20}$$

The observed influence of the axial force in the main member on the initial rotational stiffness was found to have the similar pattern as in the case with the moment resistance, as depicted in Figs. 6 and 7. According to the graphs, the reduction of the stiffness can be extremely high, >50% for the joints with small β and large γ. Similarly, for the same joints, the increase of the initial stiffness can reach 30%. For $-0.8\le n\le 0.8$, the response is generally linear, being nonlinear when $0.8<|n|\le 0.99$. In addition, the effect was observed to weaken with the increase of β and the decrease of γ. For the joints with $\beta=1.0$, the dependence on γ is negligibly little.

3.2. Chord stress function for initial rotational stiffness

To take into account the effect of the axial stresses in the main member on the initial rotational stiffness of the joint, the corresponding chord stress function was developed using the obtained numerical results. Following the above observations, the function was found dependent on three variables: β, γ and n. To compare the values of the proposed function with the FEM results, the coefficient of determination R^2, the average percent error Δ_{av} and the maximum percent error Δ_{max} were selected as the assessment criteria. On the first step, the existing chord stress functions for the moment resistance were tested for applicability to the case of the initial stiffness.

3.2.1. Existing chord stress functions for moment resistance

As a starting point for the approximation, the current chord stress function in [8] was selected, Eq. (14) (Case 1). Since it does not consider the increase of the stiffness for $n>0$, it was found to provide very inaccurate results (Table 5). Case 2, the development of Case 1 extended also for positive n, did not bring reasonable results. The similar performance was obtained for the chord stress functions proposed in [19], Cases 3 and 4, and [18], Cases 5 and 6. None of these functions considers the increase of stiffness for $n>0$, and thus cannot be extended for the initial stiffness.

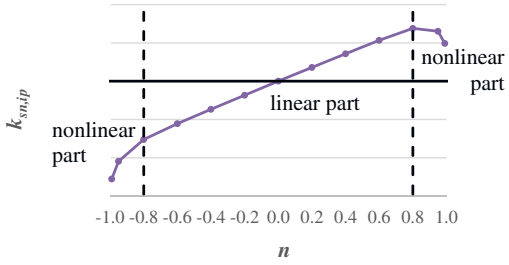

Fig. 8. Approximation model for the chord stress function.

3.2.2. Proposed chord stress function

This section develops a chord stress function for the initial stiffness, using the stated above assessment criteria. Following the numerical observations, the approximation was assumed consisting of a linear and two nonlinear parts (Fig. 8), with the following corresponding equations:

$$k_{sn,ip}=\begin{cases}1+A\cdot f(\beta)\cdot n\cdot\gamma^B-C_1\cdot(|n|-0.8)^2, & -0.99\le n<-0.8\\ 1+A\cdot f(\beta)\cdot n\cdot\gamma^B, & -0.8\le n\le -0.8\\ 1+A\cdot f(\beta)\cdot n\cdot\gamma^B-C_2\cdot(n-0.8)^2, & 0.8<n\le 0.99\end{cases} \tag{21}$$

Analyzing the FEM results, $B=2$ in Eq. (21) was found to provide the most accurate approximation for $0.25\le\beta\le 0.85$; whereas for the joints with $\beta=1.0$, the function was observed not to depend on γ. From that point of view, the curve fitting was conducted separately for the joints with $0.25\le\beta\le 0.85$ and $\beta=1.0$, proposing the linear interpolation for $0.85<\beta<1.0$. Eq. (22) presents the final chord stress function with the following parameters: $R^2=0.95$, $\Delta_{av}=1.8\%$, $\Delta_{max}=9.3\%$.

For $0.25\le\beta\le 0.85$:

$$k_{sn,ip}=\begin{cases}1+0.001\cdot\left(1+1.7\beta-2.6\beta^2\right)\cdot n\cdot\gamma^2-2.7\cdot(|n|-0.8)^2, & -0.99\le n<-0.8\\ 1+0.001\cdot\left(1+1.7\beta-2.6\beta^2\right)\cdot n\cdot\gamma^2, & -0.8<n<0.8\\ 1+0.001\cdot\left(1+1.7\beta-2.6\beta^2\right)\cdot n\cdot\gamma^2-3.1\cdot(n-0.8)^2, & 0.8<n\le 0.99\end{cases}$$

For $0.85<\beta<1.0$:

$k_{sn,ip}$ is the linear interpolation between $\beta=0.85$ and $\beta=1.0$

For $\beta=1.0$:

$$k_{sn,ip}=\begin{cases}1+0.06\cdot n-3.5\cdot(|n|-0.8)^2, & -0.99\le n<-0.8\\ 1+0.06\cdot n, & -0.8<n<0.8\\ 1+0.06\cdot n-2.8\cdot(n-0.8)^2, & 0.8<n\le 0.99\end{cases} \tag{22}$$

3.3. Validation of the proposed chord stress function

The validation of the final chord stress function was conducted with the independent FE results but using the same FE model. To prove that the proposed function is scalable in the main member width, two chord sizes were considered, 100 × 100 and 200 × 200, with $2\gamma=12.5$ and $2\gamma=25$ (Table 6). Validation was performed for two brace widths ($\beta=0.40$ and $\beta=0.90$) and two steel grades (S355 and S700).

The validation results are presented graphically in Figs. 9 and 10. As was expected, when the joints are not loaded by the axial load in the

Table 6
Validation parameters.

Main member	$100\times100\times t_0$		$200\times200\times t_0$	
t_0 [mm]	4	8	8	16
2γ	25	12.5	25	12.5
Connected member	$b_1\times b_1\times t_1$		$b_1\times b_1\times t_1$	
b_1 [mm]	40	90	80	180
β	0.40	0.90	0.40	0.90
Steel grade	S355, S700			
n	−0.99, −0.95, −0.80, −0.60, −0.40, −0.20, 0, 0.20, 0.40, 0.60, 0.80, 0.95, 0.99			

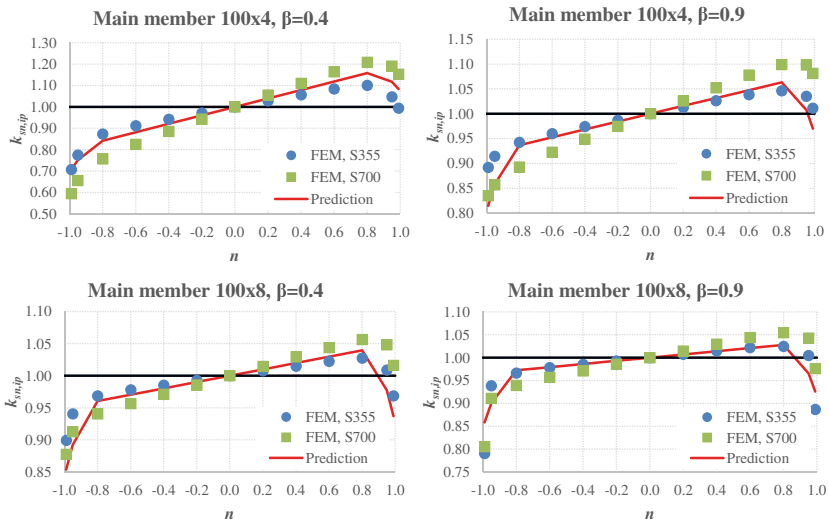

Fig. 9. Validation of the proposed chord stress function, main member size 100 mm.

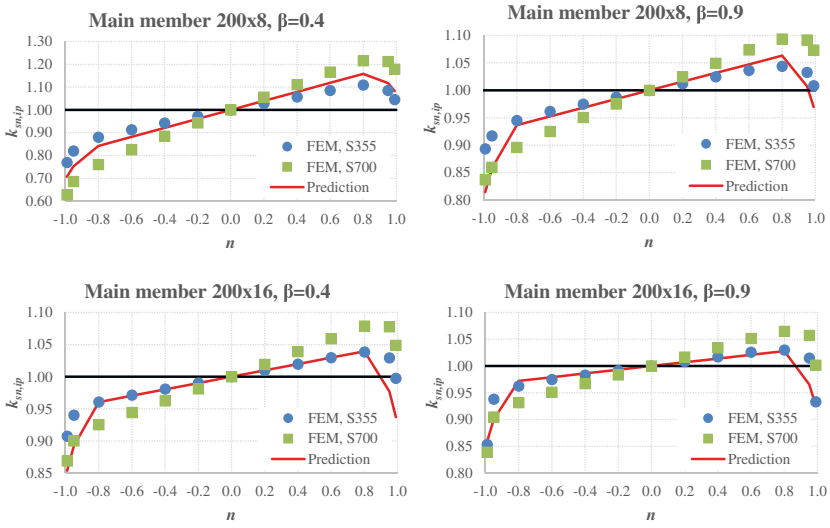

Fig. 10. Validation of the proposed chord stress function, main member size 200 mm.

main member ($n = 0$), their initial rotational stiffness, $S_{j,ini}$, is found not to depend on the steel grade: the joints made of S355 steel have exactly the same initial stiffness as the corresponding ones made of S700. However, the stresses in the main member lead to noticeable discrepancy in the stiffness values for different steel grades. The difference increases with the increase of n, leading to the same discrepancy in the chord stress function, $k_{sn,ip,FEM}$. The largest differences Δ are observed for $n = -0.99$ (16%) and $n = 0.99$ (14%).

At the same time, the proposed chord stress function $k_{sn,ip}$ is developed for all steel grades. Based on the numerical data for S500, it provides the results intermediate between S355 and S700, with the largest errors in the cases close to yielding ($n = \pm 0.95 \ldots 0.99$). However, in the practical range $-0.95 \le n \le 0.95$, the observed discrepancy between the results does not exceed 10% and can be neglected. The manual calculations of the chord stress function, presented in Table 7, show that the change of the steel grade with a constant axial force in the chord affects the relative axial force n, which finally influences the chord stress function. Therefore, in principle, the function is not

Table 7
Validation of the chord stress function. Main member 200 × 200 × 8, $2\gamma = 25$, $\beta = 0.40$.

N [kN]	A [cm^2]	f_{y0} [MPa]	n	$k_{sn,ip}$	$k_{sn,ip,FEM}$	$k_{sn,ip}/k_{sn,ip,FEM}$
−2000	59.24	355	−0.95	0.75	0.82	0.91
−2000	59.24	500	−0.68	0.87	0.85	1.02
−2000	59.24	700	−0.48	0.90	0.87	1.03

dependent on the steel grade but on the stress and strain level of the chord. The overall evaluation of the results shows that the developed chord stress function provides rather accurate prediction, with the final average error of 3.0% for steels in the range from S355 to S700.

4. Conclusions

This article analyzes the approach provided in [25] for analytical evaluation of the initial rotational stiffness for welded RHS T joints. By the comparison with the experimental data, it is shown that the original approach considerably underestimates the initial stiffness of the joints. To obtain more accurate results, the improved equation is proposed for the component 'main member flange in bending'. It is also found that the size of the fillet weld noticeably affects the initial rotational stiffness of the joint.

Based on the 3D FEM analysis of square hollow section joints, the axial stress in the main member is found to affect significantly their initial rotational stiffness, with the maximum decrease of stiffness by 50% for compressive loads and the maximum increase by 30% for tensile loads. The observed effect is found to depend on the brace-to-chord width ratio β and the chord width-to-thickness ratio γ.

To get reliable results in frame analyses, the chord stress function for the initial rotational stiffness of T joints is proposed, similar to that for moment resistance. The function is developed using the curve fitting technique, based on the obtained numerical results. The function is presented divided in three parts: the linear part in the range $-0.8 \le n \le 0.8$ and two nonlinear parts with $-0.99 \le n < -0.8$ and $0.8 < n \le 0.99$. The different functions are proposed for the range $0.25 \le \beta \le 0.85$ and $\beta = 1.0$, with the linear interpolation for $0.85 < \beta < 1.0$. In the considered range, the proposed solution matches well to the numerical results and can be recommended for using in the frame design of square hollow section joints. However, more research is required to extend the function for RHS joints.

References

[1] L.M.C. Simoes, Optimization of frames with semi-rigid connections, Comput. Struct. 60 (4) (1996) 531–539.
[2] D.E. Grierson, L. Xu, Design optimization of steel frameworks accounting for semi-rigid connections, in: G.I.N. Rozvany (Ed.), Optimization of Large Structural Systems, vol. II, Kluwer Academic Publisher, Dordrecht 1993, pp. 873–881.
[3] K. Bzdawka, Optimization of Office Building Frame With Semi-Rigid Joints in Normal and Fire ConditionsPhD Thesis 1038, Tampere Univ. Technol. Publ., 2012
[4] H. Boel, Buckling Length Factors of Hollow Section Members in Lattice GirdersMs Sci thesis Eindhoven University of Technology, Eindhoven, 2010.
[5] H.H. Snijder, H.D. Boel, J.C.D. Hoenderkamp, R.C. Spoorenberg, Buckling length factors for welded lattice girders with hollow section braces and chords, Proc. Eurosteel 2011 (2011) 1881–1886.
[6] M. Heinisuo, Ä. Haakana, Buckling of members of welded tubular truss, Nord. Steel Constr. Conf. 2015 (2015).
[7] J. Wardenier, Hollow Section Joints, Delft University of Technology, Delft, 1982.
[8] (CEN) European Committee for Standardization, Eurocode 3. Design of Steel Structures, Part 1–8: Design of Joints (EN 1993-1-8:2005)(Brussels) 2005.
[9] (IIW) International Institute of Welding, ISO 14346:2013, Static Design Procedure for Welded Hollow-section Joints - Recommendations, 2013.
[10] M. Tabuchi, H. Kanatani, T. Kamba, The local strength of welded RHS T joints subjected to bending moment, CIDECT Rep. 5AF-84/5E, 1984.
[11] J. Szlendak, Beam-column welded RHS connections, Thin-Walled Struct. 12 (1) (1991) 63–80.
[12] J.A. Packer, Moment connections between rectangular hollow sections, J. Constr. Steel Res. 25 (1–2) (1993) 63–81.
[13] Y. Yu, The Static Strength of Uniplanar and Multiplanar Connections in Rectangular Hollow SectionsDoctoral Dissertation Delft University of Technology, Delft, 1997.
[14] L. Lu, The Static Strength of I-Beam to Rectangular Hollow Section Column ConnectionsDoctoral Dissertation Delft University Press, Delft, 1997.
[15] X.-L. Zhao, Deformation limit and ultimate strength of welded T-joints in cold-formed RHS sections, J. Constr. Steel Res. 53 (2) (2000) 149–165.
[16] P. Ongelin, I. Valkonen, S.S.A.B. Domex Tube, Structural hollow sections, EN 1993 - Handbook 2016, SSAB Europe Oy, 2016.
[17] J. Wardenier, G.J. van der Vegte, D.K. Liu, Chord stress functions for K gap joints of rectangular hollow sections, Int. J. Offshore Polar Eng. 17 (3) (2007) 225–232.
[18] D.K. Liu, J. Wardenier, G.J. van der Vegte, et al., New chord stress functions for rectangular hollow section joints, Proc. Fourteenth Int. Offshore Polar Eng. Conf 2004, pp. 178–185.
[19] J. Wardenier, G.J. van der Vegte, D.K. Liu, Chord stress function for rectangular hollow section X and T joints, Proc. Seventeenth Int. Offshore Polar Eng. Conf 2007, pp. 3363–3370.
[20] A. Nizer, L.R.O. de Lima, P.C.G. da, S. Vellasco, S.A.L. de Andrade, E. da, S. Goulart, A.T. da Silva, L.F. da, C. Neves, Structural behaviour of T RHS joints subjected to chord axial force, Proc. 15th Int. Symp. Tubul. Struct. Rio Janeiro, Brazil, 27–29 May 2015 2015, pp. 371–378.
[21] A. Lipp, T. Ummenhofer, Influence of tensile chord stresses on the strength of CHS X-joints – experimental and numerical investigations, Proc. 15th Int. Symp. Tubul. Struct. Rio Janeiro, Brazil, 27–29 May 2015 2015, pp. 379–386.
[22] R.M. Korol, F.A. Mirza, Finite element analysis of RHS T-joints, J. Struct. Div. 108 (9) (1982) 2081–2098.
[23] P. Mäkeläinen, R. Puthli, F. Bijlaard, Strength. stiffness and nonlinear behaviour os simple tubular joints, IABSE Congr. Rep. 13 (1988) 635–640.
[24] P. Zoetemeijer, Design method for the tension side of statically loaded, bolted beam-to-column connections, Heron. 20 (1) (1974) 1–59.
[25] D. Grotmann, G. Sedlacek, Rotational Stiffness of Welded RHS Beam-to-Column Joints. Cidect 5BB-8/98, RWTH-Aachen, Aachen, 1998.
[26] K. Weynand, J.P. Jaspart, J.-F. Demonceau, L. Zhang, Component method for tubular joints, CIDECT Report 16F – 3/15, 2015.
[27] J. Packer, R. Puthli, G.J. van der Vegte, J. Wardenier, Discussion on the paper "Experimental and numerical assessment of RHS T-joints subjected to brace and chord axial forces", by Nizer et al., Steel Construction 9 (2016), No. 4, pages 315–322, Steel Constr. 10 (1) (2017) 89–90.
[28] M. Heinisuo, H. Perttola, H. Ronni, A step towards the 3D component method for modelling beam-to-column joints, Steel Constr. 7 (1) (2014) 8–13.
[29] A.A. Del Savio, D.A. Nethercot, P.C.G.S. Vellasco, S.A.L. Andrade, L.F. Martha, Generalised component-based model for beam-to-column connections including axial versus moment interaction, J. Constr. Steel Res. 65 (8–9) (2009) 1876–1895.
[30] K.W. Johansen, Brudlinieteorier. Copenhagen: Forlag, 191 pp. (Yield Line Theory, Translated By Cement and Concrete Association, London, 1962. 181 pp.), 1943.
[31] J. Havula, H. Myllymäki, I. Sorsa, J. Haapio, M. Heinisuo, Experimental research of welded tubular HSS T-joints, welding times and moment resistances, IIW International Conference High Strength Materials – Challenges and Applications, 2–3 July 2015, Helsinki, Finland, 2015.
[32] F. Mang, Ö. Bucak, Hohlprofilkonstruktionen, Stahlbauhandbuch, Stahlbau-Verlag-GmbH Köln, 1982.
[33] H. Kanatani, K. Fujiwara, M. Tabuchi, T. Kamba, Bending tests on T-joints of RHS chord and RHS or H-shape branch, CIDECT Programme 5AF, 1981.
[34] A.D. Christitsas, D.T. Pachoumis, C.N. Kalfas, E.G. Galoussis, FEM analysis of conventional and square bird-beak SHS joint subject to in-plane bending moment — experimental study, J. Constr. Steel Res. 63 (10) (2007) 1361–1372.
[35] M. Heinisuo, M. Garifullin, T. Jokinen, T. Tiainen, K. Mela, Surrogate modeling for rotational stiffness of welded tubular Y-joints, Proceedings of The Eighth International Workshop on Connections in Steel Structures (Connections VIII) 2016, pp. 285–294.
[36] M. Garifullin, S. Pajunen, K. Mela, M. Heinisuo, 3D component method for welded tubular T joints, Int. Symp. Tubul. Struct. Melbourne, Aust. 4–6 December 2017, 2017 Accept. Publ.
[37] Abaqus 6.12, Getting Started with Abaqus, Dassault Systèmes, Interactive edition, 2012 695 pp.
[38] M. Garifullin, S. Pajunen, K. Mela, M. Heinisuo, Finite element model for rectangular hollow section T joints, Adv. Steel Constr. (2017) Submitt.
[39] (CEN) European Committee for Standardization, Cold formed welded structural hollow sections of non-alloy and fine grain steels, Part 2: Tolerances, Dimensions and Sectional Properties (EN 10219-2:2006), 2006 Brussels.
[40] G.J. van der Vegte, Y. Makino, Further research on chord length and boundary conditions of CHS T- and X-joints, Adv. Steel Constr. 6 (3) (2010) 879–890.
[41] Ä. Haakana, In-plane Buckling and Semi-Rigid Joints of Tubular High Strength Steel TrussesMs Sci thesis Tampere University of Technology, Tampere, 2014.
[42] H. AlHendi, M. Celikag, Behavior of reverse-channel and double-reverse-channel connections to tubular columns with HSS, J. Constr. Steel Res. 112 (2015) 271–281.

III

MOMENT-ROTATION BEHAVIOR OF WELDED TUBULAR HIGH STRENGTH STEEL T JOINT

by

Havula J., Garifullin M., Heinisuo M., Mela K., & Pajunen S., 2018

Engineering Structures vol. 172, 523-537

Engineering Structures 172 (2018) 523–537

Contents lists available at ScienceDirect

Engineering Structures

journal homepage: www.elsevier.com/locate/engstruct

Moment-rotation behavior of welded tubular high strength steel T joint

Jarmo Havula[a], Marsel Garifullin[b,*], Markku Heinisuo[b], Kristo Mela[b], Sami Pajunen[b]

[a] Häme University of Applied Sciences, Hämeenlinna, Finland
[b] Tampere University of Technology, Tampere, Finland

ARTICLE INFO

Keywords:
High strength steel
Welded tubular T joint
In-plane moment-load
Moment resistance
Rotational stiffness
Ductility
Reduction coefficient

ABSTRACT

Based on recent studies, high strength steels (HSS) can be efficiently used in civil engineering, reducing the consumption of material and CO_2 emissions. The present Eurocode contains the reduction coefficients (0.8 and 0.9 depending on the steel grade) for high strength steel joints. These reduction factors lead to the excessive consumption of material, making the usage of HSS for construction not as economically viable as it might be. The scope of this paper is to present experimental results dealing with the welded in-plane moment-loaded HSS joints. Twenty tests on square hollow section T joints were performed to observe their moment-rotation relationship, studying the following parameters: (1) bending resistance, (2) rotational stiffness, (3) ductility. The results show that the reduction factors are needed only for butt-welded joints, as well as for joints with small fillet welds and made of steel grades higher than S500. The required ductility was achieved by all specimens, even when using welds smaller than full-strength fillet welds. In addition, it was shown experimentally that fillet welds considerably increase the resistance and stiffness of joints.

1. Introduction

The application field for high strength steel (HSS) joints covers a wide range of structures, including bridges, lattice masts, towers and buildings with large openings. Hollow section joints subject to bending moment are found in beam-to-column connections or as a simple joint configuration in Vierendeel girders. The beam-to-column T joint is comprised of a brace member connected at an angle of 90° to a chord member.

The developments in manufacturing processes and material technologies increased the strength of available steels worldwide [1]. Generally, the steel grade $f_y \leq 355$ MPa is considered as regular steel, although basic Eurocodes EN 1993-1-1 to EN 1993-1-11 consider steel grades up to $f_y \leq 460$ MPa, where f_y is the yield strength. Following EN 1993-1-12:2007 [2], high strength steel is defined as 460 MPa $< f_y \leq 700$ MPa. To make the usage of HSS in construction as viable as possible, more precise and accurate calculation methods should be developed for HSS structures. Attention should be paid particularly to the resistance and rotational stiffness of joints. The increase of joint resistance clearly reduces material consumption, while the increase of stiffness affects the load distribution in the structure and reduces the buckling length of members, contributing to the reduction of costs.

Currently, EN 1993-1-8:2005 [3] and EN 1993-1-12:2007 [2] contain additional rules for HSS joints. Following these rules, clause 7.1.1(4) of EN 1993-1-8:2005 requires using the factor 0.9 for the static design resistances of end-products with a nominal yield strength higher than 355 N/mm^2. This rule must be fulfilled for the design equations in Section 7; however, it does not concern the design of welds. In addition, clause 2.8 of EN 1993-1-12:2007 specifies the reduction factor 0.8 for steel grades greater than S460 up to S700. The identical requirements can be found in the latest CIDECT Design Guide No. 3 [4]. In the design of HSS joints, these factors considerably reduce the design resistance of joints, making their design very conservative.

Currently, there is no clear evidence regarding the origin of these reduction factors. It should be noted that the rules for HSS have been developed based on a very limited number of experiments with variable types of joints, especially when considering full-scale HSS joints. The lack of experimental data could have led to the necessity to reduce the design resistance of HSS joints, leading to the introduction of these factors. According to [5] and CIDECT Design Guide No. 3 [4], the need for the reduction factors can be explained by the relatively larger deformations that take place in joints with nominal yield strengths of approximately 450–460 MPa, when the plastification of the connecting tubular face occurs. A broad discussion on this issue can be found in [6]. Based on about 100 tests on HSS joints, it proposes no reduction for a steel grade S500, but implies the reduction factor 0.9 for the a grade S700 when the connected brace is loaded with an axial load.

At the same time, the reduction can be also caused by the softening of the heat affected zone (HAZ) [7–9]. According to [8], the effect of weld-induced heat on the mechanical properties of steel tubes results in

* Corresponding author.
E-mail address: marsel.garifullin@tut.fi (M. Garifullin).

https://doi.org/10.1016/j.engstruct.2018.06.029
Received 6 July 2017; Received in revised form 12 March 2018; Accepted 6 June 2018

an overall reduction around of 8% in HSS. Dunđer et al. [10] present the $t_{8/5}$ cooling time–hardness relationship for TStE 420 steel HAZ softening, clearly indicating the importance of HAZ and weld-heat input when considering the resistance of HSS welded joints. However, both EN 1993-1-8:2005 and EN 1993-1-12:2007 require no reductions in HAZ. Only the Finnish National Annex for EN 1993-1-12:2007 [11] contains a rule to reduce the yield strength, with the factors 1.0 for S500, 0.85 for S700 and linear interpolation in between. However, this reduction does not concern the design equations for hollow section joints in Section 7 of EN 1993-1-8:2005. In any case, this issue remains open and requires more research for moment-loaded joints.

Another problem of HSS joints is the high price of welding when full-strength welds are used. According to [12], full-strength fillet welds result in extremely large throat thickness, namely $1.48\,t_1$ for S420, $1.61\,t_1$ for S500 and $1.65\,t_1$ mm for S700, where t_1 is the wall thickness of the connected tube. Such large welds increase the number of welding runs and thus, taking into account the high costs of welding, make the welding process extremely expensive for HSS joints. According to [6], the full-strength fillet-weld throat thicknesses can be reduced to $1.0\,t_1$ for S500, $1.2\,t_1$ for S700 and $1.4\,t_1$ for S960, provided that they can resist the loads.

Subsequent to the above discussion, the scope of this paper is to present the experimental results of welded moment-loaded HSS joints. Twenty tests on square hollow section T joints were performed to:

- observe the moment-rotation relationship in the whole range of loading: initial stiffness, hardening stiffness, plastic and ultimate moment resistances and ductility;
- determine the need for the reduction coefficients and propose smaller ones, if possible;
- evaluate the ductility of joints and justify the use of welds that are smaller than full-strength ones.

The paper considers only joints with the brace-to-chord width ratio $\beta = b_1/b_0 \leq 0.85$, i.e., when chord face bending governs the deformation of the specimen. Joints with fillet and butt welds are considered. Fig. 1 presents the typical moment-rotation relationship for a hollow section joint with $\beta \leq 0.85$. In the figure, $M_{pl,\mathrm{exp}}$ and $M_{u,\mathrm{exp}}$ denote plastic and ultimate moment resistances, respectively; $S_{j,ini}$ and $S_{j,h}$ denote initial and hardening rotational stiffness, respectively; φ_u denotes rotation corresponding to ultimate resistance. According to [13], for this type of joints plastic moment resistance $M_{pl,\mathrm{exp}}$ is determined as the intersection of the two tangent lines corresponding to initial and hardening stiffness.

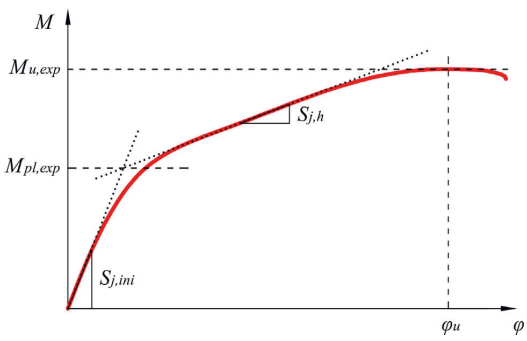

Fig. 1. Typical M-φ relationship for hollow section T joint with $\beta \leq 0.85$.

2. Literature review

2.1. Moment resistance

The first equations for the strength of moment-loaded hollow section joints can be found in [14–17]. A comprehensive research on tubular joints was conducted by Wardenier [18], who first proposed the design formulae based on the classical yield line theory. Currently, these rules are used in many design standards, such as EN 1993-1-8:2005 [3], ISO 14346:2013 [19], and CIDECT Design Guide No. 3 [4]. Some newer experimental tests are presented in [20,21]. Tabuchi et al. [22] presented experimental results for in-plane moment-loaded rectangular hollow section (RHS) T joints and examined their local failures. Szlendak [23] and Packer [24] developed design procedures for RHS connections under the moment loading. Intensive research for uniplanar and multiplanar RHS joints was conducted by Yu [25]. The deformation limit of RHS joints was investigated by Lu et al. [26] and Zhao [27]. The comparison of conventional and bird-beak RHS joints under in-plane bending moment has been conducted in [28]. Cyclic tests on welded RHS connections were performed in [29]. Fatigue tests on hollow section joints made of HSS can be found in [30]. However, most of the presented tests have been conducted for regular steels; no experiments can be found for HSS tubular joints under static moment loading.

2.2. Rotational stiffness

In addition to moment resistance, rotational stiffness is an important quantity in the design of joints, needed particularly in a global analysis model based on beam elements. In addition, initial rotational stiffness has a great effect when cost optimal solutions are sought, both in sway frames [31–35] and non-sway frames [36]. Moreover, rotational stiffness was shown to have an influence on the buckling lengths of truss members [37–39]. Grotmann and Sedlacek [13] employed the component method to propose theoretical equations for the initial rotational stiffness of RHS T joints. Later, these equations were validated against experimental results in [40].

2.3. Ductility

The ductility requirements are not as straightforward as those for moment resistance and initial stiffness, being dependent on the case. EN 1993-1-8:2005 and EN 1993-1-12:2007 provide the requirements for the basic steel material using the ultimate strain ε_u. Annex C of EN 1993-1-5:2006 [41] recommends a value of 5% for the principal strain at the ultimate limit state. To evaluate the ductility of members, the factor R, the ratio of plastic and elastic rotation, is used, being dependent on the layout of the frame and the loading conditions [42,43]. A continuous beam with $R = 3$, the most unfavorable system, is accepted in EN 1993-1-1:2005 [44] as the minimum requirement for the members belonging to the cross-section class 1, allowing the global plastic design of the frame.

Rotation capacity has been studied by Beg et al. [45], who limited the rotation capacity of the entire joint by limiting the relevant principal strains of distinct components to 10–20%. EN 1998-1:2004 [46] proposes a general limit of 0.035 rad for joint rotation to fulfil the requirements for the seismic design. This rule is aimed to allow joints form a sufficient plastic hinge to carry cyclic loads without a brittle fracture in the connection [47].

For tubular joints, the ultimate deformation limit was proposed by Lu et al. [26] to define the strength of joints that do not exhibit a pronounced peak load. Later it was discussed in [27,48]. Following this rule, the local displacement of the chord is limited to 3% of the width of the chord b_0. Applying this rule to moment-loaded joints, the rotation of the joint φ is limited to $\varphi_{lim,3\%} = 0.03b_0/(h_1/2)$, where h_1 is the height of the brace. This limit is based on the observation that hollow section

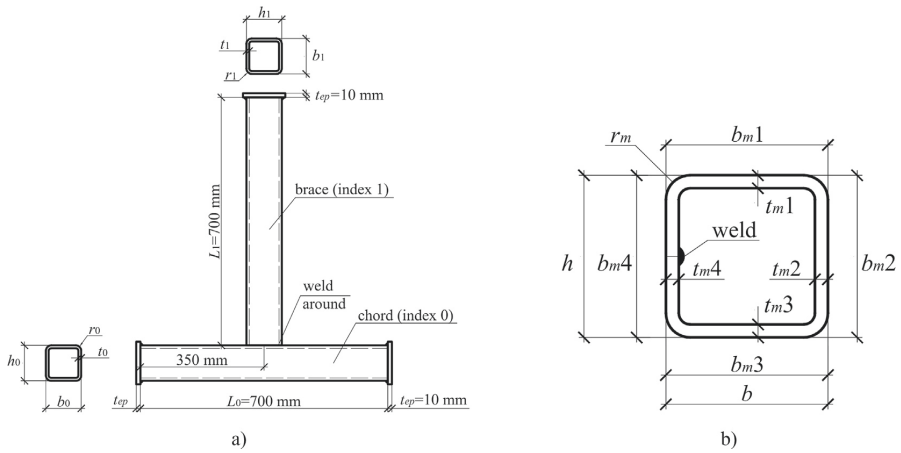

Fig. 2. Test specimen: (a) overall view, (b) measured dimensions of tube. Plate 1 corresponds to compressed flange of brace.

joints that did exhibit a peak load had a corresponding local deformation of the chord face between 2.5 and 4% of b_0 [48]. Currently the limit is adopted by the International Institute of Welding (IIW) as the ultimate deformation limit to define and compare the strength of welded hollow section connections.

3. Experimental study

A total of twenty experiments with tubular T joints were performed at the Sheet Metal Centre at Häme University of Applied Sciences (HAMK), Finland. The specimens differed in steel grade, the size of welds and the type of welding. The brace of the specimen was welded at the midpoint of the chord at an angle of 90°, as shown in Fig. 2a. The brace-to-chord width ratio β varied from 0.67 to 0.80. Both the chord and the brace had a length of 700 mm. The 170 × 170 × 10 mm plates were welded at the ends of the chord, and 120 × 120 × 10 mm plates (140 × 140 × 10 for 120 mm brace) were welded at the ends of the brace, all made of S355 steel. The measured cross-section dimensions of the tubes are presented in Table 1, where the naming of the test specimens is presented in the format [chord material]_[brace material]_[weld type] and the measured dimensions follow the notations of Fig. 2b. The thicknesses (t_{m1}, t_{m2}, t_{m3}, t_{m4}) of the tubes were measured on the four sides of each tube. Radius r_m is an average value of the measured values. Three steel grades and their combinations were considered: S420, S500 and S700. Table 2 presents the details of steels and their properties obtained from tensile coupon tests.

Three weld types, a6 and a10 fillet welds and 1/2v butt welds, were selected to determine the effect of the weld type and size on the resistance and stiffness of the joints (Table 3). The 1/2v butt welds were performed following EN ISO 9692-1:2013 [49], with no root support and with an 8 mm deep bevel all around the end of the brace (Fig. 3). The bevel shape complied with EN ISO 9692-1:2013, Table 1, Ref. No. 1.9.1, meaning a zero air gap (allowed max 2–4 mm) and a 45° angle (allowed 35–60°). However, the rules were violated in terms of the zero peak (straight part) at the bevel end (allowed 1–2 mm). The groove support was made by welding firstly a small weld at the groove tip, followed by the final load-bearing weld.

The throat thicknesses of welds a_w were chosen to be less than the required full-strength weld sizes $a_{w,fs}$. This can be justified by clause 7.3.1 (6) of EN 1993-1-8:2005, which states: “The criterion given in 7.3.1(4) may be waived where a smaller weld size can be justified both with regard to resistance and with regard to deformation capacity and rotation capacity.” The throat thicknesses were selected so that for some joints (a6 joints) the design resistance of welds was knowingly lower than the moment resistance based on chord face failure, while for others (a10 joints) it was higher. The throat thicknesses of full-strength fillet welds were determined according to [12]: $a_{w,fs} = 1.48\,t_1$ for S420, $a_{w,fs} = 1.61\,t_1$ for S500 and $a_{w,fs} = 1.65\,t_1$ for S700; where $t_1 = 8$ mm is the thickness of the brace. The ratio $a_w/a_{w,fs}$ is provided in Table 3.

Two welding processes were used: MAG (manual welding) and MAG Wise (manual welding with Wise features), developed by Kemppi Oy (Lahti, Finland) and used for robot welding. The welding positions PB and PF were determined following DIN EN ISO 6947. The specimens were welded by a certified welder, following the instructions of the steel manufacturer in terms of heat input, weld speed, and cooling time $t_{8/5}$ to obtain the required strength of the weld. All filler materials were over-matching, meaning that the yield strength of the filler materials was larger than the base material in all tests. The actual weld sizes were not measured and all calculations were performed using the nominal values.

Fig. 4 shows the test setup and the static model of the test specimen with the locations of the displacement transducers and the load cell. The corresponding measured displacements are denoted as v_{D1}, v_{D2}, v_{D3}, v_{D4} and v_{D5}. Transducers $D1$ and $D2$ measured the same displacement. Transducer $D1$ was located inside the hydraulic cylinder. Transducer $D2$ was supported from the floor and was used to validate transducer $D1$, since the hydraulic cylinder could move up under high loads, increasing the values of transducer $D1$. The force F was measured by the load cell installed at the head of the hydraulic cylinder (max load 250 kN). All tests were displacement-controlled, with the 20 mm/min loading speed.

The vertical displacement at the end of the brace δ_b was calculated according to Eq. (1), subtracting the following from displacement v_{D1}:

(1) the axial displacement v_{D5}, corresponding to the vertical displacement of the upper end of the specimen in relation to the floor, as shown in Fig. 5a.
(2) the rigid body motion of the test specimens δ_{rb} due to the displacements at the supports v_{D3} and v_{D4}, as shown in Fig. 5b.

$$\delta_b = v_{D1} - v_{D5} - \delta_{rb} = v_{D1} - v_{D5} - \frac{L_1 + h_0/2}{L_0 + t_{ep}} \cdot (v_{D4} - v_{D3}) \quad (1)$$

The local rotation of the joint φ was defined at the point where the brace was connected to the face of the chord. Generally, displacement δ_b corresponds to the global behavior of the specimen, which incorporates three simultaneous processes: the elastic bending of the brace (Fig. 6a), the elastic bending of the chord (Fig. 6b) and the local deformation of the joint (Fig. 6c). The latter is used to evaluate the moment-rotation behavior of the joint. Therefore, to obtain the local

Table 1
Measured section dimensions [mm].

Specimen	β	Member	Section	t_{m1}	t_{m2}	t_{m3}	t_{m4}	r_m	b_{m1}	b_{m3}	b_{m4}	b_{m2}
S420_S420_a6	0.67	Chord	150 × 150 × 8	7.88	8.00	7.95	8.07	21.00	151.70	151.70	151.30	151.30
		Brace	100 × 100 × 8	7.92	7.99	7.88	7.96	20.30	100.30	100.30	100.70	100.70
S500_S420_a6	0.67	Chord	150 × 150 × 8	7.89	8.05	7.90	8.03	19.50	149.60	149.60	150.00	150.00
		Brace	100 × 100 × 8	7.92	7.99	7.88	7.96	21.50	100.20	100.20	100.70	100.70
S500_S500_a6	0.67	Chord	150 × 150 × 8	7.89	8.05	7.90	8.03	20.50	149.90	149.90	151.50	151.50
		Brace	100 × 100 × 8	7.90	8.02	8.04	8.01	21.00	100.66	100.66	100.50	100.50
S700_S420_a6	0.67	Chord	150 × 150 × 8	7.84	7.95	7.89	7.97	19.50	150.70	150.70	151.60	151.60
		Brace	100 × 100 × 8	7.92	7.99	7.88	7.96	20.35	101.00	101.00	100.20	100.20
S700_S500_a6	0.67	Chord	150 × 150 × 8	7.84	7.95	7.89	7.97	19.50	150.60	150.60	150.90	150.90
		Brace	100 × 100 × 8	7.90	8.02	8.04	8.01	19.50	100.50	100.50	100.40	100.40
S700_S500_a6_WiPF	0.67	Chord	150 × 150 × 8	7.84	7.95	7.89	7.97	19.50	150.80	150.80	151.10	151.10
		Brace	100 × 100 × 8	7.90	8.02	8.04	8.01	19.50	100.60	100.60	100.55	100.55
S700_S700_a6	0.80	Chord	150 × 150 × 8	7.84	7.95	7.89	7.97	21.00	150.80	150.80	150.60	150.60
		Brace	120 × 120 × 8	7.96	7.96	8.01	7.96	20.50	120.60	120.60	120.40	120.40
S420_S420_a10	0.67	Chord	150 × 150 × 8	7.88	8.00	7.95	8.07	20.50	151.40	151.40	150.80	150.80
		Brace	100 × 100 × 8	7.92	7.99	7.88	7.96	20.00	100.94	100.94	100.33	100.33
S500_S420_a10	0.67	Chord	150 × 150 × 8	7.89	8.05	7.90	8.03	19.50	149.70	149.70	151.00	151.00
		Brace	100 × 100 × 8	7.92	7.99	7.88	7.96	20.50	100.80	100.80	100.30	100.30
S500_S500_a10	0.67	Chord	150 × 150 × 8	7.89	8.05	7.90	8.03	20.00	149.50	149.50	150.70	150.70
		Brace	100 × 100 × 8	7.90	8.02	8.04	8.01	19.50	100.50	100.50	100.40	100.40
S700_S420_a10	0.67	Chord	150 × 150 × 8	7.84	7.95	7.89	7.97	19.50	151.20	151.20	151.50	151.50
		Brace	100 × 100 × 8	7.92	7.99	7.88	7.96	22.00	100.80	100.80	100.15	100.15
S700_S500_a10	0.67	Chord	150 × 150 × 8	7.84	7.95	7.89	7.97	20.00	150.90	150.90	151.80	151.80
		Brace	100 × 100 × 8	7.90	8.02	8.04	8.01	20.00	100.60	100.60	100.50	100.50
S700_S500_a10_WiPF	0.67	Chord	150 × 150 × 8	7.84	7.95	7.89	7.97	20.50	151.20	151.20	151.90	151.90
		Brace	100 × 100 × 8	7.90	8.02	8.04	8.01	21.50	100.58	100.58	100.64	100.64
S700_S700_a10	0.80	Chord	150 × 150 × 8	7.84	7.95	7.89	7.97	20.50	150.50	150.50	151.30	151.30
		Brace	120 × 120 × 8	7.96	7.96	8.01	7.96	20.50	120.64	120.64	120.60	120.60
S420_S420_1/2v	0.67	Chord	150 × 150 × 8	7.88	8.00	7.95	8.07	20.50	150.60	150.60	151.60	151.60
		Brace	100 × 100 × 8	7.92	7.99	7.88	7.96	20.50	100.33	100.33	100.85	100.85
S500_S420_1/2v	0.67	Chord	150 × 150 × 8	7.89	8.05	7.90	8.03	19.50	149.70	149.70	150.30	150.30
		Brace	100 × 100 × 8	7.92	7.99	7.88	7.96	19.50	100.84	100.84	100.35	100.35
S500_S500_1/2v	0.67	Chord	150 × 150 × 8	7.89	8.05	7.90	8.03	20.50	149.60	149.60	151.40	151.40
		Brace	100 × 100 × 8	7.90	8.02	8.04	8.01	21.00	100.60	100.60	100.58	100.58
S700_S420_1/2v	0.67	Chord	150 × 150 × 8	7.84	7.95	7.89	7.97	20.00	150.70	150.70	151.70	151.70
		Brace	100 × 100 × 8	7.92	7.99	7.88	7.96	18.50	100.85	100.85	99.90	99.90
S700_S500_1/2v	0.67	Chord	150 × 150 × 8	7.84	7.95	7.89	7.97	20.50	150.50	150.50	151.70	151.70
		Brace	100 × 100 × 8	7.90	8.02	8.04	8.01	18.50	100.16	100.16	101.46	101.46
S700_S700_1/2v	0.80	Chord	150 × 150 × 8	7.84	7.95	7.89	7.97	19.50	150.10	150.10	150.90	150.90
		Brace	120 × 120 × 8	7.96	7.96	8.01	7.96	19.00	121.50	121.50	120.50	120.50

rotation of the joint φ, the displacement δ_b was reduced by the displacement due to elastic bending of the brace δ_{db} and the displacement due to elastic bending of the chord δ_{dc}:

$$\varphi = \frac{\delta_b - \delta_{db} - \delta_{dc}}{L_1} \tag{2}$$

Displacements of the brace and the chord were found according to the equations from strength of materials:

$$\delta_{db} = \frac{F L_1^3}{3 E I_1} \tag{3}$$

$$\delta_{dc} = \frac{M}{3 L_0^2 E I_0} \cdot \left[\left(\frac{L_0}{2} \right)^3 + \left(\frac{L_0}{2} \right)^3 \right] \cdot \left(L_1 + \frac{h_0}{2} \right) \tag{4}$$

where E is the Young's modulus of steel; I_1 and I_0 are correspondingly the second moments of inertia of the brace and the chord; $M = F \cdot (L_1 + h_0/2)$ is the bending moment defined at the line where the brace is connected to the center line of the chord. It should be noted that the paper does not consider the second order effects due to the deflection of the chord (e.g., the horizontal movement of the loading point), as well as the shear deflection of the connected members.

4. Theoretical calculations

4.1. Design moment resistance

Generally, the structural behavior of tubular joints is complicated by a non-uniform stress distribution over the surface of the chord. As it is shown in [18], the elastic stress distribution becomes particularly non-uniform for joints with small β, sharply increasing in the corners of the brace. For this reason, an analytical solution for joint resistance is very complicated and is generally replaced by a semi-analytical approach, which assumes an uniform distribution [18]. Moreover, as stresses reach the yield strength of steel and initiate plastic deformations, the stress distribution becomes more uniform, justifying the adopted assumption.

According to EN 1993-1-8:2005, the deformation of RHS T joints with $\beta \leq 0.85$ is governed by chord face failure. Since the specimens had welds smaller than full-strength welds, the resistance of welds was also checked. In accordance with the foregoing, the moment joint resistance was found by

$$M_{j,Rd} = \min \{M_{ip,1,Rd}, M_{w,Rd}\} \tag{5}$$

where $M_{ip,1,Rd}$ is the bending moment resistance based on chord face failure and $M_{w,Rd}$ is the bending moment resistance based on weld failure.

Table 2
Measured material properties.

Specimen	Chord	E_0 [GPa]	f_{y0} [MPa]	f_{u0} [MPa]	Brace	E_1 [GPa]	f_{y1} [MPa]	f_{u1} [MPa]
S420_S420_a6	S420	185	507	562	S420	181	502	557
S500_S420_a6	Optim 500 MH	196	602	662	S420	181	502	557
S500_S500_a6	Optim 500 MH	196	602	662	Optim 500 MH	185	563	627
S700_S420_a6	Optim 700 Plus MH	197	769	850	S420	181	502	557
S700_S500_a6	Optim 700 Plus MH	197	769	850	Optim 500 MH	185	563	627
S700_S500_a6_WiPF	Optim 700 Plus MH	197	769	850	Optim 500 MH	185	563	627
S700_S700_a6	Optim 700 Plus MH	197	769	850	Optim 700 Plus MH	199	734	854
S420_S420_a10	S420	185	507	562	S420	181	502	557
S500_S420_a10	Optim 500 MH	196	602	662	S420	181	502	557
S500_S500_a10	Optim 500 MH	196	602	662	Optim 500 MH	185	563	627
S700_S420_a10	Optim 700 Plus MH	197	769	850	S420	181	502	557
S700_S500_a10	Optim 700 Plus MH	197	769	850	Optim 500 MH	185	563	627
S700_S500_a10_WiPF	Optim 700 Plus MH	197	769	850	Optim 500 MH	185	563	627
S700_S700_a10	Optim 700 Plus MH	197	769	850	Optim 700 Plus MH	199	734	854
S420_S420_1/2v	S420	185	507	562	S420	181	502	557
S500_S420_1/2v	Optim 500 MH	196	602	662	S420	181	502	557
S500_S500_1/2v	Optim 500 MH	196	602	662	Optim 500 MH	185	563	627
S700_S420_1/2v	Optim 700 Plus MH	197	769	850	S420	181	502	557
S700_S500_1/2v	Optim 700 Plus MH	197	769	850	Optim 500 MH	185	563	627
S700_S700_1/2v	Optim 700 Plus MH	197	769	850	Optim 700 Plus MH	185	734	854

(1) E_0 is the Young's modulus of the chord.
(2) f_{y0} is the yield strength of the chord.
(3) f_{u0} is the ultimate strength of the chord.
(4) E_1 is the Young's modulus of the brace.
(5) f_{y1} is the yield strength of the brace.
(6) f_{u1} is the ultimate strength of the brace.

Table 3
Weld properties.

Specimen	Welding process and position	Weld	a_w [mm]	$a_{w,fs}$ [mm]	$a_w/a_{w,fs}$
S420_S420_a6	MAG & PB	a6	6	11.9	0.51
S500_S420_a6	MAG & PB	a6	6	11.9	0.51
S500_S500_a6	MAG & PB	a6	6	12.9	0.47
S700_S420_a6	MAG & PB	a6	6	11.9	0.51
S700_S500_a6	MAG & PB	a6	6	12.9	0.47
S700_S500_a6_WiPF	MAG Wise & PB + PF	a6	6	12.9	0.47
S700_S700_a6	MAG & PB	a6	6	13.2	0.45
S420_S420_a10	MAG & PB	a10	10	11.9	0.84
S500_S420_a10	MAG & PB	a10	10	11.9	0.84
S500_S500_a10	MAG & PB	a10	10	12.9	0.78
S700_S420_a10	MAG & PB	a10	10	11.9	0.84
S700_S500_a10	MAG & PB	a10	10	12.9	0.78
S700_S500_a10_WiPF	MAG Wise & PB + PF	a10	10	12.9	0.78
S700_S700_a10	MAG & PB	a10	10	13.2	0.76
S420_S420_1/2v	MAG & PB	1/2v	–	–	–
S500_S420_1/2v	MAG & PB	1/2v	–	–	–
S500_S500_1/2v	MAG & PB	1/2v	–	–	–
S700_S420_1/2v	MAG & PB	1/2v	–	–	–
S700_S500_1/2v	MAG & PB	1/2v	–	–	–
S700_S700_1/2v	MAG & PB	1/2v	–	–	–

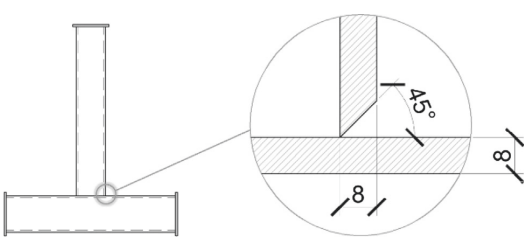

Fig. 3. 1/2v bevel welds.

4.1.1. Moment resistance based on chord face failure

The moment resistance based on chord face failure $M_{ip,1,Rd}$ was calculated according to Table 7.14 of EN 1993-1-8:2005, with the measured yield strengths and the section dimensions and taking into account the reduction factor k_{HSS}:

$$M_{ip,1,Rd} = k_n f_{y0} k_{HSS} t_0^2 h_1 \left(\frac{1}{2\eta} + \frac{2}{\sqrt{1-\beta}} + \frac{\eta}{1-\beta} \right) / \gamma_{M5}, \tag{6}$$

where k_n is the chord stress function (not needed in this case), k_{HSS} is the reduction factor for HSS, $\beta = b_1/b_0$ is the brace-to-chord width ratio, $\eta = h_1/b_0$ is the brace height-to-chord width ratio. In keeping with the conditions for the reduction factors determined in the Introduction, they would take the following values (the given steel grades refer to the chord):

$$k_{HSS} = \begin{cases} 0.9, & \text{S420} \\ 0.8, & \text{S500, S700} \end{cases} \tag{7}$$

4.1.2. Moment resistance based on fillet-weld failure

In this paper, the design resistance of fillet welds is determined using the Directional method presented in EN 1993-1-8:2005. The welds related to b_1 are assumed to carry only the axial force *P,* while the welds related to h_1 are assumed to carry the shear load (Fig. 7a).

The load *P* acting in the weld:

$$P = \frac{M}{z} = \frac{M}{h_1 - t_1}, \tag{8}$$

where the lever arm $z = h_1 - t_1$ is taken from EN 1993-1-8:2005, Figure 6.15.

The stress is calculated by dividing *P* by the throat area A_w (EN 1993-1-8:2005, 4.5.3.2(2)):

$$\sigma_w = \frac{P}{A_w} = \frac{P}{ab_1} = \frac{M}{ab_1(h_1 - t_1)} \tag{9}$$

Stresses acting in the weld (Fig. 7b):

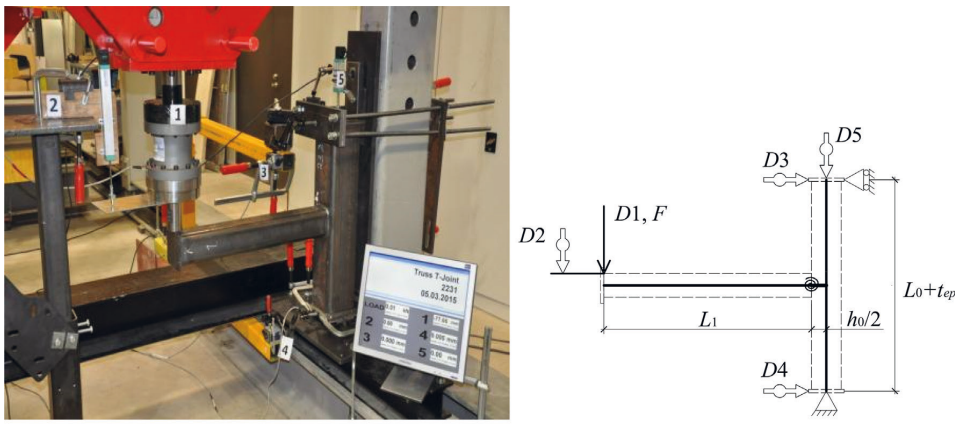

Fig. 4. Test setup: (a) test arrangement overview, (b) static model of test specimen.

$$\sigma_\perp = \tau_\perp = \frac{\sigma_w}{\sqrt{2}} \tag{10}$$

The design resistance of the fillet weld is sufficient if the following is satisfied (EN 1993-1-8:2005, 4.5.3.2(6)):

$$\sqrt{\sigma_\perp^2 + 3(\tau_\perp^2 + \tau_\parallel^2)} \leqslant \frac{f_u}{\beta_w \gamma_{M2}}, \tag{11}$$

where $\beta_w = 1$ is the correlation factor for steel grades higher or equal to S420 and f_u is the minimum ultimate strength.

By putting (10) to (11):

$$\sigma_w = \frac{f_u}{\gamma_{M2}\sqrt{2}} \tag{12}$$

Equalizing (9) to (12):

$$\frac{M_{w,N,Rd}}{ab_1(h_1 - t_1)} = \frac{f_u}{\gamma_{M2}\sqrt{2}} \tag{13}$$

Thus, the moment resistance of the weld for normal stresses:

$$M_{w,N,Rd} = \frac{1}{\sqrt{2}} ab_1(h_1 - t_1)\frac{f_u}{\gamma_{M2}} \tag{14}$$

In the case of shear force, only shear stresses act on the throat area:

$$\tau_\parallel = \frac{F}{A_w} = \frac{F}{2ah_1} \tag{15}$$

Eq. (11) takes the form:

$$\tau_\parallel = \frac{f_u}{\gamma_{M2}\sqrt{3}} \tag{16}$$

Equalizing (15) to (16):

$$F = \frac{2}{\gamma_{M2}\sqrt{3}} ah_1 f_u \tag{17}$$

The moment resistance of the weld for shear stresses:

$$M_{fw,S,Rd} = FL_1 = \frac{2}{\sqrt{3}} ah_1 \frac{f_u}{\gamma_{M2}} L_1 \tag{18}$$

The fillet weld final resistance is the minimum of the two:

$$M_{fw,Rd} = \min\{M_{fw,N,Rd}, M_{fw,S,Rd}\} \tag{19}$$

4.1.3. Moment resistance based on 1/2v butt weld failure

Similar to fillet welds, the design resistance of 1/2v butt welds is determined using the Directional method and the same assumptions. For the 1/2v butt weld, the stress components are found by

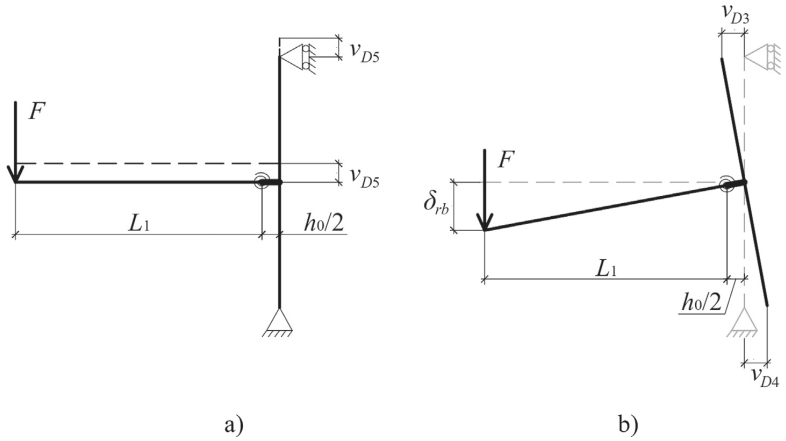

Fig. 5. Corrections to calculate the displacement at the end of the brace: (a) axial deformation of the chord, (b) motion of the supports.

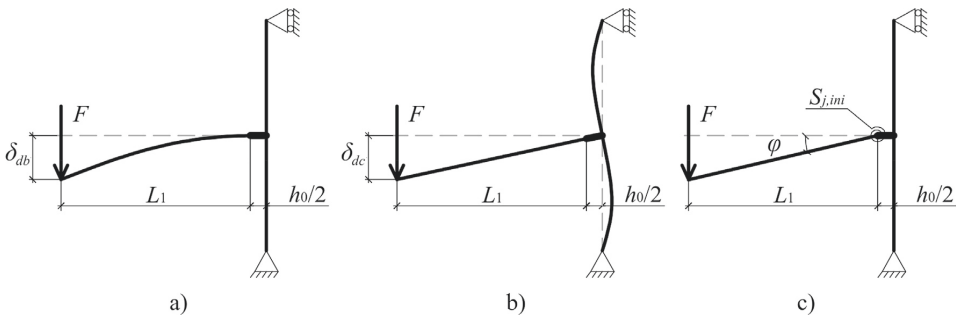

Fig. 6. Behavior of joint under loading: (a) bending of brace; (b) bending of chord; (c) local deformation of joint.

$$\sigma_{\perp} = \sigma_w; \quad \tau_{\perp} = \tau_{||} = 0 \tag{20}$$

Equalizing (20) to (11):

$$\sigma_w = \frac{f_u}{\beta_w \gamma_{M2}}, \tag{21}$$

Equalizing (9) to (21):

$$\frac{M_{bw,Rd}}{ab_1(h_1 - t_1)} = \frac{f_u}{\gamma_{M2}} \tag{22}$$

Taking into account $a = t_1$, the bending resistance of the butt weld is found by

$$M_{bw,Rd} = \frac{f_u t_1 b_1 (h_1 - t_1)}{\gamma_{M2}} \tag{23}$$

4.2. Rotation capacity

As mentioned in the Introduction, the rotation limit for the joints is calculated according to the 3%b_0 deformation rule of Lu et al. [26], leading to the following rotation limit:

$$\varphi_{\lim,3\%} = \frac{0.03 b_0}{h_1/2} = \frac{0.06}{\eta} \tag{24}$$

5. Results

All twenty tests were performed until the overall failure of the specimens. Since all joints had the brace-to-chord width ratio in the range $\beta < 0.85$, their deformation was governed by chord face failure, as shown in Fig. 8a. In addition, chord side walls buckling was observed as a minor failure mode in all specimens (Fig. 8b). Strain hardening and the membrane effect allowed the considerable post-yielding behavior of the joints. Finally, cracking in HAZ led the specimens to punching shear failure, as shown in Fig. 8c.

Graphically, the behavior of T joints can be presented by a corresponding moment-rotation (M-φ) curve. As an example, the M-φ response for case S700_S500_a6 is shown in Fig. 9; the remaining moment-rotation curves are provided in Appendix. The presented curves for all joints are found to be similar to that shown in Fig. 1, with the following clearly observed phases:

- linear elastic phase, corresponding to elastic deformations with initial rotational stiffness $S_{j,ini}$;
- transitional phase, when the yielding of the joint starts and the slope declines;
- hardening phase, corresponding to hardening stiffness $S_{j,h}$;
- final failure, when the load starts to drop, corresponding to the failure in HAZ or weld.

The following parameters were extracted from the test data and are summarized in Table 4:

- $S_{j,ini}$, initial joint stiffness (defined by the manual curve fitting);
- $S_{j,h}$, joint stiffness at the hardening phase (defined by the manual curve fitting);
- $M_{pl,\exp}$, plastic moment resistance (determined according to Fig. 1);
- $M_{u,\exp}$, ultimate moment resistance;
- φ_u, rotation corresponding to ultimate moment resistance.

The joints with $\beta = 0.80$ (cases S700_S700_a6, S700_S700_a10 and S700_S700_1/2) had a considerably smaller hardening phase than the

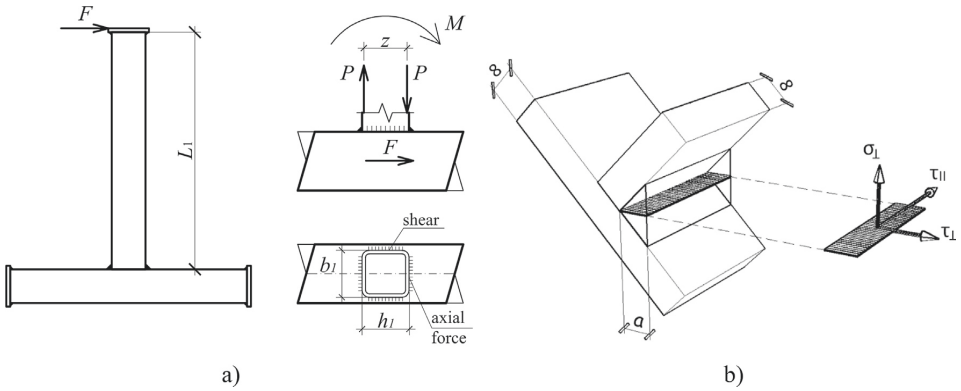

Fig. 7. Design of welds: (a) load components; (b) stress components in weld.

Fig. 8. Observed failure modes: (a) chord face failure; (b) chord side walls failure; (c) punching shear.

joints with $\beta = 0.67$. This can be explained by the different influence of β on the resistance of joints: for higher β plastic resistance increases more radically than the resistance of welds. This leads to smaller post-yielding behavior of the joint. For this reason, the manual curve-fitting approach was not so straightforward for these cases and allowed several possible solutions to determine the corresponding hardening stiffness.

To investigate the dependence of plastic resistance on the brace-to-chord width ratio β, it was normalized in respect to steel grade and geometry. Fig. 10a presents non-dimensional plastic moment resistance $M_{pl,exp}/(f_{y0}{\cdot}t_0^2{\cdot}h_1)$ in relation to β; for convenience, the points are grouped by weld size. The experimental results are compared to the theoretical equation, which is derived from Eq. (6) ($\eta = \beta$ in all cases):

$$f(\beta,\eta) = \frac{M_{ip,1,Rd}}{f_{y0}t_0^2h_1} = \frac{1}{2\eta} + \frac{2}{\sqrt{1-\beta}} + \frac{\eta}{1-\beta} \tag{25}$$

Fig. 10b presents the experimental plastic resistance normalized in relation to joint geometry $M_{pl,exp}/(t_0^2{\cdot}h_1 f(\beta,\eta))$ and plotted against chord yield strength f_{y0}. The experimental results are compared to the theoretical equation, which in this case represents a linear regression:

$$f(f_{y0}) = \frac{M_{ip,1,Rd}}{t_0^2 h_1 f(\beta,\eta)} = f_{y0} \tag{26}$$

As can be seen in Fig. 10, the experimental results confirm the general trend: the brace-to-chord width ratio β significantly affects the resistance of joints representing the main factor in their structural behavior. Moreover, the results prove the linear dependence of plastic resistance on chord yield strength. In both cases, resistance is found dependent on welds: the joints with a10 fillet welds have significantly higher resistance than those with a6 mm; the latter have higher resistance than those with butt welds. This can be explained by the fact that fillet welds enlarge the cross-section of the brace at the connection area, increasing thus the total length of the yielding mechanism and leading to higher plastic resistance. No trend was observed in relation to the influence of the brace material on the resistance of joints.

The theoretical moment resistances based on the chord face failure were calculated according to Section 3, with and without the reduction factor k_{HSS}. All theoretical data is collected in Table 5 with the following notations:

- $M_{ip,1,Rd}$, the bending moment resistance based on the chord face failure (current Eurocode rules);
- $M^*_{ip,1,Rd}$, the bending moment resistance based on the chord face failure without k_{HSS};
- $M_{w,Rd}$, the bending moment resistance based on the weld failure ($M_{fw,Rd}$ or $M_{bw,Rd}$);
- $M_{j,Rd}$, the moment resistance of the joint, $\min\{M_{ip,1,Rd}, M_{w,Rd}\}$;
- $M^*_{j,Rd}$, the moment resistance of the joint without k_{HSS}; $\min\{M^*_{ip,1,Rd}, M_{w,Rd}\}$;
- $\varphi_{lim,3\%}$, the rotation limit.

Experimental plastic resistance $M_{pl,exp}$ was compared to theoretical moment resistance based on chord face failure $M_{ip,1,Rd}$, with and

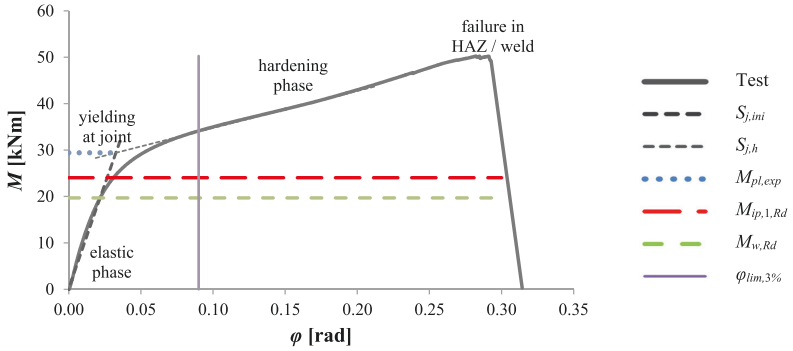

Fig. 9. Moment-rotational curve, specimen S700_S500_a6.

Table 4
Experimental results.

Specimen	β	Weld	$M_{pl,exp}$ [kNm]	$M_{u,exp}$ [kNm]	φ_u [rad]	$S_{j,ini}$ [kNm/rad]	$S_{j,h}$ [kNm/rad]
S420_S420_a6	0.66	a6	21.2	34.6	0.270	866	56
S500_S420_a6	0.67		24.3	38.6	0.235	939	68
S500_S500_a6	0.67		25.0	39.3	0.227	861	69
S700_S420_a6	0.67		27.7	41.6	0.212	926	86
S700_S500_a6	0.67		29.4	50.2	0.283	900	80
S700_S500_a6_WiPF	0.67		31.2	39.5	0.147	888	79
S700_S700_a6	0.80		61.2	67.5	0.111	2052	82
S420_S420_a10	0.67	a10	31.6	48.7	0.263	1255	71
S500_S420_a10	0.67		35.1	57.3	0.302	1285	78
S500_S500_a10	0.67		37.2	48.1	0.201	1369	69
S700_S420_a10	0.67		38.5	53.4	0.201	1310	91
S700_S500_a10	0.67		45.5	58.0	0.175	1525	89
S700_S500_a10_WiPF	0.67		37.6	51.8	0.201	1295	84
S700_S700_a10	0.80		70.1	76.0	0.102	2551	96
S420_S420_1/2v	0.67	1/2v	18.5	27.4	0.218	750	54
S500_S420_1/2v	0.67		21.1	33.4	0.230	695	60
S500_S500_1/2v	0.67		21.0	28.0	0.177	845	60
S700_S420_1/2v	0.67		24.2	33.9	0.160	763	76
S700_S500_1/2v	0.67		26.4	39.8	0.211	816	72
S700_S700_1/2v	0.81		46.8	50.7	0.085	1694	70

without k_{HSS}. Similarly, the rotation corresponding to ultimate moment resistance was compared to the rotation limit $\varphi_{lim,3\%}$. Table 6 provides the summary of the comparative analysis.

6. Discussion

6.1. Resistance

In respect of joint resistance, attention is paid to the following two issues: the need for the reduction factors k_{HSS} in case of plastic resistance (chord face failure) and other possible improvements to the resistance calculation. The results show that theoretical resistance considerably underestimates experimental plastic resistance for the joints with a10 fillet welds ($a_w/a_{w,fs}$ = 0.76…0.84) with the average $M_{ip,1,Rd}/M_{pl,exp}$ ratio of 0.58. Even without the reduction, the average ratio is 0.71. This observation justifies no need for the reduction for joints with large fillet welds ($a_w/a_{w,fs} \geq 0.75$).

For joints with a6 fillet welds ($a_w/a_{w,fs}$ = 0.45–0.51), the situation is not so straightforward. With the reduction coefficient k_{HSS}, all joints are on the safe side, with the average $M_{ip,1,Rd}/M_{pl,exp}$ ratio of 0.79. When the reduction is not taken into account, the average $M^*_{ip,1,Rd}/M_{pl,exp}$ ratio is 0.98, which also yields safe results. However, the ratio exceeds 1.0 for two cases, S700_S420_a6 and S700_S500_a6 (both have the chord made of S700). This implies the following rule: for joints with $0.45 \leq a_w/a_{w,fs} < 0.75$, no reduction may be needed, when the steel grade is below S700 (S500 can be the optimal limit). For steel grade S700, the reduction is needed; however, k_{HSS} = 0.9 seems to be sufficient, instead of the conservative value of 0.8. This conclusion is in line with the observations of [6], who proposed no reduction for S500 and the reduction factor 0.9 for S700.

Regarding the butt-welded joints, without reduction their theoretical moment resistance exceeds the experimental values in all cases, with an average $M^*_{ip,1,Rd}/M_{pl,exp}$ ratio of 1.16. At the same time, taking into account the reduction factors, all joints show safe performance, with the average $M_{ip,1,Rd}/M_{pl,exp}$ ratio being 0.94. Therefore, for butt-welded joints, reduction is required, provided that butt welds are completed as in this research and their resistance is calculated as in this paper. Table 7 contains a summary of the observations regarding the reduction coefficients.

Different findings for joints with various welds can be explained by the fact that experimental plastic resistance directly depends on the fillet weld size. Table 4 and Fig. 10 clearly show that the joints with fillet welds have higher experimental resistance than the joints with butt welds and the same geometry and material properties (compare, e.g., S420_S420_1/2v, S420_S420_a6 and S420_S420_a10). However, EN 1993-1-8:2005 does not take this phenomenon into account and

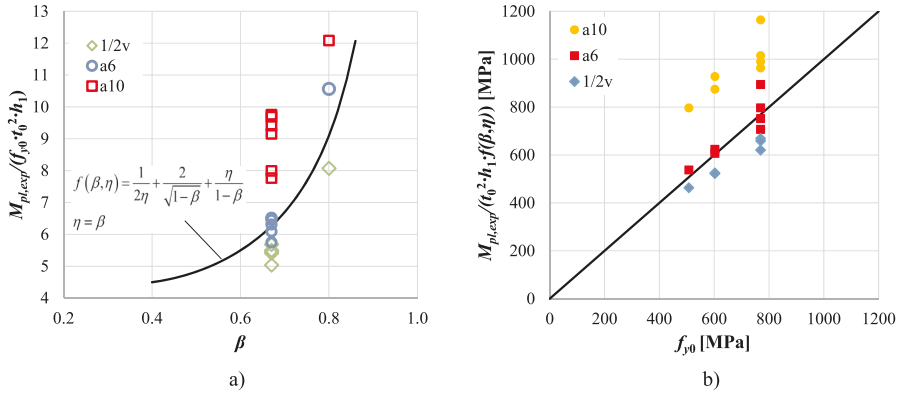

Fig. 10. (a) $M_{pl,exp}/(f_{y0}\cdot t_0^2\cdot h_1)$ in relation to β; (b) $M_{pl,exp}/(t_0^2\cdot h_1 f(\beta,\eta))$ in relation to f_{y0}.

Table 5
Theoretically calculated values.

Specimen	β	$a_w/a_{w,fs}$	$M^*_{ip,1,Rd}$ [kNm]	k_{HSS}	$M_{ip,1,Rd}$ [kNm]	$M_{w,Rd}$ [kNm]	$M^*_{j,Rd}$ [kNm]	$M_{j,Rd}$ [kNm]	Limiting factor	$\varphi_{lim,3\%}$ [rad]
S420_S420_a6	0.66	0.51	20.0	0.9	18.0	17.6	17.6	17.6	Weld	0.090
S500_S420_a6	0.67	0.51	24.1	0.8	19.3	17.6	17.6	17.6	Weld	0.089
S500_S500_a6	0.67	0.47	24.1	0.8	19.3	19.8	19.8	19.3	Chord	0.089
S700_S420_a6	0.67	0.51	30.1	0.8	24.1	17.6	17.6	17.6	Weld	0.090
S700_S500_a6	0.67	0.47	30.1	0.8	24.1	19.7	19.7	19.7	Weld	0.090
S700_S500_a6_WiPF	0.67	0.47	30.1	0.8	24.1	19.8	19.8	19.8	Weld	0.090
S700_S700_a6	0.80	0.45	52.6	0.8	42.1	39.1	39.1	39.1	Weld	0.075
S420_S420_a10	0.67	0.84	20.1	0.9	18.1	29.4	20.1	18.1	Chord	0.091
S500_S420_a10	0.67	0.84	24.1	0.8	19.3	29.3	24.1	19.3	Chord	0.090
S500_S500_a10	0.67	0.78	24.1	0.8	19.3	32.9	24.1	19.3	Chord	0.089
S700_S420_a10	0.67	0.84	29.9	0.8	23.9	29.3	29.3	23.9	Chord	0.091
S700_S500_a10	0.67	0.78	30.1	0.8	24.0	33.0	30.1	24.0	Chord	0.090
S700_S500_a10_WiPF	0.67	0.78	30.0	0.8	24.0	33.0	30.0	24.0	Chord	0.090
S700_S700_a10	0.80	0.76	53.1	0.8	42.5	65.4	53.1	42.5	Chord	0.075
S420_S420_1/2v	0.67	–	20.2	0.9	18.2	33.0	20.2	18.2	Chord	0.090
S500_S420_1/2v	0.67	–	24.2	0.8	19.3	33.0	24.2	19.3	Chord	0.090
S500_S500_1/2v	0.67	–	24.2	0.8	19.3	37.3	24.2	19.3	Chord	0.089
S700_S420_1/2v	0.67	–	30.0	0.8	24.0	32.8	30.0	24.0	Chord	0.091
S700_S500_1/2v	0.67	–	30.4	0.8	24.3	37.5	30.4	24.3	Chord	0.089
S700_S700_1/2v	0.81	–	54.6	0.8	43.7	74.1	54.6	43.7	Chord	0.075

Table 6
Comparison of the experimental and theoretical values.

Specimen	β	$a_w/a_{w,fs}$	$M^*_{ip,1,Rd}/M_{pl,\exp}$	$M_{ip,1,Rd}/M_{pl,\exp}$	$\varphi_{lim,3\%}/\varphi_u$
S420_S420_a6	0.66	0.51	0.95	0.85	0.33
S500_S420_a6	0.67	0.51	0.99	0.79	0.38
S500_S500_a6	0.67	0.47	0.96	0.77	0.39
S700_S420_a6	0.67	0.51	1.09	0.87	0.43
S700_S500_a6	0.67	0.47	1.02	0.82	0.32
S700_S500_a6_WiPF	0.67	0.47	0.96	0.77	0.61
S700_S700_a6	0.80	0.45	0.86	0.69	0.68
Average			**0.98**	**0.79**	**0.45**
S420_S420_a10	0.67	0.84	0.64	0.57	0.34
S500_S420_a10	0.67	0.84	0.69	0.55	0.30
S500_S500_a10	0.67	0.78	0.65	0.52	0.44
S700_S420_a10	0.67	0.84	0.78	0.62	0.45
S700_S500_a10	0.67	0.78	0.66	0.53	0.52
S700_S500_a10_WiPF	0.67	0.78	0.80	0.64	0.45
S700_S700_a10	0.80	0.76	0.76	0.61	0.74
Average			**0.71**	**0.58**	**0.46**
S420_S420_1/2v	0.67	–	1.09	0.98	0.41
S500_S420_1/2v	0.67	–	1.15	0.92	0.39
S500_S500_1/2v	0.67	–	1.15	0.92	0.51
S700_S420_1/2v	0.67	–	1.24	0.99	0.57
S700_S500_1/2v	0.67	–	1.15	0.92	0.42
S700_S700_1/2v	0.81	–	1.17	0.93	0.88
Average			**1.16**	**0.94**	**0.53**

provides the same theoretical resistance for joints with different weld types and sizes, as can be seen in Table 5 (slight differences of $M_{ip,1,Rd}$ are caused by deviations in the measured dimensions of the specimens). For this reason, the ratio $M_{ip,1,Rd}/M_{pl,\exp}$ is found to be unsafe for the joints with butt welds, requiring reduction; close to 1.0 for the joints with a6 fillet welds, requiring partial reduction; and very conservative for the joints with a10 fillet welds, justifying no reduction for such joints. If full-strength welds were used, the underestimation of resistance would be even greater.

To develop more generalized conclusions, the theoretical resistance of RHS joints should first be calculated incorporating the improving effect of fillet welds. This effect can be taken into account, e.g., by increasing β by means of some simple equation, as has been proposed for initial stiffness in [50]. However, such an approach has to be applied carefully: if the enlarged β is used in the cases with $\beta = 0.8$ (S700_S700_a6 and S700_S700_a10), it might exceed the limit of $\beta \leq 0.85$, thus making the chord face failure calculation invalid and requiring the resistance to be calculated based on chord side-wall crushing and brace failure. It should be noted that this paper considers the reduction factors for the joints with $\beta \leq 0.85$, i.e., when the failure of the joint is caused by chord face bending. When other failure modes prevail, the conclusions can be different.

Table 7
Summary of the reduction coefficients observations.

Reduction factor	Reduction factor for $f_y > 355$ MPa	Reduction factor for 460 MPa $< f_y \leq 700$ MPa
Reference	EN 1993–1-8:2005, clause 7.1.1(4); CIDECT Design Guide No. 3, clause 1.2.1	EN 1993–1-12:2007, clause 2.8; CIDECT Design Guide No. 3, clause 1.2.1
Existing value	0.9	0.8
Possible value:		
Butt welds	0.9	0.8
Fillet welds, $a_w/a_{w,fs} \geq 0.75$	1.0	1.0
Fillet welds, $0.45 \leq a_w/a_{w,fs} < 0.75$	1.0	1.0 for S500 0.9 for S700 Linear interpolation between

The application of MAG Wise welding did not yield noticeable improvements in the performance of the joints. Moreover, in the case of a6 joints (compare S700_S500_a6 and S700_S500_a6_WiPF), it decreased their ultimate bending resistance by 21%, in the case of a10 joints (compare S700_S500_a10 and S700_S500_a10_WiPF) by 11%.

6.2. Stiffness

The initial rotational stiffness of joints with an a10 fillet weld was found to be clearly higher than that of joints with a6 fillet welds (by 42% on average) and also 1/2v butt welds (by 63% on average). The results clearly show that in addition to moment resistance, fillet welds significantly affect also the initial rotational stiffness of tubular joints. To take this effect into account in the design, a possible solution has been proposed in [50]. A similar improving effect was also observed for hardening stiffness in these tests.

The application of MAG Wise welding did not bring noticeable improvements in the rotational stiffness of the joints. Moreover, in the

case of a10 fillet welds (compare S700_S500_a10 and S700_S500_a10_WiPF) it decreased initial and hardening stiffness by 15% and 6% respectively.

6.3. Ductility

The results show that the experimental ultimate rotation capacity of all tested joints clearly exceeded the $3\%b_0$ deformation limit, provided that no full-strength fillet welds were used. According to Table 6, the ratio $\varphi_{lim,3\%}/\varphi_u$ lies in the range of 0.33…0.61 for the joints with $\beta = 0.67$ and 0.68…0.88 for the joints with $\beta = 0.80$. Such a considerable margin justifies the use of welds smaller than full-strength fillet welds if they provide sufficient resistance.

7. Conclusions

The moment-rotation behavior of all tested specimens was found to follow the typical moment-rotation response for joints with $\beta \leq 0.85$. The rotation capacity of all specimens complies with the requirements for tubular joints, even using welds smaller than full-strength welds. This indicates that full-strength fillet welds are not needed in these joints and in this loading condition.

The experimental results show that the size of fillet welds has a significant influence on the structural behavior of joints, increasing their bending resistance and rotational stiffness. To avoid overly conservative results, such phenomenon should be taken into account in the design of tubular joints.

There is no single conclusion concerning the relevance of the reduction factors for the bending resistance of HSS joints limited by chord face failure. This issue is complicated by the fact that the current design rules do not consider the improving effect of fillet welds on the structural behavior of tubular joints. If this influence is neglected, the reduction is necessary only for butt-welded joints, as well as for joints with small fillet welds ($0.45 \leq a_w/a_{w,fs} < 0.75$) and made of steel grades higher than S500. It should be noted that these conclusions are based on the tests carried out, i.e., for square hollow sections of 8 mm thickness ($2\gamma = b_0/t_0 = 18.75$). More tests are required to establish the reliability of these observations in relation to joints with other 2γ ratio, as well as for rectangular hollow section joints. Moreover, further investigations are needed to specify the relevance of the reduction factors k_{HSS} for the bending resistance based on other failure modes, as well as for the design of welds.

Acknowledgements

The authors appreciate the financial support of the city of Hämeenlinna. The authors would like to thank SSAB Europe Oy for providing the high strength steel tubular materials and Tavastia Vocational College for manufacturing the specimens. The financial support of the Tekes project FIMECC/Digimap is also gratefully acknowledged.

Appendix A. Moment-rotation curves

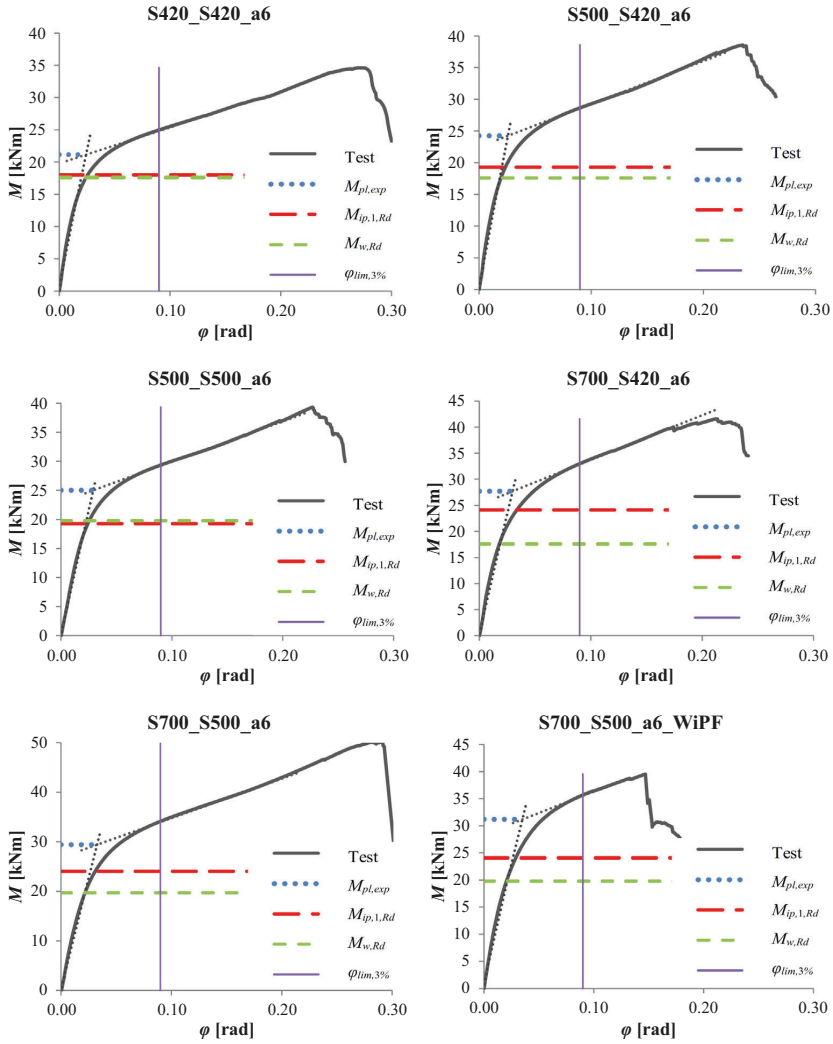

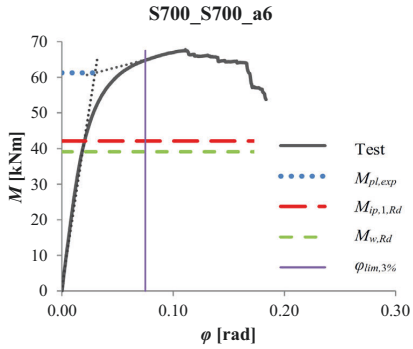
S700_S700_a6
M [kNm]
φ [rad]
Test
$M_{pl,exp}$
$M_{ip,1,Rd}$
$M_{w,Rd}$
$\varphi_{lim,3\%}$

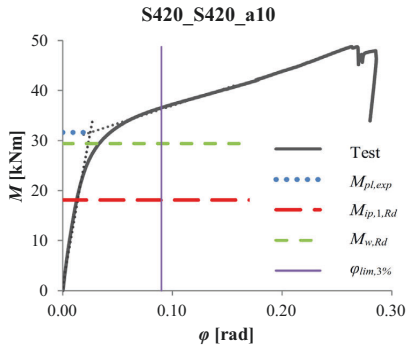
S420_S420_a10
M [kNm]
φ [rad]
Test
$M_{pl,exp}$
$M_{ip,1,Rd}$
$M_{w,Rd}$
$\varphi_{lim,3\%}$

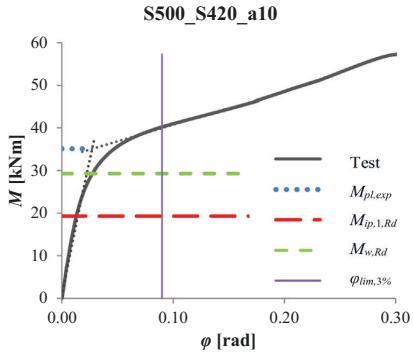
S500_S420_a10
M [kNm]
φ [rad]
Test
$M_{pl,exp}$
$M_{ip,1,Rd}$
$M_{w,Rd}$
$\varphi_{lim,3\%}$

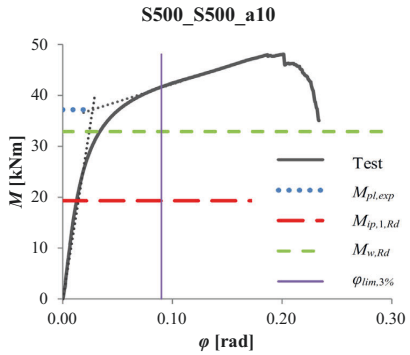
S500_S500_a10
M [kNm]
φ [rad]
Test
$M_{pl,exp}$
$M_{ip,1,Rd}$
$M_{w,Rd}$
$\varphi_{lim,3\%}$

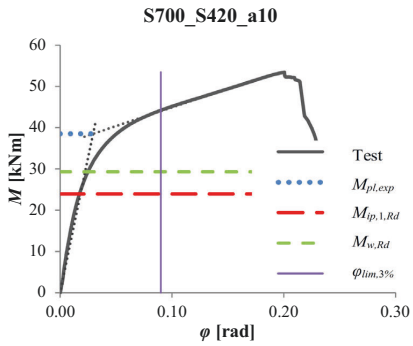
S700_S420_a10
M [kNm]
φ [rad]
Test
$M_{pl,exp}$
$M_{ip,1,Rd}$
$M_{w,Rd}$
$\varphi_{lim,3\%}$

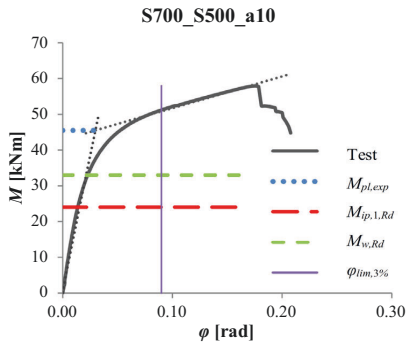
S700_S500_a10
M [kNm]
φ [rad]
Test
$M_{pl,exp}$
$M_{ip,1,Rd}$
$M_{w,Rd}$
$\varphi_{lim,3\%}$

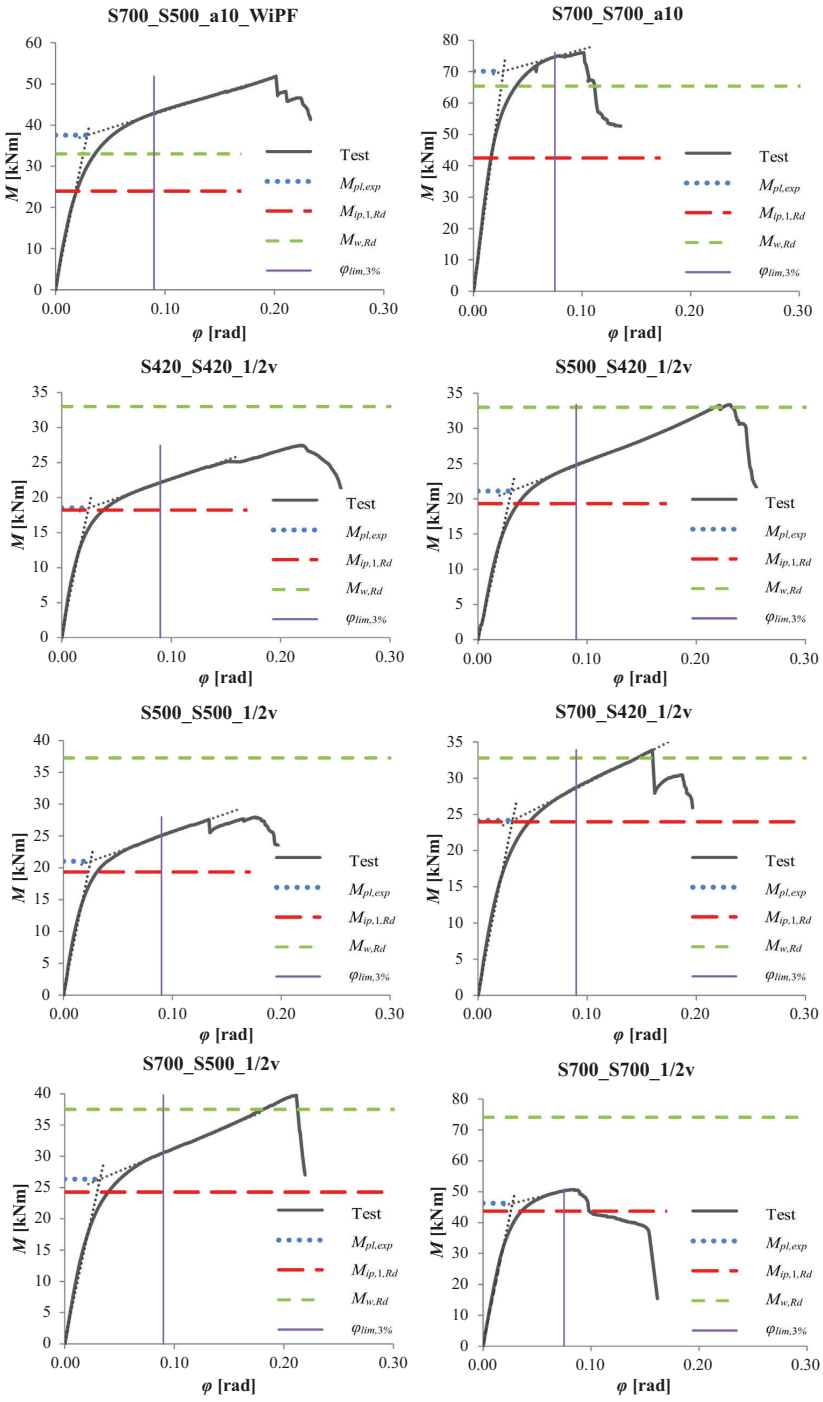
S700_S500_a10_WiPF
S700_S700_a10
S420_S420_1/2v
S500_S420_1/2v
S500_S500_1/2v
S700_S420_1/2v
S700_S500_1/2v
S700_S700_1/2v
M [kNm]
φ [rad]
Test
Mpl,exp
Mip,1,Rd
Mw,Rd
φlim,3%

References

[1] Raoul J. Use and application of high-performance steels for steel structures, 8. Zürich, Switzerland: IABSE-AIPC-IVBH; 2005.
[2] European Committee for Standardization (CEN). Eurocode 3. Design of steel structures, Part 1-12: Additional rules for the extension of EN 1993 up to steel grades S 700 (EN 1993-1-12: 2007). Brussels; 2007.
[3] European Committee for Standardization (CEN). Eurocode 3. Design of steel structures, Part 1–8: Design of joints (EN 1993-1-8:2005), Brussels; 2005.
[4] Packer JA, Wardenier J, Zhao X-L, van der Vegte GJ, Kurobane Y. Design guide for rectangular hollow section (RHS) joints under predominantly static loading. CIDECT Design Guide No. 3, 2nd ed. LSS Verlag; 2009.
[5] Zhao X-L, Heidarpour A, Gardner L. Recent developments in high-strength and stainless steel tubular members and connections. Steel Constr 2014;7(2):65–72.
[6] Feldmann M, Schillo N, Schaffrath S, Virdi K, Björk T, Tuominen N, et al. Rules on high strength steel. Luxembourg: Publications Office of the European Union; 2016.
[7] Jiao H, Zhao X-L, Lau A. Hardness and compressive capacity of longitudinally welded very high strength steel tubes. J Constr Steel Res 2015;114:405–16.
[8] Javidan F, Heidarpour A, Zhao X-L, Hutchinson CR, Minkkinen J. Effect of weld on the mechanical properties of high strength and ultra-high strength steel tubes in fabricated hybrid sections. Eng Struct 2016;118:16–27.
[9] Pirinen M. The effects of welding heat input on the usability of high strength steels in welded structures [Doctor of Science Thesis] Lappeenranta: Lappeenranta University of Technology; 2013.
[10] Dunđer M, Samardžić I, Klarić Š. Influence of cooling time Δt8/5 on welded joint properties of the thermal cycle simulated TStE 420 specimens. Tech Gaz 2007;14(1–2):47–57.
[11] Ministry of the Environment. Finnish National Annex to standard SFS-EN 1993-1-12; 2017.
[12] Ongelin P, Valkonen I. SSAB Domex Tube. Structural hollow sections. EN 1993 - Handbook 2016. SSAB Europe Oy; 2016.
[13] Grotmann D, Sedlacek G. Rotational stiffness of welded RHS beam-to-column joints. Cidect 5BB-8/98. Aachen: RWTH-Aachen; 1998.
[14] Brockenbrough RL. Strength of square-tube connections under combined loads. J. Struct Div 1972;98(12):2753–68.
[15] Korol RM, El-Zanaty M, Brady FJ. Unequal width connections of square hollow sections in Vierendeel trusses. Can J Civ Eng 1977;4(2):190–201.
[16] Kanatani H, Fujiwara K, Tabuchi M, Kamba T. Bending tests on T-joints of RHS chord and RHS or H-shape branch. CIDECT Programme 5AF; 1981.
[17] Yura JA, Edwards IF, Zettlemoyer N. Ultimate capacity of circular tubular joints. J Struct Div 1981;107(10):1965–84.
[18] Wardenier J. Hollow section joints. Delft: Delft University of Technology; 1982.
[19] International Institute of Welding (IIW). ISO 14346:2013. Static design procedure for welded hollow-section joints – Recommendations; 2013.
[20] Ishida K, Ono T, Iwata M. Ultimate strength formula for joints of new truss system using rectangular hollow sections. In: Coutie MG, Davies G, editors. Tubular structures V. Nottingham: E. & F.N. Spon; 1993. p. 511–8.
[21] Ono T, Iwata M, Ishida K. An experimental study on joints of new truss system using rectangular hollow sections. In: Wardenier J, Panjeh Shahi E, editors. Tubular structures IV. Delft: Delft University Press; 1991. p. 344–53.
[22] Tabuchi M, Kanatani H, Kamba T. The local strength of welded RHS T joints subjected to bending moment CIDECT report 5AF-84/5E Boston, Massachusetts: International Institute of Welding; 1984
[23] Szlendak J. Beam-column welded RHS connections. Thin-Walled Struct 1991;12(1):63–80.
[24] Packer JA. Moment connections between rectangular hollow sections. J Constr Steel Res 1993;25(1–2):63–81.
[25] Yu Y. The static strength of uniplanar and multiplanar connections in rectangular hollow sections [Doctoral Dissertation]. Delft: Delft University of Technology; 1997.
[26] Lu LH, de Winkel GD, Yu Y, Wardenier J. Deformation limit for the ultimate strength of hollow section joints. In: Grundy P, Holgate A, Wong B, editors. Tubular structures VI, 6th international symposium on tubular structures, Melbourne, Australia. Rotterdam: Balkema; 1994. p. 341–7.
[27] Zhao X-L. Deformation limit and ultimate strength of welded T-joints in cold-formed RHS sections. J Constr Steel Res 2000;53(2):149–65.
[28] Christitsas AD, Pachoumis DT, Kalfas CN, Galoussis EG. FEM analysis of conventional and square bird-beak SHS joint subject to in-plane bending moment — experimental study. J Constr Steel Res 2007;63(10):1361–72.
[29] Fadden M, Wei D, McCormick J. Cyclic testing of welded HSS-to-HSS moment connections for seismic applications. J Struct Eng 2015;141(2):04014109.
[30] Mang F, Bucak O, Stauf H. Fatigue behaviour of welded hollow section joints and their connections made of high-strength steels. In: Proceedings of the Third (1993) international offshore and polar engineering conference; 1993. p. 104–16.
[31] Anderson D, Hines EL, Arthur SJ, Eiap EL. Application of artificial neural networks to the prediction of minor axis steel connections. Comput Struct 1997;63(4):685–92.
[32] Grierson DE, Xu L. Design optimization of steel frameworks accounting for semi-rigid connections. Rozvany GIN, editor. Optimization of large structural systems, vol. II. Dordrecht: Kluwer Academic Publisher; 1993. p. 873–81.
[33] Simoes LMC. Optimization of frames with semi-rigid connections. Comput Struct 1996;60(4):531–9.
[34] Weynand K, Jaspart J-P, Steenhuis M. Economy studies of steel building frames with semi-rigid joints. J Constr Steel Res 1998;46(1–3):85.
[35] Haapio J, Jokinen T, Heinisuo M. Cost simulations of steel frames with semi-rigid joints using product model techniques. In: Dunai L, Ivanyi M, Jarmai K, Kovács N, Vigh LG, editors. Proceedings of Eurosteel 2011. Brussels: ECCS; 2011. p. 2151–6.
[36] Bzdawka K. Optimization of office building frame with semi-rigid joints in normal and fire conditions [PhD Thesis] Tampere: Tampere University of Technology; 2012. Publication 1038.
[37] Boel H. Buckling length factors of hollow section members in lattice girders [Ms Sci thesis] Eindhoven:: Eindhoven University of Technology; 2010.
[38] Snijder HH, Boel HD, Hoenderkamp JCD, Spoorenberg RC. Buckling length factors for welded lattice girders with hollow section braces and chords. In: Dunai L, Iványi M, Jármai K, Kovács N, Vigh LG, editors. Proceedings of the 6th European Conference on Steel and Composite Structures (Eurosteel 2011), 31 August - 2 September 2011, Budapest, Hungary. Brussels: ECCS; 2011. p. 1881–6.
[39] Heinisuo M, Haakana Ä. Buckling of members of welded tubular truss. In: Heinisuo M, Mäkinen J, editors. Proceedings of The 13th Nordic Steel Construction Conference (NSCC-2015). Tampere: Tampere University of Technology; 2015. p. 219–20.
[40] Garifullin M, Pajunen S, Mela K, Heinisuo M, Havula J. Initial in-plane rotational stiffness of welded RHS T joints with axial force in main member. J Constr Steel Res 2017;139:353–62.
[41] European Committee for Standardization (CEN). Eurocode 3. Design of steel structures. Part 1-5: Plated structural elements (EN 1993-1-5:2006), Brussels; 2006.
[42] Spangemacher R, Sedlacek G. On the development of a computer simulator for tests of steel structures. Constr Steel Des World Dev 1992:593–611.
[43] Dahl W, Langenberg P, Sedlacek G, Spangemacher R. Elastisch-plastisches Verhalten von Stahlkonstruktionen- Anforderungen und Werkstoffkennwerte. Luxembourg: EUR; 1993.
[44] European Committee for Standardization (CEN). Eurocode 3: Design of steel structures, Part 1-1: General rules and rules for buildings (EN 1993-1-1:2005). Brussels; 2005.
[45] Beg D, Zupančič E, Vayas I. On the rotation capacity of moment connections. J Constr Steel Res 2004;60(3–5):601–20.
[46] European Committee for Standardization (CEN). Eurocode 8. Design of structures for earthquake resistance, Part 1: General rules, seismic actions and rules for buildings (EN 1998-1:2004), Brussels; 2004.
[47] Wilkinson S, Hurdman G, Crowther A. A moment resisting connection for earthquake resistant structures. J Constr Steel Res 2006;62(3):295–302.
[48] Kosteski N, Packer JA, Puthli RS. A finite element method based yield load determination procedure for hollow structural section connections. J Constr Steel Res 2003;59(4):453–71.
[49] European Committee for Standardization (CEN). Welding and allied processes – Types of joint preparation – Part 1: Manual metal arc welding, gas-shielded metal arc welding, gas welding, TIG welding and beam welding of steels (ISO 9692-1:2013). Brussels;2013.
[50] Heinisuo M, Garifullin M, Jokinen T, Tiainen T, Mela K. Surrogate modeling for rotational stiffness of welded tubular Y-joints. In: Carter CJ, Hajjar JF, editors. Connections in Steel Structures VIII. Chicago, Illinois: American Institute of Steel Construction; 2016. p. 285–94.

IV

EFFECT OF WELDING RESIDUAL STRESSES ON LOCAL BEHAVIOR OF RECTANGULAR HOLLOW SECTION JOINTS. PART 1 – DEVELOPMENT OF NUMERICAL MODEL

by

Garifullin M., Launert B., Heinisuo M., Pasternak H., Mela K. & Pajunen S., Apr 2018

Bauingenieur vol. 93 (April), 152-159

Bei diesem Beitrag handelt es sich um einen wissenschaftlich begutachteten und freigegebenen Fachaufsatz („reviewed paper").

Effect of welding residual stresses on local behavior of rectangular hollow section joints

Part 1 – Development of numerical model

M. Garifullin, B. Launert, M. Heinisuo, H. Pasternak, K. Mela, S. Pajunen

Abstract Welded tubular joints are widely used in structural engineering due to their excellent resistance and stiffness in contrast to open sections, as well as simpler end preparation. Welding residual stresses that occur in these joints after the welding process can affect their structural behavior. Some recent experimental studies have shown that this effect can be considerable. This study numerically evaluates the influence of welding residual stresses on the behavior of rectangular hollow section T joints. The paper consists of two parts. Part I develops and validates a finite element model for the joints directly taking into account welding residual stresses by means of an upstream thermomechanical simulation of the welding process. It is proven that particular attention needs to be paid to the discretization of the model, the material properties and the adequate description of the weld heat input. The validation with experimental results shows that the developed numerical model properly captures the local structural behavior of tubular joints and can be efficiently used for further investigations. Part II employs the constructed model to investigate the effect of welding residual stresses on the resistance and initial stiffness of the considered joints.

Einfluss der Schweißeigenspannungen auf die Tragfähigkeit von Rechteck-Hohlprofil-Knoten Teil 1: Entwicklung eines numerischen Modells

Zusammenfassung Geschweißte Hohlprofilknoten sind aufgrund besserer Festigkeits – und Steifigkeitseigenschaften im Vergleich zu offenen Profilen sowie ihrer einfacheren Fertigung weit verbreitet. Schweißeigenspannungen, die infolge des Fügens der Einzelkomponenten mittels Schweißen entstehen, können deren Tragverhalten zum Teil stark beeinflussen, was auch durch einige neuere Untersuchungen belegt wird. Dieser Beitrag beschreibt eine erweiterte Vorgehensweise für die Finite-Elemente-Modellierung am Beispiel eines T-Knotens aus Rechteckhohlprofilen. Der Beitrag gliedert sich in zwei Teile. Teil 1 beinhaltet die Entwicklung und Validierung eines numerischen Modells, welches Schweißeinflüsse durch eine vorangehende thermomechanische Simulation explizit modelliert und diese in nachfolgende Berechnungsschritte einbezieht. Dabei werden die Bedeutung einer geeigneten Vernetzung des Modells, der Materialeigenschaften und eines zutreffenden Schweißwärmeeintrags diskutiert. Die Validierung mit experimentellen Ergebnissen zeigt die Eignung des entwickelten numerischen Modells und dass dieses das lokale Tragverhalten entsprechender Knotenverbindungen korrekt erfasst. Es kann daher für nachfolgende Untersuchungen weiterverwendet werden. Teil 2 zeigt die diesbezüglich durchgeführten Parameterstudien, um die Auswirkungen der Schweißeigenspannungen auf die Tragfähigkeit und die Anfangssteifigkeit der untersuchten Knotenverbindung darzustellen.

Marsel Garifullin, M. Sc.
marsel.garifullin@tut.fi
Prof., Ph.D, Markku Heinisuo
markku.heinisuo@tut.fi
Ph.D, Kristo Mela
kristo.mela@tut.fi
Assoc. Prof., Ph.D, Sami Pajunen
sami.pajunen@tut.fi
Tampere University of Technology
Korkeakoulunkatu 10, 33720 Tampere, Finland
Benjamin Launert, M.Sc., SFI/IWE
benjamin.launert@b-tu.de
Prof. Dr.-Ing. habil. Hartmut Pasternak
hartmut.pasternak@b-tu.de
Brandenburgische Technische Universität
Platz der Deutschen Einheit 1, 03046 Cottbus

1 Introduction

Welded hollow section joints are widely used in the building industry due to their excellent strength and simple end preparations. Although welding enables fast and simple connection of sections, it represents a complex thermomechanical process, which takes place at very high temperatures. When a welded joint is cooled to room temperature, the occurring shrinkage of the material leads to high residual stresses in the welded zone. To ensure that welding residual stresses have no negative effect on the structural behavior of tubular joints, these stresses should be taken into account in the analysis.

Many papers evaluate experimentally residual stresses in welded connections. In [1] it is shown that residual stresses can lead to the reduction of tensile strength for butt-welded plates by 10 %. Some authors came to the conclusion that the reduction of tensile strength of high strength steel (HSS) butt joints can reach 3 % to 8 % [2], and even 15 % [3]. Similar results are obtained in [4]. Some other studies dealing on the same issue can be found in [5], [6], [7]. A comprehensive numerical analysis on welding residual stresses in component-type welded I-girders is provided in [8].

However, very few publications evaluate welding residual stresses in relation to hollow section joints. Brar & Singh [9] have proved that it is possible to increase the tensile strength of tubular X joints by 24 % due to reduction of residual stresses in the heat affected zones (HAZ) by changing welding input parameters. In [10] it is shown that the load-bearing capacity of square hollow section T joints can vary by 10 % depending on the welding sequence. At the same time, the paper does not directly compare the structural behavior of joints considering and neglecting welding residual stresses.

Modern numerical methods and software allow analysing the residual stresses induced by the welding process. One possible solution is the finite element analysis (FEA), which is implemented in a broad range of software. This paper creates a finite element (FE) model to investigate the beha-

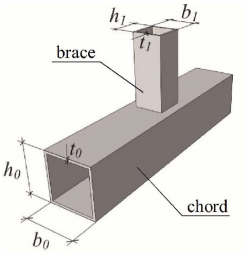

b_0	Chord width
h_0	Chord height
t_0	Chord thickness
f_{y0}	Chord material yield strength
b_1	Brace width
h_1	Brace height
t_1	Brace thickness
β	b_1/b_0 ratio
γ	$b_0/2t_0$ ratio
a	Weld throat thickness

Fig. 1. Notations of T joint
Bild 1. Bezeichnungen am T-Knoten

vior of rectangular hollow section (RHS) T joints taking into account welding residual stresses. Section 2 provides a brief overview on the structural behavior of RHS T joints. Section 3 develops the FE model of the joint taking into account welding residual stresses and validates it with the experimental data. A T joint represents the simplest joint configuration, when a brace is connected to a chord at an angle of 90°. Notations of the T joint are provided in **figure 1**. Only joints with fillet welds are investigated. The companion paper (Part II) employs the constructed model to evaluate the effect of welding residual stresses on the resistance and initial stiffness of the considered joints.

2 Theoretical background for structural behavior of RHS T joints

2.1 Local design model for RHS T joints

The local beam model for semi-rigid tubular T joints has been developed in [11]. The models are depicted in **figure 2a** and figure 2b for in-plane bending and axial brace loading, respectively. In the figure, $S_{j,ini}$ and $C_{j,ini}$ denote initial rotational and axial stiffness that are modelled by rotational and linear springs respectively. It should be noted that the springs are located at the upper flange of the chord and are connected to the chord axis by a rigid beam.

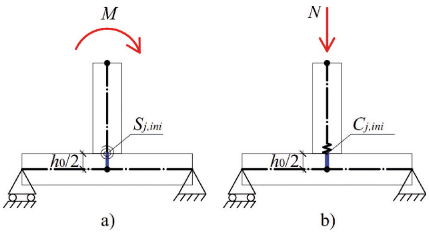

Fig. 2. Local design models for RHS T joint: a) in-plane bending; b) axial brace loading
Bild 2. Lokale Berechnungsmodelle für T-Knoten aus Rechteck-Hohlprofilen: a) Biegung in der Ebene; b) Axiallast aus Pfosten

Generally, displacements and rotations measured during analyses reflect the global behavior of the joint, which includes deformations of the chord and the brace, as well as local deformations of the joint. The latter represents deformations at the connection area, where the brace and the chord meet. In particular, to obtain the local rotation of the joint φ in case of in-plane bending, the rotation of the brace φ_{br} and the rotation of the chord φ_{ch} are subtracted from the rotation in the end of the brace φ_{tot} (**figure 3**):

$$\varphi = \varphi_{tot} - \varphi_{br} - \varphi_{ch} \quad (1)$$

In case of axial loading of the brace, two parameters are extracted: the vertical displacement in the end of the brace δ_{br} and the vertical displacement in the bottom flange of the chord δ_{bot}, as shown in **figure 4**a. The local displacement of the joint δ is then

$$\delta = \delta_{br} - \delta_{bot} - \delta_{sh} \quad (2)$$

where δ_{sh} is the shortening of the brace (not shown in the figure). The motions of the members are supposed to be elastic (assuming that plastic deformations occur only in the connection area); therefore, the values φ_{br}, φ_{ch}, and δ_{sh} are calculated manually using well-known beam equations from the strength of materials.

In case of axial brace loading, the axial force N causes bending of the chord, which results in additional normal stress in its faces [12]. To eliminate this effect, compensating moments $M_{0,END} = 0.25N(l_0 - h_1)$ are applied at the ends of the chord, resulting in the desired zero moment in the area of connection, as shown in figure 4b.

2.2 Structural behavior of T joints

The behavior of tubular joints demonstrates certain similarities in case of in-plane bending and axial brace loading and is best described by corresponding action-deformation curves. The initial stiffness and resistance of joints are found graphically, using the manual curve-fitting approach. To evaluate the deformation capacity of joints, the so-called 3% deformation limit φ_{lim} (δ_{lim}) is calculated in accordance with [13]. Following this rule, for a joint loaded by an axial force in the brace, the deformation limit is found as

$$\delta_{lim} = 0.03\, b_0 \quad (3)$$

Similarly, for a joint loaded by an in-plane moment:

$$\varphi_{\text{lim}} = \frac{0.03 b_0}{h_1/2} = 0.06 b_0/h_1 \quad (4)$$

Initial stiffness $S_{j,ini}$ ($C_{j,ini}$) is found as the tangent line in the elastic phase of the curve. Here, S corresponds to the rotational stiffness and C to the axial stiffness. In accordance with EN 1993–1–8: 2005 [14], the indices j and ini correspond to "joint" and

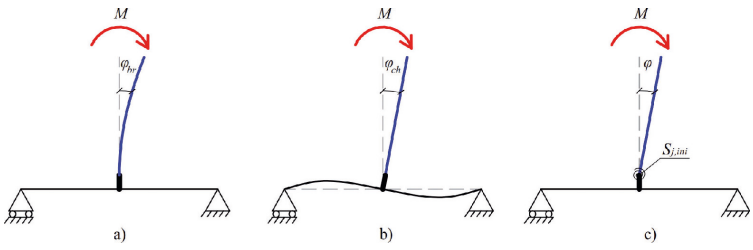

Fig. 3. Behavior under in-plane bending: a) elastic rotation of the brace; b) elastic rotation of the chord; c) local rotation of the joint
Bild 3. Verhalten unter Biegung in der Ebene: a) Elastische Verdrehung des Pfostens; b) Elastische Verdrehung des Gurtes; c) lokale Verdrehung am Knoten

"initial phase" respectively. The resistance of the joint is determined depending on its brace-to-chord width ratio β, as proposed in [15]. For joints with $\beta \leq 0.85$, bending of the chord top face governs the deformation of the whole joint and the action-deformation curve has a clearly observed hardening phase, as shown in **Figure 5**. In this case, the plastic resistance M_{pl} (N_{pl}) is determined according to [16] as the intersection of two tangent lines corresponding to initial stiffness $S_{j,ini}$ ($C_{j,ini}$) and hardening stiffness $S_{j,h}$ ($C_{j,h}$). Ultimate resistance M_u (N_u) in this case usually corresponds to very large deformations, considerably exceeding the deformation limit; therefore, it is rarely considered for such joints. Oppositely, the behavior of joints with $0.85 < \beta \leq 1.0$ is generally governed by buckling of their chord side walls; the resistance of such joints is determined differently [17]. It should be noted that when $0.85 < \beta \leq 1.0$, the finite element modeling of the joint becomes complicated, because the fillet weld reaches the rounded corner of the chord section (between the web and the upper flange). When $\beta = 1.0$ (the chord and the brace are of equal width), a fillet weld cannot be performed and is replaced by a partial/full penetration butt weld. As the focus of this study is on T joints with fillet welds, only joints with $\beta \leq 0.85$ are considered in this paper.

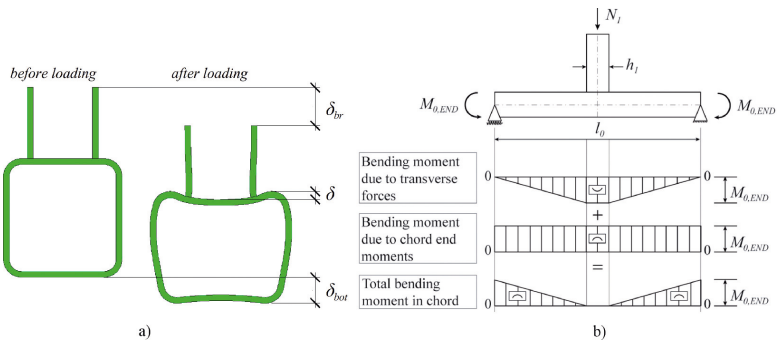

Fig. 4. a) Behavior under axial loading; b) bending moment in chord caused by transverse forces, compensating moments and their combined effect [12]
Bild 4. a) Verhalten unter Axiallast aus Pfosten; b) Biegemomente im Gurt durch Querkräfte, Kompensationsmomente und Überlagerung [12]

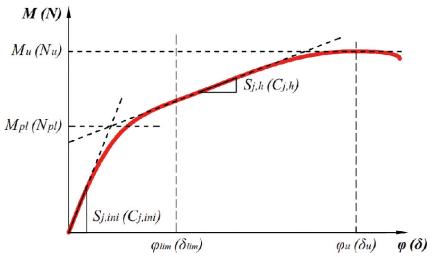

Fig. 5. Action-deformation curve for T joint with $\beta \leq 0.85$
Bild 5. Last-Verformungs-Kurve T-Knoten für $\beta \leq 0.85$

3 FE model for RHS T joints with welding residual stresses

3.1 Abaqus Welding Interface

Currently there are various programs for finite element modeling and simulation of welding processes, such as Abaqus Welding Interface [18], Sysweld [19], Simufact Welding [20], and Virfac [21]. In this study, Abaqus Welding Interface (AWI) was employed, as it provides wide opportunities both for welding simulation and for subsequent structural analyses of the joints in Abaqus [22]. AWI represents an Abaqus plug-in for simulating of the welding process, employing a sequentially coupled approach for the thermal stress analysis [18]. AWI constructs both the thermal and mechanical models, including the necessary step definitions, step-dependent boundary conditions and step-dependent temperature field specifications.

AWI generally considers welds consisting of multiple beads (layers), as shown in **figure 6**. Each bead is then assumed divided into chunks corresponding to the actual weld pools. The sequence of welding is later defined by the introduction of passes, which determine the chunk (or a number of chunks) being activated at a particular time.

3.2 Finite element discretization

In the first step, a short study was conducted to determine the most suitable finite element. Tubular joints are best simulated using at least two quadratic hexahedral elements across the wall thickness [23]. To obtain adequate distribution of residual stresses with AWI, models should have sufficient number of layers, i.e., three, four and even more. However, such models have extremely large calculation time when quadratic finite elements are used. Reasonable results can be also obtained using linear hexahedral elements with incompatible modes [24].

To find the most suitable finite element for further simulations, a short study was conducted in Abaqus/Standard without AWI. A joint was considered under in-plane bending with a 100 x 100 x 6 chord and a 50 x 50 x 5 brace, both made of S355 and with a = 5 mm weld. Three types of finite elements were chosen for comparison: linear hexahedral (C3D8 in Abaqus), linear hexahedral with incompatible modes (C3D8I in Abaqus) and quadratic hexahedral with reduced integration (C3D20R in Abaqus). Three elements in thickness direction were employed, for both the chord and the brace. The moment-rotation response of the joints is presented in **figure 7**, where all three finite element types provide the same structural behavior of the joint. Therefore, the linear full-integration hexahedral element (C3D8 in Abaqus) was chosen for further investigations, as the one with minimum calculation time.

3.3 FE model for RHS T joint

AWI requires welded members modelled as a single part with suitable partitioning for the definition of base and filler

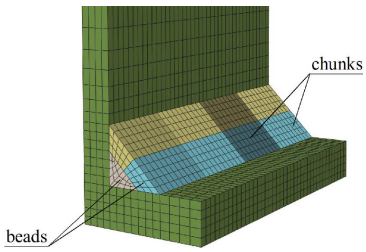

Fig. 6. Division of weld into beads and chunks
Bild 6. Einteilung der Schweißnaht in Lagen und Längsabschnitte

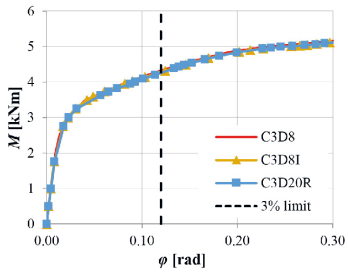

Fig. 7. Results of finite element analysis
Bild 7. Ergebnisse der Finite-Elemente-Berechnung

materials; therefore, in this study the brace, the chord and the weld were modelled as one geometric object. To exclude possible effects of the chord boundary conditions, its length was selected as $6b_0$, while the brace length was chosen as $4b_1$, as shown in **figure 8**a. To capture large temperature and stress gradients due to welding, the used mesh was refined near the connection area. The RHS profiles were modelled as cold-formed sections with rounded corners according to [25]. Residual stresses due to cold-forming were not considered.

Attention should be paid particularly to the gap between the chord and the brace. In practice, a small gap exists between the connected members due to their geometrical imperfections. If it is ignored during modeling, the brace and the chord are connected directly, forming an enlarged connection area. This does not correspond to reality, where the connection is performed only through the fillet weld. Therefore, a small gap was introduced to the FE model for computational purposes only, as shown in figure 8b. To determine the required width of the gap, three gap sizes (0 mm, 0.2 mm and 0.5 mm) were considered for the same joint (chord 150 x 150 x 8, brace 80 x 80 x 8, S355, a = 8 mm fillet weld). For simplicity, the sections were connected with a tie constraint. The M-φ responses of the tested models are provided in **figure 9**a. As can be noticed, all three joints have the same initial stiffness with slight deviations of the ultimate resistance. The discrepancy occurs in the area of large deformations, which is out of practical interest. Therefore, the effect of gap size was found negligible, and a gap of 0.5 mm was assumed for further investigations, as the one providing clear partitioning with reasonable aspect ratio of the elements.

It should be noted, when such a model is loaded by an in-plane bending moment, the nodes of the compressed brace flange could penetrate the surface of the chord, as shown in figure 9b. In reality, such penetration is impossible and should be prevented by introducing a contact interaction in the FE model. However, a short study has shown that the penetration takes place only at very high deformations, far beyond the deformation limit (figure 9a) and does not influence the results in the practical range of interest.

Only fillet welds are considered in this paper, with a throat angle of 45 °. Welds with throat thickness of $a \leq 5$ mm are assumed to consist of a single bead, while welds with $a > 5$ mm consist of three beads. Division into beads is conducted so that they have approximately equal volumes of metal, i.e., equal areas of the cross section. Modelling of the weld and its division into chunks is provided in figure 8c. This paper considers only the joints, in which the brace and the chord are made of a single steel grade. The material of welds is assumed to match that for the base parts. To simulate properly the welding process, the following properties were introduced in the material model: thermal conductivity, specific heat, density and latent heat for the thermal analysis; as well as expansion coefficient, Young's modulus and plastic stress-strain curve for the mechanical analysis. They all were considered as temperature-dependent and were extracted from Simufact.material 2016 library, where they are based on [26] for S355 and [27] for S690. It should be noted that the influence of phase transformation was ne-

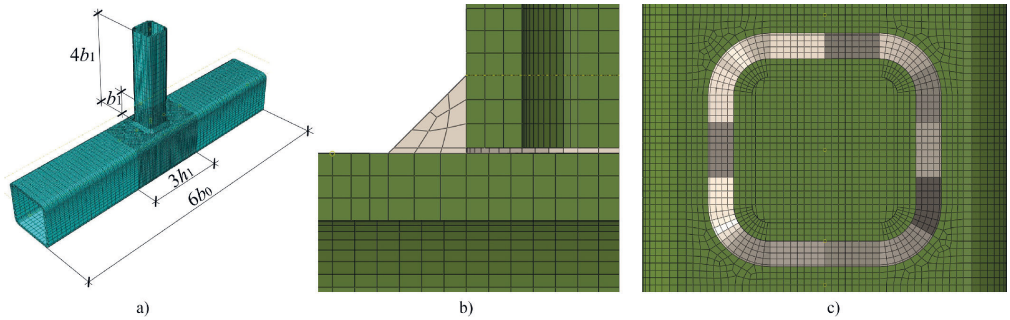

Fig. 8. FE model: a) meshing; b) gap between connected members; c) weld chunking
Bild 8. FE-Modell: a) Vernetzung; b) Spalt zwischen verschweißten Bauteilen; c) Längseinteilung Schweißnaht

glected. On the other hand, this local effect should not dramatically act on the overall stress distribution in joints [28].

3.4 Calibration of weld heat input

For a realistic assessment of temperatures, the weld heat input has to be properly introduced in the FE model, i. e., the activation of chunks representing the welding speed and the corresponding target torch heat-up temperature. The welding speed is set in accordance with available welding procedure specifications (WPS) for semi-mechanized metal active gas (MAG) welding [29], depending on the weld throat thickness. The target torch heat-up temperature represents the maximum temperature that is applied to the specimen during the welding process. It is determined so that both welded parts in the welding area are heated up to the melting temperature at the required depth. This criterion guarantees the quality of the weld. In this paper, it was evaluated visually by the expansion of the calculated 1 500 °C isotherm during the welding process. The optimal shape of this isotherm should be possibly close to the ellipsoid, while the "angular" shape usually means insufficient heating of the welded zone. Some trial analyses have shown that the default torch heat-up temperature of 1 500 °C does not provide the required depth of the melted zone (**figure 10**a). The temperature of 2 000 °C provides the expansion of the isotherm to the required depth (figure 10b). For the temperature of 2 500 °C the welded zone expands severely through the thickness of the brace, partly reaching its inner surface (figure 10c), which is usually not the case in practice. The observed discontinuity of the isotherm at the edges of the connected members is mainly caused by the gap. From the above observations, the required torch heat-up temperature was assumed equal to 2 000 °C. A more detailed calibration of the weld heat input requires a comparison with experimental results, e. g., macro sections [8].

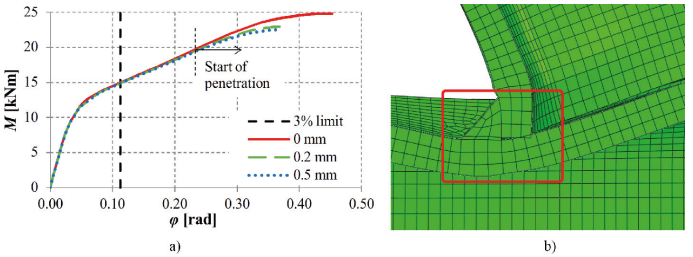

Fig. 9. Gap: a) effect of gap size; b) penetration of brace nodes to chord surface
Bild 9. Spalt: a) Einfluss der Spaltgröße; b) Eindringen des Pfostenknotens in die Gurtoberfläche

3.5 Mesh convergence study

Mesh convergence was studied on the developed model with the 100 x 100 x 6 chord and the 50 x 50 x 5 brace, made of S355 steel and with a = 5 mm weld. To reduce the calculation time, the welding process was simulated in AWI assuming the whole weld consisting of a single chunk, i.e., the whole weld was inserted simultaneously. Three mesh sizes were considered: 3 mm (two elements in thickness direction), 2 mm (three elements in thickness direction) and 1 mm (six elements in thickness direction). In other directions, the mesh size was determined so that the elements had an aspect ratio close to 1 near the connection area. The evaluation was conducted by extracting von Mises stresses in two paths: ABCD in longitudinal direction and MNOP in transverse direction, as shown in **figure 11**. Both paths were located on the outer surface of the connected members.

The von Mises stresses along the paths ABCD and MNOP are presented in **figure 12** and **figure 13**, respectively. Residual stresses reach their maximum in the weld area (sections BC and NO), where all models provide more or less the same values with some minor deviations. Extending further to the surface of the chord, both in longitudinal and transverse directions (sections AB and MN), stresses tend to reduce to the yield level. Spreading to the surface of the brace (section CD and OP), stresses decrease even stronger, beyond the yield level. At the distance of 5 mm from the weld in all directions (sections CD, MN and OP), a severe drop of stresses is observed, followed by a subsequent recovery. These observations clearly show that the 3 mm mesh is too coarse for such joint and cannot capture the local changes of stresses close to the weld area. Compared to the 1 mm mesh, the 2 mm mesh underestimates the local deviations of stresses on the surface of the brace and the weld; however, the difference is not so large on the surface of the chord, which plays the major role in the local behavior of such joints.

It is recalled here that Abaqus generally calculates stresses in the integration points of elements. To construct stress distributions maps, the program extrapolates values from the integration points to the corresponding nodes; therefore, the resulting stresses may lead to unreliable results in unfavourable cases. Moreover, when mesh refinement is evaluated, calculation time becomes a very important factor. The overall calculation time accounts for 0.72, 3.86 and 9.93 hours for 3 mm, 2 mm and 1 mm mesh correspondingly, considering that the simplest welding sequence is used. All calculations were performed on a personal computer with an Intel Core i7–4710HQ CPU, 2.50 GHz clock frequency and 16 GB RAM, using multiple processors parallelization. If a more sophisticated sequence is employed, e. g., the weld is divided into n chunks; the calculation time must be approximately multiplied by n, extremely complicating further investigations. For these reasons, 2 mm mesh was chosen as the optimal solution for this joint by the criteria of the results accuracy and reasonable calculation time. Extending this conclusion further, the preferable mesh size for similar cases can be recommended as $t_0/3$ or $a/3$.

3.6 Validation

The validation of the developed FE model was conducted with the results of [30]. The paper presents twenty experiments of HSS square hollow section T joints under in-plane bending, which were performed at the Sheet Metal Centre of Häme University of Applied Sciences, Finland. **Table 1** presents the details of the two joints selected for the validation. The test arrangement and the specimen dimensions are presented in **figure 14**. The connected members were produced of S420 steel. Material properties of the weld overmatched those of the members. The elastic properties and the plastic stress-strain response for S420 steel at room temperature were obtained from tensile coupon tests. The

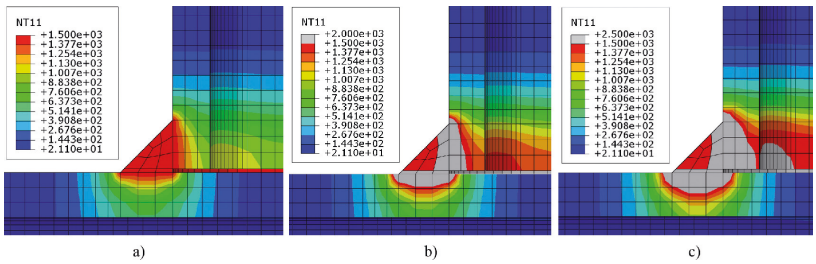

Fig. 10. Temperature distribution [°C] for various torch heat-up temperatures: a) 1500 °C, "angular" shape of 1500 °C isotherm; b) 2000 °C, ellipsoid shape of 1500 °C isotherm; c) 2500 °C, ellipsoid shape of 1500 °C isotherm with considerable expansion through the thickness of the sections

Bild 10. Temperaturverteilung [°C] für verschiedene Aufheiztemperaturen: a) 1500 °C, „ecki ger" Verlauf der 1500 °C Isotherme; b) 2000 °C, ellipsoider Verlauf der 1500 °C Isotherme; c) 2500 °C, ellipsoider Verlauf der 1500 °C Isotherme mit starker Durchwärmung in Blechdickenrichtung

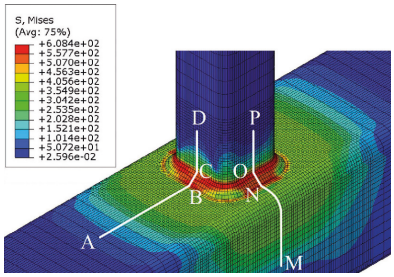

Fig. 11. Distribution of von Mises stresses [MPa] for 1 mm mesh size and the analysed paths

Bild 11. Von Mises Vergleichsspannung [MPa] für 1 mm Netzdichte und Pfadauswertungen

plastic stress-strain curves at elevated temperatures were extracted from Simufact.material 2016, scaling those for S355 by the coefficient $k = 420/355 \approx 1.18$. The thermomechanical parameters were assumed equal to those for S355. For both joints, the welding process was simulated in AWI, assuming double C-shaped welding sequence, as was used in the experiments. The welding simulation was followed by a nonlinear static analysis under in-plane bending. No geometric imperfections were considered.

Figure 15 provides the visual comparison between the deformed shapes obtained experimentally and numerically for Joint 1111. The results show that the developed FE model properly captures chord face plastification and chord web buckling. At the same time, certain difference is observed in relation to the overall failure of the joints. In reality, the joints failed from the cracking in the heat affected zone, reflected by a sharp drop in the moment-rotation response. Oppositely, in Abaqus, the damage mechanics to predict crack propagation were not introduced and the joints failed at higher loads, forming the clearly observed plateau in the moment-rotation response (**figure 16**). For this reason, this FE model is unreliable for the prediction of the ultimate load.

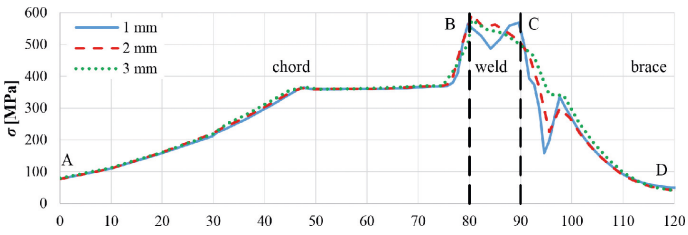

Fig. 12. Von Mises stress distribution along path ABCD

Bild 12. Von Mises Vergleichsspannung Pfad ABCD

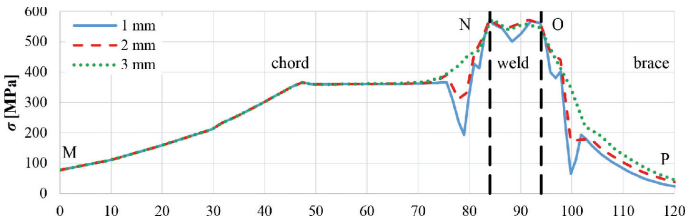

Fig. 13. Von Mises stress distribution along path MNOP

Bild 13. Von Mises Vergleichsspannung Pfad MNOP

Figure 16 presents the moment-rotation curves for the tested joints. As can be seen, the FE model provides good correlation in the elastic phase, with accurate initial stiffness. Very close results are observed in the hardening phase for Joint 1111, almost repeating the experimental curve. Small difference in the hardening phase is noticed for Joint 1121, which can be caused by the difference in the material properties. A comparison of the mechanical response is provided in Table 1. The FE model effectively predicts the plastic moment resistance, with errors smaller than 5 %. The results show that the developed model provides reasonable results and can be used for evaluation of the

structural behavior of joints in further parametric studies.

4 Conclusions

This paper develops and validates a FE model for RHS T joints, which takes into account welding residual stresses. This model is constructed in Abaqus/Standard software using the Abaqus Welding Interface (AWI) for the implementation of welding effects in the model.

To capture severe temperature and stress gradients due to welding, the constructed model requires sufficient number of elements near the welds, which considerably increases the calculation time using quadratic finite elements. For that reason, linear solid elements (C3D8 in Abaqus) with at least three elements in thickness direction are recommended for welding simulation in combination with subsequent loading situations. In the area affected by residual stresses, the mesh should be refined with a recommended mesh size of $t_0/3$ or $a/3$. Outside this area, a coarser mesh can be used to reduce computational efforts.

To provide reasonable results, material properties need to be determined as temperature-dependent. In practice, measuring of these properties is extremely expensive and challenging. In this paper, the material properties for S355 and S690 were extracted from Simufact.material 2016 and scaled for other steels proportionally to their nominal yield strength. Besides, the influence of phase transformation was neglected. For these reasons, material properties used in this paper may differ to some extent from reality.

Although the effects of welding are directly considered in this approach, AWI still simplifies the actual welding process. In AWI, the heat application is strongly idealized by controlling temperature in the contact faces of the weld and the weld itself. The setting of this temperature together with the chunk activation requires careful calibration. Incorrect selection of these parameters can lead to unrealistic results. In this particular approach, setting of these parameters was based on the assessment of the simulated 1 500 °C isotherms.

The validation with the experimental results has shown that the developed model properly captures

Table 1. Joints used in validation: details and structural behavior
Tabelle 1. Knoten zur Validierung: Randbedingungen und Tragverhalten

					$S_{j,ini}$[kNm/rad]			M_{pl}[kNm]		
Joint	Chord	Brace	Material	a [mm]	FEM	Test	FEM/Test	FEM	Test	FEM/Test
1111	150 x 150 x 8	100 x 100 x 8	S420	6	1401	1115	1.26	20.6	20.5	1.01
1121	150 x 150 x 8	100 x 100 x 8	S420	10	1778	1692	1.05	31.0	32.2	0.96

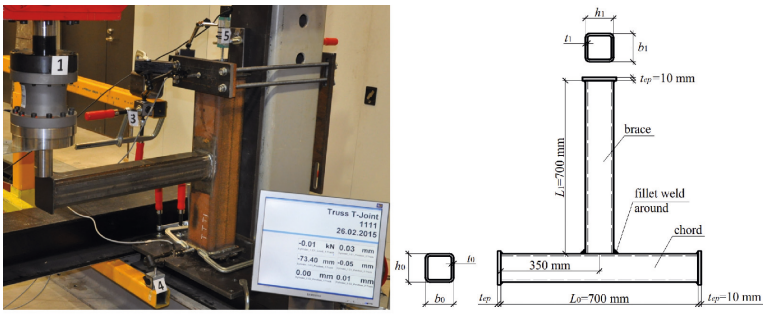

a) b)

Fig. 14. Tests: a) test arrangement; b) specimen dimensions
Bild 14. Experimentelle Ergebnisse: a) Versuchsaufbau; b) Probenabmessungen

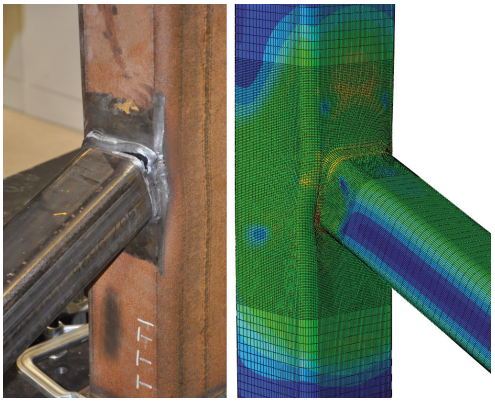

Fig. 15. Comparison between experimental and numerical results, Joint 1111
Bild 15. Vergleich zwischen experimentellen und numerischen Ergebnissen, Knoten 1111

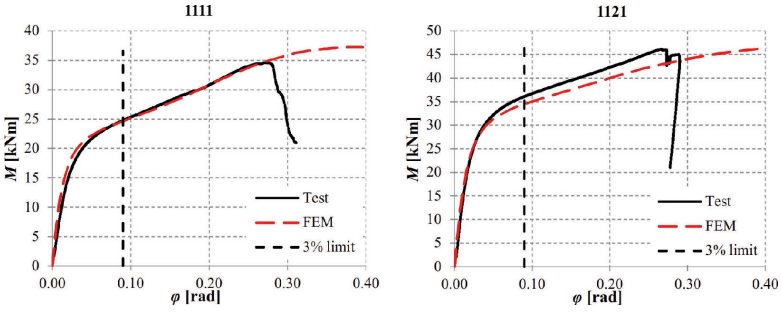

Fig. 16. Moment-rotation curves for Joints 1111 and 1121
Bild 16. Momenten-Rotations-Beziehung für Knoten 1111 und 1121

the local behavior of joints in the field of interest and can be used effectively for studying the effects of welding residual stresses in HSS tubular joints. The effect of welding residual stresses on the structural behavior of RHS T joints will be further discussed in Part II.

Acknowledgements

The authors gratefully acknowledge the financial support from KAUTE Foundation for the research reported in this paper.

Literature

[1] *Chen, C. et al.:* Influence of welding on mechanical properties of high strength steel butt joints. Proceedings of Eurosteel 2017.

[2] *Hochhauser, F. et al.:* Influence of the soft zone on the strength of welded modern HSLA steels. *In:* Welding in the World, Vol. 56 (2012), Iss. 5–6, pp. 77–85.

[3] *Khurshid, M.; Barsoum, Z.; Barsoum, I.:* Load carrying capacities of butt welded joints in high strength steels. *In:* Journal of Engineering Materials and Technology, Vol. 137 (2015), Iss. 4, pp. 41003.

[4] *Rodrigues, D.M. et al.:* Numerical study of the plastic behaviour in tension of welds in high strength steels. *In:* International Journal of Plasticity, Vol. 20 (2004), Iss. 1, pp. 1–18.

[5] *Teng, T. et al.:* Analysis of residual stresses and distortions in T-joint fillet welds. *In:* International Journal of Pressure Vessels and Piping, Vol. 78 (2001), Iss. 8, pp. 523–538.

[6] *Knödel, P.; Gkatzogiannis, S.; Ummenhofer, T.:* Practical aspects of welding residual stress simulation. *In:* Journal of Constructional Steel Research, Vol. 132 (2017), pp. 83–96.

[7] *Günther, H.-P. et al.:* Welded Connections of High-Strength Steels for the Building Industry. *In:* Welding in the World, Vol. 56 (2012), Iss. 5–6, pp. 86–106.

[8] *Pasternak, H.; Launert, B.; Krausche, T.:* Welding of girders with thick plates – Fabrication, measurement and simulation. *In:* Journal of Constructional Steel Research, Vol. 115 (2015), pp. 407–416.

[9] *Brar, G.S.; Singh, C.S.:* FEA of residual stress in cruciform welded joint of hollow sectional tubes. *In:* Journal of Constructional Steel Research, Vol. 102 (2014), pp. 44–58.

[10] *Moradi Eshkafti, M.:* Influence of various welding sequence schemes on the load bearing capacity of square hollow section T-joint. Cottbus, Brandenburg University of Technology, Dissertation, 2017.

[11] *Garifullin, M. et al.:* 3D component method for welded tubular T joints. *In: Heidarpour, A.; Zhao, X.-L. (Eds.):* Tubular Structures XVI – Proceedings of the 16th International Symposium on Tubular Structures (ISTS 2017), Melbourne, Australia, 4–6 December 2017. Taylor & Francis Group, London, 2018, pp. 165–173.

[12] *Packer, J. et al.:* Discussion on the paper "Experimental and numerical assessment of RHS T-joints subjected to brace and chord axial forces", by Nizer et al., Steel Construction 9 (2016), No. 4, pages 315–322. *In*: Steel Construction, Vol. 10 (2017), Iss. 1, pp. 89–90.

[13] *Lu, L.:* The static strength of I-beam to rectangular hollow section column connections. Delft University Press, Dissertation, 1997.

[14] EN 1993–1–8:2005, Eurocode 3: Design of steel structures – Part 1–8: Design of joints, Brussels, 2005.

[15] *Zhao, X.-L.; Hancock, G.J.:* T-joints in rectangular hollow sections subject to combined actions. *In:* Journal of Structural Engineering, Vol. 117 (1991), Iss. 8, pp. 2258–2277.

[16] *Kosteski, N.; Packer, J.A.:* Welded Tee-to-HSS Connections. *In:* Journal of Structural Engineering, Vol. 129 (2003), Iss. 2, pp. 151–159.

[17] *Zhao, X.-L.:* Deformation limit and ultimate strength of welded T-joints in cold-formed RHS sections. *In:* Journal of Constructional Steel Research, Vol. 53 (2000), Iss. 2, pp. 149–165.

[18] *Shubert, M.; Pandheeradi, M.:* An Abaqus Extension for 3-D Welding Simulations. *In:* Materials Science Forum, Vol. 768–769 (2013), pp. 690–696.

[19] *Bate, S.K.; Charles, R.; Warren, A.:* Finite element analysis of a single bead-on-plate specimen using SYSWELD. *In:* International Journal of Pressure Vessels and Piping, Vol. 86 (2009), Iss. 1, pp. 73–78.

[20] *Islam, M. et al.:* Simulation-based numerical optimization of arc welding process for reduced distortion in welded structures. *In:* Finite Elements in Analysis and Design, Vol. 84 (2014), pp. 54–64.

[21] *Majumdar, A.; D'Alvise, L.:* Application of welding simulation method to simulate additive manufacturing. *In:* Proceedings of the International Symposium on Visualization in Joining&Welding Science through Advanced Measurements and Simulation (Visual-JW2014), 2014, pp. 105–106.

[22] Abaqus 6.12. Getting Started with Abaqus: Interactive Edition. Dassault Systèmes, 2012.

[23] *van der Vegte, G.J.; Wardenier, J.; Puthli, R.S.:* FE analysis for welded hollow-section joints and bolted joints. *In:* Proceedings of the Institution of Civil Engineers – Structures and Buildings, Vol. 163 (2010), Iss. 6, pp. 427–437.

[24] *Bursi, O.S.; Jaspart, J.P.:* Calibration of a Finite Element Model for Isolated Bolted End-Plate Steel Connections. *In:* Journal of Constructional Steel Research, Vol. 44 (1997), Iss. 3, pp. 225–262.

[25] EN 10219–2:2006: Cold formed welded structural hollow sections of non-alloy and fine grain steels – Part 2: Tolerances, dimensions and sectional properties, Brussels, 2006.

[26] *Voss, O.:* Untersuchung relevanter Einflußgrößen auf die numerische Schweißsimulation. Aachen, Shaker, Dissertation, 2001.

[27] *Schröter, F.:* Höherfeste Stähle für den Stahlbau – Auswahl und Anwendung. *In:* Bauingenieur 78 (2003), Heft 9, S. 426–432.

[28] *Launert, B. et al.:* Measurement and numerical modeling of residual stresses in welded HSLA component-like I-girders. *In:* Welding in the World, Vol. 61 (2017), Iss. 2, pp. 223–229.

[29] *Aichele, G.:* Leistungskennwerte für Schweißen und Schneiden. 2., überarbeitete und erweiterte Auflage. Fachbuchreihe Schweißtechnik, DVS-Verlag GmbH, Düsseldorf, 1994.

[30] *Havula, J. et al.:* Experimental research of welded tubular HSS T-joints, welding times and moment resistances. *In:* IIW International Conference High Strength Materials – Challenges and Applications, 2–3 July 2015, Helsinki, Finland, 2015.

V

EFFECT OF WELDING RESIDUAL STRESSES ON LOCAL BEHAVIOR OF RECTANGULAR HOLLOW SECTION JOINTS. PART 2 – PARAMETRIC STUDIES

by

Garifullin M., Launert B., Heinisuo M., Pasternak H., Mela K. & Pajunen S., May 2018

Bauingenieur vol. 93 (May), 207-213

Bei diesem Beitrag handelt es sich um einen wissenschaftlich begutachteten und freigegebenen Fachaufsatz („reviewed paper").

Effect of welding residual stresses on local behavior of rectangular hollow section joints

Part 2 – Parametric studies

M. Garifullin, B. Launert, M. Heinisuo, H. Pasternak, K. Mela, S. Pajunen

Abstract Welding residual stresses that occur in tubular joints after the welding process affect their structural behavior. To ensure that these stresses do not negatively act on the load-bearing capacity of joints, their influence should be carefully investigated. This paper represents the second part of a study that numerically evaluates the structural behavior of rectangular hollow section T joints taking into account welding residual stresses. The finite element model developed in Part 1 is now used to evaluate their effect on the resistance and initial stiffness of tubular joints. The conducted parametric analyses show that welding residual stresses have a positive influence of 1–19 % on the plastic resistance of tubular joints and insignificantly reduce their initial stiffness. At the same time, the behavior of the considered joints is found not to depend on the welding sequence.

Einfluss der Schweißeigenspannungen auf die Tragfähigkeit von Rechteck-Hohlprofil-Knoten Teil 2: Parameterstudien

Zusammenfassung Schweißeigenspannungen können das Tragverhalten geschweißter Hohlprofilknoten zum Teil stark beeinflussen. Um mögliche negative Einflüsse auf die Tragfähigkeit auszuschließen, sollte der Eigenspannungseinfluss mitberücksichtigt werden. Dieser Beitrag bildet den zweiten Teil einer numerischen Untersuchung an geschweißten Rechteck-Hohlprofil-Knoten unter Berücksichtigung der vorgenannten Spannungen. Darin werden in Teil 1 entwickelten Modelle dazu verwendet, deren Auswirkungen auf die Tragfähigkeit und die Anfangssteifigkeit der Knotenverbindung darzustellen. Die Ergebnisse zeigen im untersuchten Parameterfeld eine Traglaststeigerung zwischen 1 % und 19 %. Die Anfangssteifigkeit wird generell nur geringfügig reduziert. Gleichzeitig wird gezeigt, dass die Schweißreihenfolge in den untersuchten Fällen keinen nennenswerten Einfluss auf die Tragfähigkeit ausübt.

Marsel Garifullin, M.Sc.
marsel.garifullin@tut.fi
Prof., Ph.D, Markku Heinisuo
markku.heinisuo@tut.fi
Ph.D, Kristo Mela
kristo.mela@tut.fi
Assoc. Prof., Ph.D, Sami Pajunen
sami.pajunen@tut.fi
Tampere University of Technology
Korkeakoulunkatu 10, 33720 Tampere, Finland
Benjamin Launert, M.Sc., SFI/IWE
benjamin.launert@b-tu.de
Prof. Dr.-Ing. habil. Hartmut Pasternak
hartmut.pasternak@b-tu.de
Brandenburgische Technische Universität
Platz der Deutschen Einheit 1, 03046 Cottbus

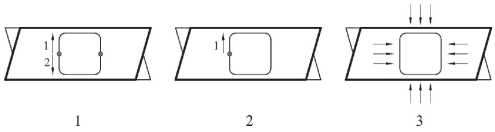

Fig. 1. Welding sequences
Bild 1. Schweißreihenfolgen

1 Introduction

This paper represents the second part of the study investigating the effect of welding residual stresses on the structural behavior of rectangular hollow section (RHS) T joints. The finite element model of the joint with welding residual stresses was developed and validated in Part 1 [1]. This paper employs the constructed model to evaluate the effect of welding residual stresses on the resistance and initial stiffness of the considered joints. Section 2 evaluates the effect of welding residual stresses considering various welding sequences. Section 3 conducts parametric studies to investigate the structural behavior of joints with varying parameters, such as steel grade, chord wall thickness and weld throat thickness. Finally, the observed results are discussed in Section 4. The welding process is simulated using the Abaqus Welding Interface [2], and the subsequent static loading is performed in Abaqus/Standard [3]. The paper investigates only joints with fillet welds. The considered joints are subjected to in-plane bending and axial force in the brace.

2 Influence of welding residual stresses using various welding sequences

This study investigates the effect of welding residual stresses on the resistance and stiffness of RHS T joints. The analysis is conducted on a single joint with a 100 x 100 x 6 chord and a 50 x 50 x 5 brace with a = 5 mm weld under in-plane bending and axial loading in the brace. The weld is assumed to be comprised of a single bead. Three welding sequences are considered and presented in **figure 1**. Sequence 1 represents the sequence used by the steel manufacturer SSAB, when the weld bead consists of two consecutive C-shaped paths. Sequence 2 corresponds to its minor simplification, when the bead is conducted by a single progressive path. Sequence 3 represents the most simplified variant, when the whole weld is inserted simultaneously to the model. This hypothetical case has no connection to reality, but is considered here for comparison, because it requires much less computational time. Sequences 1 and 2 activate one chunk per pass, Sequence 3 activates all chunks in a single pass. Definition of passes and chunks is discussed in Part 1.
All three sequences were simulated in AWI and the obtained residual stresses are presented in **figure 2**. As can be

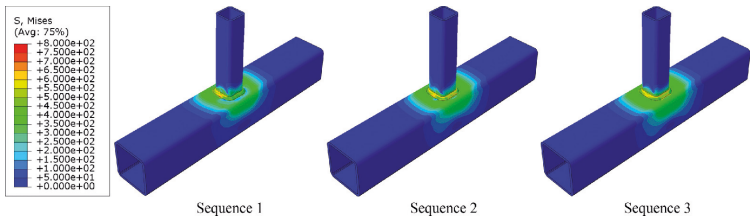

Fig. 2. Von Mises residual stresses [MPa] for Sequences 1–3
Bild 2. Von Mises Vergleichseigenspannung [MPa] für Schweißreihenfolgen 1–3

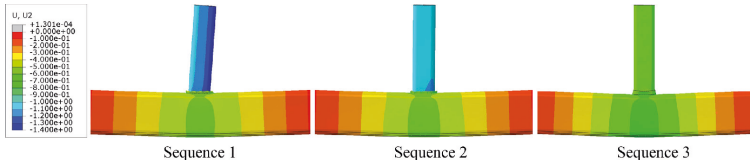

Fig. 3. Welding-induced displacements [mm] along brace axis for various sequences, scaled 15 times
Bild 3. Schweißbedingte Verformungen [mm] des Pfostens für verschiedene Schweißreihenfolgen, 15fache Überhöhung

seen, all cases have similar stress distribution patterns, with the stress-affected zones located in the chord top face and in the upper half of chord webs. In most parts of the zones, the stresses reach yielding, extreme values occur in the weld. As expected, the stress distribution pattern is symmetrical for Sequence 3.

In terms of deformations, all three sequences show similar patterns: shrinkage occurring in the welding area during the post-welding cooling leads to bending of the chord in the plane of the joint, as shown in **figure 3**. The largest deformations are observed for Sequence 1 (1.3 mm), the smallest for Sequence 3 (0.94 mm). The out-of-plane deformations are relatively small and are not shown. Similar results are reported in [4]. In addition, Sequence 1 shows a large deviation of the brace from its vertical position, resulting in a horizontal displacement of 0.8 mm at its end.

Afterwards, the joints with the considered welding sequences were loaded separately by an in-plane bending moment and an axial brace force using a nonlinear static finite element analysis (FEA). The results are presented in **figure 4**, where "No welding" corresponds to the model, which was analysed considering fillet weld geometry but ignoring welding residual stresses. As can be seen, all three sequences provide practically the same responses, both in the case of bending and axial loading, which differ from the original model without welding. Compared to "No welding", Sequences 1–3 have considerably larger moments in the transitional phase, with a smaller difference in the hardening phase. In both loading cases, the curves with and without welding proceed almost parallel to each other. This indicates that the plastification of the chord top face develops similarly in all models, but welding residual stresses postpone its initiation.

To evaluate the effect of welding-induced deformations, they were extracted from "Sequence 1" and were applied to "No welding" as initial geometric imperfections, this model is named as "No welding+U". This case shows almost identical behavior as "No welding", meaning that welding-induced imperfections have no influence on the behavior of the joint, and the observed differences for Sequences 1–3 are predominantly caused by welding residual stresses. Ultimate resistance is the same for the models with and without

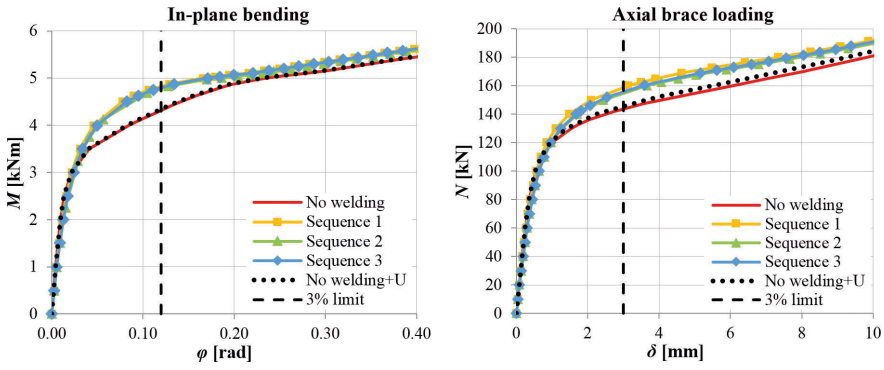

Fig. 4. Action-deformation curves for joints with various welding sequences
Bild 4. Last-Verformungs-Kurven für Knoten mit verschiedenen Schweißreihenfolgen

Table 1. Structural behavior of joints with various welding sequences. Relative values in relation to "No welding"
Tabelle 1. Tragverhalten von Knoten mit unterschiedlichen Schweißreihenfolgen. Bezogene Werte in Bezug auf „No welding" (kein Schweißeinfluss)

	In-plane bending				Axial brace loading			
	M_{pl} [kNm]		$S_{j,ini}$ [kNm/rad]		N_{pl} [kN]		$C_{j,ini}$ [kN/mm]	
	Absolute	Relative	Absolute	Relative	Absolute	Relative	Absolute	Relative
No welding	4.38	**1.00**	226	**1.00**	131.8	**1.00**	240	**1.00**
Sequence 1	4.62	**1.05**	210	**0.93**	152.3	**1.16**	227	**0.94**
Sequence 2	4.55	**1.04**	199	**0.88**	148.5	**1.13**	230	**0.96**
Sequence 3	4.61	**1.05**	195	**0.86**	148.7	**1.13**	239	**1.00**
No welding + U	4.39	**1.00**	227	**1.00**	133.8	**1.01**	244	**1.01**

welding and is not shown in the figure. In addition, all models demonstrate the required deformation capacity, clearly exceeding the deformation limit introduced in Part 1 [1].
The plastic resistance and initial stiffness of the tested models are determined according to Part 1 [1] and provided in **table 1**. The results show that the consideration of welding stresses leads to higher resistance (4–5 % for in-plane bending and 13–16 % for axial loading) and lower initial stiffness (7–14 % for in-plane bending and 4–6 % for axial loading) of the joints.

3 Parametric studies

This section uses the FE model for studying the influence of welding residual stresses on joints with varying parameters, such as steel grade, chord wall thickness and the throat thickness of the weld. According to [5], joints with $\beta \leq 0.85$ primarily fail from the plastification of the top chord flange and, therefore, demonstrate similar local behavior under static loading. For that reason, the parametric study is not conducted in relation to β. The studies are conducted for both in-plane bending and axial brace loading. The small difference between the tested sequences in Section 2 indicates that the simplified approach of Sequence 3 can be employed for further investigations, as it provides reasonable results with comparatively small computational time.

3.1 Influence of steel grade

Firstly, the effect of steel grade on the distribution of welding residual stresses on the joint used in Section 2 is studied. Apart from S355, two additional steel grades were considered: S500 and S690, both for the connected members and the weld material. The material properties for S690 were taken from Simufact.material 2016. The properties for S500 were obtained from S355: the plastic stress-strain curves were scaled by multiplying by a factor $k = 500/355 \approx 1.41$, the remaining properties were kept the same. **figure 5** provides the distribution of residual von Mises stresses close to the welding area. As can be seen, on the top flange of the chord, the stress distributions are similar for all grades, reaching the distance of $2h_1 \ldots 2.5h_1$ from the centre of the brace. On the chord web, the length of the distribution area increases for higher steels, reaching the bottom flange for S690. The values of stresses correlate with the steel grade, increasing with the nominal yield strength. The maximum stresses are observed locally in the weld and the adjacent parts of the brace.
The distribution of stresses along paths ABCD and MNOP (according to **figure 11**, Part 1) is presented in **figure 6** and **figure 7** correspondingly. Reaching the maximum in the weld, the stresses distribute evenly by 30 mm in both directions on the surface of the chord, with a clearly observed

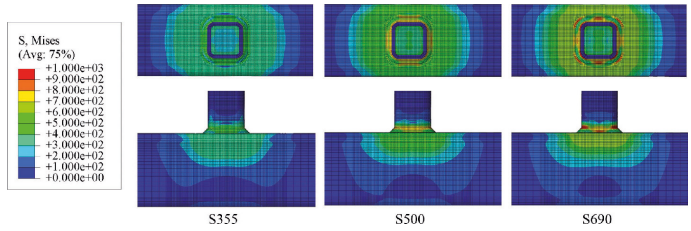

Fig. 5. Comparison of residual stresses [MPa] for various steel grades
Bild 5. Vergleich der Eigenspannungen [MPa] für unterschiedliche Stahlgüten

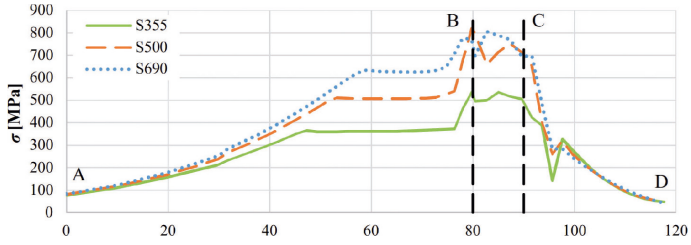

Fig. 6. Von Mises stresses along longitudinal path ABCD
Bild 6. Von Mises Vergleichsspannung, Längspfad ABCD

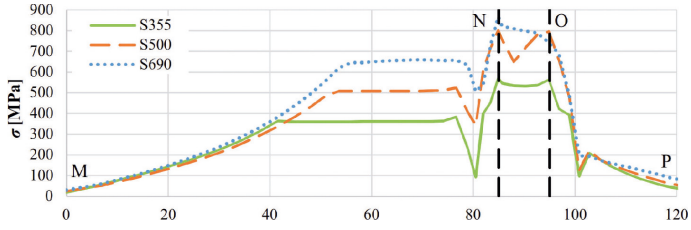

Fig. 7. Von Mises stresses along transversal path MNOP
Bild 7. Von Mises Vergleichsspannung, Querpfad MNOP

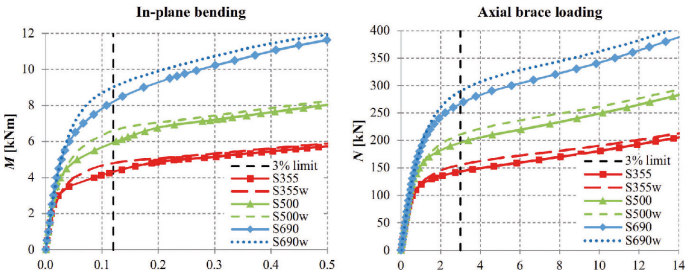

Fig. 8. Action-deformation curves for joints with various steel grades
Bild 8. Last-Verformungs-Kurven für Knoten mit unterschiedlichen Stahlgüten

Table 2. Structural behavior of joints with various steel grades
Tabelle 2. Tragverhalten von Knoten mit unterschiedlichen Stahlgüten

Material	S355	S355w	S355w / S355	S500	S500w	S500w / S500	S690	S690w	S690w/ S690
M_{pl} [kNm]	4.40	4.62	**1.05**	6.18	6.39	**1.04**	7.56	8.60	**1.14**
M_u [kNm]	6.61	6.67	**1.01**	9.25	9.34	**1.01**	12.63	12.77	**1.01**
$S_{j,ini}$ [kNm/rad]	226	195	**0.86**	226	211	**0.93**	227	244	**1.08**
N_{pl} [kN]	131.8	145.8	**1.11**	182.4	203.7	**1.12**	256.9	283.9	**1.11**
N_u [kN]	287.3	287.4	**1.00**	400.2	400.1	**1.00**	543.7	545.3	**1.00**
$C_{j,ini}$ [kN/mm]	240	227	**0.94**	240	234	**0.98**	240	251	**1.04**

Table 3. Joints with various chord wall thickness
Tabelle 3. Knoten mit unterschiedlichen Gurtwandstärken

Joint	Chord	2γ	Brace	a [mm]	Material
1	100 x 100 x 6	16.6	50 x 5	5	S355
2	100 x 100 x 4	25	50 x 4	5	S355
3	100 x 100 x 3	33.3	50 x 3	5	S355

plateau with the values approximately equal to the yield strength. Beyond the plateau, the stresses gradually decline to zero. On the other hand, the decrease of the stresses on the surface of the brace is more rapid, with no plateau observed.

The behavior of each joint under an in-plane bending moment and an axial brace force is illustrated in **figure 8**, where the index w corresponds to the models with welding residual stresses. The results show that the improving effect, observed for S355, remains also for higher steel grades. The exact values of plastic resistance, ultimate resistance and initial stiffness are collected in **table 2**. As can be seen, the consideration of residual stresses leads to 4–14 % higher plastic resistance against bending moment and 11–12 % higher resistance against axial loading. At the same time, ultimate resistance is practically not affected by welding stresses. Initial stiffness is slightly lower for S355 and S500 but insignificantly higher for S690; in practice, these changes of initial stiffness can be neglected. At least no negative effects are found when the residual stresses are present.

3.2 Influence of chord wall thickness

This section investigates the effect of welding residual stresses on the behavior of joints with various wall thickness of the connected members. According to [5], the behavior of the joint with $\beta \leq 0.85$ is governed by the deformation of the chord top face; therefore, the wall thickness of the brace is of less importance than that of the chord. The latter is best characterized by the chord width-to-thickness ratio $\gamma = b_0/2t_0$, which for simplicity is often considered as $2\gamma = b_0/t_0$. Chapter 7 of [5] provides the following limitations for this ratio: $10 \leq 2\gamma \leq 35$. The thickness of the brace is determined so that it does not exceed that of the chord. Three joints are considered in this study, as shown in **table 3**. The first one represents a joint with a very thick wall; the second joint with $2\gamma = 25$ corresponds to an intermediate case; while Joint 3 relates to its upper bound. Each model was constructed with and without AWI and then loaded by an in-plane bending moment and an axial brace force.

The visual comparison of welding residual stresses after simulation in AWI is provided in **figure 9**, the distribution along paths ABCD and MNOP in **figure 10** and **figure 11** correspondingly. As can be seen, all joints have similar stress distribution patterns, with slightly larger stress distribution zones for high 2γ. Moreover, the maximum stresses in the welding areas are smaller for thinner walls, i. e., for larger γ. The behavior of each joint under an in-plane bending moment and an axial brace force is shown in **figure 12** and collected in **table 4**, where index w corresponds to the models with welding residual stresses. According to the results, the models with welds simulated with AWI show higher resistance than those without. Moreover, the improving effect of welding residual stresses is more pronounced for the joints with thinner walls: plastic moment resistance increases by 19 % for $2\gamma = 25$ and $2\gamma = 33.3$, while plastic axial resistance increases by 17 % for $2\gamma = 33.3$. At the same time, the joints with high 2γ are weakly affected by residual stresses in terms of their initial stiffness. As before, no changes are observed for ultimate resistance.

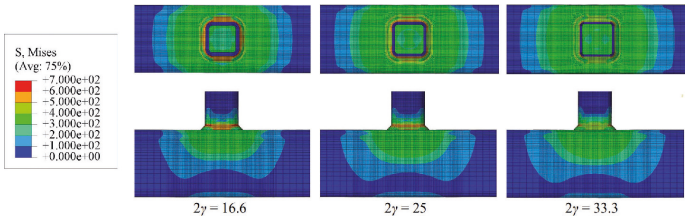

Fig. 9. Comparison of residual stresses [MPa] for various wall thickness
Bild 9. Vergleich der Eigenspannungen [MPa] für unterschiedliche Wandstärken

3.3 Influence of weld throat thickness

The last parametric study is conducted in relation to weld throat thickness. The analyses are based on the joint from Section 2 with three throat thicknesses: 3, 5 and 8 mm. According to [6], the throat thickness for a full-strength fillet weld is 6 mm for this joint. Each joint was constructed with and without AWI and loaded separately by an in-plane moment and an axial brace force. **Figure 13** provides the visual comparison of the residual stress distribution for the tested joints. As can be seen, for larger throat thicknesses, the stresses propagate further along the chord face and chord web. The analysis of stresses along paths ABCD and MNOP is not given here because the geometry of the joint varies along with the weld size.

The structural behavior of each joint under an in-plane bending and an axial brace loading is provided in **figure 14** and **table 5**, where index w corresponds to the models with welding residual stresses. As can be seen, larger welds increase the dimensions of the brace and lead to higher plastic resistance and initial stiffness. As before, the presence of residual stresses positively affects the bearing capacity of joints. For moment-loaded joints, the improving effect declines from 19 % for a = 3 mm to 1 % for a = 8 mm. At the same time, for axial-loaded joints, it has no correlation with the size of the weld and remains at the level of 8–11 %. The stresses slightly reduce the initial stiffness of joints, almost not affecting their ultimate resistance.

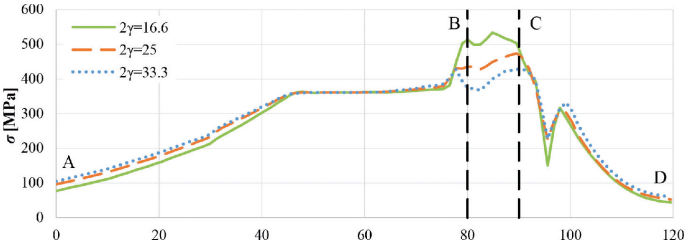

Fig. 10. Von Mises stresses along longitudinal path ABCD
Bild 10. Von Mises Vergleichsspannung Längspfad ABCD

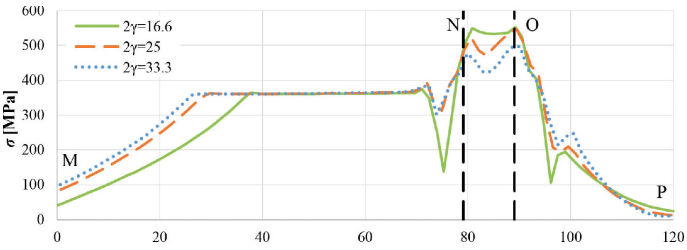

Fig. 11. Von Mises stresses along transversal path MNOP
Bild 11. Von Mises Vergleichsspannung Querpfad MNOP

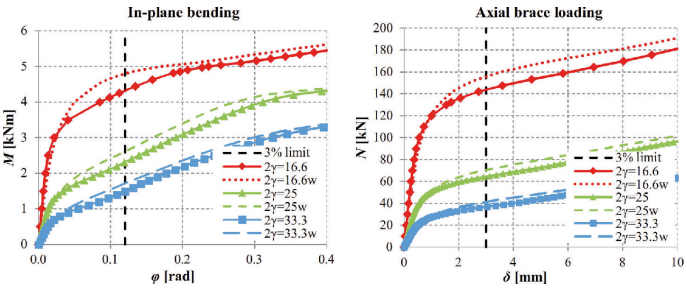

Fig. 12. Action-deformation curves for joints with various wall thickness
Bild 12. Last-Verformungs-Kurven für Knoten mit unterschiedlichen Wandstärken

4 Discussion

The conducted FE analyses have shown that for all joints investigated in this paper, AWI provides a similar distribution pattern of welding residual stresses, which is depicted in **figure 15**. The stresses reach their maximum values in the body of the weld. It should be noted that extreme values are observed on the straight parts of the weld, but not in the corners. On the top flange of the chord, the stresses spread to the length of $4h_1 \ldots 5h_1$. On the chord web, they extend to $0.5h_0 \ldots h_0$, reaching the bottom flange for S690 and large weld throat thickness. In the brace, the area affected by the stresses generally does not exceed b_1.

The conducted FE analyses under static loading have demonstrated that welding residual stresses increase the plastic resistance of joints, especially at the hardening phase. The improving effect is observed for all joints and is found not to depend on the welding sequence used in AWI. This contradicts with the results of [7], who reports a 8–10 % difference between the resistances of joints with different welding sequences. The parametric studies have shown that the increase of plastic bending resistance is in the range of

Table 4. Structural behavior of joints with various wall thickness
Tabelle 4. Tragverhalten von Knoten mit unterschiedlichen Wandstärken

2γ	16.6	16.6w	16.6w/16.6	25	25w	25w/25	33.3	33.3w	33w/33
M_{pl} [kNm]	4.40	4.62	**1.05**	1.37	1.62	**1.19**	0.73	0.87	**1.19**
M_u [kNm]	6.61	6.67	**1.01**	5.33	5.38	**1.01**	3.94	3.96	**1.00**
$S_{j,ini}$ [kNm/rad]	226	195	**0.86**	85	80	**0.94**	43	41	**0.97**
N_{pl} [kN]	131.8	145.8	**1.11**	54.1	59.9	**1.11**	28.1	32.7	**1.17**
N_u [kN]	287.3	287.4	**1.00**	175.5	176.2	**1.00**	127.9	128.2	**1.00**
$C_{j,ini}$ [kN/mm]	240	227	**0.94**	93	93	**1.00**	47	47	**1.01**

1–19 %. The improving effect is more pronounced for higher steel grades, smaller chord wall thickness and smaller weld throat thickness. Plastic axial resistance is improved by 8–17 %. For this case, the improving effect is more pronounced for smaller chord wall thickness but is weakly dependent on the other studied parameters. Residual stresses also affect the initial and rotational stiffness of joints, reducing it by 5–14 %. A positive influence on the initial stiffness is observed only for S690 steel. Such changes of stiffness are usually found insignificant in the practical range of interests. Ultimate resistance is almost not influenced by residual stresses in this study.

The nature of the observed phenomenon is not clear. Generally, it can be caused by welding residual stresses and / or resulted deformations. Figure 4 clearly shows that the deformations obtained from the welding process do not affect the local behavior of joints; therefore, the improving effect is primarily connected with residual stresses. In reality, these stresses are always present in joints and obviously cannot be avoided. The observed positive effect demonstrates the difference between two FE modelling approaches for tubular joints: one considering residual stresses and one neglecting them. Ignoring these stresses leads to mostly small underestimation of the plastic resistance of the joint, leading thus to safe results. Moreover, the complexity of welding simulation in AWI does not allow to employ it widely for general simulations. From that point of view, neglecting welding residual stresses is fully justified in the FE analyses of tubular joints, which behaviour is governed by chord plastification failure in the investigated parameter range. The findings of this paper may be verified by more sophisticated calculations in the future.

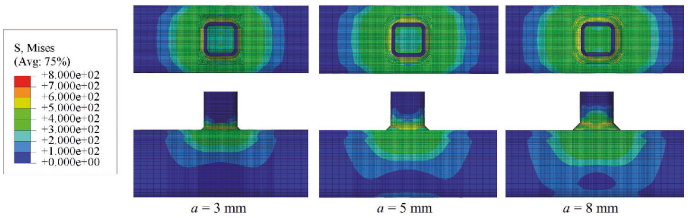

Fig. 13. Comparison of residual stresses [MPa] for various weld throat thickness
Bild 13. Vergleich der Eigenspannungen [MPa] für unterschiedliche Kehlnahtdicken

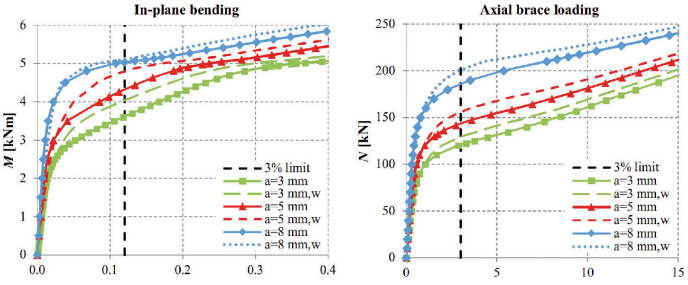

Fig. 14. Action-deformation curves for joints with various weld throat thickness
Bild 14. Last-Verformungs-Kurven für Knoten mit unterschiedlichen Kehlnahtdicken

5 Conclusions

All the joints studied in this paper demonstrate a positive effect of welding residual stresses on their plastic resistance. The observed influence is found not to depend on welding sequences; therefore, an idealized sequence is recommended for simulation to reduce calculation time. At the same time, the conducted parametric studies have shown that the effect depends on steel grade, chord wall thickness and weld throat thickness.

This paper considers the joints with fillet welds from $a = 3$ mm to $a = 8$ mm, $\beta \leq 0.85$, $10 \leq 2\gamma \leq 35$ and steel grades from S355 to S690. The research can be further extended to explore additional cases and develop more generalized conclusions. Additional studies are also required to eliminate the possible scaling effect, considering different chord sizes. A further experimental validation of the obtained findings may be possible by comparing welded T joints with the joints that received a stress-relief heat treatment prior to loading. Such a comparison will allow to experimentally evaluate the influence of welding residual stresses on the structural behavior of tubular joints. The presented results can serve as a starting point for studying the issue of welding residual stresses in relation to HSS tubular joints.

Table 5. Structural behavior of joints with various weld throat thickness
Tabelle 5. Tragverhalten von Knoten mit unterschiedlichen Kehlnahtdicken

a [mm]	3	3w	3w/3	5	5w	5w/5	8	8w	8w/8
M_{pl} [kNm]	2.76	3.27	**1.19**	4.40	4.62	**1.05**	4.70	4.77	**1.01**
M_u [kNm]	5.12	5.26	**1.03**	6.61	6.67	**1.01**	6.70	6.69	**1.00**
$S_{j,ini}$ [kNm/rad]	180	171	**0.95**	226	195	**0.86**	326	284	**0.87**
N_{pl} [kN]	107.6	116.5	**1.08**	131.8	145.8	**1.11**	179.5	197.5	**1.10**
N_u [kN]	285.9	286.0	**1.00**	287.3	287.4	**1.00**	289.2	289.2	**1.00**
$C_{j,ini}$ [kN/mm]	186	176	**0.95**	240	227	**0.94**	355	336	**0.95**

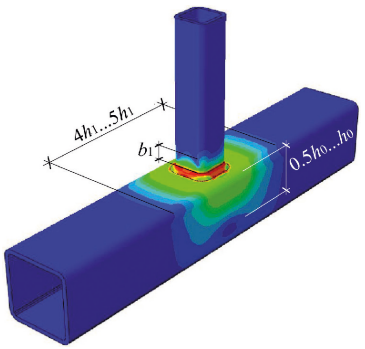

Fig. 15. Distribution of welding residual stresses in joint
Bild 15. Verteilung der Schweißeigenspannungen im Knoten

Acknowledgements

The authors gratefully acknowledge the financial support from KAUTE Foundation for the research reported in this paper.

Literature

[1] *Garifullin, M.; Launert, B.; Heinisuo, M.; Pasternak, H.; Mela, K.; Pajunen, S.:* Effect of welding residual stresses on local behavior of rectangular hollow section joints, Part 1 – Development of numerical model. *In:* Bauingenieur 93 (2018), Iss. 4, pp. 152–159

[2] *Shubert, M.; Pandheeradi, M.:* An Abaqus Extension for 3-D Welding Simulations. *In:* Materials Science Forum, Vol. 768–769 (2013), pp. 690–696.

[3] Abaqus 6.12. Getting Started with Abaqus: Interactive Edition. Dassault Systèmes, 2012.

[4] *Teng, T. et al.:* Analysis of residual stresses and distortions in T-joint fillet welds. *In:* International Journal of Pressure Vessels and Piping, Vol. 78 (2001), Iss. 8, pp. 523–538.

[5] EN 1993–1–8:2005, Eurocode 3: Design of steel structures – Part 1–8: Design of joints. Brussels, 2005.

[6] *Ongelin, P.; Valkonen, I.:* SSAB Domex Tube. Structural hollow sections. EN 1993 – Handbook 2016. SSAB Europe Oy, 2016.

[7] *Moradi Eshkafti, M.:* Influence of various welding sequence schemes on the load bearing capacity of square hollow section T-joint. Cottbus, Brandenburg University of Technology, dissertation, 2017.

Buchempfehlungen

Olzem, O. und Hoffstadt, J.
Abwicklung von Bauvorhaben
Von den Grundstücksfragen über Planung und Ausführung bis zur Abnahme
8. Auflage 2018, 225 Seiten, 78 Abbildungen, 7 Tabellen, gebunden.
Rudolf Müller Verlag
ISBN: 978–3–481–03668–3
59,– Euro

Das Buch führt Architekten, Planer und Bauherren Schritt für Schritt durch alle Planungsphasen sowie den gesamten Bauablauf und ermöglicht so eine reibungslose und rechtssichere Abwicklung und Umsetzung von Bauprojekten.
Der praxisorientierte Wegweiser unterstützt vom ersten Entwurf bis zur Abnahme und Abrechnung und vermittelt praxisnah bau- und planungsrechtliche Themen wie Genehmigungsverfahren, Bauvertrag und Bauausführung, Kostenplanung. Anhand eines konkreten Beispielprojektes mit Architektenvertrag, Honorarabrechnung, vollständigen Planunterlagen inklusive Baubeschreibung, Kostenschätzung und -berechnung sowie Ausschreibungsunterlagen erläutern die Autoren chronologisch und anschaulich die zeitlichen, rechtlichen und organisatorischen Abläufe. Die detaillierten Unterlagen des Beispielprojektes dienen als Vorlage für eigene Projekte und stehen im Anhang sowie als Online-Download zur Verfügung.
Die vorliegende Auflage des Werkes wurde anhand der derzeit gültigen baurechtlichen und bautechnischen Regelwerke komplett aktualisiert und um ein Kapitel zum Thema BIM im Planungsprozess erweitert.

www.rudolf-mueller.de

Reichert, F., Reuber, N., Siegburg , F.
Handbuch Vergabe von Architekten- und Ingenieurleistungen
2017, 340 Seiten, gebunden
Werner Verlag
ISBN 978–3–8041–4663–1
74,– Euro, auch als E-Book erhältlich

Die Vergabe von Architekten- und Ingenieurleistungen durch öffentliche Auftraggeber wird durch die, im April 2016 in Kraft getretene, Vergaberechtsreform grundlegend neu gestaltet. Die VOF fällt weg, Rechtsgrundlagen sind die Vergabeverordnung (VgV) für Vergaben oberhalb der Schwellenwerte sowie die neue Unterschwellenvergabeordnung (UVgO), ebenfalls berücksichtigt wird die Sektorenverordnung (SektVO).
Die Autoren zeigen die Fallstricke im neuen Vergabeverfahren ober- und unterhalb der Schwellenwerte auf und wie man sie vermeidet. Sie geben eine umfangreiche, praxisorientierte Anleitung zur Gestaltung von Planerverträgen.
Das Buch wendet sich an alle Teilnehmer, Auftraggebervertreter oder Berater im Vergabeverfahren für Architekten- und Ingenieurleistungen.

www.wolterskluwer.de

VI

COLD-FORMED RHS T JOINTS WITH INITIAL GEOMETRICAL IMPERFECTIONS

by

Garifullin M., Bronzova M., Heinisuo M., Mela K., & Pajunen S., 2018

Magazine of Civil Engineering vol. 4(80), 81-94

doi: 10.18720/MCE.80.8

Cold-formed RHS T joints with initial geometrical imperfections

Сварные узлы холодногнутых труб прямоугольного сечения с начальными несовершенствами

M. Garifullin,
Tampere University of Technology, Tampere, Finland
M.K. Bronzova,
Peter the Great St. Petersburg Polytechnic University, St. Petersburg, Russia
M. Heinisuo,
K. Mela,
S. Pajunen,
Tampere University of Technology, Tampere, Finland

Аспирант М.Р. Гарифуллин,
Технологический университет Тампере, Тампере, Финляндия
студент М.К. Бронзова,
Санкт-Петербургский политехнический университет Петра Великого, г. Санкт-Петербург, Россия
д-р техн. наук, профессор М. Хейнисуо,
канд. техн. наук, старший научный сотрудник К. Мэла,
канд. техн. наук, доцент С. Паюнен,
Технологический университет Тампере, Тампере, Финляндия

Key words: hollow section joint; resistance; initial stiffness; finite element analysis; imperfection

Ключевые слова: трубный узел; прочность; начальная жесткость; метод конечных элементов; несовершенства

Abstract. Generally, numerical simulations of structures are carried out in such a way as to most accurately repeat their real behavior. The current rules for finite element modeling of tubular joints oblige scientists and engineers to construct their numerical models considering initial imperfections. However, not all joints are sensitive to initial imperfections. Often consideration of initial imperfections brings no reasonable improvements in the accuracy of results, but severely complicates numerical simulations. In such cases, the effect of geometrical imperfections can be effectively replaced by a simple theoretical equation or neglected entirely. This paper evaluates the effect of initial geometrical imperfections on the structural behavior of cold-formed rectangular hollow section T joints. Imperfections are simulated using the conventional approach for thin-walled structures, applying corresponding buckling modes to the perfect geometry. The paper analyzes several buckling modes and their combinations to identify the most rational technique for simulation of imperfections under in-plane bending and axial loading. Based on the obtained results, parametric studies are conducted to investigate the effect of initial imperfections on joints with various geometry and material properties. The results demonstrate that initial imperfections reduce the resistance and initial stiffness of joints. However, the observed effect has been found sufficiently small to be safely ignored in computational analyses.

Аннотация. Как правило, конечно-элементный анализ строительных конструкций проводится таким образом, чтобы максимально точно повторить их реальную работу. Современные требования к конечно-элементному анализу трубных узлов обязывают ученых и инженеров учитывать влияние начальных несовершенств. Однако, как показывает практика, не все узлы чувствительны к начальным несовершенствам. Часто учет несовершенств не позволяет получить более точные результаты, однако серьезно усложняет расчет конструкций. В таких случаях влияние несовершенств может быть учтено простой аналитической формулой или не учитываться вообще. Данная статья исследует влияние начальных геометрических несовершенств на несущую способность Т-образных узлов из труб прямоугольного сечения. Несовершенства моделируются при помощи традиционного для тонкостенных конструкций метода, когда соответствующая форма потери устойчивости узла прикладывается к его идеальной геометрии. Чтобы определить наиболее целесообразный подход к моделированию несовершенств для изгиба в плоскости узла и продольного сжатия, статья анализирует несколько форм потери устойчивости, а также их возможные комбинации. На основании полученных данных статья проводит параметрические исследования, чтобы определить влияние несовершенств на работу узлов с различной геометрией и свойствами стали. Результаты показали, что начальные несовершенства уменьшают несущую способность трубных узлов. Однако наблюдаемый

Гарифуллин М.Р., Бронзова М.К., Хейнисуо М., Мэла К., Паюнен С. Сварные узлы холодногнутых труб прямоугольного сечения с начальными несовершенствами. 2018. № 4(80). С. 81–94.

негативный эффект достаточно мал и позволяет проводить расчет конструкций без учета влияния геометрических несовершенств.

1. Introduction

To provide most reliable results, numerical simulations are carried out in such a way as to most accurately repeat the real behavior of structures. Generally, the finite element analysis of tubular joints incorporates nonlinear large deflection theory for displacements, a nonlinear elastic-plastic material law as well as initial imperfections [1]. Initial imperfections include the deviations of geometry, imperfections in boundary conditions and residual stresses. Cold-formed tubular welded joints are generally influenced by initial geometrical imperfections, welding residual stresses and the residual stresses that occur from the cold-forming process.

The influence of welding residual stresses on structural behavior of rectangular hollow section joints was investigated in [2, 3] and was found negligible. Residual stresses in tubular joints obtained from cold-forming process were studied in [4–6]. However, very limited research is dedicated to studying initial geometrical imperfections in tubular joints. Most of the current papers conduct finite element analyses ignoring deviations in geometry of tubular members [7–10]. Although such an approach can be fully justified for members with very thick walls, it is not clear, whether or not the same can be assumed for tubes with relatively thin walls. These joints may behave similarly to thin-walled structures, which demonstrate considerable reduction of resistance due to imperfections in geometry [11, 12]. Moreover, the effect of initial imperfections might differ for the joints made of high strength steels, which are known to be particularly sensitive to any uncertainties. If the influence of initial imperfections is considerable, ignoring them in the design of tubular joints can lead to the overestimation of their load-bearing capacity, leading thus to unsafe results.

This paper investigates numerically the effect of initial geometrical imperfections on the resistance and initial stiffness of rectangular hollow section (RHS) T joints. A T joint represents the simplest joint configuration, when a brace is welded to a chord at an angle of 90°, as shown in Figure 1a. Section 2 develops the finite element (FE) model for RHS T joints and briefly describes its structural behavior under in-plane bending M_{ip} and axial brace loading N. The loading cases are demonstrated in Figure 1b. Initial imperfections are modelled by applying the scaled buckling modes to perfect geometry. Section 3.1 considers various buckling modes and their combinations by comparing the structural behavior of perfect and imperfect FE models. Finally, Section 3.2 provides parametric studies of RHS T joints with varying geometry and steel grades. The paper investigates only butt-welded joints, with no welding imperfections considered.

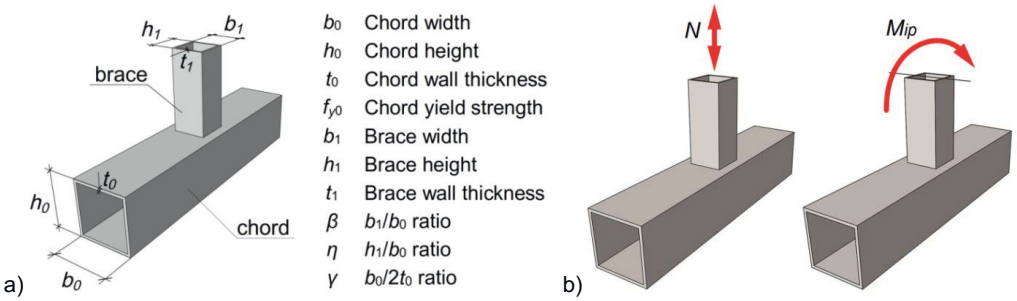

Figure 1. RHS T joint: a) notations; b) loading cases

2. Methods

2.1. Development of FE model

The FE model for RHS T joints under in-plane bending was developed in [13]. This paper conducts numerical analyses employing the FE package Abaqus/Standard [14]. Cold-formed sections were modeled with round corners, according to EN 10219-2:2006 [15]. Residual stresses due to cold-forming were not considered. To exclude the possible effects of chord boundary conditions, its length was selected as $6b_0$, as recommended in [16], while the brace length was chosen as $4b_1$, as shown in Figure 2a. The wall thickness of the brace t_1 was chosen so that it did not exceed the thickness of the chord t_0. Following the recommendations of [17], the sections were modelled using solid quadratic finite

elements with reduced integration (C3D20R), with two elements in the thickness direction. To capture large stress gradients, the mesh was refined near the connection area.

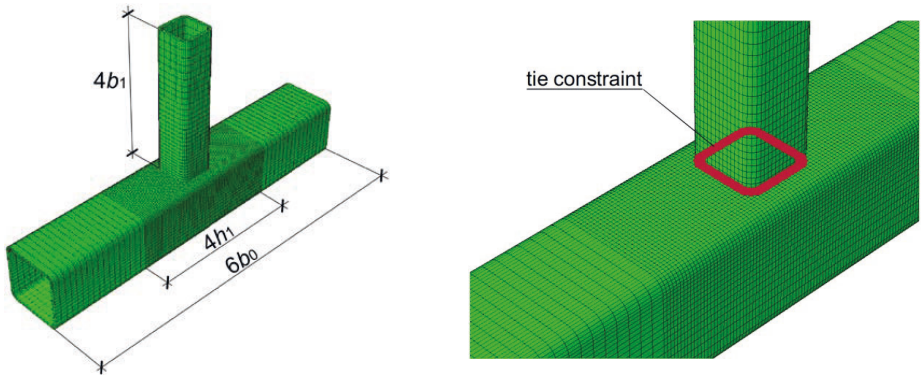

Figure 2. FE model: a) meshing; b) welds modeling

The joints were modelled with butt welds, considering them as the continuation of the brace parent material. The connection was simulated using the tie constraint [14], which ties two separate surfaces together with no relative motion between, as shown in Figure 2b. This approach allows using individual meshes for the connected members with no direct matching of their nodes [18]. All calculations employed the elastic-plastic material model with linear strain hardening according to EN 1993-1-5:2006 [19], with the Young's modulus of E = 210 GPa and the Poisson's ratio of v = 0.3, as shown in Figure 3a.

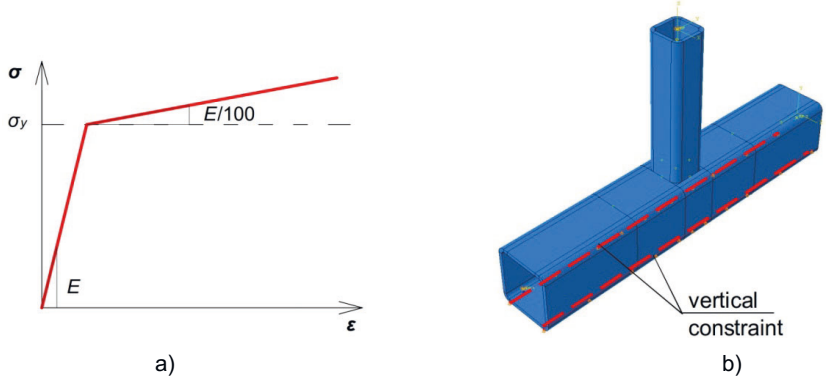

Figure 3. a) Material model; b) boundary conditions to prevent bending of the chord

Loading was performed using a force-controlled nonlinear static analysis. The load was applied to the end of the brace by a concentrated in-plane moment M or an axial force N. In case of axial brace loading, the axial force N causes in-plane bending of the chord, producing additional normal stresses on its faces. These stresses affect the structural behavior of tubular joints, reducing their resistance and initial stiffness [20]. To eliminate this effect, the bottom flange of the chord was restrained along the whole length against vertical displacements, as shown in Figure 3b.

2.2. Modeling imperfections

Currently, there are two main approaches for the implementation of geometrical imperfections to the perfect model. The first method represents measuring the real imperfections of members using non-contact 3D deformation scanners [21, 22]. The measured imperfections are then added to the FE model. Such a method provides a very realistic distribution of imperfections along the surface of members but is very time-consuming and is not widely used due to the high price of the measuring equipment.

The second approach is described in Appendix C.5 of EN 1993-1-5:2006 [19] and it represents the simulation of equivalent imperfections. On the first step, a linear buckling analysis is performed. The

obtained buckling modes are then scaled and implemented to a model with perfect geometry. The direction of the applied imperfections should be such that the lowest resistance is obtained. Although the resulting distribution of imperfections in this case represents a rather simplified pattern, this straightforward method is widely used, particularly for thin-walled structures [23, 24]. This approach is employed in the present study in all FE analyses. According to EN 1993-1-8:2005 [25], the most typical failure modes for RHS T joints are chord face bending for $\beta \leq 0.85$ and chord side walls failure for $0.85 < \beta \leq 1.0$. This means that local deformations in RHS T joints are generally located in the chord. Therefore, this paper considers geometrical imperfections only in relation to the chord member.

When imperfections are applied based on a linear buckling analysis, attention should be paid on two issues. The first one concerns the shape and the amplitude of imperfections. To apply imperfections in the most unfavorable way, their shape should possibly repeat the deformation pattern of the joint under the corresponding load. Figure 4a shows the typical deformation pattern of the RHS T joint under an axial brace loading. In this case, imperfections can be applied as the concavity of the chord top face x_1 and the convexity of its web x_2. The deformation of the RHS T joint under in-plane bending can be considered as a combination of a compressed and a tensile part. In this case, geometrical imperfections can be applied similarly using the corresponding buckling modes.

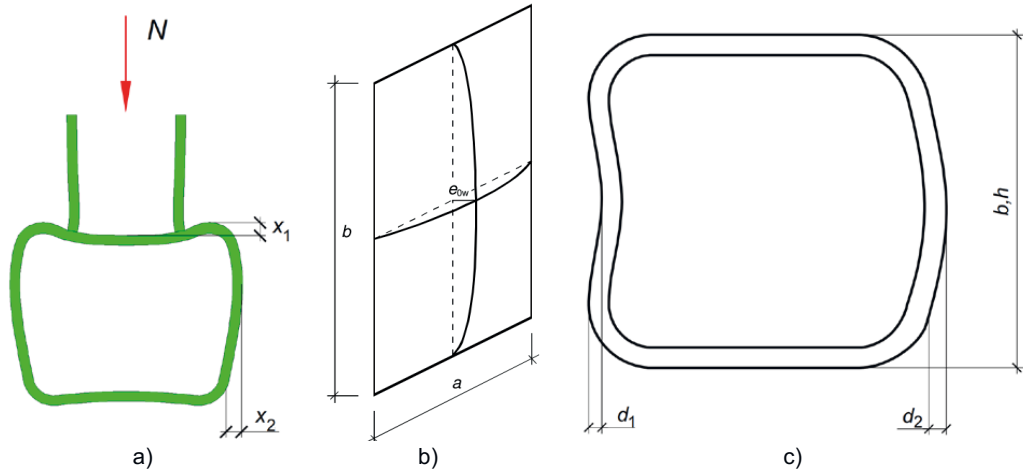

Figure 4. a) Deformation shape of RHS T joint under axial brace loading; b) limitations provided in EN 1993-1-5:2006 [19]; c) limitations provided in EN 10219-2:2006

According to [4], maximum measured imperfections can be conservatively used to predict lower bound strength in the FE analysis. The required magnitudes of imperfections can be found in Eurocode. Appendix C.5 of EN 1993-1-5:2006 [19] specifies local imperfections equal to $e_w = a/200$ or $b/200$, as shown in Figure 4b. In relation to a RHS chord, these values respectively correspond to $b_0/200$ and $h_0/200$. The same amplitudes are used in many publications [26, 27]. Another value can be found in EN 10219-2:2006 [15], which limits the concavity and convexity of cold-formed RHS tubes by 0.8 % with a minimum of 0.5 mm, see d_1 and d_2 in Figure 4c. This corresponds to the values of $b_0/125$ and $h_0/125$. The same limit can be found in [28]. Experimental measurements of the imperfections on hollow sections [5, 29, 30] demonstrate that real imperfections generally do not exceed these amplitudes. This paper employs the values of $b_0/125$ and $h_0/125$, as the most conservative limitations.

The second issue of this approach relates to the combination rules for buckling modes, i.e. the number of buckling modes to be applied and their corresponding scaling factors. Generally, the deformation pattern of the joint is governed by the first buckling mode [4]. However, if the difference between the first and subsequent eigenvalues is small, some subsequent buckling modes can also contribute to the overall deformation. To take into account several buckling modes, a combination rule for their imperfections should be considered. Appendix C of EN 1993-1-5:2006 [19] states that any buckling mode can be taken as the leading imperfection, and the accompanying modes may have their values reduced to 70 %. This leads to the following combination rule:

$$e_0 = e_1 + 0.7\left(e_2 + e_3 + ... + e_n\right), \quad (1)$$

where e_0 is the total amplitude, e_n is the amplitude from buckling mode n, n is the amount of considered buckling modes. It should be noted that the summation should be conducted very thoroughly, paying attention to the shape of buckling modes. Eq. (1) considers the amplitudes at some particular point of interest. This paper considers the imperfections of the chord; therefore, Eq. (1) regulates the convexity of the chord side walls, denoted as x_2 in Figure 4a. Therefore, it should include only those modes that have the maximum (or at least considerable) deformation in the chord side walls. The direction of imperfections is also important: if negative buckling modes are included Eq. (1), they have to be multiplied by negative scaling factors to be applied in the proper direction.

2.3. Structural behavior of RHS T joints

The local beam model for semi-rigid tubular T joints has been developed in [31]. The models under in-plane bending moment and axial brace loading are depicted in Figure 5, where $S_{j,ini}$ and $C_{j,ini}$ denote initial rotational and axial stiffnesses, which are modelled by rotational and linear springs, respectively. It should be noted that the springs are located at the upper flange of the chord and they are connected to the chord axis by a rigid beam.

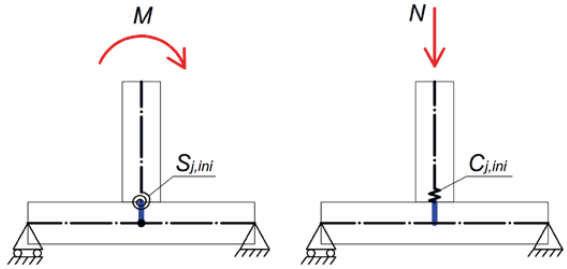

Figure 5. Design local models for RHS T joint: a) in-plane bending; b) axial brace loading

Generally, displacements and rotations measured in a FE analysis reflect the global behavior of the joint, including deformations of the chord and the brace, as well as the local deformations of the joint. The latter represents the deformations at the connection area, where the brace and the chord meet. In particular, to obtain the local rotation of the joint φ in case of in-plane bending, the rotation of the brace φ_{br} and the rotation of the chord φ_{ch} are subtracted from the measured rotation in the end of the brace φ_{tot} (Figure 6):

$$\varphi = \varphi_{tot} - \varphi_{br} - \varphi_{ch} \quad (2)$$

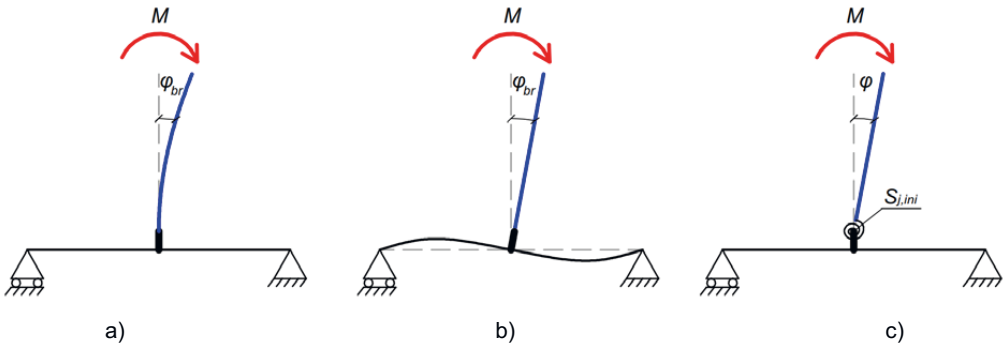

Figure 6. Behavior under in-plane bending: a) elastic rotation of the brace; b) elastic rotation of the chord; c) local rotation of the joint

To obtain local displacements in case of axial loading, the displacement in the end of the brace δ_{tot} is reduced by the brace shortening δ_{sh}:

$$\delta = \delta_{tot} - \delta_{sh} . \quad (3)$$

The motions of the members are supposed to be elastic (assuming that plastic deformations occur only in the connection area); therefore, the values φ_{br}, $\varphi_{ch,}$ and δ_{sh} are calculated manually using the well-known beam equations from strength of materials:

$$\varphi_{br} = \frac{Ml_1}{EI_1}; \quad \varphi_{ch} = \frac{Ml_0}{12EI_0}; \quad \delta_{sh} = \frac{Nl_1}{EA_1} \quad (4)$$

where l_0 and l_1 are respectively the lengths of the chord and the brace, I_0 and I_1 are respectively the second moments of area of the chord and the brace, A_1 is the cross-sectional area of the brace, E is the Young's modulus.

The structural behavior of tubular joints demonstrates certain similarities in case of in-plane bending and axial brace loading and it is best described by corresponding load-deformation curves. The initial stiffness and resistance of joints are found graphically, using a manual curve-fitting approach. To evaluate the deformation capacity of joints, the 3%b_0 deformation limit is calculated in accordance with [32]. Following this rule, for a joint loaded by an axial brace force, the deformation limit δ_{lim} is found as

$$\delta_{\lim} = 0.03b_0 \quad (5)$$

Similarly, for a joint loaded by an in-plane moment the deformation limit $\varphi_{\lim}$ is

$$\varphi_{\lim} = \frac{0.03b_0}{h_1/2} = \frac{0.06}{\eta} \quad (6)$$

Initial stiffness $S_{j,ini}$ ($C_{j,ini}$) is found as the tangent line in the elastic phase of the curve, as shown in Figure 7. The resistance of joints is determined depending on their brace-to-chord width ratio β [33]. For the joints with $\beta \le 0.85$, bending of the chord top face governs the deformation of the whole joint, and the load-deformation curve has a clearly observed hardening phase, as shown in Figure 7. In this case, plastic resistance M_{pl} (N_{pl}) is determined as the intersection of two tangent lines corresponding to initial stiffness $S_{j,ini}$ ($C_{j,ini}$) and hardening stiffness $S_{j,h}$ ($C_{j,h}$), as demonstrated in [34]. Ultimate resistance M_u (N_u) in this case usually corresponds to very large deformations, considerably exceeding the deformation limit; therefore, it is not considered in this paper.

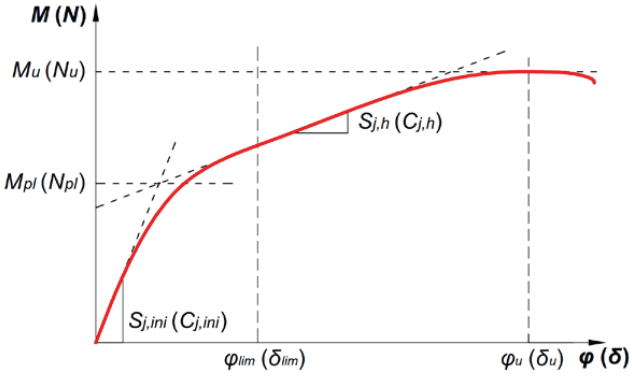

Figure 7. Load-deformation curve for T joint with $\beta \le 0.85$

The behavior of joints with $0.85 < \beta \le 1.0$ is generally governed by chord side walls buckling. Instead of a well-developed hardening phase, the action-deformation curves of such joints have a clear peak load M_{max} (N_{max}). The resistance of such joints depends on the correlation between this peak load and the 3%b_0 deformation limit [35]. If a joint has a peak load M_{max} (N_{max}) at a deformation smaller than φ_{lim} (δ_{lim}), the peak load is considered to be the resistance of the joint, as shown in Figure 8a. If a joint has a peak load M_{max} (N_{max}) at a deformation larger than φ_{lim} (δ_{lim}), resistance is determined as equal to the load at the deformation limit, as shown in Figure 8b.

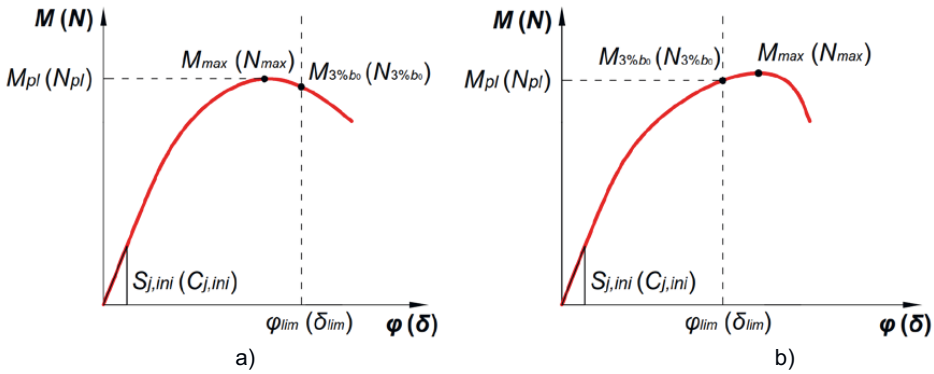

Figure 8. Load-deformation curves for T joint with 0.85 < β ≤ 1.0

3. Results and Discussion

3.1. Influence of initial imperfections on structural behavior of joints

This section investigates the effect of initial geometric imperfections on the structural behavior of RHS T joints under two loading cases: an axial load and an in-plane bending moment. Attention is paid particularly on the buckling modes and their possible combinations that can be used to the proper modeling of imperfections. All analyses were conducted on a single joint with a 100 x 100 x 6 mm chord and a 60 x 60 x 6 mm brace (β = 0.6), made of S355 steel grade.

On the first step, a linear buckling analysis was conducted for the case of in-plane bending and axial brace loading to obtain desired buckling modes. Figure 9 presents the first 10 buckling modes for the case of in-plane bending. As can be seen, Modes 3–10 represent local buckling of the brace and they cannot be applied to simulate chord imperfections. Modes 1 and 2 most closely correspond to the deformation pattern under the moment loading; however, major displacements are observed in the end of the brace, but not in the chord web. For this reason, buckling modes obtained from in-plane bending were found inapplicable for the simulation of imperfections for the considered joint.

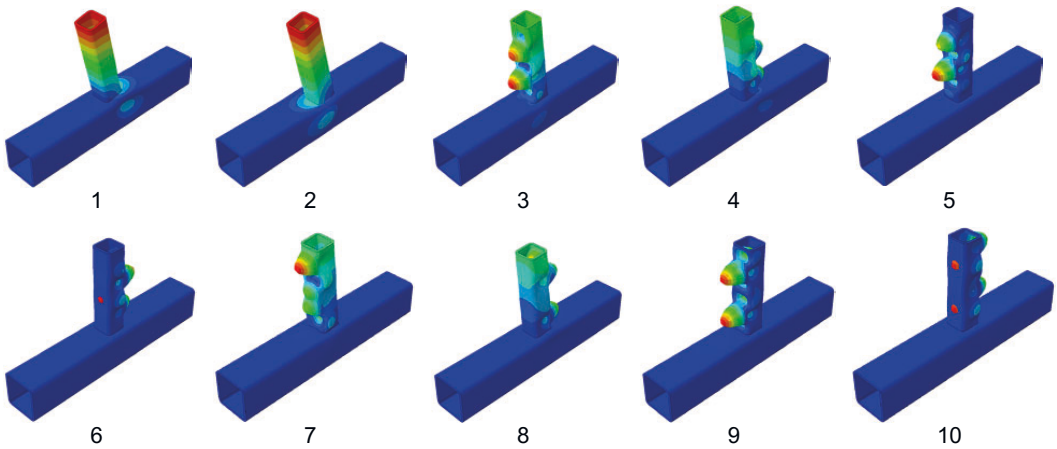

Figure 9. Buckling modes, in-plane bending

The buckling modes for axial loading are provided in Figure 10. A negative Mode 1 represents a buckling mode closest to the real deformation pattern of the joint under an axial load (compare with Figure 4a). Modes 4 and 9 correspond to the lateral buckling of the chord and cannot be used to simulate local imperfections of the cross-section. Modes 5 and 10 are located in the brace. Modes 7 and 8 are similar to Modes 1 and 6, respectively. Mode 3 represents the buckling of the chord side walls in opposite

direction, i.e. inwards the tube. Based on these observations, Modes 1, 2 and 6 were selected as the most reliable for the simulation of imperfections, both in the case of in-plane bending and axial loading.

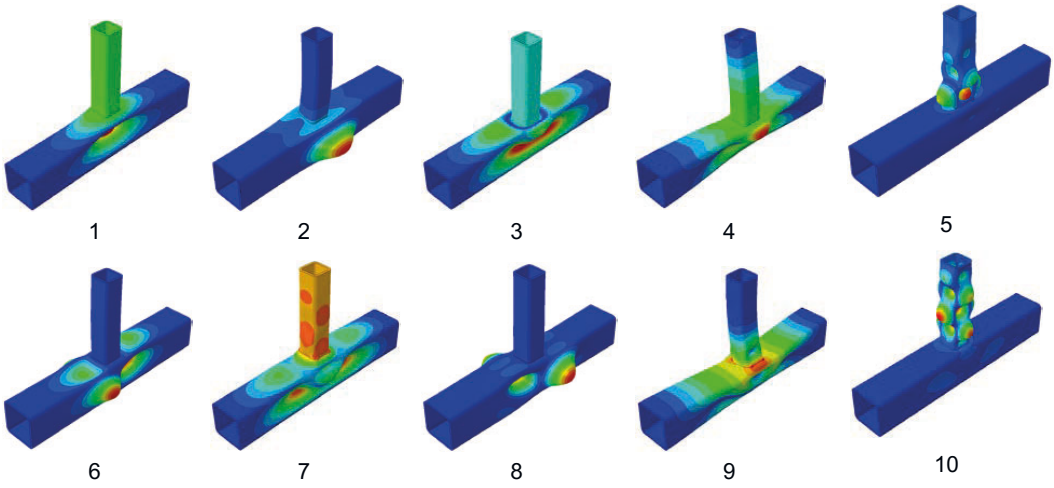

Figure 10. Buckling modes, axial loading

On the second step, a nonlinear static analysis was conducted for the joint separately under in-plane bending and axial loading. The analyses were conducted with and without imperfections. Imperfections were simulated using Modes 1, 2 and 6 for both loading cases. Each buckling mode was first applied independently and then in a combination with others. The combination was introduced according to Eq. (1), employing the following equation:

$$e_0 = e_1 + 0.7e_2 + 0.7e_6 \tag{7}$$

The scaling factors for the buckling modes were selected such that the total convexity on the web e_0 was equal to the assumed limitation of $h_0/125$ = 0.8 mm. Being negative, Mode 1 was applied in the opposite direction. The outcome of the numerical analyses included the plastic resistance and initial stiffness of the analyzed joints. The results are presented in Table 1, where "Imperfect-N" relates to the model with imperfections obtained from a buckling mode *N*. "Imperfect-C" corresponds to the model with imperfections obtained from the combination of buckling modes, Eq. (7). The results are presented in absolute values and in relation to "Perfect" model.

Table 1. Structural behavior of joints with various imperfections

	M_{pl} [kNm]		$S_{j,ini}$ [kNm/rad]		N_{pl} [kN]		$C_{j,ini}$ [kN/mm]	
Perfect	3.15	1	262.0	1	121.9	1	219.9	1
Imperfect-1	3.12	0.99	256.9	0.98	120.1	0.98	210.4	0.96
Imperfect-2	3.15	1.00	262.0	1.00	121.9	1.00	220.0	1.00
Imperfect-6	3.15	1.00	262.1	1.00	122.9	1.01	220.0	1.00
Imperfect-C	3.13	1.00	259.0	0.99	120.8	0.99	214.3	0.97

As can be seen, the influence of initial geometric imperfections on the structural behavior is negligibly small. The reduction of resistance does not exceed 1 % for moment load and 2 % for axial load. For initial stiffness, the values account for 2 % and 4 % respectively. For both loading cases, the most conservative results are observed employing buckling Mode 1, i.e. the mode that as close as possible corresponds to the deformation pattern of the joint under an axial brace loading. This buckling mode can be considered further as the bounding buckling mode. Although in this section it corresponded to the first computed buckling mode, its number can be different for other joints.

3.2. Parametric studies for joints with various geometry and steel grades

This section evaluates the effect of geometric imperfections on the structural behavior of RHS T joints with varying geometries and steel grades. The variations of geometry are considered in relation to chord wall thickness and the width of the brace. As in Section 3.1, firstly a linear buckling analysis was

conducted for every joint, followed by a nonlinear static analysis. Initial imperfections were simulated using the bounding buckling mode that maximally repeats the deformation of the joint under an axial load. The results are evaluated in relation to resistance and initial stiffness, separately under moment and axial loading.

3.2.1. Joints with various steel grade

Consider firstly the effect of steel grade on the behavior of the joint. The analyses were conducted on the same joint as was used in Section 3.1. In addition to S355, the study considered steel grades S500 and S700, employing similar bi-linear material models. The results are presented in Figure 11 and Table 2, where indices *p* and *i* relate to perfect and imperfect models, respectively. As can be seen, the small influence of initial imperfections remains also for higher steel grades. Similarly, imperfections reduce plastic moment and axial resistance by 1 % and 2 % respectively. Initial rotational and axial stiffness is reduced by 2 % and 4 % respectively.

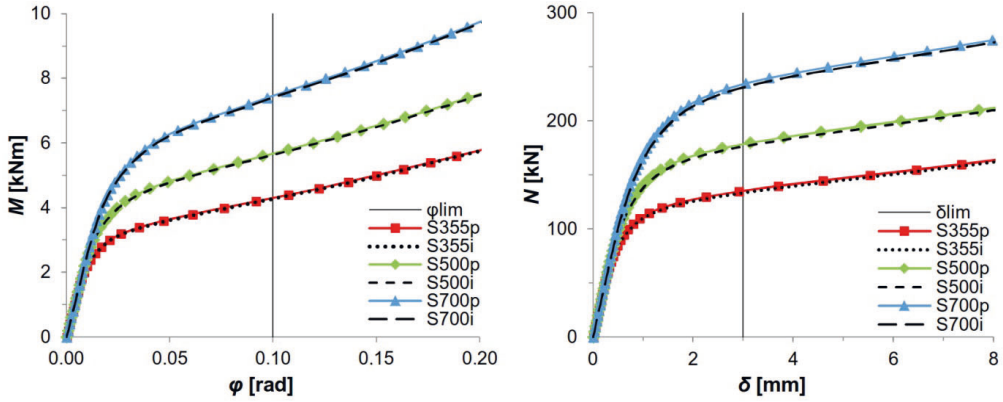

Figure 11. Influence of initial imperfections on joints with various steel grades

Table 2. Influence of initial imperfections for joints with various steel grades

Steel grade	S355p	S355i	S355i/ S355p	S500p	S500i	S500i/ S500p	S700p	S700i	S700i/ S700p
M_{pl} [kNm]	3.15	3.12	0.99	4.26	4.23	0.99	5.73	5.69	0.99
$S_{j,ini}$ [kNm/rad]	262.0	256.9	0.98	262.0	256.9	0.98	262.0	256.9	0.98
N_{pl} [kN]	121.9	120.1	0.98	165.4	162.6	0.98	221.7	218.2	0.98
$C_{j,ini}$ [kN/mm]	219.9	210.4	0.96	219.9	210.4	0.96	219.9	210.4	0.96

3.2.2. Joints with various chord wall thickness

The next parametric study investigates the effect of initial geometric imperfections on the behavior of joints with varying chord wall thickness. Generally, this thickness is characterized by the chord width-to-thickness ratio $\gamma = b_0/2t_0$, which for simplicity is often considered as $2\gamma = b_0/t_0$. Chapter 7 of EN 1993-1-8:2005 [25] limits 2γ in the range of $10 \le 2\gamma \le 35$. Initial geometrical imperfections are known to considerably reduce the resistance of thin-walled members [4]. For this reason, a more pronounced effect can be expected for the joints with 2γ close to its upper limit.

Section 3.1 evaluated the joint with $2\gamma = 100/6 = 16.6$, which is close to the lower bound of γ. In the following, two additional chord thicknesses are considered: $2\gamma = 25.0$ ($t_0 = 4$ mm) and $2\gamma = 33.3$ ($t_0 = 3$ mm). The thickness of the brace was selected as equal to the thickness of the chord. The results are presented graphically in Figure 12 and collected in Table 3, where indices *p* and *i* relate to perfect and imperfect models, respectively. As can be seen, the effect of initial imperfections is more pronounced for joints with thinner walls, reducing their moment and axial resistance by 3 % for $2\gamma = 33.3$. A more pronounced infunence is observed for initial stiffness: rotational stiffness is reduced by 4 %, while axial stiffness is reduced by 6 %.

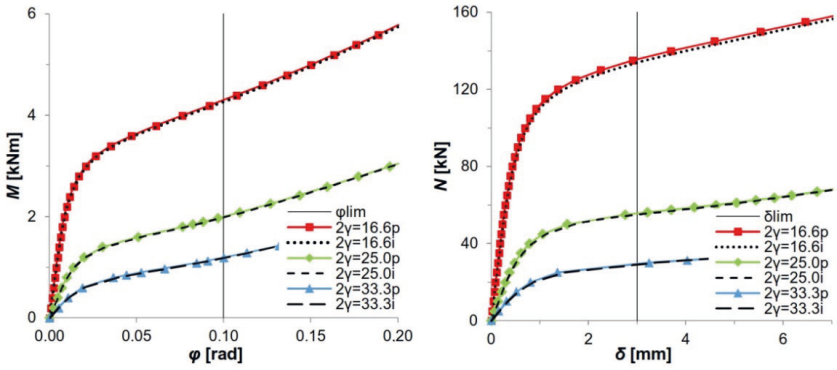

Figure 12. Influence of initial imperfections on joints with various chord wall thickness

Table 3. Influence of initial imperfections for joints with various chord wall thickness

2γ	16.6p	16.6i	16.6i/ 16.6p	25.0p	25.0i	25.0i/ 25.0p	33.3p	33.3i	33.3i/ 33.3p
M_{pl} [kNm]	3.15	3.12	0.99	1.29	1.27	0.98	0.67	0.65	0.97
$S_{j,ini}$ [kNm/rad]	262.0	256.9	0.98	86.4	84.1	0.97	39.6	38.1	0.96
N_{pl} [kN]	121.9	120.1	0.98	48.8	47.9	0.98	25.0	24.3	0.97
$C_{j,ini}$ [kN/mm]	219.9	210.4	0.96	70.9	67.6	0.95	31.9	30.1	0.94

3.3. Joints with various brace width

The third and the last parametric study evaluates the influence of initial imperfections of joints with different brace widths. Generally, the brace width is represented by the brace-to-chord width ratio β. EN 1993-1-8:2005 [25] limits β for RHS T joints in the range of $0.25 \le \beta \le 1.0$. All previous analyses considered the joints with $\beta = 0.6$ and demonstrated a negligibly small effect of initial imperfections. Although this finding can be justified for the joints that fail from chord face bending, the results can differ for the joints with other failure modes, e.g. chord side walls buckling, which is critical when $0.85 < \beta \le 1.0$.

Consider the structural behavior of equal-width joints ($\beta = 1.0$). The analyses were conducted for a joint with a 100x100 chord and a 100x100 brace, made of S355, with three chord wall thicknesses: $2\gamma = 16.6$ ($t_0 = 6$ mm), $2\gamma = 25.0$ ($t_0 = 4$ mm) and $2\gamma = 33.3$ ($t_0 = 3$ mm). The wall thickness of the brace was selected as equal to the wall thickness of the chord. The resistance of the joints was determined according to Figure 8. The structural behavior of the joints is illustrated in Figure 13 and summarized in Table 4, where indices *p* and *i* relate to perfect and imperfect models, respectively. As can be seen, the negative influence of initial imperfections observed for joints with $\beta = 0.6$ remains also for equal-width joints. Similarly, the effect is more pronounced for the joints with thinner walls, reducing their moment and axial resistance by 2% and 5% respectively for $2\gamma = 33.3$. In relation to initial stiffness, the reducing effect does not exceed 7%. It should be noted that the effect is more pronounced for axial loading than for in-plane bending.

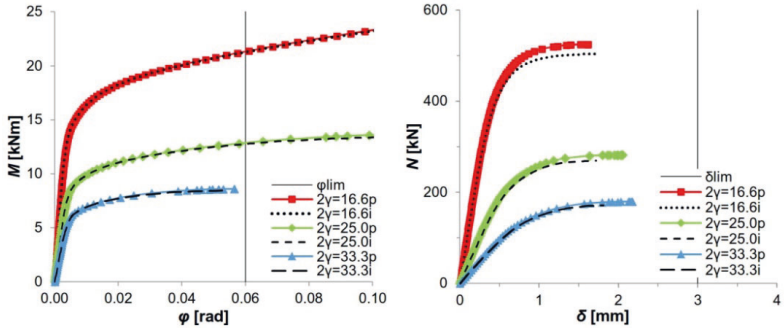

Figure 13. Influence of initial imperfections on joints with $\beta = 1.0$

Garifullin M., Bronzova M., Heinisuo M., Mela K., Pajunen S., Cold-formed RHS T joints with initial geometrical imperfections. *Magazine of Civil Engineering*. 2018. No. 4(80). Pp. 81–94. doi:10.18720/MCE.80.8

Table 4. Influence of initial imperfections on joints with β = 1.0

2γ	16.6p	16.6i	16.6i/ 16.6p	25.0p	25.0i	25.0i/ 25.0p	33.3p	33.3i	33.3i/ 33.3p
M_{pl} [kNm]	21.34	21.29	1.00	12.85	12.77	0.99	8.61	8.44	0.98
$S_{j,ini}$ [kNm/rad]	4281	4237	0.99	2332	2295	0.98	1578	1538	0.97
N_{pl} [kN]	525.3	503.7	0.96	282.0	269.3	0.95	179.9	171.2	0.95
$C_{j,ini}$ [kN/mm]	1181	1102	0.93	429	403	0.94	213	201	0.94

3.4. Discussion

In this paper, geometrical imperfections were modelled applying scaled buckling modes to the perfect geometry. Buckling modes were obtained from linear buckling analyses for the corresponding loading type. The comparative buckling analyses under axial loading have showed that the first buckling mode most closely corresponds to the deformation pattern of T joints, being thus the most desirable for the simulation of initial imperfections. The consideration of higher buckling modes as well as their possible combinations brought no noticeable changes in further results and therefore was found unnecessary. At the same time, all buckling modes resulted from in-plane bending loading were located in the brace and therefore could not be employed to simulate local deformations of the chord walls. For this reason, imperfections for both loading cases were modelled using the first buckling mode obtained from axial loading. This resulted to the fact that the observed influence of imperfections was less pronounced for in-plane bending than for axial loading. In all cases studied in this paper, the first buckling mode was negative and was multiplied by a negative scaling factor to be applied in the proper direction.

The conducted parametric studies have demonstrated a small negative influence of initial imperfections on both design resistance and initial stiffness of the investigated joints. The effect was observed for the joints governed by chord face bending ($\beta \le 0.85$) as well as the joints with chord side walls buckling as the dominating failure mode ($\beta > 0.85$). The structural properties were found to decrease for the joints with thinner walls, particularly those with 2γ ratio close to its upper limit specified by the Eurocode ($2\gamma = 35$). For the joints beyond this limit ($2\gamma > 35$), the effect is expected to be more pronounced, making these joints behave similar to thin-walled sections. At the same time, the negative effect of imperfections showed no correlation with steel grade in the considered range from S355 to S700.

The maximum observed reduction of resistance accounted 3 % and 5 % for in-plane bending moment and axial loading respectively. In practice, these reductions are taken into account by partial safety factors and thus do not have to be considered in theoretical calculations. At the same time, initial imperfections reduce initial rotational stiffness by 4 % and initial axial stiffness by 7 %. Since the accuracy requirements for initial stiffness are not as strict as for resistance, these small reductions of stiffness are acceptable and can be ignored in the design. It should be noted that in this paper imperfections were modelled rather conservatively, using the maximum allowed value of $h_0/125$. The experimental measurements of on RHS tubes [5, 29, 30] demonstrate that real imperfections are generally smaller than this amplitude. Moreover, imperfections were applied in the most unfavorable way, i.e. providing the most unsafe behavior. In real members, the distribution of imperfections is more random. These findings allow to conclude that initial geometrical imperfections do not seriously affect the structural behavior of RHS T joints in the range defined by the regulations of the Eurocode.

4. Conclusions

This paper analyzed the effect of initial geometric imperfections on the structural behavior of tubular joints. In this study, initial geometrical imperfections were simulated using the conventional approach for thin-walled sections, applying corresponding buckling modes scaled in accordance with allowable fabrication tolerances. The comparative FE analyses for RHS joints with perfect and imperfect geometry have showed that the effect of initial geometric imperfections on the strength of joints is smaller than that observed for thin-walled cold-formed structures. For this reason, geometrical imperfections can be neglected in the design of RHS T joints with no serious consequences on their design results.

The presented results can serve as a starting point for studying the issue of initial imperfections in relation to welded tubular joints. This paper considered the joints that follow the requirements of Eurocode, i.e. $0.25 \le \beta \le 1.0$, $10 \le 2\gamma \le 35$, steel grades from S355 to S700, under in-plane bending and axial loading. For joints with $\beta \le 0.85$, chord face bending governs the deformation of the joint under all loading cases; therefore, the obtained conclusions can be extended also for the case of out-of-plane bending. Some comparative numerical analyses can be conducted to eliminate a possible scaling effect,

considering joints with different sections of the chord. Moreover, some calculations can be useful to extend the conclusions for other welded connections, including K and X joints, as well as circular hollow section joints. In addition, particularly important results can be obtained considering geometrical imperfections in welds, i.e., the deviations of fillet welds from their nominal dimensions.

References

1. *European Committee for Standardization (CEN). Eurocode 3.* Design of steel structures. Part 1-6: Strength and Stability of Shell Structures (EN 1993-1-6:2007). Brussels, 2007.
2. Brar G.S., Singh C.S. FEA of residual stress in cruciform welded joint of hollow sectional tubes. *Journal of Constructional Steel Research.* 2014. Vol. 102. Pp. 44–58.
3. Moradi Eshkafti M. *Influence of various welding sequence schemes on the load bearing capacity of square hollow section T-joint.* PhD thesis. Cottbus: Brandenburg University of Technology, 2017.
4. Dubina D., Ungureanu V., Landolfo R. *Design of Cold-formed Steel Structures: Eurocode 3: Design of Steel Structures, Part 1-3: Design of Cold-formed Steel Structures* . ECCS, 2012.
5. Jiao H., Zhao X.-L. Imperfection, residual stress and yield slenderness limit of very high strength (VHS) circular steel tubes. *Journal of Constructional Steel Research.* 2003. Vol. 59. No. 2. Pp. 233–249.
6. Feldmann M., Schillo N., Schaffrath S., Virdi K., Björk T., Tuominen N., Veljkovic M., Pavlovic M., Manoleas P., Heinisuo M., Mela K., Ongelin P., Valkonen I., Minkkinen J., Erkkilä J., Pétursson E., Clarin M., Seyr A., Horváth L., Kövesdi B., Turán P., Somodi B. *Rules on high strength steel.* Luxembourg: Publications Office of the European Union, 2016.
7. Pavlenko A.D., Rybakov V.A., Pikht A.V., Mikhailov E.S. Non-uniform torsion of thin-walled open-section multi-span beams. *Magazine of Civil Engineering.* 2016. Vol. 67, No. 7. Pp. 55–69.
8. de Matos R.M.M.P., Costa-Neves L.F., de Lima L.R.O., Vellasco P.C.G.S., da Silva J.G.S. Resistance and elastic stiffness of RHS "T" joints: Part I - Axial brace loading. *Latin American Journal of Solids and Structures.* 2015. Vol. 12. No. 11. Pp. 2159–2179.
9. Christitsas A.D., Pachoumis D.T., Kalfas C.N., Galoussis E.G. FEM analysis of conventional and square bird-beak SHS joint subject to in-plane bending moment — experimental study. *Journal of Constructional Steel Research.* 2007. Vol. 63. No. 10. Pp. 1361–1372.
10. Tusnina O.A., Danilov A.I. The stiffness of rigid joints of beam with hollow section column. *Magazine of Civil Engineering.* 2016. Vol. 64. No. 4. Pp. 40–51.
11. Nazmeeva T.V., Vatin N.I. Numerical investigations of notched C-profile compressed members with initial imperfections. Magazine of Civil Engineering. 2016. Vol. 62. No. 2. Pp. 92–101.
12. Zeinoddini V., Schafer B.W. Global Imperfections And Dimensional Variations In Cold-Formed Steel Members. *International Journal of Structural Stability and Dynamics*. 2011. Vol. 11. No. 5. Pp. 829–854.
13. Garifullin M., Pajunen S., Mela K., Heinisuo M., Havula J. Initial in-plane rotational stiffness of welded RHS T joints with axial force in main member. *Journal of Constructional Steel Research.* 2017. Vol. 139. Pp. 353–362.
14. *Abaqus 6.12.* Getting Started with Abaqus: Interactive Edition . Dassault Systèmes, 695 p., 2012.
15. *European Committee for Standardization (CEN). Cold formed welded structural hollow sections of non-alloy and fine grain steels.* Part 2: Tolerances, dimensions and sectional properties (EN 10219-2:2006). Brussels, 2006.

Литература

1. European Committee for Standardization (CEN). Eurocode 3. Design of steel structures. Part 1-6: Strength and Stability of Shell Structures (EN 1993-1-6:2007). Brussels, 2007.
2. Brar G.S., Singh C.S. FEA of residual stress in cruciform welded joint of hollow sectional tubes // Journal of Constructional Steel Research. 2014. Vol. 102. Pp. 44–58.
3. Moradi Eshkafti M. Influence of various welding sequence schemes on the load bearing capacity of square hollow section T-joint. PhD thesis . Cottbus: Brandenburg University of Technology, 2017.
4. Dubina D., Ungureanu V., Landolfo R. Design of Cold-formed Steel Structures: Eurocode 3: Design of Steel Structures, Part 1-3: Design of Cold-formed Steel Structures . ECCS, 2012.
5. Jiao H., Zhao X.-L. Imperfection, residual stress and yield slenderness limit of very high strength (VHS) circular steel tubes // Journal of Constructional Steel Research. 2003. Vol. 59. № 2. Pp. 233–249.
6. Feldmann M., Schillo N., Schaffrath S., Virdi K., Björk T., Tuominen N., Veljkovic M., Pavlovic M., Manoleas P., Heinisuo M., Mela K., Ongelin P., Valkonen I., Minkkinen J., Erkkilä J., Pétursson E., Clarin M., Seyr A., Horváth L., Kövesdi B., Turán P., Somodi B. Rules on high strength steel. Luxembourg: Publications Office of the European Union, 2016.
7. Павленко А.Д., Рыбаков В.А., Пихт А.В., Михайлов Е.С. Стесненное кручение многопролетных тонкостенных балок открытого профиля // Инженерно-строительный журнал. 2016. № 7(67). С. 55–69
8. de Matos R.M.M.P., Costa-Neves L.F., de Lima L.R.O., Vellasco P.C.G.S., da Silva J.G.S. Resistance and elastic stiffness of RHS "T" joints: Part I - Axial brace loading // Latin American Journal of Solids and Structures. 2015. Vol. 12. № 11. Pp. 2159–2179.
9. Christitsas A.D., Pachoumis D.T., Kalfas C.N., Galoussis E.G. FEM analysis of conventional and square bird-beak SHS joint subject to in-plane bending moment — experimental study // Journal of Constructional Steel Research. 2007. Vol. 63. № 10. Pp. 1361–1372.
10. Туснина О.А., Данилов А.И. Жесткость рамных узлов сопряжения ригеля с колонной коробчатого сечения // Инженерно-строительный журнал. 2016. № 4(64). С. 40–51.
11. Назмеева Т.В., Ватин Н.И. Численные исследования сжатых элементов из холодногнутого просечного С-профиля с учетом начальных несовершенств // Инженерно-строительный журнал. 2016. № 2(62). С. 92–101.
12. Zeinoddini V., Schafer B.W. Global Imperfections And Dimensional Variations In Cold-Formed Steel Members // International Journal of Structural Stability and Dynamics. 2011. Vol. 11. № 5. Pp. 829–854.
13. Garifullin M., Pajunen S., Mela K., Heinisuo M., Havula J. Initial in-plane rotational stiffness of welded RHS T joints with axial force in main member // Journal of Constructional Steel Research. 2017. Vol. 139. Pp. 353–362.
14. Abaqus 6.12. Getting Started with Abaqus: Interactive Edition . Dassault Systèmes, 695 p., 2012.
15. European Committee for Standardization (CEN). Cold formed welded structural hollow sections of non-alloy and fine grain steels. Part 2: Tolerances, dimensions and

16. van der Vegte G.J., Makino Y. Further research on chord length and boundary conditions of CHS T- and X-joints. *Advanced Steel Construction.* 2010. Vol. 6. No. 3. Pp. 879–890.
17. van der Vegte G.J., Wardenier J., Puthli R.S. FE analysis for welded hollow-section joints and bolted joints. *Proceedings of the Institution of Civil Engineers — Structures and Buildings.* 2010. Vol. 163. No. SB6. Pp. 427–437.
18. AlHendi H., Celikag M. Behavior of reverse-channel and double-reverse-channel connections to tubular columns with HSS. *Journal of Constructional Steel Research*. 2015. Vol. 112. Pp. 271–281.
19. *European Committee for Standardization (CEN). Eurocode 3.* Design of steel structures. Part 1-5: Plated structural elements (EN 1993-1-5:2006). Brussels, 2006.
20. Packer J., Puthli R., van der Vegte G.J., Wardenier J. Discussion on the paper “Experimental and numerical assessment of RHS T-joints subjected to brace and chord axial forces”, by Nizer et al., Steel Construction 9 (2016), No. 4, pages 315–322. *Steel Construction.* 2017. Vol. 10. No. 1. Pp. 89–90.
21. Tran A.T., Veljkovic M., Rebelo C., da Silva L.S. Resistance of cold-formed high strength steel circular and polygonal sections - Part 2: Numerical investigations. *Journal of Constructional Steel Research.* 2016. Vol. 125. Pp. 227–238.
22. Zhao X., Tootkaboni M., Schafer B.W. Laser-based cross-section measurement of cold-formed steel members: Model reconstruction and application. *Thin-Walled Structures.* 2017. Vol. 120. Pp. 70–80.
23. Schafer B.W., Peköz T. Computational modeling of cold-formed steel: characterizing geometric imperfections and residual stresses. *Journal of Constructional Steel Research.* 1998. Vol. 47. Pp. 193–210.
24. Rybakov V.A., Al Ali M., Panteleev A.P., Fedotova K.A., Smirnov A. V. Bearing capacity of rafter systems made of steel thin-walled structures in attic roofs. Magazine of Civil Engineering. 2017. Vol. 76. No. 8. Pp. 28–39.
25. *European Committee for Standardization (CEN). Eurocode 3.* Design of steel structures, Part 1–8: Design of joints (EN 1993-1-8:2005). Brussels, 2005.
26. Hoang V.L., Demonceau J.-F., Jaspart J.-P. Resistance of through-plate component in beam-to-column joints with circular hollow columns. *Journal of Constructional Steel Research.* 2014. Vol. 92. Pp. 79–89.
27. Pavlovčič L., Detzel A., Kuhlmann U., Beg D. Shear resistance of longitudinally stiffened panels-Part 1: Tests and numerical analysis of imperfections. *Journal of Constructional Steel Research.* 2007. Vol. 63. Pp. 337–350.
28. Ongelin P., Valkonen I. *SSAB Domex Tube. Structural hollow sections.* EN 1993 - Handbook 2016. SSAB Europe Oy, 2016.
29. Hayeck M., Nseir J., Saloumi E., Boissonnade N. Experimental characterization of steel tubular beam-columns resistance by means of the Overall Interaction Concept. *Thin-Walled Structures*. 2017. Vol. In press.
30. Ellobody E., Young B. Structural performance of cold-formed high strength stainless steel columns. *Journal of Constructional Steel Research.* 2005. Vol. 61. No. 12. Pp. 1631–1649.
31. Garifullin M., Pajunen S., Mela K., Heinisuo M. 3D component method for welded tubular T joints. *Tubular Structures XVI – Proceedings of the 16th International Symposium on Tubular Structures (ISTS 2017).* Melbourne, Australia, 2017 / ed. Heidarpour A., Zhao X.-L. London: Taylor & Francis Group, 2018. Pp. 165–173.
32. Lu L.H., de Winkel G.D., Yu Y., Wardenier J. Deformation

sectional properties (EN 10219-2:2006) . Brussels, 2006.
16. van der Vegte G.J., Makino Y. Further research on chord length and boundary conditions of CHS T- and X-joints // Advanced Steel Construction. 2010. Vol. 6, No. 3. Pp. 879–890.
17. van der Vegte G.J., Wardenier J., Puthli R.S. FE analysis for welded hollow-section joints and bolted joints. Proceedings of the Institution of Civil Engineers — Structures and Buildings. 2010. Vol. 163, No. SB6. Pp. 427–437.
18. AlHendi H., Celikag M. Behavior of reverse-channel and double-reverse-channel connections to tubular columns with HSS. Journal of Constructional Steel Research. 2015. Vol. 112. Pp. 271–281.
19. European Committee for Standardization (CEN). Eurocode 3. Design of steel structures. Part 1-5: Plated structural elements (EN 1993-1-5:2006) . Brussels, 2006.
20. Packer J., Puthli R., van der Vegte G.J., Wardenier J. Discussion on the paper “Experimental and numerical assessment of RHS T-joints subjected to brace and chord axial forces”, by Nizer et al. Steel Construction 9 (2016), No. 4, pages 315–322 // Steel Construction. 2017. Vol. 10, № 1. Pp. 89–90.
21. Tran A.T., Veljkovic M., Rebelo C., da Silva L.S. Resistance of cold-formed high strength steel circular and polygonal sections - Part 2: Numerical investigations // Journal of Constructional Steel Research. 2016. Vol. 125. Pp. 227–238.
22. Zhao X., Tootkaboni M., Schafer B.W. Laser-based cross-section measurement of cold-formed steel members: Model reconstruction and application // Thin-Walled Structures. 2017. Vol. 120. Pp. 70–80.
23. Schafer B.W., Peköz T. Computational modeling of cold-formed steel: characterizing geometric imperfections and residual stresses // Journal of Constructional Steel Research. 1998. Vol. 47. Pp. 193–210.
24. Рыбаков В.А., Ал Али М., Пантелеев А.П., Федотова К.А., Смирнов А.В. Несущая способность стропильных систем из стальных тонкостенных конструкций в чердачных крышах // Инженерно-строительный журнал. 2018. № 8(76). С. 28–39.
25. European Committee for Standardization (CEN). Eurocode 3. Design of steel structures, Part 1–8: Design of joints (EN 1993-1-8:2005) . Brussels, 2005.
26. Hoang V.L., Demonceau J.-F., Jaspart J.-P. Resistance of through-plate component in beam-to-column joints with circular hollow columns // Journal of Constructional Steel Research. 2014. Vol. 92. Pp. 79–89.
27. Pavlovčič L., Detzel A., Kuhlmann U., Beg D. Shear resistance of longitudinally stiffened panels-Part 1: Tests and numerical analysis of imperfections // Journal of Constructional Steel Research. 2007. Vol. 63. Pp. 337–350.
28. Ongelin P., Valkonen I. SSAB Domex Tube. Structural hollow sections. EN 1993 - Handbook 2016 . SSAB Europe Oy, 2016.
29. Hayeck M., Nseir J., Saloumi E., Boissonnade N. Experimental characterization of steel tubular beam-columns resistance by means of the Overall Interaction Concept // Thin-Walled Structures. 2017. Vol. In press.
30. Ellobody E., Young B. Structural performance of cold-formed high strength stainless steel columns // Journal of Constructional Steel Research. 2005. Vol. 61. № 12. Pp. 1631–1649.
31. Garifullin M., Pajunen S., Mela K., Heinisuo M. 3D component method for welded tubular T joints // Tubular Structures XVI – Proceedings of the 16th International Symposium on Tubular Structures (ISTS 2017). Melbourne, Australia, 2017 / ed. Heidarpour A., Zhao X.-L.

Гарифуллин М.Р., Бронзова М.К., Хейнисуо М., Мэла К., Паюнен С. Сварные узлы холодногнутых труб прямоугольного сечения с начальными несовершенствами. 2018. № 4(80). С. 81–94.

limit for the ultimate strength of hollow section joints. *Tubular Structures VI. 6th International Symposium on Tubular Structures.* Melbourne, Australia / ed. Grundy P., Holgate A., Wong B. Rotterdam: Balkema, 1994. Pp. 341–347.

33. Zhao X.-L., Hancock G.J. T-joints in rectangular hollow sections subject to combined actions. *Journal of Structural Engineering.* 1991. Vol. 117. No. 8. Pp. 2258–2277.
34. Grotmann D., Sedlacek G. *Rotational stiffness of welded RHS beam-to-column joints.* Cidect 5BB-8/98 . Aachen: RWTH-Aachen, 1998.
35. Zhao X.-L. Deformation limit and ultimate strength of welded T-joints in cold-formed RHS sections. *Journal of Constructional Steel Research.* 2000. Vol. 53. No. 2. Pp. 149–165.

London: Taylor & Francis Group, 2018. Pp. 165–173.

32. Lu L.H., de Winkel G.D., Yu Y., Wardenier J. Deformation limit for the ultimate strength of hollow section joints // Tubular Structures VI. 6th International Symposium on Tubular Structures. Melbourne, Australia / ed. Grundy P., Holgate A., Wong B. Rotterdam: Balkema, 1994. Pp. 341–347.
33. Zhao X.-L., Hancock G.J. T-joints in rectangular hollow sections subject to combined actions // Journal of Structural Engineering. 1991. Vol. 117. № 8. Pp. 2258–2277.
34. Grotmann D., Sedlacek G. Rotational stiffness of welded RHS beam-to-column joints. Cidect 5BB-8/98 . Aachen: RWTH-Aachen, 1998.
35. Zhao X.-L. Deformation limit and ultimate strength of welded T-joints in cold-formed RHS sections // Journal of Constructional Steel Research. 2000. Vol. 53. № 2. Pp. 149–165.

Marsel Garifullin,
+7(999)034-60-70; marsel.garifullin@tut.fi

Maria Bronzova,
+7(921)330-25-29; bronzochka@mail.ru

Markku Heinisuo,
+358(40)596-58-26; markku.heinisuo@tut.fi

Kristo Mela,
+358(40)849-05-63; kristo.mela@tut.fi

Sami Pajunen,
+358(40)849-05-71; sami.pajunen@tut.fi

Марсель Ринатович Гарифуллин,
+7(999)034-60-70;
эл. почта: marsel.garifullin@tut.fi

Мария Константиновна Бронзова,
+7(921)330-25-29;
эл. почта: bronzochka@mail.ru

Маркку Хейнисуо,
+358(40)596-58-26;
эл. почта: markku.heinisuo@tut.fi

Кристо Мэла,
+358(40)849-05-63; эл. почта: kristo.mela@tut.fi

Сами Паюнен,
+358(40)849-05-71;
эл. почта: sami.pajunen@tut.fi

Garifullin M., Bronzova M., Heinisuo M., Mela K., Pajunen S., Cold-formed RHS T joints with initial geometrical imperfections. *Magazine of Civil Engineering*. 2018. No. 4(80). Pp. 81–94. doi:10.18720/MCE.80.8

VII

SURROGATE MODELING FOR ROTATIONAL STIFFNESS OF WELDED TUBULAR Y-JOINTS

by

Heinisuo M., Garifullin M., Jokinen, T., Tiainen, T. & Mela K., 2016

Connections in Steel Structures VIII: Proceedings of the Eighth International Workshop on Connections in Steel Structures, May 24-26, 2016, Boston, pp. 285-294

VIII

INITIAL AXIAL STIFFNESS OF WELDED RHS T JOINTS

by

Garifullin M., Bronzova M., Pajunen S., Mela K., & Heinisuo M., 2019

Journal of Constructional Steel Research vol. 153, 459-472

Journal of Constructional Steel Research 153 (2019) 459–472

Contents lists available at ScienceDirect

Journal of Constructional Steel Research

Initial axial stiffness of welded RHS T joints

Marsel Garifullin [a,*], Maria Bronzova [b,c], Sami Pajunen [a], Kristo Mela [a], Markku Heinisuo [a]

[a] Tampere University of Technology, Tampere, Finland
[b] Peter the Great St.Petersburg Polytechnic University, Saint Petersburg, Russia
[c] Technical University of Munich, Munich, Germany

ARTICLE INFO

Article history:
Received 22 June 2018
Received in revised form 9 October 2018
Accepted 28 October 2018
Available online xxxx

Keywords:
Rectangular hollow section
Tubular joint
Initial stiffness
Axial stiffness
Component method

ABSTRACT

Recently, CIDECT (International Committee for the Development and Study of Tubular Structures) has proposed the component method as a unified approach for the design of many types of connections, including welded tubular joints. Although CIDECT provides clear and simple equations for the resistance of welded tubular joints, the design of initial stiffness remains complicated and includes a number of uncertainties. This paper analyzes the theoretical approach for the initial axial stiffness of rectangular hollow section T joints. The validation against experimental data has shown that the component method considerably overestimates the stiffness of T joints. The paper develops new equations for the stiffness of the components "chord face in bending" and "chord side walls in compression". The equations are based on simplified mechanical models, employing finite element analyses to calculate the parameters for which analytical solutions are found extremely complicated. In addition, the article numerically investigates the effect of chord axial stresses on the axial stiffness of joints and proposes a corresponding chord stress function.

1. Introduction

Welded tubular structures are used in a wide range of trusses and frames. In such structures, rectangular hollow section (RHS) joints combine high strength and simple end preparations. The main properties of tubular joints include their design resistance and stiffness. Generally, in the design of joints, the main attention of engineers and scientists is paid to design resistance, while the stiffness of joints is usually disregarded. However, initial stiffness is known to be essential in the global analysis of frames and trusses, since it affects the distribution of forces between members. In addition, it has been shown [1–3] that initial rotational stiffness plays the key role when considering buckling of tubular truss members.

Particular attention should be paid to axial stiffness, which represents the stiffness of a joint under an axial force acting along its brace. Fig. 1a shows an RHS T joint loaded by an axial force. A T joint represents the simplest joint configuration, when a brace is welded to a chord at an angle of 90°. Considering a beam model for such a joint (Fig. 1b), its axial stiffness $C_{j,ini,N}$ can be presented by a linear spring located on the surface of the chord [4]. The importance of axial stiffness for such joints can be demonstrated in a shallow Vierendeel girder, shown in Fig. 1c. When the girder is analyzed using the frame theory, then in addition to rotational stiffness, the axial stiffness of its joints should be taken into account. The local deformations of the joints can reduce the height of the girder *e*. Such reduction can be particularly noticeable for shallow girders. Finally, this increases axial forces acting in the chords, making the design unsafe.

The current design rules for RHS T joints in EN 1993-1-8:2005 [5] and CIDECT Design Guide No. 3 [6] are based on the failure mode approach and allow calculating design resistance, providing however no information for initial stiffness. Most of the publications and design guides on the topic [7–9] deal with the resistance of RHS joints, and very few of them investigate their stiffness. A formula for the initial axial stiffness of circular hollow section joints was presented by Mäkeläinen et al. [10]. Grotmann & Sedlacek [11] investigated the initial stiffness of RHS joints under in-plane bending. An extensive parametric study of axially-loaded joints was conducted by de Matos et al. [12], but no theoretical equation was proposed for initial stiffness. Costa-Neves [13] developed the equation for the axial stiffness of RHS-to-IPE connections, which was later accepted by CIDECT [14] and extended for RHS joints with some modifications.

One of the most reliable solutions for the design of initial stiffness can be provided by the component method. It was invented by Zoetemeijer [15] for bolted beam-to-column connections and developed by Tschemmernegg [16]. Later it was extended to column bases by Wald [17] and fire resistance by Leston-Jones [18]. Girão Coelho & Bijlaard [19] employed the method to investigate the behavior of high strength steel end-plate connections. Da Silva [20] developed the component method for joints under arbitrary loading. For bolted end-plate joints the method was used by Heinisuo et al. [21].

* Corresponding author.
E-mail address: marsel.garifullin@tut.fi (M. Garifullin).

https://doi.org/10.1016/j.jcsr.2018.10.025
0143-974X/

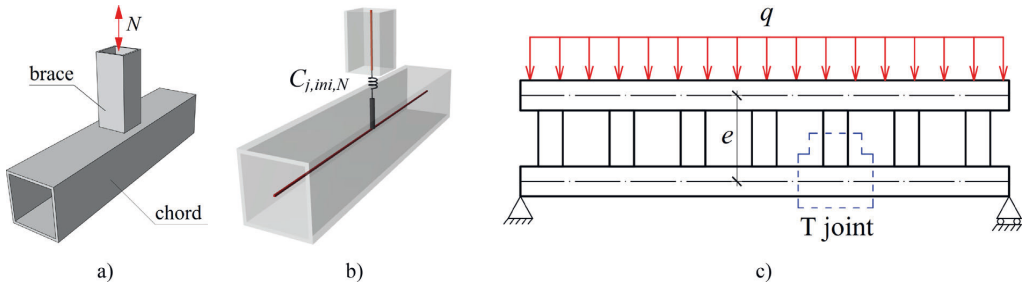

Fig. 1. a) RHS T joint loaded by axial force; b) axial stiffness modelled by a linear spring; c) Vierendeel girder.

Decomposing the joint into basic parts (components), the component method determines joint resistance and stiffness by combining the resistance and stiffness of these components. Being a unified approach for the design of various types of joints, the method was adopted by EN 1993-1-8:2005 [5] for joints connecting H or I sections. Weynand & Jaspart [22] proposed the method for hollow section joints. The main principles of the component method for tubular joints were developed in the CIDECT reports 5BP [23] and 16F [14]. The documents identify the main components of RHS joints and present a detailed procedure to calculate their design resistance. However, the information concerning initial stiffness is very limited: the provided equations for the stiffness of the components are not distinguished between various loading cases, and, therefore, the design of initial stiffness remains questionable.

This paper investigates the theoretical approach for the initial axial stiffness of RHS T joints. Section2 briefly describes and discusses the current design procedure for axial stiffness, which is provided in the CIDECT report 16F [14] (hereinafter – CIDECT). Section3 validates the design approach against the experimental data available in the literature. Section4 develops and experimentally validates new stiffness equations for two individual components. The equations are based on simple mechanical models, employing finite element modeling to replace complicated analytical solutions. Finally, Section5 numerically investigates the effect of chord axial stresses on the axial stiffness of RHS T joints and develops a corresponding chord stress function. The developed solutions are limited only for joints following the requirements of EN 1993-1-8:2005 [5].

2. Current theoretical approach for the initial axial stiffness of RHS T joints

The main notations of RHS T joints are provided in Fig. 2a. The theoretical approach for the initial stiffness of tubular joints employs the component method, as presented in CIDECT [14]. The component method assumes the axial load to be transferred from the brace to the chord face through four loading zones located at the corners of the brace. The mechanical behavior of the joint can then be modelled by a system of springs, as shown in Fig. 2b. Generally, the springs represent the following components:

a) chord face in bending,
b) chord side walls in tension / compression,
c) chord side walls in shear,
d) chord face under punching shear,
e) brace flange / webs in tension / compression,
f) chord section in distortion,
g) welds.

The behavior of the springs is assumed to be elastic. The initial stiffness of the joint is computed by combining the corresponding stiffnesses of the components using the combination rules for the systems of springs. In particular, initial axial stiffness $C_{j,ini,N}$ is calculated as.

$$C_{j,ini,N} = \frac{E}{\sum_i \frac{1}{k_i}} \tag{1}$$

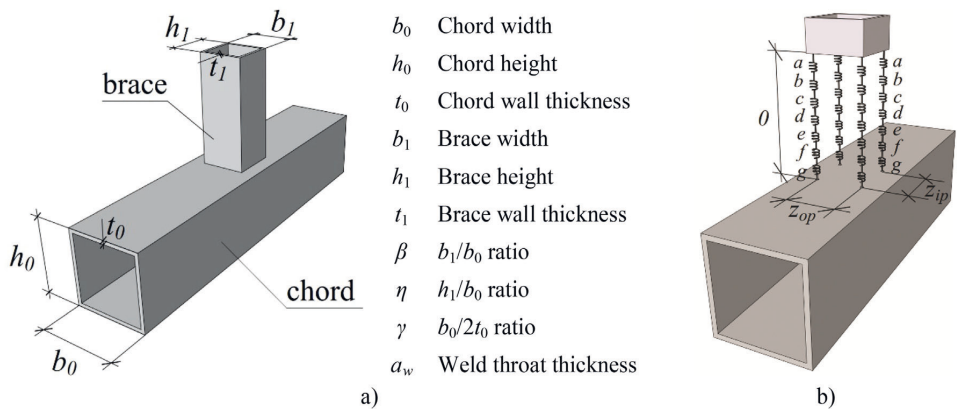

Fig. 2. RHS T joint: a) notations; b) component model.

where E is Young's modulus, and k_i is the stiffness of component i. In this paper, k_i defines the sum of the four components (springs) in the corners of the brace; therefore, each component is counted in Eq. (1) only once. According to [4], only components a "chord face in bending" and b "chord side wall in compression / tension" play a noticeable role in the axial stiffness of RHS T joints. The other components have substantially greater stiffness and can be considered as infinite for practical purposes. Taking into account the aforementioned assumptions, Eq. (1) can be reduced to

$$C_{j,ini,N} = \frac{E}{\frac{1}{k_a} + \frac{1}{k_b}} \tag{2}$$

where k_a is the stiffness of the component "chord face in bending" and k_b is the stiffness of the component "chord side walls in compression / tension". According to CIDECT [14], the stiffness of the latter is assumed to be the same in tension and in compression. This paper considers joints only under compressive axial load; therefore, the component b is referred to as "chord side walls in compression" for simplicity. For joints with large β, the stiffness of the component "chord face in bending" becomes relatively high, i.e. $0.1k_a > k_b$, and can be also ignored in the design of initial stiffness. In this case, Eq. (2) can be simplified to

$$C_{j,ini,N} = Ek_b \tag{3}$$

2.1. Component "Chord face in bending"

As been said before, the stiffness of the component "chord face in bending" has to be calculated only for the joints in which this component noticeably contributes to the design of stiffness. To be consistent with the design of resistance specified in EN 1993-1-8:2005 [5], such joints can be limited to those governed by chord face failure, i.e. $\beta \le 0.85$. However, this component might become irrelevant even for smaller β if the cross-section of the brace is increased by large fillet welds [24].

Two possible options are available to compute the stiffness of this component. The first one was developed by Costa-Neves [13] for RHS-to-IPE connections. Later it was accepted by CIDECT [14] in a form presented in Eq. (4).

$$k_a = \frac{t_0^3}{14.4\beta_0 L_{stiff}^2}\left(\frac{L_{stiff}^2}{bt_0}\right)^{1.25} \cdot \frac{\frac{c}{L_{stiff}} + \left(1-\frac{b}{L_{stiff}}\right)\tan\theta}{\left(1-\frac{b}{L_{stiff}}\right)^3 + \frac{10.4\left(1.5-1.6\frac{b}{L_{stiff}}\right)}{\left(\frac{L_{stiff}}{t_0}\right)^2}} \tag{4}$$

where b and c are respectively the width and the height of the brace, i.e., $b = b_1$ and $c = h_1$. L_{stiff} is the stiffness length determined as $L_{stiff} = d + r$, where d and r represent the width of the chord top face flat area and the chord inner corner radius, respectively. Notations b, c, d and r are illustrated in Fig. 3. The reduction factor β_0 is found as

$$\beta_0 = \begin{cases} 1, & \frac{b+c}{L} \ge 0.5 \\ 0.7 + 0.6\frac{b+c}{L}, & \frac{b+c}{L} < 0.5 \end{cases} \tag{5}$$

$$L = d + 0.5r$$

The angle θ is defined as

$$\theta = \begin{cases} 35 - 10b/L_{stiff}, & b/L_{stiff} < 0.7 \\ 49 - 30b/L_{stiff}, & b/L_{stiff} \ge 0.7 \end{cases} \tag{6}$$

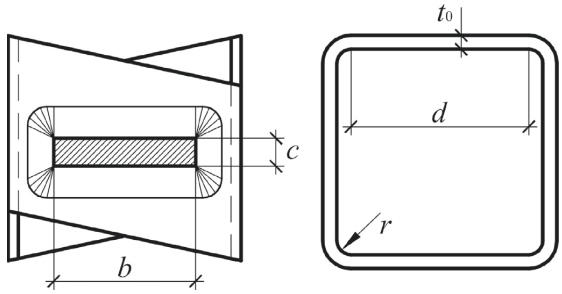

Fig. 3. Design model for component "chord face in bending".

The validity range of Eq. (4) is defined by the following limitations:

$$10 \le L_{stiff}/t_0 \le 50; \quad 0.08 \le b/L_{stiff} \le 0.75; \quad 0.05 \le c/L_{stiff} \le 0.20 \tag{7}$$

For RHS joints, the last limitation in Eq. (7) is transformed into

$$0.05 \le h_1/L_{stiff} \approx h_1/b_0 = \eta \le 0.20 \tag{8}$$

Obviously, this requirement can be fulfilled only for very small braces, meaning that Eq. (4) violates by default its validity range for most of RHS joints. However, Eq. (4) will be examined in this paper.

The second option for the stiffness of the component "chord face in bending" has been presented in [25] and accepted as an alternative approach in CIDECT [14]. It represents the following equation:

$$k_a = \frac{\pi t_0^3}{12(1-\nu^2)C_t\left(\frac{b_0-t_0}{2}\right)^2} \tag{9}$$

where ν is Poisson's ratio and C_t is a coefficient assumed as 0.18. It should be noted that Eq. (9) represents a function of the chord geometry and does not depend on the size of the brace, making its reliability doubtful for tubular joints. CIDECT [14] provides no information regarding its validity range.

2.2. Component "Chord side walls in compression"

The stiffness of the component "chord side walls in compression" was originally developed in [26] and later studied in [27]. The component employs the model of an RHS chord loaded by two transverse plates of the same width as the chord, as shown in Fig. 4a. CIDECT [14] provides the following equation for its stiffness:

$$k_b = \frac{2 \cdot 0.7 \cdot b_{eff,c,wc} \cdot t_0}{h_0} \tag{10}$$

where $b_{eff,c,wc}$ is the effective width, defined as

$$b_{eff,c,wc} = t_1 + 2\sqrt{2}a_w + 5t_0 \tag{11}$$

where t_1 is the thickness of the loading plate. In case of an RHS joint, the load is transferred through the whole section of the tubular brace, as shown in Fig. 4b, and Eq. (11) should be modified as

$$b_{eff,c,wc} = h_1 + 2\sqrt{2}a_w + 5t_0 \tag{12}$$

However, the applicability of Eq. (10) for tubular joints remains questionable. Firstly, as can be seen in Fig. 4a, Eq. (10) has been developed for X joints and CIDECT [14] does not specify its reliability for T joints. Secondly, Eqs. (10)–(12) do not include β as a variable, i.e., provide the same solution for joints with the same h_1 but various

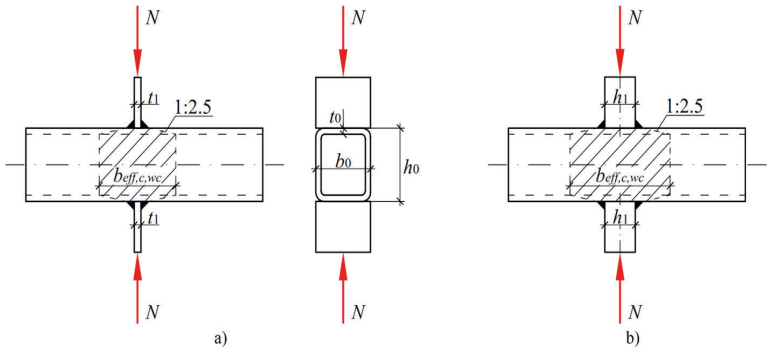

Fig. 4. Component "chord side walls in compression": a) original design model; b) its extension to RHS joints.

b_1. Since these equations have been developed for $\beta = 1.0$, their applicability for joints with smaller β remains unclear.

3. Validation of the current theoretical approach

This part validates the current approach for the initial axial stiffness of RHS T joints with the experimental results available in the literature. Usually the publications dealing with experimental investigations of joints provide no direct values of initial stiffness. For this reason, initial stiffness was determined graphically, as a tangent line in the beginning of available load-displacement curves. The described procedure is illustrated in Fig. 5, where $C_{j,ini,N}$ denotes initial axial stiffness. Although the accuracy of this approach is doubtful, it represents the only possible method to obtain experimental stiffness from available publications. Moreover, the design of initial stiffness does not require such high level of accuracy as the design of resistance, assuming 30% discrepancy in both directions. This fact can fully justify the possible inaccuracy of this method. For simplicity, initial axial stiffness is denoted as C further in this paper.

A pioneering experimental work on T joints has been conducted by Kato & Nishiyama [28]. However, the authors presented only the global deformations of joints, including chord bending. Later a series of tests under various loading was conducted by Zhao & Hancock [29], but only three load-displacement curves can be found for T joints under pure axial loading. One T joint was selected from the tests of Davies & Crockett [30]. Nizer et al. [31] conducted six tests on T joints with and without axial loading in the chord. Generally, axial stresses in the chord are found to affect the stiffness of T joints; therefore, only one joint free from chord pre-loading have been selected for the validation. Some results have been found in the most recent tests of Becque & Wilkinson [32].

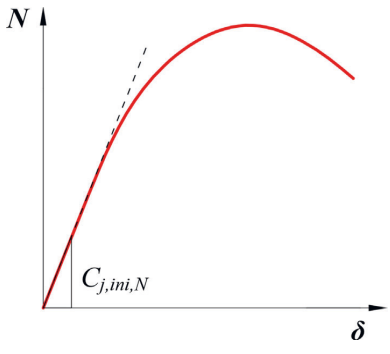

Fig. 5. Graphical approach for determination of initial axial stiffness.

Attention should be also paid to the publications that analyze the behavior of RHS X joints, e.g. [33,34]. Due to the similarities in the behavior of T and X joints, these joints are often considered together. In particular, EN 1993-1-8:2005 [5] and CIDECT Design Guide No. 3 [6] provide the same equations for the design resistances of RHS T and X joints. However, the design of initial stiffness might differ. To investigate this issue in details, a comparative analysis was conducted based on the experimental results of Feng & Young, who conducted a series of tests on stainless steel RHS T [35] and X [36] joints. The tests were carried out in such a way that the geometry of X joints repeated the geometry of some T joints. The stiffness of the joints with matching geometry was determined and collected in Table 1, where the joints are arranged in the ascending order of β. The graphical comparison of the behavior of some matching joints is provided in Fig. 6.

It can be seen that X joints have noticeably higher experimental stiffness than matching T joints. The difference is particularly pronounced for the cases with $\beta = 1.0$, reaching an order of magnitude for some joints. The observed difference can be explained by the various contribution of the components to the overall stiffness of the joint. If β is small, the stiffness is mostly governed by the component "chord face in bending", which behaves similarly for both types of joints. This leads to relatively small difference between the stiffness of T and X joints. Oppositely, the stiffness of the joints with large β is mostly influenced by the component "chord side walls in compression", which obviously behaves differently for T and X joints. This leads to a significant difference in the stiffness of the matching T and X joints. These results demonstrate that initial stiffness has to be calculated differently for T and X joints. Although a common equation can be adopted for the component "chord face in bending", individual equations for T and X joints should be derived for the component "chord side walls in compression". For this reason, X joints are not employed in the validation and this paper considers only T joints.

Attention should be also paid to stainless steel joints. Due to the nonlinear stress-strain responses of stainless steels [34], the equation developed for joints made of carbon steels may be invalid for joints made of stainless steels. For this reason, the latter were excluded from in the validation, in particular the abovementioned tests of Feng & Young [35]. Table 2 presents the summary of the tests used for the validation. Table 3 provides the details of the joints and their experimental initial stiffness C_{exp}, which was determined according to Fig. 5.

Theoretically, initial stiffness was calculated according to Section2. For the joints with $\beta \le 0.85$, the stiffness of the component "chord face in bending" was computed using both available options, Eqs. (4) and (9), corresponding to k_{a1} and k_{a2} respectively. The stiffness of the component "chord side walls in compression" was calculated by Eq. (10). It should be noted that most of the joints were welded with fillet welds, which are known to considerably increase their initial stiffness [37]. In this paper, the influence of fillet welds was taken into account using

Table 1
Comparison of stiffness of T and X joints. The names of joints in accordance with [35,36].

X joint	C_X [kN/mm]	T joint	C_T [kN/mm]	C_X/C_T	β
XD-C140x3-B40x2-P0	75	TD-C140x3-B40x2	42	1.8	0.50
XH-C110x4-B150x6-P0	200	TH-C110x4-B150x6	50	4.0	0.75
XD-C50x1.5-B40x2-P0	200	TD-C50x1.5-B40x2	67	3.0	0.80
XD-C40x2-B40x2-P0	1900	TD-C40x2-B40x2	167	11.4	1.00
XD-C50x1.5-B50x1.5-P0	1700	TD-C50x1.5-B50x1.5	100	17.0	1.00
XD-C140x3-B140x3-P0	4250	TD-C140x3-B140x3	175	24.3	1.00
XH-C150x6-B150x6-P0	2000	TH-C150x6-B150x6	338	5.9	1.00
XH-C200x4-B200x4-P0	1500	TH-C200x4-B200x4	145	10.3	1.00
XN-C40x2-B40x2-P0	2000	TN-C40x2-B40x2	100	20.0	1.00

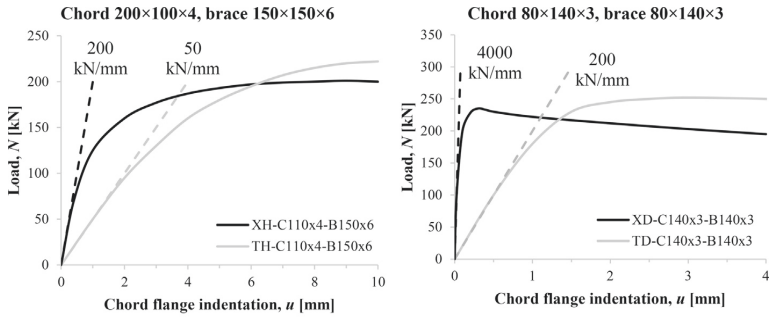

Fig. 6. Comparison of T and X joints with matching geometry: a) $\beta = 0.75$, b) $\beta = 1.0$.

Table 2
Summary of tests used for the validation.

No.	Authors	Reference
1–3	Zhao & Hancock, 1991	[29]
4	Nizer et al., 2016	[31]
5–6	Becque & Wilkinson, 2017	[32]
7	Davies & Crockett, 1996	[30]

the approach of de Matos et al. [12], which replaces the actual brace section by an equivalent butt-welded section with the following width:

$$b_{eq} = b_1 + 1.6a_w \tag{13}$$

The equivalent brace width was used further to calculate the equivalent brace-to-chord width ratio:

$$\beta_{eq} = b_{eq}/b_0 \leq 1.0 \tag{14}$$

The equivalent brace-to-chord width ratio was further used to compute the stiffnesses k_a and k_b. Two joint stiffnesses, C_1 and C_2, were calculated according to Eq. (2), respectively employing k_{a1} and k_{a2} for the component "chord face in bending". For the joints with $\beta > 0.85$, only the component "chord side walls in compression" was considered, and joint stiffness C was determined according to Eq. (3).

Table 4 provides a detailed comparison of initial stiffness calculated theoretically and experimentally. Regarding the joints with $\beta \leq 0.85$, if k_a is calculated using the first approach, Eq. (4), then theoretical stiffness two times overestimates the experimental. Oppositely, if k_a is calculated using the alternative approach, Eq. (9), the results are significantly underestimated, with the average C_2 / C_{exp} ratio of 0.08. For the joints with $\beta > 0.85$, the stiffness is overestimated more than two times. All these findings clearly show that the CIDECT equations for the initial stiffness of RHS T joints cannot serve as a reliable tool in the design of tubular joints and more accurate equations have to be developed.

4. New equations for the stiffness of components

Given the unsatisfactory prediction of initial axial stiffness by the current theoretical approach, this section develops a more accurate solution for RHS T joints. Following the component method, the paper proposes new equations for the components "chord face in bending" and "chord side walls in compression". To avoid extremely complicated

Table 3
Details of joints used for the validation.

No.	Joint	b_0 [mm]	h_0 [mm]	t_0 [mm]	r^a [mm]	b_1 [mm]	h_1 [mm]	t_1 [mm]	β	2γ	a_w [mm]	E^b [GPa]	C_{exp} [kN/mm]
1	S1B1C11	51	102	4.9	4.9	51	51	4.9	1.00	10.4	4.6	200	570
2	S1B1C12	51	102	3.2	3.2	51	51	4.9	1.00	15.9	4.6	200	330
3	S1B1C23	102	102	4	4	51	51	4.9	0.50	25.5	4.6	200	74
4	TN02N0	140	80	4	4	100	100	3	0.71	35.0	5.0	200	280
5	T1	200	200	6	14	100	100	8	0.50	33.3	4.0	210*	75
6	T4	400	400	16	24	200	200	12.5	0.50	25.0	6.3	210*	400
7	MPJT1	150	150	6.2	9.3	90	90	6.2	0.60	24.2	6.2	210*	230

[a] Nominal inner corner radius.
[b] Young's modulus of the chord steel (* if a value not provided by authors).

Table 4
Validation of the theoretical approach.

No.	Joint	β	β_{eq}	E [GPa]	k_{a1} [mm]	k_{a2} [mm]	k_b [mm]	C_1 [kN/mm]	C_2 [kN/mm]	C_{exp} [kN/mm]	C_1/C_{exp}	C_2/C_{exp}
	$\beta \le 0.85$											
3	S1B1C23	0.50	0.57	200	0.661	0.043	4.612	116	8.4	74	1.6	0.11
4	TN02N0	0.71	0.77	200	4.064	0.022	9.390	567	4.4	280	2.0	0.02
5	T1	0.50	0.53	210	0.747	0.037	5.935	139	7.7	75	1.9	0.10
6	T4	0.50	0.53	210	2.317	0.178	16.670	427	36.9	400	1.1	0.09
7	MPJT1	0.60	0.67	210	2.883	0.074	8.017	445	15.3	230	1.9	0.07
	Average										**2.0**	**0.08**
	Variance										**0.3**	**0.001**
	$\beta > 0.85$											
1	S1B1C11	1.00	1.00	200	–	–	5.952	1190	–	570	2.1	–
2	S1B1C12	1.00	1.00	200	–	–	3.514	703	–	330	2.1	–
	Average										**2.1**	
	Variance										**0.0**	

analytical solutions for these components, the paper considers simplified mechanical models and employs the concept of equivalent length and width, which are determined numerically. The developed equations are further validated against the same experimental results.

4.1. Stiffness of the component "chord face in bending"

Consider an RHS T joint with a $b_0 \times h_0 \times t_0$ chord loaded axially by a $b_1 \times h_1$ brace, as shown in Fig. 7a. Generally, the thickness of the brace t_1 does not influence the structural properties of tubular joints [38]; therefore, it is not considered in this section. Since the influence of fillet welds is considered independently (see Section3), it is ignored in this study. The top face of the chord can be replaced by a simply supported plate with an equivalent length l_{eff} and a span $L = b_0 - 2\,t_0$. The load N can be assumed applied through an infinitely rigid plate of the size $b_1 \times l_{eff}$. This design model can be simplified further to a 2D beam model, shown in Fig. 7b. The vertical displacement of point A (mid-point of the 2D beam) is found as

$$v(A) = \frac{N(L-b_1)^3}{48EI} \tag{15}$$

where I is the second moment of area of the cross-section A-A. Then, Eq. (15) can be written as

$$v(A) = \frac{N(L-b_1)^3}{4El_{eff}t_0^3} \tag{16}$$

The stiffness of the component can be found as

$$k_a = \frac{N}{v(A)E} = \frac{4l_{eff}t_0^3}{(L-b_1)^3} \tag{17}$$

The equivalent length l_{eff} remains the only unknown variable in Eq. (17). In this paper, it was determined numerically, employing the finite element (FE) software Abaqus/Standard [39]. To exclude a possible effect of the chord end conditions, the length of the chord was selected as $6b_0$ [40], while the brace length was chosen as b_1, as shown in Fig. 8a. According to [41], the model was constructed using quadratic solid finite elements with reduced integration (C3D20R), with two elements in the thickness direction. Since initial stiffness was the only requested outcome of the analyses, only elastic properties were introduced to the material model, with Young's modulus of 210 GPa and Poisson's ratio of 0.3. The brace was connected to the chord top face using a tie

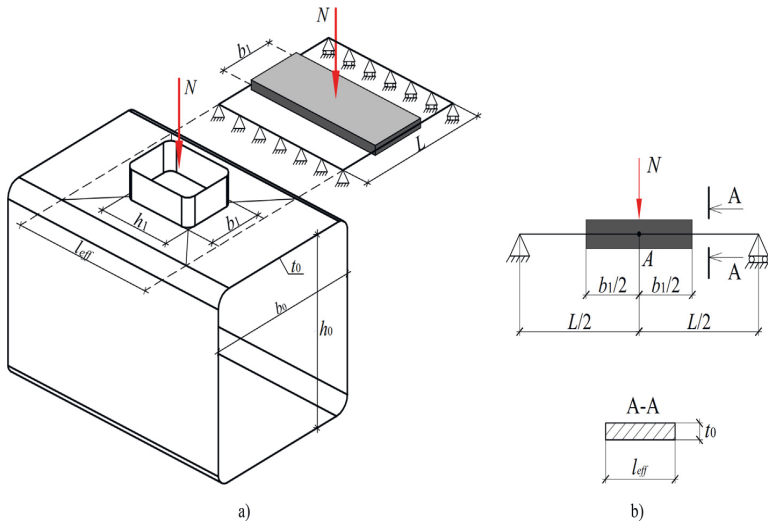

Fig. 7. Component "chord face in bending": a) spatial design model; b) 2D design model.

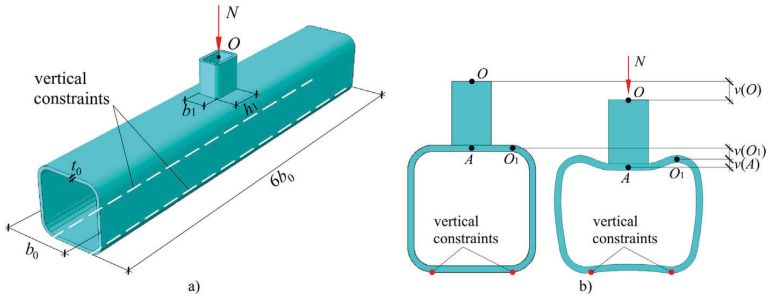

Fig. 8. FE model: a) overall view; b) location of points with measured displacements.

Table 5
Values of variables used in FEM.

Variable	Considered values
b_0 [mm]	100; 150; 200; 250; 300
$\beta = b_1 / b_0$	0.25; 0.40; 0.55; 0.70; 0.85
$2\gamma = b_0 / t_0$	10; 15; 20; 25; 30; 35
$\alpha = h_1 / b_1$	0.5; 1.0; 1.5; 2.0

constraint. To avoid the contribution of the brace to the deformation of the joint, it was modelled with increased Young's modulus of $210 \cdot 10^4$ GPa. The compressive axial load was applied using a single increment to point O, connected by a rigid body to the upper face of the brace. To avoid bending of the chord from the transverse force, it was restrained against vertical displacements along its length, as shown in Fig. 8a.

Fig. 8b demonstrates two vertical displacements measured in the analyses: $v(O)$ corresponding to the displacement of the loading point O and $v(O_1)$ corresponding to the global displacement of the upper flange of the chord. The shortening of the brace was neglected due to its relatively high Young's modulus. The local displacement corresponding to the component "chord face in bending" was found as

$$v(A) = v(O) - v(O_1) \tag{18}$$

Following Eq. (16), the equivalent length l_{eff} was calculated as

$$l_{eff} = \frac{N(L-b_1)^3}{4Et_0^3 v(A)} \tag{19}$$

The equivalent length l_{eff} was determined for a series of joints with varying parameters b_0, b_1, h_1 and t_0. To avoid considering an extra variable h_0, only square hollow section were analyzed. For convenience, parameters b_1, h_1 and t_0 were correspondingly replaced by their relative ratios $\beta = b_1 / b_0$, $\alpha = h_1 / b_1$ and $2\gamma = b_0 / t_0$. EN 1993-1-8:2005 [5] provides the following limitations for these ratios: $0.25 \le \beta \le 1.0$, $0.5 \le \alpha \le 2.0$ and $10 \le 2\gamma \le 35$. Based on the numerical observations, for $\beta > 0.85$ the contribution of the component "chord face in bending" to the overall stiffness of the joint becomes negligibly small; therefore, the upper bound for β was reduced to 0.85. Table 5 provides the values for the considered variables.

Using Eq. (17), l_{eff} was calculated for varying joint parameters with $v(A)$ obtained by the finite element analysis. To analyze the behavior of l_{eff}, it was plotted against the introduced variables. As can be seen from Fig. 9, l_{eff} depends linearly on b_0 and α. According to Fig. 10, the dependence on β was assumed linear, while the influence of 2γ was found comparatively small and thus was ignored. To be consistent with the current terminology, α was replaced by the commonly used ratio $\eta = h_1 / b_0$. Finally, l_{eff} was approximated as

$$l_{eff} = h_1(2-\beta) + 1.25b_0(1-\beta) \qquad \beta \le 0.85 \tag{20}$$

In relation to the numerical results, the proposed equation demonstrated sufficient accuracy, with $R^2 = 0.980$, $R^2_{adj} = 0.979$ and the average relative error of 4.1%. Since the component "chord face in bending" behaves similarly for T and X joints, the proposed equation can be also extended for X joints.

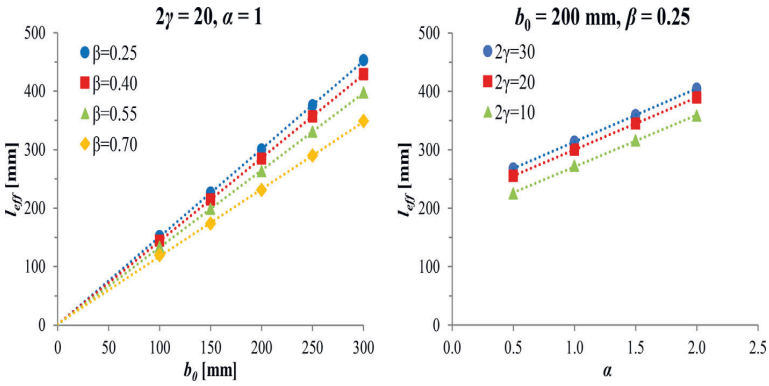

Fig. 9. Dependence of l_{eff} on b_0 and α.

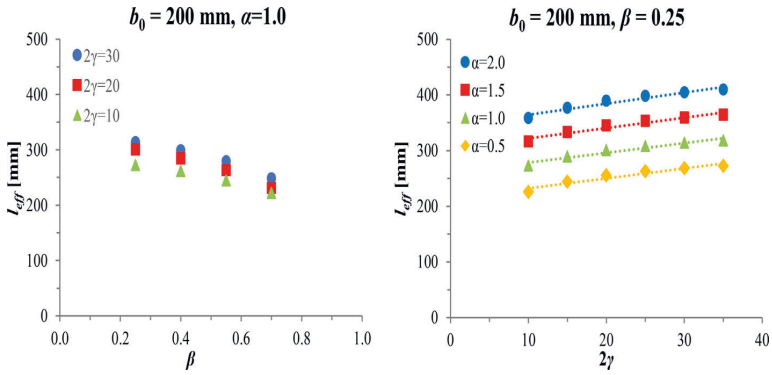

Fig. 10. Dependence of l_{eff} on β and 2γ.

4.2. Stiffness of the component "chord side walls in compression"

Consider an RHS T joint with a $b_0 \times h_0 \times t_0$ chord loaded axially by a $b_1 \times h_1$ brace with an axial force N. Fig. 11a shows the approximate deformation pattern for the compressed chord side wall. Considering it separately, the chord side wall can be replaced by a simply supported column of length $H = h_0 - t_0$ with an equivalent width b_{eff} and loaded by a compressive force $N/2$. It can be further simplified to a 2D beam model, shown in Fig. 11b.

The vertical displacement at the end of the column (point B) can be found as

$$v(B) = \frac{0.5NH}{EA} = \frac{NH}{2Eb_{eff}t_0} \tag{21}$$

Then the stiffness of the component "chord side walls in compression" can be calculated as

$$k_b = \frac{N}{Ev(B)} = \frac{2b_{eff}t_0}{H} \tag{22}$$

This equation looks similar to Eq. (10) if b_{eff} and H are respectively replaced by $b_{eff,c,wc}$ and h_0. However, Eq. (22) does not take into account the coefficient 0.7, which is present in Eq. (10). The origin of this coefficient is difficult to trace. Probably, it represents a correction factor between the gradients for load introduction, as demonstrated by Grotmann & Sedlacek [11]:

$$r = \frac{\sqrt{3}}{2.5} = 0.693 \approx 0.7 \tag{23}$$

However, Grotmann & Sedlacek [11] employ a slightly different equation for the stiffness of this component and use this correction factor for the effective width b_{eff}. In this section, the equivalent width b_{eff} is determined by a series of numerical analyses, which by default consider this correction factor. This section employs the results of the FE analyses conducted for the component "chord face in bending". According to Fig. 8b, displacement $v(B)$ was found as equal to displacement $v(O_1)$. Moreover, additional analyses were conducted to consider joints with $\beta = 1.0$. These joints experienced no chord face bending; therefore, displacement $v(B)$ was calculated as equal to displacement $v(O)$. According to Eq. (22), the equivalent width b_{eff} was found as

$$b_{eff} = \frac{NH}{2Et_0v(B)} \tag{24}$$

To analyze the behavior of b_{eff}, it was plotted against the introduced variables. The effective width b_{eff} was found to depend linearly on b_0 and

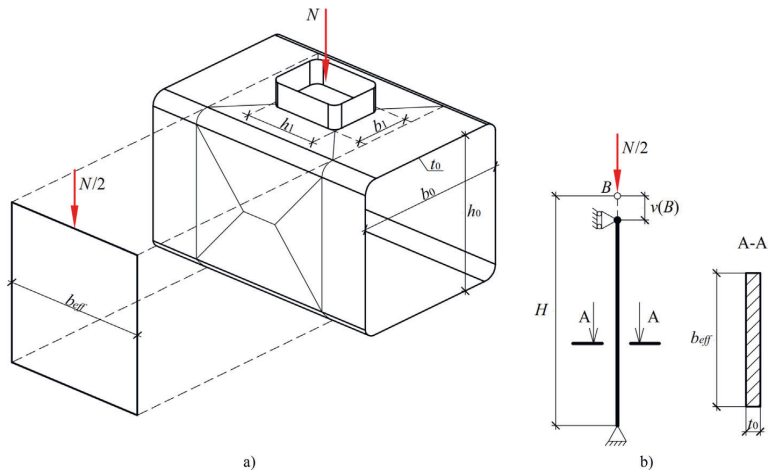

Fig. 11. Component "chord side walls in compression": a) spatial design model; b) 2D design model.

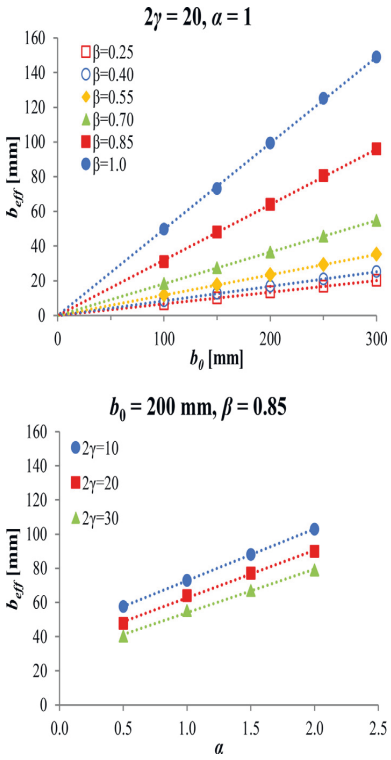

Fig. 12. Dependence of b_{eff} on b_0 and α.

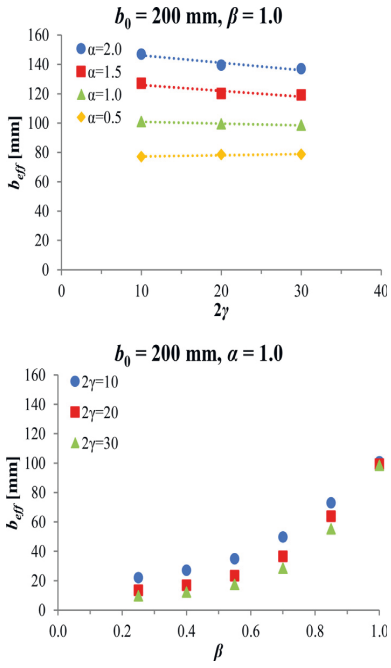

Fig. 13. Dependence of b_{eff} on 2γ and β.

α, as shown in Fig. 12. Similar to the component "chord face in bending", the influence of 2γ was found negligibly small and was ignored. At the same time, considerable nonlinear behavior was observed in relation to β, as shown in Fig. 13. To be consistent with the current terminology, α was replaced by the commonly used ratio $\eta = h_1 / b_0$. Finally, a curve fitting approach approximated b_{eff} as

$$b_{eff} = 0.025\left(h_1(9\beta - 1) + \frac{2.4b_0}{1.2-\beta}\right) \tag{25}$$

In relation to the numerical results, the accuracy of the proposed equation was justified by $R^2 = 0.96$, $R^2_{adj} = 0.95$ and the average relative error of 11.2%. The component "chord side walls in buckling" governs the behavior of joints with $\beta > 0.85$. Table 1 demonstrated a clear difference between T and X joints with matching geometry. For this reason, the equations developed for this component cannot be extended for X joints and are limited only for T joints.

4.3. Validation of the proposed equations

The developed equations were validated against the same experimental data as was used in Section3. The stiffnesses of the components were calculated in accordance with the developed Eqs. (17) and (22), both neglecting (denoted as k_a and k_b) and considering the influence of fillet welds (denoted as $k_{a,eq}$ and $k_{b,eq}$). The corresponding theoretical stiffnesses are denoted as C and C_{eq}, respectively. Both were compared to experimental stiffness C_{exp}. The results of the validation are summarized in Table 6. For all the joints with $\beta \le 0.85$, the theoretical prediction underestimates the experimental values, if fillet welds are ignored. If welds are taken into account, the prediction is more accurate and the C / C_{exp} ratio exceeds 1.0 in most cases, except joints T1 and T4. For these two joints, the exact throat thicknesses of welds were not provided by the authors and were determined as equal to $t_1/2$, as the minimum specified in the paper. If measured throat thicknesses were used instead, the ratio could have been closer to 1.0. The joints with $\beta = 1.0$ also demonstrate accurate prediction; however, any certain conclusions are complicated by the small amount of joints of available for the validation. It should be noted that for the joints with $\beta = 1.0$, the consideration of fillet welds does not bring any reasonable changes, since β cannot exceed 1.0. Generally, the results show that the developed equations provide sufficiently accurate prediction of initial axial stiffness and can be effectively used in the design of RHS T joints.

Attention should be paid also to the approach that was employed to consider the influence of fillet welds. The results of the validation show that if welds are disregarded, initial stiffness in noticeably underestimated. The used solution allowed to compensate the observed underestimation for most of joints and obtain more accurate prediction of stiffness, although demonstrating excessive stiffness for joints 3 and 7. Unless a more accurate equation is developed based on extensive numerical and/or experimental values, this solution can be effectively employed as a rule of thumb for RHS T joints under axial loading. A similar approach was proposed for moment-loaded RHS joints in [37].

5. Chord stress function for initial axial stiffness

According to Wardenier [38], axial forces in the chord affect the structural behavior of RHS T joints. In particular, the reduction of resistance is determined by the so-called chord stress functions, the simplest of which is provided in EN 1993-1-8:2005 [5], Eq. (26). Some other functions for RHS T and X joints can be found in [42,43].

$$k_n = \begin{cases} 1.3 - \dfrac{0.4|n|}{\beta} \le 1.0, & n>0 \\ 1.0, & n<0 \end{cases} \tag{26}$$

Table 6
Validation of the proposed theoretical approach

No.	Joint	β	β_{eq}	k_a [mm]	$k_{a,eq.}$ [mm]	k_b [mm]	$k_{b,eq.}$ [mm]	C [kN/mm]	C_{eq} [kN/mm]	C_{exp} [kN/mm]	C / C_{exp}	C_{eq}/ C_{exp}
	$\beta \le 0.85$											
3	S1B1C23	0.50	0.57	0.452	0.720	1.019	1.161	63	89	**74**	0.85	1.20
4	TN02N0	0.71	0.77	1.395	3.016	3.097	3.455	192	322	**280**	0.69	1.15
5	T1	0.50	0.53	0.349	0.419	1.513	1.604	60	70	**75**	0.79	0.93
6	T4	0.50	0.53	1.900	2.212	4.077	4.268	272	306	**400**	0.68	0.76
7	MPJT1	0.60	0.67	1.777	3.255	2.039	2.302	199	283	**230**	0.87	1.23
	Average										**0.77**	**1.06**
	Variance										**0.01**	**0.03**
	$\beta > 0.85$											
1	S1B1C11	1.00	1.00	–	–	2.445	2.445	489	489	**570**	0.86	0.86
2	S1B1C12	1.00	1.00	–	–	1.569	1.569	314	314	**330**	0.95	0.95
	Average										**0.90**	**0.90**
	Variance										**0.00**	**0.00**

where n is the relative axial stress:

$$n = \frac{\sigma_0}{f_{y0}} = \frac{N_0}{A_0 f_{y0}} \tag{27}$$

where A_0 is the cross-sectional area of the chord and N_0 is the axial force in the chord. Although EN 1993-1-8:2005 [5] assumes negative n for tension and positive n for compression, most of publications [42–44] employ the inverse sign convention for n, which is also used in this paper.

In addition to resistance, a similar influence of chord axial stresses is also observed on the initial stiffness of tubular joints. Garifullin et al. [45] have shown that compressive normal stresses in the chord reduce the initial rotational stiffness of RHS T joints by 40%, while tensile stresses increase it by 30%. Such phenomenon might be particularly important for frame structures, where the stiffness of joints has to be considered in the global analysis. Such serious influence of chord axial stresses on initial stiffness can noticeably change the distribution of forces in the members of frames, affecting the results of the global analysis. This section numerically evaluates the effect of chord axial forces on the initial axial stiffness of RHS T joints and develops a corresponding chord stress function $k_{sn,N}$.

5.1. Numerical simulations

The analyses were conducted numerically, employing the same FE model as was used in Section4. The scope of the study was restricted to square hollow sections to exclude the consideration of the additional variable b_0/h_0. All analyses were conducted for a joint with a 3.0 m long chord made of 300 × 300 mm cross-section. Following the requirements of EN 1993-1-8:2005 [5], the chord wall thickness t_0 varied from 8.5 mm ($2\gamma = 35$) to 30 mm ($2\gamma = 10$), whereas the brace width changed from 75 mm ($\beta = 0.25$) to 300 mm ($\beta = 1.00$), as shown in Table 7. The length of the brace was selected as equal to b_1. The brace wall thickness t_1 was determined so that it did not exceed the wall thickness of the chord t_0. The relative stress n in the chord was determined according to Eq. (27). All calculations employed the elastic-ideal plastic material model with $E = 210$ GPa and $\nu = 0.3$. The analyses were conducted in two steps: after an axial load was applied to the chord on the first step, the end of the brace was loaded with a concentrated axial force N using only one increment to find the initial stiffness of the joint.

Table 7
Parameters of joints used in numerical simulations.

Chord	$300 \times 300 \times t_0$				
	t_0 [mm]	8.5	10	20	30
	2γ	35	30	15	10
Brace	$b_1 \times b_1 \times t_1$				
	b_1 [mm]	75	180	255	300
	β	0.25	0.60	0.85	1.00
Steel grade	S355, S500, S700				
n	−0.95, −0.90, −0.80, −0.60, −0.30, 0, 0.30, 0.60, 0.80, 0.90, 0.95				

According to the obtained results, chord axial stresses significantly affected the initial axial stiffness of the joints. Figs. 14 and 16 plot the ratio C/C_0 for the joints with varying 2γ and β, where C is the stiffness with a relative axial stress n, C_0 is the stiffness with no axial stress. As can be seen, the observed effect has the similar pattern as in the case with initial rotational stiffness [45]. The maximum 35% reduction of stiffness is observed for compressive loads and 30% increase for tensile loads. The effect is particularly pronounced for the joints with small β and large 2γ. Moreover, the effect depends on the steel grade, increasing with the increase of yield strength, as shown in Fig. 15.

5.2. Chord stress function for initial axial stiffness

To take into account the influence of chord axial stresses, a corresponding chord stress function (CSF) was developed based on the obtained numerical results. Following the above observations, the function was found dependent on four variables: β, γ, f_{y0} (i.e., steel grade) and n. The assessment criteria included the coefficient of determination R^2, the adjusted coefficient of determination R^2_{adj}, the average percent error Δ_{av} and the maximum percent error Δ_{max}.

Firstly, the paper tested the existing chord stress functions for resistance for their applicability to initial stiffness. The results are summarized in Table 8. Case 1 represents the current CSF in EN 1993-1-8:2005 [5], Eq. (26), providing very inaccurate results. Similar performance was observed for the functions proposed in [43], Case 3, and [42], Case 5. In addition, none of these functions considers the increase of stiffness for tensile stresses. Cases 2, 4 and 6 represent the corresponding improvements of Cases 1, 3 and 5, originating from their general equations and adjusted using a curve fitting approach. As can be seen, none of the latter brings reasonable improvements in accuracy. These results demonstrate that the existing chord stress functions for resistance are inapplicable for initial stiffness.

A new CSF was developed based on the obtained numerical results. For some combinations of β and γ, the influence of chord axial forces is found to be negligibly small, as presented on Fig. 17a for S700 and $n = -0.95$. In the figure, the black dots represent the tested cases. In particular, the reduction of initial stiffness does not exceed 5% for the joints with small 2γ and large β; therefore, the introduction of a CSF seems unreasonable for these joints, particularly if its possible error exceeds 5%. For the remaining combinations of β and 2γ, the reduction is considerable, with the maximum value at the largest 2γ and smallest β. Following these observations, the analyzed area of joints was divided into two zones, as shown on Fig. 17b. The grey area corresponds to the joints for which no CSF is proposed, while the yellow zone denotes the

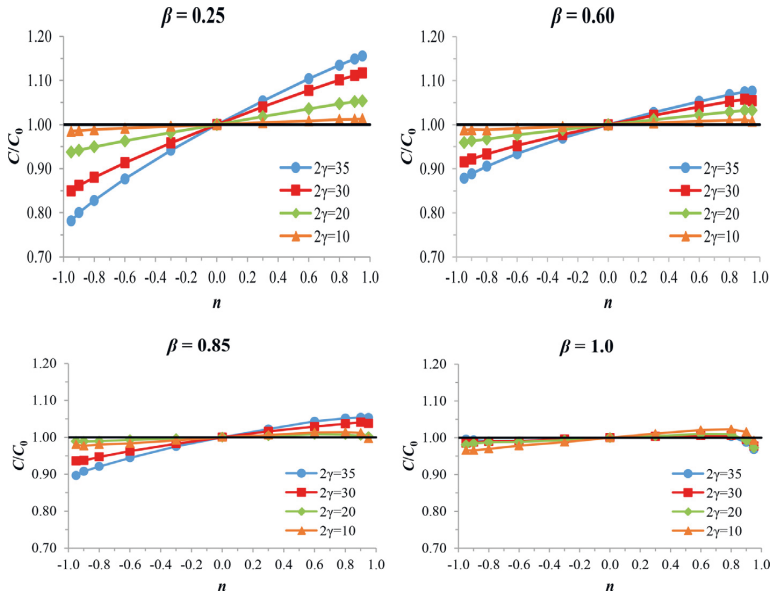

Fig. 14. Dependence of the effect on 2γ, S355.

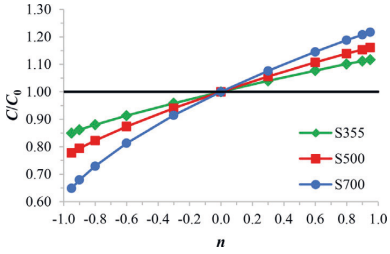

Fig. 15. Dependence of the effect on steel grade ($2\gamma = 30, \beta = 0.25$).

area with the proposed CSF. The domain of CSF was specified with additional numerical analyses:

$$2\gamma \geq 12; \quad \beta \leq 0.9; \quad 40\beta - 2\gamma \leq 11 \tag{28}$$

According to Fig. 15, the proposed CSF was assumed to behave linearly for steel grades with 355 MPa ≤ f_{y0} ≤ 500 MPa and nonlinearly for S700. For steel grades 500 MPa < f_{y0} < 700 MPa, the values are proposed to be found by linear interpolation. The developed CSF is provided in

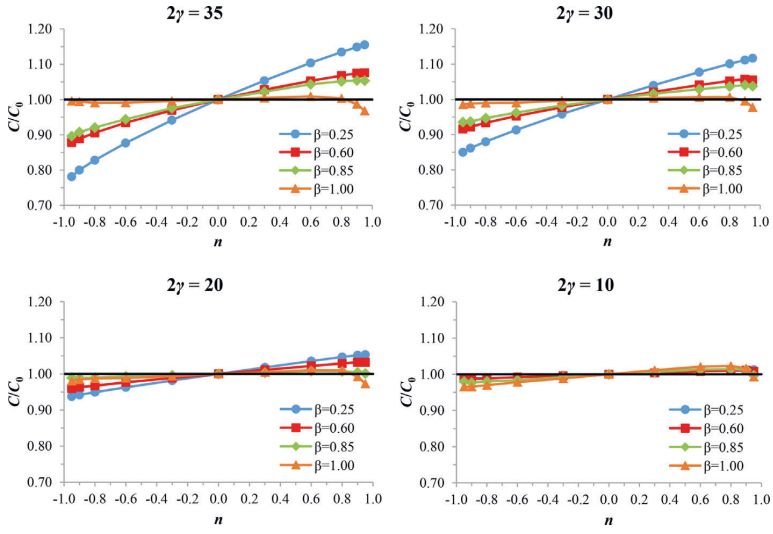

Fig. 16. Dependence of the effect on β, S355.

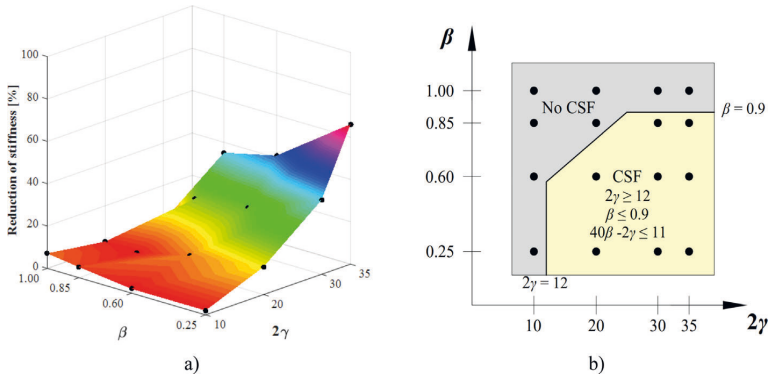

Fig. 17. a) Dependence on β and γ (S700, $n = -0.95$); b) domain of the proposed CSF.

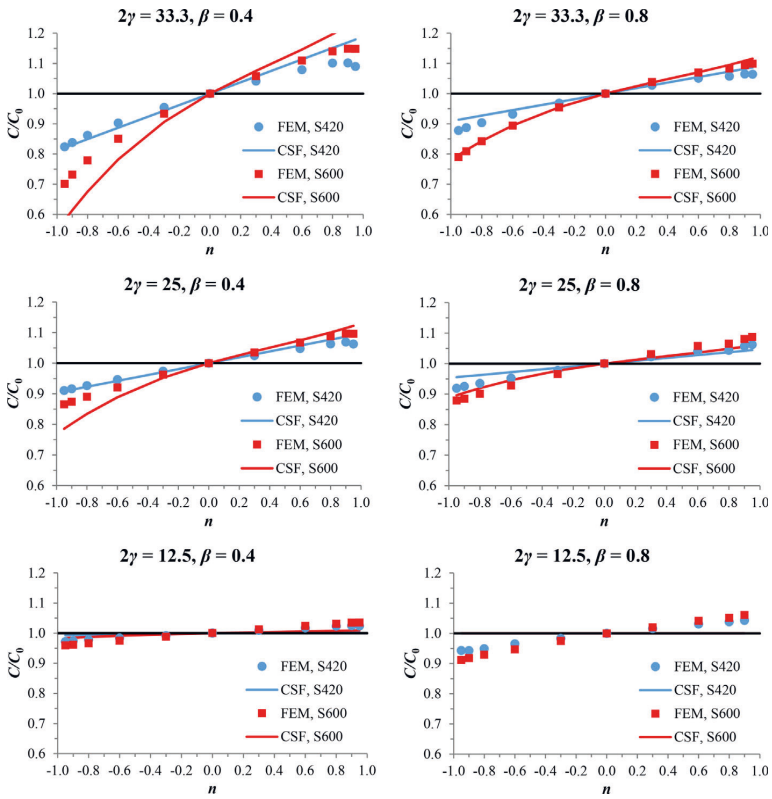

Fig. 18. Validation of the proposed CSF.

Eq. (29).

For $355\ \text{MPa} \le f_{y0} \le 500\ \text{MPa}$:

$$k_{sn,N} = 1 + 10^{-5} f(\beta) f(\gamma) f\left(f_{y0}\right) n$$

For $500\ \text{MPa} < f_{y0} < 700\ \text{MPa}$:

$k_{sn,N}$ is the linear interpolation between S500 and S700 (29)

For $f_{y0} = 700\ \text{MPa}$:

$$k_{sn,N} = 1 + 0.0008 f(\beta) f(\gamma) \left(n^3 - 1.25 n^2 + 0.01 f\left(f_{y0}\right) n\right)$$

where

$$f(\beta) = -2\beta^2 + 1.6\beta + 0.3$$
$$f(\gamma) = 1.3\gamma^2 - 38 \quad (30)$$
$$f\left(f_{y0}\right) = 0.02 {f_{y0}}^{1.4}$$

Table 8
Approximation based on the existing chord stress functions for the resistance.

Case	Equation	A	B	C	R^2	R^2_{adj}	Δ_{av} [%]	Δ_{max} [%]
1	$k_{sn,ip} = \begin{cases} 1.3-\frac{0.4\lvert n\rvert}{\beta} \le 1.0, & n<0 \\ 1.0, & n>0 \end{cases}$	–	–	–	0.30	0.30	17.0	141.1
2	$k_{sn,ip} = 1 + A\frac{n}{\beta+B}, \quad -0.99 \le n \le 0.99$	0.1	0.13	–	0.58	0.58	6.4	23.8
3	$k_{sn,ip} = \begin{cases} (1-\lvert n\rvert)^{0.6-0.5\beta}, & n<0 \\ (1-\lvert n\rvert)^{0.1}, & n>0 \end{cases}$	–	–	–	0.26	0.26	21.0	75.5
4	$k_{sn,\,ip} = (1+n)^{A+B\beta}$	0.45	0	–	0.47	0.47	29.9	73.7
5	$k_{sn,\,ip} = (1-n^2)^{0.8-0.8\beta+0.01\gamma}$	–	–	–	0.01	0.01	25.8	87.2
6	$k_{sn,\,ip} = (1-n^2)^{A+B\beta+C\gamma}$	0.1	0.1	0.1	0.01	0.01	53.1	99.0

Table 9
Details of joints used for validation of CSF.

Chord, $b_0 \times h_0 \times t_0$	2γ	Brace, $b_1 \times h_1 \times t_1$	β	Steel grade
$100 \times 100 \times 3$	33.3	$40 \times 40 \times 3$	0.4	S420
$100 \times 100 \times 4$	25.0	$80 \times 80 \times 3$	0.8	S600
$100 \times 100 \times 8$	12.5			

5.3. Validation of the proposed chord stress function

The validation of the proposed CSF was conducted with a series of independent FE results and employing the same FE model. To prove that the function is scalable in the chord width, the validation was conducted for the different chord size, 100 × 100 mm. The validation was performed for three chord wall thicknesses, two brace widths and two steel grades, as shown in Table 9. Although the grade S600 is not generally produced, it was used for scientific purposes, as an intermediate grade between S500 and S700. The brace wall thickness was selected so that it did not exceed that of the chord.

Fig. 18 presents the graphical validation of the developed chord stress function, plotting the ratio C/C_0 in relation to n, where C is the stiffness with a relative axial stress n, C_0 is the stiffness with no axial stress. As can be seen, the proposed CSF provides a sufficiently accurate prediction, with $R^2 = 0.94$, $R^2_{adj} = 0.93$, the average error is 2.3% and the maximum error is 17.3%. The case with $2\gamma = 12.5$ and $\beta = 0.8$ represents the only joint outside the domain of the CSF, meaning that no CSF is needed for it ($k_{sn,N} = 1.0$). The numerical simulations demonstrate 9% maximum reduction of initial stiffness for this joint, which is acceptable in practice. Taking the chord stress function into account, Eq. (1) can be modified as follows:

$$C_{j,ini,N} = \frac{k_{sn,N} E}{\sum_i \frac{1}{k_i}} \tag{31}$$

6. Conclusions

This paper considers the initial axial stiffness of tubular joints, employing the component method proposed by CIDECT. The paper considered the existing CIDECT approach for initial axial stiffness of RHS T joints and validated it against the existing experimental results. The validation has demonstrated that the existing equations for the stiffness of individual components lead to inaccurate results and cannot be reliable in the computational analysis. Moreover, in most cases, the stiffness equation for the component "chord face in bending" has violated its validity range. In addition, the direct comparison of the experimental stiffness of T and X joints with matching geometry have shown that X joints have considerably higher axial stiffness than T joints, therefore, they cannot be used to validate the theoretical approach for T joints.

Following the adopted component method, the paper has proposed new equations for the stiffness of the components "chord face in bending" and "chord side walls in compression". The equations are based on simple mechanical modes, employing the concept of the effective length and width. Given that chord face bending develops similarly for T and X joints, a common equation has been proposed for the stiffness of the component "chord face in bending". At the same time, the equation for the component "chord side walls in compression" has been limited only for T joints, given the abovementioned differences between the stiffness of T and X joints.

The developed equation were validated against the same experimental values. When the influence of fillet welds was disregarded, the prediction inconsiderably underestimated the stiffness of joints. The employed solution of de Matos et al. for fillet welds allowed to compensate the underestimation and obtain more accurate results, although overestimating the stiffness of some joints. In general, the proposed equations has demonstrated good correlation with the experimental results and can be recommended for the design of axially loaded RHS T joints.

It should be noted that the conducted research was considerably complicated by the small amount of the available experimental results. The second challenging issue was the determination of initial stiffness from the experimental data. In this paper, it was determined graphically based on the presented load-deformation curves. This approach is rather complicated and might lead to inaccurate results. Such researches, where theoretical solutions are evaluated with existing experimental data, can be conducted more effectively if in addition to resistance and load-deformation curves, authors also provide the exact values of initial stiffness.

The second part of the paper investigated the influence of chord axial stresses on the initial axial stiffness of RHS T joints. The conducted numerical simulations demonstrated that compressive stresses reduce stiffness by 35%, while tensile stresses increase it by 30%. The effect was found dependent on the geometry and the steel grade of joints, being particularly strong for joints with high 2γ, small β and high steel grades. To take this influence into account, the paper has developed a corresponding chord stress function. The validation with a series of independent numerical data has shown the sufficient accuracy of the proposed function, which can be further verified against new experimental results.

References

[1] H. Boel, Buckling Length Factors Of Hollow Section Members In Lattice Girders, Master Thesis Eindhoven University of Technology, Eindhoven, 2010.
[2] H.H. Snijder, H.D. Boel, J.C.D. Hoenderkamp, R.C. Spoorenberg, Buckling length factors for welded lattice girders with hollow section braces and chords, Proceedings of the 6th European Conference on Steel and Composite Structures (Eurosteel 2011), 31 August - 2 September 2011, Budapest, Hungary 2011, pp. 1881–1886.
[3] Ä. Haakana, In-plane Buckling And Semi-Rigid Joints Of Tubular High Strength Steel Trusses, Master of Science Thesis Tampere University of Technology, Tampere, 2014.
[4] M. Garifullin, S. Pajunen, K. Mela, M. Heinisuo, 3D component method for welded tubular T joints, Tubular Structures XVI: Proceedings of the 16th International Symposium for Tubular Structures (ISTS 2017, 4–6 December 2017, Melbourne, Australia) 2018, pp. 165–173.
[5] CEN, Eurocode 3: Design of steel structures – part 1-8: Design of joints (EN 1993-1-8:2005). Brussels, 2005.
[6] J.A. Packer, J. Wardenier, X.-L. Zhao, G.J. van der Vegte, Y. Kurobane, Design guide for rectangular hollow section (RHS) joints under predominantly static loading, CIDECT Design Guide 3 (2009) 2nd ed. LSS Verlag.

[7] Y. Yu, The Static Strength Of Uniplanar And Multiplanar Connections In Rectangular Hollow Sections, PhD thesis Delft University of Technology, Delft, 1997.
[8] J.J. Cao, J.A. Packer, G.J. Yang, Yield line analysis of RHS connections with axial loads, J. Constr. Steel Res. 48 (1) (1998) 1–25.
[9] X.-L. Zhao, J. Wardenier, J.A. Packer, G.J. van der Vegte, Current static design guidance for hollow-section joints, Proc. Inst. Civ. Eng. — Struct. Build. 163 (6) (2010) 361–373.
[10] P. Mäkeläinen, R. Puthli, F. Bijlaard, Strength, stiffness and nonlinear behaviour of simple tubular joints, IABSE Congr. Rep. 13 (1988) 635–640.
[11] D. Grotmann, G. Sedlacek, Rotational Stiffness of Welded RHS Beam-to-Column Joints, Cidect 5BB-8/98. Aachen: RWTH-Aachen, 1998.
[12] R.M.M.P. de Matos, L.F. Costa-Neves, L.R.O. de Lima, P.C.G.S. Vellasco, J.G.S. da Silva, Resistance and elastic stiffness of RHS "T" joints: part I – Axial brace loading, Lat. Am. J. Solids Struct. 12 (11) (2015) 2159–2179.
[13] L.F. Costa-Neves, Monotonic and Cyclic Behaviour of Minor-Axis and Hollow Section Joints in Steel and Composite Structures, Doctoral Thesis University of Coimbra, 2014.
[14] K. Weynand, J.-P. Jaspart, J.-F. Demonceau, L. Zhang, Component Method for Tubular Joints, CIDECT Report 16F – 3/15, 2015.
[15] P. Zoetemeijer, Design method for the tension side of statically loaded, bolted beam-to-column connections Heron. 20 (1) (1974) 1–59.
[16] F. Tschemmernegg, A. Tautschnig, H. Klein, C. Braun, C. Humer, Zur Nachgiebigkeit von Rahmenknoten – Teil 1, Stahlbau 56 (10) (1987) 299–306 (in German).
[17] F. Wald, Column Bases, CTU Prague, Prague, 1995.
[18] L. Leston-Jones, The Influence of Semi-rigid Connections on the Performance of Steel Framed Structures in Fire, PhD Thesis University of Sheffield1997.
[19] A.M. Girão Coelho, F.S.K. Bijlaard, Experimental behaviour of high strength steel end-plate connections, J. Constr. Steel Res. 63 (9) (2007) 1228–1240.
[20] L.S. da Silva, Towards a consistent design approach for steel joints under generalized loading, J. Constr. Steel Res. 64 (9) (2008) 1059–1075.
[21] M. Heinisuo, H. Ronni, H. Perttola, A. Aalto, T. Tiainen, End and base plate joints with corner bolts for rectangular tubular member, J. Constr. Steel Res. 75 (2012) 85–92.
[22] K. Weynand, J.-P. Jaspart, Extension of the component method to joints in tubular construction, tubular Structures IX: Proceedings of the Ninth International Symposium and Euroconference, Dusseldorf, Germany 3-5 (2001) (April 2001) 517–524.
[23] J.-P. Jaspart, C. Pietrapertosa, K. Weynand, E. Busse, R. Klinkhammer, Development of a Full Consistent Design Approach for Bolted and Welded Joints in Building Frames and Trusses between Steel Members Made of Hollow and / or Open Sections – Application of the Component Method, Vol. 1, 2005 Practical guidelines. CIDECT Report: 5BP-4/05.
[24] M. Garifullin, M. Bronzova, T. Jokinen, M. Heinisuo, B. Kovačič, Effect of fillet welds on initial rotational stiffness of welded tubular joints, Procedia Eng. 165 (2016) 1643–1650.
[25] C. Málaga-Chuquitaype, A.Y. Elghazouli, Component-based mechanical models for blind-bolted angle connections, Eng. Struct. 32 (10) (2010) 3048–3067.
[26] J.-P. Jaspart, Doctor of Science Thesis, Etude de la semi-rigidité des noeuds poutercolonne et son influence sur la résistance et la stabilité des ossatures en Acier, University of Liège (in French), 1991.
[27] C. López-Colina, M.A. Serrano-López, F.L. Gayarre, J.J. Del Coz-Díaz, Stiffness of the component "lateral faces of RHS" at high temperature, J. Constr. Steel Res. 67 (12) (2011) 1835–1842.
[28] B. Kato, I. Nishiyama, T-joints made of rectangular tubes, International Specialty Conference on Cold-Formed Steel Structures. 3 (1980) 663–679.
[29] X.-L. Zhao, G.J. Hancock, T-joints in rectangular hollow sections subject to combined actions, J. Struct. Eng. 117 (8) (1991) 2258–2277.
[30] G. Davies, P. Crockett, The strength of welded T-DT joints in rectangular and circular hollow section under variable axial loads, J. Constr. Steel Res. 37 (1) (1996) 1–31.
[31] A. Nizer, L.R.O. de Lima, P.C.G.S. Vellasco, S.A.L. de Andrade, E. da S. Goulart, A.T. da Silva, L.F. Costa-Neves, Experimental and numerical assessment of RHS T-joints subjected to brace and chord axial forces, Steel Constr. 9 (4) (2016) 315–322.
[32] J. Becque, T. Wilkinson, The capacity of grade C450 cold-formed rectangular hollow section T and X connections: an experimental investigation, J. Constr. Steel Res. 133 (2017) 345–359.
[33] M. Pandey, B. Young, High Strength Steel Tubular X-Joints — An Experimental Insight under Axial Compression, Tubular Structures XVI: Proceedings of the 16th International Symposium for Tubular Structures (ISTS 2017, 4–6 December 2017, Melbourne, Australia), 2018 223–230.
[34] K.J.R. Rasmussen, B. Young, Tests of X- and K-joints in SHS stainless steel tubes, J. Struct. Eng. 127 (10) (2001) 1173–1182.
[35] R. Feng, B. Young, Experimental investigation of cold-formed stainless steel tubular T-joints, Thin-Walled Struct. 46 (10) (2008) 1129–1142.
[36] R. Feng, B. Young, Tests and behaviour of cold-formed stainless steel tubular X-joints, Thin-Walled Struct. 48 (12) (2010) 921–934.
[37] M. Heinisuo, M. Garifullin, T. Jokinen, T. Tiainen, K. Mela, Surrogate modeling for rotational stiffness of welded tubular Y-joints, Connections in Steel Structures VIII (2016) 285–294.
[38] J. Wardenier, *Hollow section joints*. Delft University Press, Delft, 1982 https://doi.org/10.1016/j.lithos.2018.10.034.
[39] Abaqus Abaqus, 6.12. Getting Started with Abaqus: Interactive Edition. Dassault Systèmes, 695 p, 2012.
[40] G.J. van der Vegte, Y. Makino, Further research on chord length and boundary conditions of CHS T- and X-joints, Adv. Steel Constr. 6 (3) (2010) 879–890.
[41] G.J. van der Vegte, J. Wardenier, R.S. Puthli, FE analysis for welded hollow-section joints and bolted joints, Proc. Inst. Civ. Eng. — Struct. Build. 163 (SB6) (2010) 427–437.
[42] D.K. Liu, J. Wardenier, G.J. van der Vegte, New Chord Stress Functions for Rectangular Hollow Section Joints, The Fourteenth International Offshore and Polar Engineering Conference 2004, pp. 178–185.
[43] J. Wardenier, G.J. van der Vegte, D.K. Liu, Chord Stress Function for Rectangular Hollow Section X and T Joints, Proceedings of the Seventeenth International Offshore and Polar Engineering Conference 2007, pp. 3363–3370.
[44] A. Lipp, T. Ummenhofer, Influence of tensile chord stresses on the strength of CHS X-joints – Experimental and numerical investigations, Tubular Structures XV: Proceedings of the 15th International Symposium on Tubular Structures, Rio de Janeiro, Brazil 27-29 (2015) (May 2015) 379–386.
[45] M. Garifullin, S. Pajunen, K. Mela, M. Heinisuo, J. Havula, Initial in-plane rotational stiffness of welded RHS T joints with axial force in main member, J. Constr. Steel Res. 139 (2017) 353–362.